

Copyright  
by  
Matthew Maclean Russell  
2003

**The Dissertation Committee for Matthew Maclean Russell certifies that this  
is the approved version of the following dissertation:**

**Predicting Secondary Organic Aerosol Formation Rates and  
Concentrations in Southeast Texas**

**Committee:**

---

David T. Allen, Supervisor

---

Howard M. Liljestrand, Supervisor

---

Kerry A. Kinney

---

Richard L. Corsi

---

Elena C. McDonald-Buller

**Predicting Secondary Organic Aerosol Formation Rates and  
Concentrations in Southeast Texas**

**by**

**Matthew Maclean Russell, B.Eng, MSE.**

**Dissertation**

Presented to the Faculty of the Graduate School of

The University of Texas at Austin

in Partial Fulfillment

of the Requirements

for the Degree of

**Doctor of Philosophy**

**The University of Texas at Austin**

**December, 2003**

## **Acknowledgements**

I acknowledge my advisor David Allen for his supervision during my graduate studies; he sets the example for dedication and achievement at his profession. I acknowledge Yosuke Kimura (Yo); his help made this work possible and he is the engine that drives our research group. Finally, I acknowledge my friends and family; their support, friendship and love make what I do possible.

# **Predicting Secondary Organic Aerosol Formation Rates and Concentrations in Southeast Texas**

Publication No. \_\_\_\_\_

Matthew Maclean Russell, Ph.D.

The University of Texas at Austin, 2003

Supervisors: David T. Allen, Howard M. Liljestr nd

Elevated concentrations of atmospheric particulate matter are a significant public health concern, yet the sources, composition and formation mechanisms for this class of pollutants remain poorly understood. This work addresses these knowledge gaps, especially for Southeast Texas. This dissertation reports: 1) the development of a conceptual model of fine particulate matter (less than 2.5  $\mu\text{m}$  in diameter,  $\text{PM}_{2.5}$ ) for Southeast Texas including estimates of primary and secondary organic aerosol (SOA) concentrations, 2) the development of a photochemical grid model tool that implements a flexible chemical mechanism and a module to predict SOA formation, and 3) the application of the tool to Southeast Texas to estimate the spatial distribution, temporal distribution, and precursors of SOA formation.

PM<sub>2.5</sub> concentrations in Southeast Texas during 2000-2001 were found to be close to, but not in excess of, the annual National Ambient Air Quality Standard for PM<sub>2.5</sub>. PM<sub>2.5</sub> mass concentrations, composition and diurnal patterns were found to be relatively consistent throughout Southeast Texas and from season to season. The major components of PM<sub>2.5</sub> were found to be ammonium sulfate and organic carbon; the majority of organic carbon is primary yet secondary organic carbon is significant during the ozone season. The conceptual model contributes greatly to understanding PM<sub>2.5</sub> pollution in this area.

A state-of-the-science photochemical grid model was modified to include a flexible chemical mechanism and a module to predict SOA formation. The tool was used in this work to model SOA formation rates from aromatics and monoterpenes in Southeast Texas during the ozone season, using a new chemical mechanism designed for this purpose. SOA formation was found to come predominantly from biogenic monoterpenes, particularly from  $\alpha$ -pinene/ozone and  $\beta$ -pinene/nitrate-radical reactions. SOA formation rates were predicted to peak in the evening during the episode considered here. The levels, spatial distribution, and biogenic nature of the SOA formation are consistent with the limited ambient SOA information collected during this period. Sensitivity simulations showed that SOA formation is proportional to existing particulate matter concentrations and proportional to precursor emission rates. The model results are, most importantly, a guide for identifying knowledge gaps to model SOA air pollution.

## Table of Contents

List of Tables.....	x
List of Figures .....	xiii
Table of Acronyms.....	xx
1.0 Introduction.....	1
1.1 Particulate Matter Pollution .....	1
1.2 Urban aerosol and ozone formation .....	4
1.3 Research Objectives .....	6
1.4 Dissertation structure.....	7
2.0 Literature Review .....	8
2.1 Secondary Organic Aerosol Formation – Theory .....	8
2.2 Secondary Organic Aerosol Formation – Modeling .....	13
2.3 SOA mechanisms in photochemical grid models. ....	19
2.4 Secondary Organic Aerosol Formation – Analysis of Ambient Data .....	26
2.5 Summary .....	32
3.0 Methods – Part 1: Conceptual Model for attributing PM <sub>2.5</sub> sources and Empirical model for SOA in Southeast Texas .....	34
3.1 Fine particulate matter data in Southeast Texas.....	34
3.2 Development of SOA Empirical Model for Southeast Texas .....	41
4.0 Results-Part 1: PM <sub>2.5</sub> Conceptual Model and SOA Empirical Model.....	65
4.1 Conceptual Model of PM <sub>2.5</sub> in Southeast Texas.....	65
FRM Mass Analysis.....	65
TEOM Mass Analysis .....	70
Spatial distribution of FRM mass.....	79
FRM composition analysis.....	84

4.2 SOA Empirical model .....	90
Seasonal and spatial trends in total OC and EC .....	90
SOA empirical model results .....	94
Secondary OC and ground-level ozone.....	100
Primary and Secondary OC during TXAQS 2000 .....	105
5.0 Methods-Part 2: Modeling SOA formation in a Grid Model .....	110
5.1 Episode Selection .....	110
5.2 Chemical Mechanism Development .....	114
5.3 Emissions Inventory development .....	130
Anthropogenic emissions processing .....	133
Biogenic emissions processing.....	143
SOA precursor emissions summary .....	144
5.4 TXAQS Episode Model Performance.....	147
5.5 SOA Model Development.....	154
5.5 Model Applications .....	168
6.0 Results – Part 2: Base Case Model Results and Sensitivity Applications ....	174
6.1 Base Case Model Results .....	175
Domain-wide SOA formation.....	176
Monitoring location SOA formation.....	191
SOA formation evaluation.....	197
6.2 Sensitivity Simulations Results.....	204
Reaction Mechanism Sensitivity.....	206
Mo concentration sensitivity.....	209
SOA precursor sensitivity.....	212
Ozone precursor sensitivity.....	215
6.3 Chapter Summary.....	224

7.0 Conclusions and Recommendations.....	227
Appendix A: Emissions Inventory Processing for the TXAQS modeling episode.....	232
Appendix B: Integration of a flexible SAPRC99-generated chemical mechanism into CAMx 3.10. ....	239
Overview .....	240
The Chemical Mechanism and Its Solver .....	241
Source code modifications .....	247
Modifications to SAPRC99 Software .....	251
Modifications to CAMx31 .....	257
Guidelines for implementing a modified chemical mechanism into CAMx31 .....	260
Appendix C: Modifications to the Emitdb.xls tool. ....	263
Processing multiple speciation profiles .....	265
Calculating splitfactors for s99soa model species.....	266
Appendix D: Modifications made to GLOBEIS version 2.2. ....	270
Speciation of total monoterpene emissions by tree species. ....	271
Calculation of s99 and s99soa emissions from biogenic sources.....	293
Appendix E: SAPRC99 .RXN Input files for the s99soa and s99soa2 chemical mechanisms .....	298
s99soa.rxn.....	298
s99soa2 .....	307
References .....	316
Vita .....	324

## List of Tables

Table 3.1: PM <sub>2.5</sub> speciation sites in Southeast Texas included in this analysis. Each site had valid PM <sub>2.5</sub> speciation data and ozone data for one or two full year periods. ‘C’ numbers in the site names refer to Texas Continuous Air Monitoring Station (CAMS) IDs. A short name for each site is indicated in bold. Sites with only one year of data in the analysis are denoted by (1).....	43
Table 3.2: Regression results for the set of OC and EC measurements on days assumed to have no secondary OC and to be representative of primary OC and EC at the Southeast Texas monitoring sites. The slope represents OC <sub>1</sub> /EC and the intercept represents OC <sub>2</sub> . Italics indicate the standard error of each estimate. The data are not shown wherever the regression was not significant at the 90% confidence level, except for the Conroe site during Mar-Oct (shaded). The regression was significant at the 80% confidence level for this site/period, and the site was included because of its importance to the study. ....	61
Table 4.1 : Mean, standard deviation, maximum and number of FRM mass concentrations for the January 1st, 2000-December 31st, 2001 period and for the January 1st, 2001-December 31st, 2001 period. Each monitoring site was active for the entire period under which it is listed. ....	67
Table 4.2: Mean OC, EC and fractions of OC and EC in total PM <sub>2.5</sub> for six sites in Southeast Texas. Means are taken over the two-year period 8/15/2000 through 8/15/2002.....	91
Table 4.3. Mean <b>primary</b> OC by month. a) Regression primary OC. b) Lower bound primary OC. Italics indicate the standard deviation of each estimate. Data for which the initial regression was not valid are not included. Bold numbers indicate the month with the highest mean primary OC for that site (only for sites when all months of data are available).....	96
Table 4.4: Mean <b>secondary</b> OC by month. a) Regression secondary OC. b) Upper bound secondary OC. Italics indicate the standard deviation of each estimate. Data for which the initial regression was not valid are not included. Bold numbers indicate the month with the highest mean secondary OC for that site (only for sites when all months of data are available).....	97
Table 5.1. Input files for modeling the TXAQS modeling episode with CAMx version 3.10. ....	113

Table 5.2: Estimated aromatic emissions from all anthropogenic sources in Texas in each yield/reactivity category. These estimates were made with emissions data listed in Appendix A and speciation profiles listed in Table 5.7.....	119
Table 5.3. List of model species in s99soa and s99soa2 mechanisms that represent VOC compounds in the emissions inventory. Some descriptions taken from SAPRC documentation (Carter 2000). ....	121
Table 5.4. Speciated Texas anthropogenic emissions from area/offroad mobile, onroad mobile, and point sources. (% by mass).....	125
Table 5.5. Speciated Texas anthropogenic VOC emissions, from all sources. The list continues from column to column. (% by mass).....	126
Table 5.6 Lumped mechanism parameters for intermediate model species (APR) and condensable reaction products (COC) in the s99soa2 mechanism. Parameters were derived using spreadsheet calculations and using the Texas anthropogenic emissions profile. ....	129
Table 5.7: Sources of speciation profiles for different emissions groups .....	135
Table 5.8 All aromatic compounds in emitdb.xls and that are found in speciation profiles. Also shown is their assigned yield classification.....	137
Table 5.9. Emissions of SOA precursors input to the TXAQS episode on August 31 <sup>st</sup> , 2000. (AR1H: high-SOA yield/low-reactivity aromatics. AR2H: high-SOA yield/high-reactivity aromatics. AR2L: low-SOA yield/high-reactivity aromatics) Units are in tons/day .....	146
Table 5.10 Yield parameter data for four-parameter yield model.....	157
Table 5.11. Format of SOA parameters input file.....	164
Table 5.12. Format of Mo fields file.....	164
Table 5.13. Format of PBL layer fields file.....	164
Table 5.14. Modifications and additions to the CAMx31 source code for the SOA formation model.....	165
Table 5.15 Yield parameter data for lumped intermediate model species using the four-parameter yield model.....	167
Table 5.16. List of sensitivity simulations.....	170
Table 6.1. Daily total formation of SOA in tons from each reaction pathway for 8/29/2000, 8/30/2000 and 8/31/2000. (HYA = high-yield aromatics, LYA = low-yield aromatics).....	176
Table 6.2. List of sensitivity simulations.....	205
Table A1: Area & off-road (non-road) sources.....	234
Table A2: On-road (mobile) sources.....	235
Table A3: Point sources .....	236
Table A4: Biogenic sources .....	238

Table B1. Terminology used in the Appendix .....	241
Table B2. Modifications/additions to SAPRC99 software subroutines to produce source code to be integrated into CAMx31.....	254
Table B3: modifications to CAMx31.....	258
Table D1. Percentage of each compound in total monoterpene emissions (Geron et al. 2000). N denotes the number of samples used to determine the speciation. The first row of data is an average speciation profile across all 95 other profiles. mt_link was added to link each genus/species with internal GLOBEIS emissions factors. ....	273
Table D2. Modifications made to GLOBEIS2.2 to calculate emissions of individual monoterpene compounds. ....	277
Table D3: Speciation profile of non-isoprene, non-terpene biogenic VOC's. The original profile was given in mass C. Also shown is mass of each compound (input to emit_db.xls) and splitfactors for s99/s99soa species (output from emit_db.xls). ....	294
Table D4. Modifications to GLOBEIS2.2 to produce s99 or s99soa model species. These were made in addition to those listed in Table D2 above. ....	295

## List of Figures

Figure 1.1. Typical urban dry mass composition of PM <sub>2.5</sub> . The majority of urban PM <sub>2.5</sub> mass may be secondary in origin. ....	3
Figure 1.2 For various Texas cities, maximum concentrations of PM <sub>2.5</sub> components collected between 3/97 and 3/98 (Tropp et al. 1998). Also shown are the maximum recorded 1-hour average ozone concentrations in 1997 (USEPA 2002). ....	5
Figure 3.1 a) FRM mass sampling network in SE Texas, b) TEOM sampling network in SE Texas, and c) FRM speciation network in SE Texas .....	38
Figure 3.2: Scatterplot of OC and EC concentrations for all measurements on days with maximum ozone concentrations less than 40 ppb a)Mauriceville b)Conroe c)Galveston d)Hamshire e)Aldine f)Bayland Park g)Deer Park h)HRM-3 i)Channelview. Data points are divided into one of four seasons: Feb-Apr, May-Jul, Aug-Oct and Nov-Jan.....	49
Figure 3.3: Product of frequency of hourly resultant wind direction and mean resultant wind speed for each wind direction at the Deer Park site. Data is shown separately for the November-February, March-June and July-October period. ....	52
Figure 3.4. Number of OC-EC data points used in the regression estimates (in parenthesis) by site and season. Total numbers of data points in the dataset are indicated by the height of each column.....	53
Figure 3.5: Scatterplot of OC and EC concentrations for all measurements used in the final regression (max ozone less than 40ppb and extreme events removed). a)Mauriceville b)Conroe c)Galveston d)Hamshire e)Aldine f)Bayland Park g)Deer Park h)HRM-3 i)Channelview. Regression equations are shown for the sites with two full years of data. ....	59
Figure 3.6. Number of data points (days) for which SOC concentrations were calculated (in parenthesis) by site and season. Total numbers of data points in the dataset are indicated by the height of each column. ....	62
Figure 4.1. Monthly variations in mean FRM mass concentrations. The data points show mean FRM mass concentrations over all sites that were active during the entire two-year 2000-2001 period. Bars show one standard deviation for all data in that month, i.e. both intersite and intrasite variability. Also shown are the mean FRM mass concentrations for Clinton and Clute (no bars shown for these individual sites). ....	69

Figure 4.2. Monthly variations in maximum FRM mass concentrations. The vertical bars show the range between the lowest and highest maximum over all sites that were active during the entire two-year 2000-2001 period. Also shown are the maximum FRM mass concentrations for Clinton and Clute. ....	70
Figure 4.3. Mean daily TEOM mass (24-hour average) vs. FRM mass for all site/date combinations with 24 valid hourly TEOM mass concentrations and concurrent FRM mass concentrations. The data are limited to sites that were active during the entire March 2000 – February 2002 period. ....	72
Figure 4.4. Mean diurnal pattern of TEOM mass concentrations from hourly-averaged TEOM data. The mean for each hour is taken over all sites and dates. The data are limited to sites that were active during the entire March 2000 – February 2002 period. Bars show one standard deviation for all data in that hour, i.e. both intersite and intrasite variability. Also shown are the mean diurnal patterns for Houston East and Hamshire (no bars shown for these individual sites). ....	74
Figure 4.5. Mean diurnal patterns of PM <sub>2.5</sub> and ozone at the Conroe site on days when maximum ozone is greater than 80 ppb at Conroe (high ozone days) and on days when maximum ozone is less than 80 ppb at Conroe (low ozone days). The data are limited to the entire March 2000 – February 2002 period. ....	76
Figure 4.6. a) Frequency of mean hourly TEOM mass concentration (24 hour averaged) when the maximum hourly TEOM mass on that day exceeds 40 µg/m <sup>3</sup> . b) Frequency of the ratio of 25th percentile hourly TEOM mass to maximum hourly TEOM mass on days when the maximum hourly TEOM mass exceeds 40 µg/m <sup>3</sup> . The analysis was limited to dates with 24 hours of valid TEOM mass concentrations. ....	78
Figure 4.7. a) Ratio of 25th percentile FRM mass to maximum FRM mass, versus maximum FRM mass for a given day. The 25th percentile and maximum are taken over all the monitoring sites on a given day with at least 5 valid FRM mass measurements. b) Distribution of the values of the ratio of 25th percentile FRM mass to maximum FRM mass. ....	80
Figure 4.8. Forty-eight hour back trajectories calculated using the HYSPLIT model, for days when maximum FRM concentration observed in the region was greater than 20 µg/m <sup>3</sup> and all monitors recorded relatively high concentrations (regional events). ....	82

Figure 4.9: Forty-eight hour back trajectories calculated using the HYSPLIT model, for days when maximum FRM concentration observed in the region are greater than 20 $\mu\text{g}/\text{m}^3$ and at least some monitors recorded low mass concentrations (local events).....	83
Figure 4.10. (Preceding Pages) Mean composition of $\text{PM}_{2.5}$ during a) November-January, b) February-April, c) May-July and d) August-October. The difference between the sum of the major component concentrations and the total mass concentration is classified as ‘other’, such that the total height of each column equals the mean total $\text{PM}_{2.5}$ mass concentration for that site and season. Data are limited to the sites that were active during the entire two-year period beginning September 1st, 2000 and ending August 31st, 2002.....	88
Figure 4.11: Monthly mean OC (top) and EC (bottom) concentrations over all six monitoring sites with valid data for the two-year 8/15/2000 – 8/15/2002 period. Error bars represent one standard deviation from the mean over all sites, i.e. showing inter- and intra-site variability. Monthly mean OC and EC are also shown for both Aldine and Galveston which recorded the highest and lowest overall mean OC and EC respectively. There are no error bars reported for these sites.....	93
Figure 4.12. <b>Regression</b> mean monthly primary OC (top) and <b>regression</b> mean monthly secondary OC (bottom). This is the same data that is presented in Tables 4.3a and 4.4a.....	98
Figure 4.13. <b>Lower-bound</b> mean monthly primary OC (top) and <b>upper-bound</b> mean monthly secondary OC (bottom). This is the same data that is presented in Tables 4.3b and 4.4b.....	99
Figure 4.14: Scatter plot of mean daily ozone concentration vs. predicted secondary organic carbon at the same site and date. a)Galveston, b)Aldine, c)Hamshire, d)Bayland Park, e) Deer Park and f) Conroe.....	104
Figure 4.15 (Preceding pages) Measured total OC and predicted secondary OC (both regression and upper-bound) at all sites with valid data during this period a) Galveston, b) HRM-3, c) Hamshire, d) Aldine, e) Bayland Park and f) Conroe. Note some days have valid total OC and no secondary OC because these were excluded from the regression based on one of the arguments given in section 3.2.....	109

Figure 5.1: TXAQS episode modeling domain. The three largest grids were the primary modeling domains (Regional, East Texas and HGBPA). The two smallest 2km grids (HG and BPA) were not considered in this research. (This figure was obtained from the TCEQ). .....	112
Figure 5.2: Illustration of series/parallel nature of aromatic reactions to form condensable organic compounds.....	121
Figure 5.3. Illustration of aromatic-SOA formation in a) s99soa and b) s99soa2 (Dechapanya et al. 2003b). ARO represents a lumped aromatic species. APR represents intermediate aerosol precursors. COC represents condensable (or semi-volatile) organic compounds. ....	129
Figure 5.4. Monitored (top row) and modeled (bottom row) ozone concentrations on Aug 28 <sup>th</sup> , 2000 at 2pm, 4pm, 6pm and 8pm.....	149
Figure 5.5. Monitored (top row) and modeled (bottom row) ozone concentrations on Aug 29 <sup>th</sup> , 2000 at 2pm, 4pm, 6pm and 8pm.....	150
Figure 5.6. Monitored (top row) and modeled (bottom row) ozone concentrations on Aug 30 <sup>th</sup> , 2000 at 2pm, 4pm, 6pm and 8pm.....	151
Figure 5.7. Monitored (top row) and modeled (bottom row) ozone concentrations on Aug 31 <sup>st</sup> , 2000 at 2pm, 4pm, 6pm and 8pm.....	152
Figure 5.8. Interpolated Mo concentrations for August 31 <sup>st</sup> , 2000, 6 pm. ....	161
Figure 6.1. Time series of total SOA mass formed in the SOA-formation subdomain for the most significant formation pathways (top seven in Table 6.1). ....	177
Figure 6.2. Daily SOA formation in grams under the PBL for reactions of aromatics with the hydroxyl radical. 8/30/2000.....	179
Figure 6.3. Daily SOA formation in grams under the PBL for reactions of monoterpenes with the hydroxyl radical. 8/30/2000.....	180
Figure 6.4. Daily SOA formation in grams under the PBL for reactions of monoterpenes with the nitrate radical. 8/30/2000.....	181
Figure 6.5. Daily SOA formation in grams under the PBL for reactions of monoterpenes with ozone. 8/30/2000.....	182
Figure 6.6. Locations of FRM speciation monitoring stations in Southeast Texas. ....	183
Figure 6.7. Mean-grid cell SOA formation rates in $\mu\text{g}/\text{m}^3$ -hour in the SOA-formation subdomain. For each grid column, formation was normalized by volume under the PBL.....	186
Figure 6.8. Daily SOA formation in $\mu\text{g}/\text{m}^3$ under the PBL for reactions of aromatics with the hydroxyl radical. 8/30/2000.....	188
Figure 6.9. Daily SOA formation in $\mu\text{g}/\text{m}^3$ under the PBL for reactions of monoterpenes with the hydroxyl radical. 8/30/2000.....	189

Figure 6.10. Daily SOA formation in $\mu\text{g}/\text{m}^3$ under the PBL for reactions of monoterpenes with the nitrate radical. 8/30/2000. ....	190
Figure 6.11. Daily SOA formation in $\mu\text{g}/\text{m}^3$ under the PBL for reactions of monoterpenes with ozone. 8/30/2000.....	191
Figure 6.12. SOA formation rates in $\mu\text{g}/\text{m}^3$ - hour, in the grid cell where the Deer Park monitoring station is located. The scale on the abscissa is at a maximum of <b>0.03</b> $\mu\text{g}/\text{m}^3$ .....	193
Figure 6.13. SOA formation rates in $\mu\text{g}/\text{m}^3$ - hour, in the grid cell where the Galveston monitoring station is located. The scale on the abscissa is at a maximum of <b>0.03</b> $\mu\text{g}/\text{m}^3$ .....	194
Figure 6.14. SOA formation rates in $\mu\text{g}/\text{m}^3$ - hour, in the grid cell where the Aldine monitoring station is located. The scale on the abscissa is at a maximum of <b>0.50</b> $\mu\text{g}/\text{m}^3$ .....	195
Figure 6.15. SOA formation rates in $\mu\text{g}/\text{m}^3$ - hour, in the grid cell where the Conroe monitoring station is located. The scale on the abscissa is at a maximum of <b>0.50</b> $\mu\text{g}/\text{m}^3$ .....	196
Figure 6.16. Aromatic SOA formation per hour, averaged over all grid cells in the SOA-formation subdomain. Solid lines show the s99soa mechanism, dashed lines show the s99soa2 mechanism.....	208
Figure 6.17. Mean-grid cell daily SOA formation rates for the base case, 200%, 50% and homogeneous Mo sensitivity simulations.....	210
Figure 6.18. Mean-grid cell hourly SOA formation rates for the base case (solid lines) and the homogeneous Mo concentration case (dashed lines).....	211
Figure 6.19. Mean-grid cell daily SOA formation rate in SOA-subdomain on Aug 30 <sup>th</sup> , 2000. Results are shown for the base case and for the 50% and 200% biogenic monoterpene (bMT) emission reductions and the 50% and 200% aromatic (ARO) emissions reductions. ....	214
Figure 6.20. Mean-grid cell daily SOA formation rate in SOA-subdomain on Aug 30 <sup>th</sup> , 2000. Results are shown for the base case and for the 10%, 50% and 200% anthropogenic NO <sub>x</sub> (aNO <sub>x</sub> ) emissions reductions. ....	217
Figure 6.21. a) Maximum ozone decrease in each grid cell, and b) Maximum ozone increase in each cell (relative to base case) with 10% anthropogenic NO <sub>x</sub> , Aug 30, 2000. ....	218
Figure 6.22. Reduction (relative to base case) in daily SOA formation with 10% anthropogenic NO <sub>x</sub> for a) monoterpene-NO <sub>3</sub> pathways and b) monoterpene-O <sub>3</sub> pathways. A negative 'reduction' means SOA formation increased relative to the base case. ....	219

Figure 6.23. Reduction (relative to base case) in daily SOA formation with 10% anthropogenic NO <sub>x</sub> for all SOA formation reactions. ....	220
Figure 6.25. a) Maximum ozone decrease at any hour and b) reduction in daily total SOA formation rates for Aug 30, 2000, in the 10% anthropogenic light-olefin emissions case. ....	223
Figure B.1: Algorithm diagram of CAMx solution to chemical mechanism using the IEH solver. Each box represents a subroutine in CAMx31; each arrow represents a subroutine call. ....	250
Figure B.2: Algorithm diagram of chemical mechanism solution with the IEH solver using imported SAPRC generated source code. The mechanism specific routines ierxn, ierate, iejac and ieslow now are ‘empty’ and simply call the SAPRC generated code. Each box represents a subroutine in CAMx31; each arrow represents a subroutine call. ....	251
Figure C.1 Flow chart of organic compound assignments in emitdb.xls. See text for further details. Each box is a worksheet in emitdb.xls. ....	269
Figure D1. Spatial distribution of $\alpha$ -pinene emissions in Southeast Texas, in lbs/day on Sep 1 <sup>st</sup> , 2000. ....	279
Figure D2. Spatial distribution of $\beta$ -pinene emissions in Southeast Texas, in lbs/day on Sep 1 <sup>st</sup> , 2000. ....	280
Figure D3. Spatial distribution of d-limonene emissions in Southeast Texas, in lbs/day on Sep 1 <sup>st</sup> , 2000. ....	281
Figure D4. Spatial distribution of $\Delta^3$ carene emissions in Southeast Texas, in lbs/day on Sep 1 <sup>st</sup> , 2000. ....	282
Figure D5. Spatial distribution of sabinene emissions in Southeast Texas, in lbs/day on Sep 1 <sup>st</sup> , 2000. ....	283
Figure D6. Spatial distribution of $\alpha$ -terpinene emissions in Southeast Texas, in lbs/day on Sep 1 <sup>st</sup> , 2000. ....	284
Figure D7. Spatial distribution of $\beta$ -phellandrene emissions in Southeast Texas, in lbs/day on Sep 1 <sup>st</sup> , 2000. ....	285
Figure D8. Spatial distribution of camphene emissions in Southeast Texas, in lbs/day on Sep 1 <sup>st</sup> , 2000. ....	286
Figure D9. Spatial distribution of $\gamma$ -terpinene emissions in Southeast Texas, in lbs/day on Sep 1 <sup>st</sup> , 2000. ....	287
Figure D10. Spatial distribution of myrcene emissions in Southeast Texas, in lbs/day on Sep 1 <sup>st</sup> , 2000. ....	288
Figure D11. Spatial distribution of ocimene emissions in Southeast Texas, in lbs/day on Sep 1 <sup>st</sup> , 2000. ....	289
Figure D12. Spatial distribution of p-cymene emissions in Southeast Texas, in lbs/day on Sep 1 <sup>st</sup> , 2000. ....	290

Figure D13. Spatial distribution of terpinolene emissions in Southeast Texas, in lbs/day on Sep 1 <sup>st</sup> , 2000. ....	291
Figure D14. Spatial distribution of $\alpha$ -thujene emissions in Southeast Texas, in lbs/day on Sep 1 <sup>st</sup> , 2000.....	292
Figure D15. ‘Model Parameters’ window in updated version of GLOBEIS2.2. There is now an option box for choosing which mechanism to consider. ....	295

## Table of Acronyms

AIRS	Aerometric Information Retrieval System
BPA	Beaumont – Port Arthur
CAMx (CAMx31)	Comprehensive Air Quality Model with Extensions (version 3.10)
CB-IV (CBIV) (CB4)	Carbon Bond IV chemical mechanism
CMC	Chemical Mechanism Compiler
COC	Condensable Organic Compound (synonymous here with SVOC)
EC	Elemental Carbon
EI	Emissions Inventory
EPA	Environmental Protection Agency
EPS2	Emissions Preprocessor System version 2.0
FAC	Fractional Aerosol Coefficient
FRM	Federal Reference Method (for monitoring PM <sub>2.5</sub> )
GC-ARCH	Gulf Coast Aerosol Research and Characterization Program
GLOBEIS (GLOBEIS2.2)	Global Biosphere Emissions and Interactions System (version 2.2)
HG	Houston-Galveston
HGBPA	Houston-Galveston & Beaumont-Port Arthur
HYA	High (SOA) yield aromatics
IEH	Implicit-Explicit Hybrid (Numerical Solution Scheme)
LYA	Low (SOA) yield aromatics
NAAQS	National Ambient Air Quality Standard
NIOSH	National Institute for Occupational Safety and Health
OC	Organic Carbon (in PM <sub>2.5</sub> )
OC <sub>1</sub>	Primary organic carbon associated with combustion, i.e. emitted with EC
OC <sub>2</sub>	Primary organic carbon not associated with combustion
ODE	Ordinary Differential Equation
PBL	Planetary Boundary Layer
PM	Particulate Matter
PM <sub>2.5</sub>	Particulate Matter with aerodynamic diameters less than 2.5 microns
POC	Primary Organic Carbon (in PM <sub>2.5</sub> )

PTFE	Polytetrafluoroethylene (filter material)
RACM	Regional Atmospheric Chemistry Model
RADM (RADM2)	Regional Acid Deposition Mechanism
s99	Standard, fixed parameter version of the SAPRC99 chemical mechanism
s99soa (s99soa2)	Chemical mechanisms developed in this research based on SAPRC99, but modified for SOA modeling
SAPRC (SAPRC99) (SAPRC97)	Statewide Air Pollution Research Center chemical mechanism development software. (suffix indicates year of release, i.e. 99 or 97)
SETX (SE Texas)	Southeast Texas
SOA	Secondary organic aerosol
SOC	Secondary organic carbon (in PM <sub>2.5</sub> )
SVOC	Semi-volatile organic carbon. (Synonymous here with COC)
TCEQ	Texas Commission on Environmental Quality
TEOM	Tapered Element Oscillating Microbalance
TOT	Thermal Optical Transmittance
TXAQS (TEXAQS2000)	Texas Air Quality Study (in the year 2000)
UAM	Urban Airshed Model
VOC	Volatile Organic Compound

## **1.0 Introduction**

### **1.1 Particulate Matter Pollution**

Airborne particulate matter consists of solid or liquid particles in the atmosphere, generally in the size range of a few nanometers to tens of microns. The particles are directly emitted to the atmosphere by both biogenic and anthropogenic sources (primary particulate matter) and are formed in the atmosphere through the reactions of both biogenic and anthropogenic emissions (secondary particulate matter). Elevated concentrations of particulate matter (PM) are correlated with adverse cardio-respiratory health effects. PM also contributes to visibility degradation and its chemical components can cause damage to vegetation and other structures upon deposition. Particles with diameters less than 2.5 microns, referred to as PM<sub>2.5</sub>, are of particular concern because they can deposit deep in the lungs of humans and animals. PM<sub>2.5</sub> and PM<sub>10</sub> (particles with diameters less than 10 microns, which includes PM<sub>2.5</sub>) are criteria pollutants in the United States and must be regulated by mandate of the U.S. Clean Air Act. The U.S. Environmental Protection Agency (E.P.A.) promulgated a National Ambient Air Quality Standard (NAAQS) for PM<sub>2.5</sub> in 1997. Ambient concentrations below the NAAQS must be attained to protect public health. Many areas in the U.S. (and around the world) consistently have levels of PM<sub>2.5</sub> that exceed the NAAQS.

Regulations for PM are typically based on total mass; however, PM is comprised of numerous chemical components and is present as particles with diameters that range from 10<sup>-3</sup> to 10<sup>2</sup> microns. The fraction of urban PM smaller

than 2.5 microns typically contains the vast majority of individual particles, the majority of particle surface area, and a substantial fraction of total PM mass (this is possible since a smaller number of large particles contain proportionally more of the total mass) (Seinfeld and Pandis 1998). The research presented in this dissertation focuses on PM<sub>2.5</sub> since this is recognized as the fraction of PM that is of most concern to public health. More specifically, this research examines the organic carbon content of PM<sub>2.5</sub>.

Figure 1.1 shows a typical urban PM<sub>2.5</sub> composition. The figure also shows which components are emitted directly to the atmosphere (primary components) and which components are formed in the atmosphere through chemical reaction (secondary components). The principal components of PM<sub>2.5</sub> are secondary inorganic ions, primary material, and organic carbon (OC), which is both primary and secondary. Water is also a component of PM<sub>2.5</sub> and is determined by the relative humidity of the atmosphere. The processes and sources that lead to the formation of the inorganic components are relatively well understood. The processes and sources that lead to the formation of the organic components, however, are less well understood, primarily because there are thousands of organic species that can exist in PM<sub>2.5</sub>, many of which are difficult to identify and quantify.

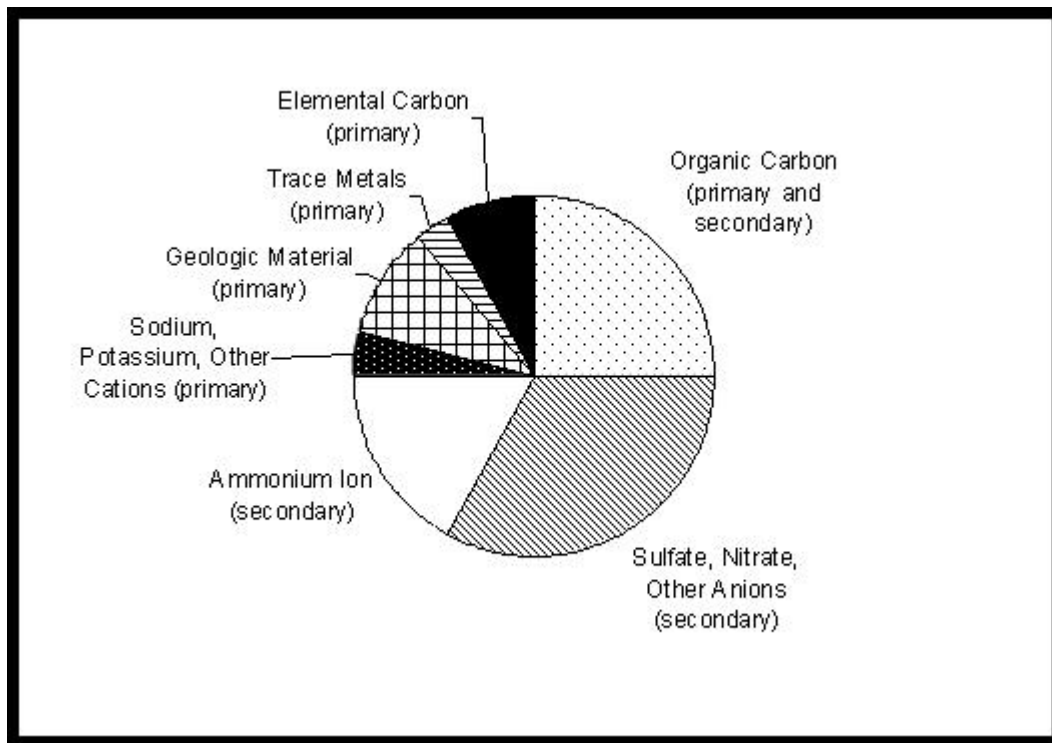


Figure 1.1. Typical urban dry mass composition of PM<sub>2.5</sub>. The majority of urban PM<sub>2.5</sub> mass may be secondary in origin.

Secondary organic matter in PM, also called secondary organic aerosol (SOA), is comprised of reaction products of the oxidation of volatile organic compounds (VOC). These products have low enough vapor pressures to partition either completely to the particle phase or exist in equilibrium between the gas and particle phase. There are numerous VOCs, both biogenic and anthropogenic, that can react to form SOA and SOA has been estimated to contribute up to 80% of the organic mass of PM<sub>2.5</sub> during short (2-6 hours) periods (Pandis et al. 1992; Turpin and Huntzicker 1995). The exact reaction pathways leading to SOA and the identity of the reaction products remain relatively unknown for all but a few

VOCs. However, empirical approximations of total SOA mass formed per mass reacted (also called the SOA yield) have been determined experimentally for a number of VOCs. This research will model the atmospheric processes that lead to SOA formation.

## **1.2 Urban aerosol and ozone formation**

Many of the reactions that lead to SOA formation play important roles in ground-level ozone formation, which itself is a secondary pollutant that results from the reaction of gas-phase pollutants. Ground-level ozone is also a criteria pollutant and it exceeds its NAAQS in many areas of the U.S. Urban areas that experience high ozone concentrations may also experience high SOA concentrations. Houston, Texas, has recorded some of the highest ozone concentrations in the U.S. In addition, high levels of OC have been found in  $PM_{2.5}$  in Houston as shown in Figure 1.2.

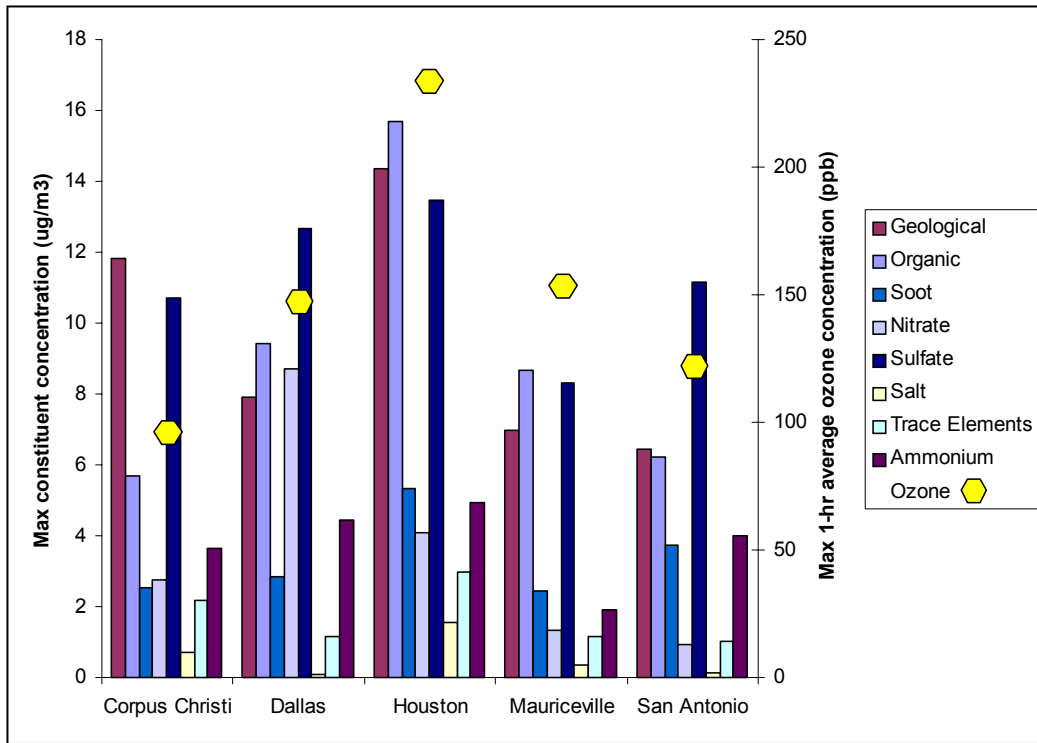


Figure 1.2 For various Texas cities, maximum concentrations of PM<sub>2.5</sub> components collected between 3/97 and 3/98 (Tropp et al. 1998). Also shown are the maximum recorded 1-hour average ozone concentrations in 1997 (USEPA 2002).

In the past ten years many advances have been made in understanding the sources of SOA and the processes that govern SOA formation. There are few examples, however, of analysis of spatial and temporal characteristics of SOA formation in polluted airsheds. As a result, the best approach to controlling SOA pollution is still relatively uncertain. The overall objective in this research was to develop a tool to test the sensitivity of SOA formation to parameters that govern its formation in an actual polluted airshed. The tool was applied, in this research,

to the urban and industrial areas of Southeast Texas (which includes Houston). This is a first step in developing a better understanding of this air pollutant.

### 1.3 Research Objectives

The identities of the majority of individual compounds that make up SOA remain unknown. Most of these compounds are difficult to identify and quantify, making it impossible to quantitatively determine the secondary organic composition of  $PM_{2.5}$ . There are, however, methods to estimate the fraction of *total* secondary organic carbon in  $PM_{2.5}$ . **The first objective of this research is to estimate spatial and seasonal trends in the secondary organic fraction of  $PM_{2.5}$  in Southeast Texas.** This objective is accomplished by developing an **empirical model** for SOA in Southeast Texas.

There are thousands of atmospheric reactions that contribute to the formation of particulate matter, and in particular SOA. Grid models make use of reduced chemical mechanisms that represent the actual reactions by a more practical reduced set of reactions. These mechanisms ‘lump’ together VOCs that react similarly. These mechanisms are usually hard-coded into grid model programs making it difficult to change them without extensively altering source code. Because SOA formation differs significantly from compound to compound, it is necessary to treat these compounds explicitly (i.e. un-lumped). **The second objective of this research is to include a model for SOA formation in an existing grid model for ozone, and to make the chemical mechanism a**

**flexible, user-controlled part of the model.** This model is referred to as the **physico-chemical model** for SOA formation.

SOA formation is dependent on many variables, and the sensitivity of SOA formation, spatially and temporally, to these variables remains relatively unknown. Furthermore, SOA and ozone may have a similar sensitivity to certain emissions reductions. **The final objective of this research is to use the physico-chemical model to test the sensitivity of SOA formation to many key parameters that determine SOA formation.** This objective is accomplished by implementing the **physico-chemical model** for SOA in a grid model and applying the model to Southeast Texas.

#### **1.4 Dissertation structure**

The literature review in the next chapter reviews the physical-chemical processes that lead to SOA formation and presents examples of computer and empirical models for SOA in the literature. Following the Literature Review, the methods and results for the SOA empirical model are presented in two separate chapters. The first chapter summarizes the data sources used to develop a conceptual model for  $PM_{2.5}$  and an empirical model for SOA in Southeast Texas; the second chapter presents the results. Following the data analysis chapters are a Methods and Results chapter presenting the physico-chemical model for SOA and the results of model simulations. Finally, a Conclusions chapter lists the major findings of this research and recommendations for further modeling of SOA.

## **2.0 Literature Review**

The development of a SOA model requires an understanding of the processes of SOA formation. Therefore, the first two sections of this chapter present an overview of this theory and a discussion of the current limitations and knowledge gaps for modeling SOA. Finally, the third section of this review discusses empirical models for estimating SOA concentrations from ambient data. A brief summary section concludes the chapter and highlights the important concepts that are presented in the Literature Review. The term aerosol is used often in this chapter to describe suspended material in the atmosphere. For purposes of this discussion it is synonymous with particulate matter.

### **2.1 Secondary Organic Aerosol Formation – Theory**

Formation of secondary organic aerosol is a result of two general processes: oxidation of a volatile organic compound gas (VOC) and partitioning of subsequent semi-volatile reaction products (SVOC for semi-volatile organic compound) into the aerosol phase. Once in the aerosol phase, SVOC species are considered secondary organic aerosol (SOA). In this chapter, VOC refers to a reactive organic gas whose reaction products can form SOA. SVOC refers to those reaction products that partition between the gas and aerosol phase.

Literally thousands of VOCs in the atmosphere may be oxidized; however, SVOC species tend to be produced by parent VOCs with six or more carbon atoms. More specifically, aromatics, terpenes and high molecular weight alkanes

and alkenes (with six or more carbon atoms) are the VOC groups suspected of forming the majority of SOA based on their emissions rates and the affinity of their reaction products to partition to the aerosol phase (Grosjean and Seinfeld 1989; Pandis et al. 1992). *Which* VOCs produce SOA is relatively well known simply by observations of total aerosol formation when individual VOCs are oxidized in smog chambers. *How* VOC's produce SOA is only beginning to become clear, and important knowledge gaps remain.

SOA formation is closely linked to ozone formation since SOA precursors are oxidized by radicals that drive the formation of ground-level ozone, and ozone itself. The primary oxidants leading to SOA are O<sub>3</sub>, and the OH and NO<sub>3</sub> radicals (the latter is important for oxidation of monoterpenes). Reaction pathways from VOC to SVOC remain relatively unknown for the majority of SOA precursors because SVOC products generally result from multi-step reactions and these products are difficult to identify and quantify. Nevertheless, a number of studies have identified certain individual compounds or compound groups that contribute to SOA. More recent studies have succeeded in reporting the identity and stoichiometric yields of the majority of SVOC products from a few important SOA precursors (Yu et al. 1999; Kalberer et al. 2000; Jaoui and Kamens 2001). In other studies, reaction mechanisms have been proposed for the formation of these species and these studies suggest that SVOC species tend to be later generation oxidation products of the parent VOC. For example, Kamens et al. (1999) proposed a 73-reaction model to account for total SOA formed from the reaction of  $\alpha$ -pinene in sunlight in the presence of NO<sub>x</sub>. Again it is important to note that

reaction pathways, SVOC identities and SVOC stoichiometric yields are known for very few VOCs. The detailed theory of individual VOC reaction pathways goes beyond the scope of this research and the theory to follow will concentrate mostly on the second process of SOA formation: partitioning of SVOCs between the gas and aerosol phases.

A common way of representing partitioning of any compound between gas and aerosol phase is by using the following partition coefficient (Yamasaki et al. 1982):

$$K_p = \frac{F/TSP}{A} \quad (2.1)$$

$K_p$  = gas - particle partitioning coefficient ( $\text{m}^3/\mu\text{g}$ )

$F$  = particle phase species concentration ( $\mu\text{g}/\text{m}^3$ )

$A$  = gas phase species concentration ( $\mu\text{g}/\text{m}^3$ )

$TSP$  = total suspended particle matter concentration ( $\mu\text{g}/\text{m}^3$ )

In all cases,  $\text{m}^3$  refers to volume of atmosphere.

A long-standing theory was that partitioning of organics into the aerosol phase occurred via physical adsorption (Junge 1977). In this case it was shown that  $K_p$  for an individual compound could be derived as (Pankow 1987):

$$K_p = \frac{RTN_s A_{TSP} e^{(Q_d - Q_v)/RT}}{P_L} \quad (2.2)$$

$N_s$  = moles of adsorption sites (mol/cm<sup>2</sup>)

$A_{TSP}$  = surface area of the TSP (cm<sup>2</sup>/μg)

T = temperature (K)

R = gas constant (= 8.314 J/mol K)

$P_L$  = is liquid vapor pressure of pure organic compound (Pa)

$Q_d$  = enthalpy of desorption (kJ/mol)

$Q_v$  = enthalpy of volatilization (kJ/mol)

It has also been suggested that partitioning may be occurring via absorption of organics into a pre-existing organic liquid phase on particulate matter. This absorptive partitioning is governed by gas/liquid equilibrium of a non-ideal organic solution (Raoult's Law in non-ideal solution):

$$P_i = \gamma_{OM} x_i P_L \quad (2.3)$$

$P_i$  = partial pressure of i in gas phase (atm)

$x_i$  = mole fraction of i in absorbing organic matter

$\gamma_{OM}$  = activity coefficient of the species in the absorbing organic matter

In this case, a  $K_p$  as defined in Equation 2.1 can be derived from Equation 2.3 as (Pankow 1994):

$$K_p = \frac{F_{OM} / TSP}{A} = \frac{RTf_{OM}}{10^6 M_{OM} \gamma_{OM} P_L} \quad (2.4)$$

$F_{OM}$  = aerosol organic phase species concentration ( $\text{ng}/\text{m}^3$ )

$f_{OM}$  = fraction of organic matter in the aerosol

$M_{OM}$  = mean molar mass of the organic matter ( $\text{g}/\text{mol}$ )

Observations of  $\log K_p$  vs.  $\log P_L$  for compound classes (e.g. PAH's) often show slopes close to  $-1$ , i.e.

$$\log K_p = -\log P_L + b \quad (\text{for a compound class}) \quad (2.5)$$

This relationship has been used to suggest the validity of both Equations 2.2 and 2.4, thus both adsorption and absorption (Pankow 1994). This relationship also implies that many of the other variables in Equations 2.2 and 2.4 are relatively constant within compound classes, which is likely over typical ranges of  $P_L$ , i.e. up to five orders of magnitude (Cousins and Mackay 2001). These observations are however based on VOCs from primary emissions. It is difficult to determine these relationships for SVOC reaction products since the identities of these reaction products are difficult to determine, and their physical properties make them difficult to quantify. Nevertheless, certain studies have succeeded in inferring partitioning characteristics of SVOC in SOA and have suggested that absorption (i.e. Equations 2.3 and 2.4) better characterizes this partitioning (Jang et al. 1997; Liang et al. 1997; Jang and Kamens 1998).

It should be noted that in the case of a single SVOC formed in aerosol-free air there is a threshold gas concentration below which no SOA will form because there is no absorbing phase present and the reaction product has not reached its vapor pressure in the gas phase. In absence of an existing absorbing phase, SOA may initially form via nucleation or adsorption to existing non-organic material (Seinfeld and Pandis 1998). Although this lower threshold must be taken into account, the presence of absorbing material is highly likely in most urban or polluted atmospheres such that reaction products will quickly partition to the aerosol phase when formed. Absorption theory is widely accepted as the partitioning process for SOA in most modern research.

## **2.2 Secondary Organic Aerosol Formation – Modeling**

This section describes methods for modeling SOA formation. A ‘model’ refers here to the mathematical representation of SOA formation according to theory discussed in the previous section. The models in this section should not be confused with grid models, which are discussed later.

Ideally, a model of SOA formation would explicitly account for the formation mechanisms of individual SVOCs and then partition these into the aerosol based on  $K_p$  values calculated using equations of the form Equations 2.2 and/or 2.4. However, for many of the VOCs that react to produce SVOCs, detailed reaction pathways and individual reaction products are still unknown. As a result, SOA formation was originally estimated as fixed fractions of VOC

emissions. These fractions, called fractional aerosol coefficients (FAC), were unique to each VOC (Grosjean and Seinfeld 1989).

An improvement on FACs were empirical yield coefficients which were also unique to each VOC (e.g. Hatakeyama et al. 1989; Izumi and Fukuyama 1990; Pandis et al. 1991; Zhang et al. 1992). Yield coefficients (Y) are defined as:

$$Y = \frac{\Delta M_o}{\Delta HC} \quad (2.6)$$

$\Delta HC$  = the amount of hydrocarbon reacted ( $\mu\text{g}/\text{m}^3$ )

$\Delta M_o$  = the organic aerosol mass produced ( $\mu\text{g}/\text{m}^3$ )

Both the numerator and denominator in Equation 2.6 are functions of many variables, yet Y values found from smog chamber experiments were originally approximated as constant. Although crude, constant yields predict SOA formation as a function of the *reacted* VOC as opposed to FAC's that predict SOA as a function of *available* (total emitted) VOC. In reality, many parent VOCs will produce more than one SVOC, which themselves may undergo oxidation to produce additional condensable species.

From absorption partitioning theory, Odum et al. (1996) showed that if a parent hydrocarbon reacted to produce multiple SVOC products ( $i=1,2,..n$ ), the yield for compound i, ( $Y_i$ ), will take the form:

$$Y_i = M_o \left( \frac{\alpha_i K_{om,i}}{1 + K_{om,i} M_o} \right) \quad (2.7)$$

$M_o$  = total absorbing organic aerosol mass ( $\mu\text{g}/\text{m}^3$ )

$\alpha_i$  = the stoichiometric coefficient of the reaction product  $i$  (mass/mass)

$K_{om,i}$  = the partitioning coefficient of  $i$  to the organic phase,

i.e. defined as  $K_{om} = \frac{F_{OM} / M_o}{A}$

More importantly, the total aerosol yield will be the sum of  $Y_i$  over all  $i$ :

$$Y = \sum_i Y_i = M_o \sum_i \left( \frac{\alpha_i K_{om,i}}{1 + K_{om,i} M_o} \right) \quad (2.8)$$

This relationship (Equation 2.8) is a major improvement over constant yields since it accounts for yield of SVOC products ( $\alpha$ ) and for pseudo-ideal solution theory that governs the partitioning (i.e. yield is dependent on total absorbing mass  $M_o$ ). For most VOCs, SVOC reaction products are not known; therefore,  $\alpha_i$  and  $K_{om,i}$  values cannot be explicitly calculated. However Equation 2.8 has been fit to smog chamber data (measured  $Y$  and  $M_o$ ) using the assumption that there are two (hypothetical) first-generation reaction products that form SOA, i.e. using four fitting parameters:  $\alpha_1$ ,  $\alpha_2$ ,  $K_{om,1}$  and  $K_{om,2}$ . These four parameters are available for many VOCs that are known to produce SOA when oxidized (Odum et al. 1996; Hoffmann et al. 1997; Odum et al. 1997b; Griffin et al. 1999;

Yu et al. 1999; Kalberer et al. 2000). Some research suggests that the same four parameters can describe the SOA yield of similar compounds, such as groups of aromatics (Odum et al. 1997b). In addition, these partitioning parameters can vary (and are often reported separately) depending on the oxidant reacting with the parent VOC (Hoffmann et al. 1997; Griffin et al. 1999). This method is however limited by the fact that  $\alpha_1$ ,  $\alpha_2$ ,  $K_{om,1}$  and  $K_{om,2}$  are fitting parameters and are approximations of the average stoichiometric yields and partitioning coefficients of numerous SVOC species.

Recently, a number of researchers have been able to predict the identity and stoichiometric yields of the majority (by mass) of the reaction products of a few SOA precursors (Yu et al. 1999; Kalberer et al. 2000; Jaoui and Kamens 2001). Pankow et al. (2001) were able to accurately model the overall yield of SOA from some of these compounds as the sum of the individual yields according to Equation 2.8. These researchers used various methods to calculate activity coefficients for a mixture of the reaction products in the aerosol phase and thus an *actual*  $K_p$  for each compound. Kamens et al. (1999) were also able to predict SOA formation reasonably well from  $\alpha$ -pinene knowing the majority of reaction pathways and reaction product identities and using partitioning theory based on Equation 2.4. These two studies modeled SOA formation in smog chambers based on actual compounds (as opposed to hypothetical compounds) and the studies lend support to absorption partitioning theory, Equations 2.3 and 2.4, and to the use of Equation 2.8 to model SOA formation. However, this ‘bottom-up’

approach is still not practical for modeling total SOA because reaction product data are still limited to a handful of compounds.

Empirical estimates of overall SOA yield, for example the ‘4-parameter’ data, are available for a number of VOCs but the major limitation to these data is that  $\alpha$  and  $K_p$  values are fitting parameters. In actuality  $\alpha$  and  $K_p$  for a single SVOC will depend on many environmental variables. The stoichiometric yields (as defined by Odum et al (1996)) of reaction products depend on the availability of oxidants in the individual reactions of parent and intermediate VOC’s. Partitioning coefficients depend on the temperature (both directly and indirectly through  $P_L$ ) and composition of the absorbing medium (through  $\gamma$ ). An important question is how sensitive empirical  $\alpha$  and  $K_p$  values are to these environmental variables. A number of experimental and modeling studies have been conducted to address this question and some important points are discussed below.

Bowman et al. (1997) suggest that a hypothetical  $\alpha$ , the average stoichiometric yield of SVOC reaction products, is relatively insensitive to whether the SVOCs are first or second generation reaction products. However other research has shown evidence to the contrary for certain aromatics;  $\alpha$  depends on the availability of other reacting compounds, especially when precursor concentrations are high (Dechapanya et al. 2003a). Until reaction mechanisms are better characterized for more SOA precursors, using empirical  $\alpha$  values will remain an important limitation to predicting SOA.

The composition of the absorbing phase affects  $K_p$  via the activity coefficient of the compound and the mean molecular weight of the absorbing

mass. Empirical  $K_p$  are estimated from data in smog chambers, generally with no pre-existing organic aerosol and low relative humidity; thus, partitioning mainly occurs to a mixture of SVOC products. Some studies have shown that water may be mixed with organic material in the absorbing phase and thus directly affect the partitioning of organic compounds (Saxena et al. 1995; Edney et al. 2000; Cocker et al. 2001a; Cocker et al. 2001b). Seinfeld et al. (2001) used a detailed SOA formation model to suggest that aerosol water increases the partitioning of SVOC's to the aerosol mainly via decreasing the mean MW of the absorbing mixture and to a lesser extent through changes in activity coefficient. Bowman and Karamalegos (2002) suggest that different mixes of SVOC products may be significant to the empirical  $K_p$  (and thus SOA predictions) and this effect is enhanced by aerosol water. Other researchers have also found different partitioning behavior in different aerosol types with different organic compositions (Jang et al. 1997; Jang and Kamens 1998). While it is clear that  $K_p$  values will change as aerosol composition changes, it is unclear how to account for this change using empirical  $K_p$  values.

Temperature is another important factor in the partitioning of SVOC species both directly and indirectly via the vapor pressure. A number of researchers have investigated how temperature affects both empirical and compound specific  $K_p$  values (Kamens et al. 1999; Strader et al. 1999; Sheehan and Bowman 2001). In each case, the authors found that the effect of temperature is most significant via the vapor pressure, and used a known empirical method to calculate  $P_L$  as a function of T. Strader et al. (1999) found that modeled SOA

formation may be enhanced in cooler winter months as a result of lower temperatures and favorable aerosol formation. Sheehan and Bowman (2001) found that modeled SOA could increase by 20-150% per 10°C temperature decrease using empirical  $K_p$  values. Clearly, temperature will determine the extent of SOA formation and should be accounted for when modeling SOA formation.

The formation of SOA is ideally modeled separately for each partitioning SVOC species. However, the formation and physical properties of *all* partitioning species must be known to accurately predict the partitioning of individual species, since this process is dependent on the composition of the organic aerosol. At present, these data are available only for reaction products of a few SOA compounds. Empirical estimates of SOA yields are available for a larger number of SOA precursors; however, these estimates are limited in that they are representative of the environmental conditions of controlled experiments. Nevertheless, empirical methods are, for now, the best option to predict total SOA.

### **2.3 SOA mechanisms in photochemical grid models.**

Three-dimensional photochemical grid models (or grid models) that account for emissions, transport, chemical reaction and removal of gas phase pollutants provide an excellent framework for modeling SOA. These models have several limitations; however, they represent the state of the science in modeling photochemical processes in urban and regional areas, and are widely used by

government agencies to set policy to control ground-level ozone. A critical review of these models is given by Russell and Dennis (2000).

Grid models are formulated to strike a balance between computational efficiency and representation of complex atmospheric processes. The two main processes that lead to SOA formation are chemical reaction of VOC's and partitioning of reaction products, so an important consideration is how grid models represent VOC's. This representation is dependent on the chemical mechanism, which represents the chemistry of thousands of gas species by a reduced set of representative or surrogate model species. Surrogate model species can represent individual compounds or compound groups, for example in the mechanism of the Statewide Air Pollution Research and Control center (SAPRC/SAPRC97/SAPRC99) (Carter 1990, 1995), in the Regional Acid Deposition Mechanism (RADM/RADM2)(Stockwell et al. 1990), and in the Regional Atmospheric Chemistry Model (RACM) (Stockwell et al. 1997). Surrogate model species can also represent reactive elements such as bond types, for example, in the Carbon Bond IV mechanism (CB-IV) (Gery et al. 1989). The latter is used widely in regulatory models because of its computational efficiency. As explained in previous sections, SOA formation is unique for individual VOCs and depends on the physical properties of individual reaction products. Therefore, a challenge for modeling SOA in grid models is to use mechanisms with surrogate species, yet be able to accurately represent SOA formation of individual compounds.

Grid models have the potential to provide valuable insight into the sources of SOA as well as the spatial and temporal distribution of SOA formation. Since SOA modeling is a relatively new area of research, there are a limited number of SOA grid models, and each has a unique way of representing both the chemistry and partitioning functions. The rest of this section summarizes some important studies where SOA formation has been included into grid models.

There are two general approaches to modeling SOA in a grid model: explicitly and implicitly. In an explicit model for SOA, the chemical mechanism predicts the formation of SVOC species based on appropriate reaction rates and reactant concentrations. The SVOC that is formed is partitioned between gas and aerosol phase according to pseudo-ideal solution theory, i.e. the gas and aerosol concentrations of species  $i$  depend on the mole fraction of  $i$ , which in turn depends on total amount of SVOC species from all VOCs. This results in a non-linear set of  $n$  equations with  $n$  unknowns that must be solved iteratively. The gas/particle partitioning is also a function of temperature, vapor pressure and activity coefficients of the compound in the absorbing mixture. In an implicit model for SOA, SOA formation is usually calculated from yield coefficients where total SOA formation is a function of reacted VOC. Yield coefficients are based on smog chamber data, and as discussed in the previous section, they can be formulated to account for pseudo-ideal solution theory and temperature effects.

First attempts to include SOA in grid models were implicit and made use of fractional aerosol coefficients or constant yields (e.g. Pilinis and Seinfeld 1988; Pandis et al. 1992; Lurmann et al. 1997). Since the understanding of SOA

formation has improved, constant yield predictions are considered outdated; nevertheless, these early predictions provided insight into the major characteristics of SOA formation. Notably, Pandis et al. (1992) included SOA formation in a grid model that was applied to the Los Angeles basin. These researchers used an early version of SAPRC as the chemical mechanism. Their results were significant in that they predicted both anthropogenic and biogenic precursors were important in forming SOA in the Los Angeles basin.

Strader et al. (1999) improved upon the method of Pandis by modeling SOA formation explicitly using two hypothetical first generation SVOC products from each of 21 VOCs. The chemical mechanism was based on SAPRC97 with additional reactions and SVOC species, and the model was applied to the San Joaquin valley in California. The authors used empirical  $\alpha$  values to determine the relative SOA contributions of each hypothetical SVOC. In addition, this modeling was the first to explicitly account for pseudo-ideal solution and the effects of temperature on SOA formation (although no effect of aerosol water was considered). The 'solution' of organic matter was assumed to be entirely composed of secondary organics, and no primary absorbing material (organic or otherwise) is accounted for. One significant finding was that SOA concentrations were strongly dependent on temperature, and there was an optimal temperature for SOA formation.

An almost identical approach was taken by Schell et al. (2001) to model SOA formation in Central Europe. The authors used 7 species to produce 8 first generation SVOC products in a mechanism based on a European version of

RADM2. SOA is solved explicitly, and pseudo-ideal solution and temperature effects are accounted for; however, primary absorbing material and activity coefficient changes are neglected. One interesting feature is that biogenic precursors are oxidized by O<sub>3</sub> and the OH and NO<sub>3</sub> radicals, and aerosol formation differs depending on the oxidant. The authors found that both biogenic and anthropogenic compounds are significant in producing SOA in this area.

A series of three recent articles describe the development of a detailed model for SOA, including chemical mechanism development (Griffin et al. 2002b), partitioning of SVOC species (Pun et al. 2002a), and application of the model to the Southern California area (Griffin et al. 2002a). The chemical mechanism is based upon SAPRC97/99, RACM and a master chemical mechanism as described by (Jenkin et al. 1997). The mechanism predicts 42 condensable species that are both first and later generation reaction products. These 42 surrogate species have ‘average’ structural and reaction properties. However, because of computational limitations, the 42 species are further grouped into five hydrophilic and five hydrophobic condensable products. A unique feature of this particular model is that it not only explicitly models SOA formation in a solution of both primary and secondary organic compounds, but also models uptake of water soluble organics and accounts for this effect on liquid water content of the aerosol. Although, the formulation of the model is relatively advanced and incorporates much of the theory on partitioning of organic compounds, there are still several assumptions made about the identity of the condensable reaction products and their physical properties. This model was

applied to Southern California (Griffin et al. 2002a). The authors found that SOA from anthropogenic sources dominated aerosol in the urban area, and that biogenic precursors contributed more in the rural areas than urban areas. The SOA was dominated by hydrophobic SVOC's from both biogenic and anthropogenic precursors.

The studies referenced in the preceding paragraphs are presented because their objective is similar to this research: to comprehensively model both biogenic and anthropogenic SOA formation in an airshed. There are a number of other examples of SOA models: in grid models, e.g. (Meng et al. 1998; Pun et al. 2002b), in box models, e.g. (Barthelmie and Pryor 1999; Kamens and Jaoui 2001), and in Lagrangian trajectory models (Andersson-Skold and Simpson 2001). It should be noted that the discussion has neglected particle size distribution. A number of the studies referenced above model inorganic and primary aerosols in addition to SOA, and some resolve the particulate matter into size ranges. Modeling the size distribution of SOA is challenging given the lack of data on the subject. This research does not consider size distributions.

There are three important considerations for modeling SOA. First, the chemical mechanism determines how accurately one can predict the formation of SVOC reaction products, in terms of identity and reaction pathways. The chemical mechanism is typically the most computationally expensive part of the modeling process, and the more SVOC products formed, the more computation

time will be necessary. SOA models ideally require a mechanism that can represent individual chemical compounds.

The second important factor is whether or not to model SOA formation explicitly or implicitly. Most models choose to model the formation explicitly which accurately accounts for the gas/particle partitioning of the condensable species. However, an explicit solution is also very computationally expensive because a non-linear set of equations needs to be solved numerically. A major limitation to explicit solutions is that primary OC emission inventories are almost non-existent; therefore, this component must be ignored as an absorbing phase, and gas/particle partitioning occurs to a solution of strictly secondary compounds. In addition, partitioning depends on the vapor pressure of the specific SVOC compound, and the vapor pressures of most of these compounds remain unknown. These limitations may not warrant the accuracy gained by explicitly solving the gas/particle partitioning. Although implicit yields are highly simplified, it is unclear how much less accurate they are than explicit solutions with hypothetical condensable products.

The third important factor is consideration of environmental variables on SVOC partitioning. Temperature has been shown to have a large impact on SOA formation and is typically factored into any SOA formation mechanism. Both implicit and explicit solutions can be made to correct for temperature; however, this correction is again based on assumed vapor pressures for the hypothetical SVOC species. The interaction of the SVOCs in the aerosol phase with other aerosol components is probably the least understood process in SOA formation.

This requires detail on the identity of all/many organic compounds in the aerosol phase and this simply does not exist. The activity coefficient for the SVOC in the absorbing medium is almost always assumed to be unity.

#### **2.4 Secondary Organic Aerosol Formation – Analysis of Ambient Data**

Organic carbon in aerosols can be primary, emitted directly into the atmosphere, and secondary, formed in the atmosphere via chemical reaction. It has proved difficult to directly measure the relative amounts of primary versus secondary organic carbon, because there are hundreds of individual organic compounds in an urban aerosol, some primary and some secondary, many of which are difficult to identify and quantify using current technologies. A thorough review of this subject is given by Turpin et al. (2000). Secondary organic carbon in PM can, however, can be estimated indirectly from other measured PM characteristics.

Typically, ambient concentrations of *total* organic carbon (OC) and elemental carbon (EC) are measured using filter-based sampling over a 2- to 24-hour period. There are a number of different thermal methods to analyze for EC and OC, but generally a single sample is heated in absence of oxygen to volatilize a fraction of the organic compounds (OC), and then heated at a higher temperature in the presence of oxygen to combust the remaining organic compounds (EC). The split between OC and EC depends on the heating/combustion methods and is thus operationally defined. Some modern non-

filter based instruments have the ability to measure total OC in near real-time, however these instruments are not widely used.

One successful indirect way of estimating SOA is to compare relative amounts of OC and EC. SOA is the mass of secondary organic carbon plus the non-carbon mass associated with these compounds. OC can be primary and secondary, but EC is considered to be entirely primary, and can be used as a tracer for primary emissions. When relative amounts of OC to EC are high, for example as indicated by the ratio of OC to EC, this is an indicator of high fractions of SOA. This method is also referred to as the EC tracer method and is one of the only ways to estimate total SOA from ambient measurements. The following paragraphs discuss the application of the EC tracer method. This method was pioneered by Turpin and Huntzicker (1991, 1995).

There is almost always primary OC associated with EC, which is emitted due to combustion of carbon compounds. OC can also be emitted without EC, for example, emissions of plant waxes from biogenic sources. To distinguish these two types of primary OC, OC emitted with EC will be referred to as  $OC_1$  and OC emitted without EC will be referred to as  $OC_2$ . It is normally considered that an emission source will have a characteristic  $OC_1/EC$  ratio. Therefore, at a given location, over time, average  $OC_1/EC$  and  $OC_2$  in the ambient air will be relatively constant. This average ambient  $OC_1/EC$  and  $OC_2$  reflect the contribution from all emission sources that influence this location. If  $OC_1/EC$  and  $OC_2$  are known or can be estimated, and OC (total) and EC are measured, secondary organic carbon can be estimated as:

$$OC_{\text{secondary}} = OC_{\text{total}} - OC_{\text{primary}} = OC_{\text{total}} - (OC_1 + OC_2) \quad (2.9)$$

Estimating primary OC for a given area is not trivial. The inherent assumption that  $OC_1/EC$  and  $OC_2$  are constant over space and time is probably not accurate. The spatial distribution of  $OC_1/EC$  and  $OC_2$  depend on the distribution of emission sources in a given area and it has been shown that  $OC_1/EC$  can differ considerably between emissions sources (Gray et al. 1986). In addition, the relative amounts of primary OC and EC and can vary throughout the day (Turpin and Huntzicker 1995). There are two approaches to estimating primary OC, 1) estimate primary carbon emissions directly from emissions inventories, and 2) estimate primary carbon emissions indirectly from statistical analysis of ambient OC and EC concentrations.

The first approach, emission inventory development, requires detailed knowledge of aerosol emission rates and composition from all aerosol sources for a given area. Most detailed emissions inventories currently available focus on gas phase ozone precursors, not aerosol species. Compilation of emissions inventories is an enormous undertaking. This approach was used to estimate an average  $OC_1/EC$  for the Los Angeles Basin of 2.2 (Gray et al., 1986). Aside from this example, direct estimation of  $OC_1/EC$  and  $OC_2$  from emissions inventories is uncommon.

The second approach, statistical analysis of ambient OC and EC, has been used successfully in several studies to predict SOA concentrations (Turpin and

Huntzicker 1991, 1995; Castro et al. 1999; Strader et al. 1999; Lim and Turpin 2002). The basis of this method is to choose a subset of OC and EC measurements when no secondary OC carbon is expected. These measurements are used to develop an expression for primary OC as a function of EC, which is then used to predict primary OC on any day. Secondary organic carbon is then calculated according to Equation 2.9. The subset of primary OC and EC measurements is chosen based on one or more of the following conditions (Turpin and Huntzicker 1991, 1995):

- Select measurement periods with little to no photochemical activity.
- Select measurement periods when accumulation of primary emissions may be occurring, as indicated by high levels of EC and light winds. Minimum OC and EC on these days may represent average primary emissions.
- Observe correlations of OC to EC over certain periods. When these correlate well this may indicate that both the OC and EC component are primary. However, at locations that experience pollutant transport, there may be a consistent fraction of SOA in the aerosol and OC and EC would still correlate well.
- Recognize that  $OC_1/EC$  and  $OC_2$  will vary from location to location and should be estimated separately for each measurement location.

Using a subset of measurements that are assumed to be strictly primary, an expression for primary OC can be developed, for example, by linear regression of OC and EC:

$$(\text{OC})_{\text{primary}} = a \cdot \text{EC} + b \quad (2.10)$$

This empirical model accounts for both types of primary OC discussed earlier, i.e.,  $\text{OC}_1 (= a \cdot \text{EC})$  and  $\text{OC}_2 (= b)$ . SOA is estimated from secondary organic carbon concentrations accounting for non-carbon mass associated with the OC. In similar studies, SOA has been assumed to be 1.2-1.4 times the secondary organic carbon concentrations; however, recent evidence suggests that this factor may be as high as 2.1 and that it may vary with location, depending on the age of the particulate matter (Turpin and Lim 2001).

The EC tracer method has been used to gain valuable insight into spatial and temporal variations in SOA concentrations. Turpin and Huntzicker (1995) found up to 80% of 2-hour averaged OC samples in summer in Los Angeles could be secondary. In addition, they found that maximum SOA concentrations occurred in late afternoon to early evening, 1-2 hours later than maximum ozone concentrations, and that highest SOA was at downwind non-urban locations. Similarly, Strader et al. (1999) found highest 3-hour averaged SOA to occur in late afternoon and early evening in the San Joaquin Valley, in wintertime. These authors suggested that relatively high wintertime SOA formation was favored by lower temperatures. More recently, Lim and Turpin (2002) found that 1-hour

averaged SOA could be as high as 88% of OC in Atlanta in late summer. These authors found that SOA peaked either in late afternoon from ‘fresh’ SOA formation or at night/early morning from transported SOA precursors that favorably formed aerosol during lower nighttime temperatures and higher relative humidity. In all three studies, the researchers found that SOA was a significant fraction of OC only during short periods (1-4 hours), and primary OC was the dominant component of OC over a 24-hour period. The studies do however provide evidence that SOA formation is linked to ozone formation given that diurnal patterns of both pollutants are similar. The studies also show that SOA formation may be strongly dependent on environmental conditions, most importantly ambient temperature.

The EC tracer method is one of the only ways to estimate total SOA concentrations from ambient data. The greatest limitation of the method is that there is no information about the individual compounds that make up the organic carbon. This in turn prevents associating the SOA with particular sources. There are a number of other ways to detect the presence of SOA in PM, most of which involve assessing the physical properties of the aerosol. These include measuring the aerosol size distribution over time, measuring for specific single compounds or functional groups that are associated with SOA, and measuring the  $^{14}\text{C}/^{13}\text{C}$  ratio to determine geologically modern carbon (which could come from biogenic SOA). These methods may provide additional insight into the sources of SOA; however, they cannot be used to determine total SOA concentrations.

## 2.5 Summary

Secondary organic aerosol is comprised of thousands of individual organic compounds, many of which are difficult to identify and quantify, and this is currently the biggest limitation to measuring and modeling SOA. The limited research available has supported the theory that SOA is formed by oxidation of gas-phase organic compounds and subsequent absorption/adsorption of the reaction products to existing particulate matter. However, a comprehensive model for SOA requires knowledge of thousands of complex reaction pathways and knowledge of thousands of components in particulate matter and these data do not exist, nor is this approach practical.

The formation of SOA has been approximated with empirical relationships between the amount of VOC reacted and the amount of total SOA formed. These relationships are known for many VOC's that are thought to be the greatest contributors to SOA and have been the basis for SOA prediction in photochemical grid models. These models have provided valuable insight into the formation potential of certain VOC's and thus certain emissions sources. Although empirical yields are less than ideal, they can be formulated to take into account some of the factors that govern gas/particle partitioning.

There are indirect ways to measure ambient SOA concentrations using organic carbon (OC) and elemental carbon (EC), and these methods are the sole methods for estimating the total contribution of SOA to PM concentrations. However, these methods are limited in that they provide no information on

individual SOA compounds which could be used to link SOA to certain emissions sources.

The following Methods chapter describes the methodology used to examine PM in Southeast Texas and to formulate an empirical model to predict SOA concentrations.

### **3.0 Methods – Part 1: Conceptual Model for attributing PM<sub>2.5</sub> sources and Empirical model for SOA in Southeast Texas**

Southeast Texas experiences some of the worst ozone pollution in the U.S., and PM<sub>2.5</sub> is likely also a pollutant of concern. To date, however, there is limited analysis of PM<sub>2.5</sub> concentrations in this area to support this hypothesis. As a prelude to analyzing SOA in Southeast Texas, a conceptual model for attributing PM<sub>2.5</sub> sources was developed by analyzing PM<sub>2.5</sub> mass and composition characteristics. The conceptual model puts the current research objectives in perspective by characterizing the PM<sub>2.5</sub> pollution problem and quantifying the contribution of OC to PM<sub>2.5</sub>. The data used both in the conceptual model and in the SOA empirical model were from the same sources, and the first section of this chapter describes how these data were collected. The second section describes the development of the SOA empirical model. Conceptual model results are presented in the first section of the Results chapter; SOA empirical model results are presented in the second section of the Results chapter. It should be noted that PM<sub>2.5</sub> and ‘fine particulate matter’ are used interchangeably throughout the rest of this thesis.

#### **3.1 Fine particulate matter data in Southeast Texas.**

The first study of regional fine PM in Texas (Tropp et al. 1998) suggested that two major urban and industrial areas in Southeast Texas, the Houston-Galveston area and the Beaumont-Port Arthur area, are close to exceeding the

new National Ambient Air Quality Standard (NAAQS) for PM<sub>2.5</sub> or particulate matter less than 2.5 μm in aerodynamic diameter. Sites in the industrial area of Houston, known as the Houston Ship channel, measured annual average PM<sub>2.5</sub> mass that exceeded the annual average standard of 15 μg/m<sup>3</sup>. In addition, annual average mass concentrations at several other sites in Southeast Texas exceeded 10 μg/m<sup>3</sup>. The major components of PM<sub>2.5</sub> in Southeast Texas are organic carbon and sulfate, which each comprise 20 - 30% on average of the fine particulate matter mass at Southeast Texas sites. A preliminary analysis of the data collected in 1997 and 1998 suggested that local sources could at times influence PM<sub>2.5</sub> in Houston; however, there was a relatively high background concentration of PM<sub>2.5</sub> mass and a significant contribution from regional sources such as large-scale dust and smoke events (Walk et al. 1999).

Much more extensive measurements of PM<sub>2.5</sub> mass, size and composition were made beginning in 2000. In August and September 2000, a major fine particulate matter field study began: the Gulf Coast Aerosol Research and Characterization Study (GC-ARCH). GC-ARCH is one of EPA's Supersites for fine particulate matter and produced fine particulate matter data with greater spatial and temporal resolution than had previously been available. As part of this program, the Texas Commission on Environmental Quality (TCEQ) collected data on Federal Reference Method (FRM) 24-hour averaged PM<sub>2.5</sub> mass concentrations, PM<sub>2.5</sub> composition, and near continuous PM<sub>2.5</sub> mass concentration data with Tapered Element Oscillating Microbalance (TEOM) samplers. These routine data are reported to EPA and are available in the Aerometric Information

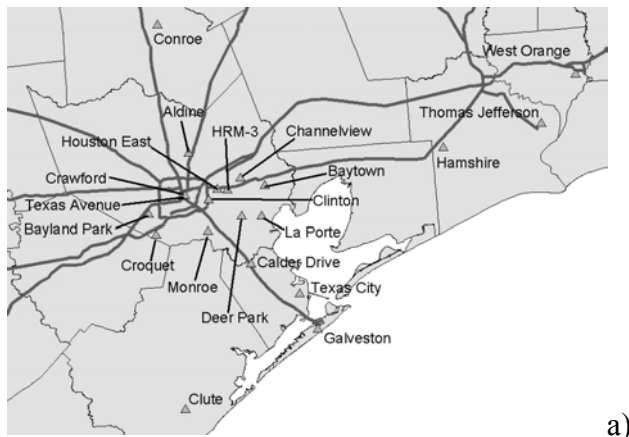
Retrieval System (AIRS) database (USEPA 2002). The conceptual model for  $PM_{2.5}$  presented in this research is the first analysis of much of this routine  $PM_{2.5}$  data collected during GC-ARCH.

The majority of FRM monitoring sites in Southeast Texas only measure total  $PM_{2.5}$  mass using Partisol®-Plus Model 2025  $PM_{2.5}$  Sequential Samplers (Rupprecht & Patashnick Co. Inc.). Air samples are drawn through an inlet that removes particles with aerodynamic diameters greater than 2.5  $\mu m$ , and the remaining particles are passed through a filter. Samples are collected over a 24-hour period. Total mass is determined gravimetrically from polytetrafluoroethylene (PTFE or Teflon) filters. A subset of FRM monitoring sites also measure  $PM_{2.5}$  speciation using the same samplers. In this case,  $PM_{2.5}$  particles are passed in parallel through PTFE and quartz fiber filters. Total mass is determined gravimetrically from the PTFE filters. The PTFE filters are also used to quantify mass of chemical elements using Energy Dispersive X-Ray Fluorescence (XRF) and soluble ions using ion chromatography. The quartz fiber filters are used to quantify total, organic, elemental and carbonate carbon determined by thermal optical transmittance (TOT) and instrumentation specified by the NIOSH method 5040 (Birch and Cary 1996; NIOSH 1996, 1998). Concurrent measurements of flow rate through the sampler and ambient temperature, relative humidity and barometric pressure during the collection are used to determine the mass concentration (or component mass concentration) over the sampling period.

One exception to this methodology is at the Deer Park 2 monitoring site. In addition to the Partisol®-Plus Model 2025 PM<sub>2.5</sub> Sequential Sampler, this site uses URG-MASS 400 and URG 450 samplers for total PM<sub>2.5</sub> mass and speciation sampling respectively. Total mass and elemental analyses are determined from PTFE filters. Organic, elemental and carbonate carbon are determined from quartz fiber filters. However, the determination of soluble ion concentrations is from a nylon filter as opposed to a PTFE filter. Because the OC and EC measurements were made on quartz filters and according to the same protocol, Deer Park OC and EC is assumed to be comparable to OC and EC at other sites. Sampler operation and sample collection is performed by the TCEQ for both types of samplers; chemical analysis is performed by Research Triangle Institute (RTI) for both types of samplers.

The TEOM sampler (Rupprecht and Patashnick Co.) is an EPA-accepted method for determining total PM<sub>2.5</sub> mass concentration over sampling periods as short as 5 minutes. In this work, hourly averaged PM<sub>2.5</sub> mass are reported. TEOM data collection was performed by the TCEQ.

The monitoring network for FRM mass is shown in Figure 3.1a. Subsets of these monitoring sites measure TEOM mass (Figure 3.1b) and FRM speciation (Figure 3.1c).



a)



b)



c)

Figure 3.1 a) FRM mass sampling network in SE Texas, b) TEOM sampling network in SE Texas, and c) FRM speciation network in SE Texas

To complement the PM<sub>2.5</sub> data, hourly ozone and NO<sub>x</sub> concentrations and meteorological data (temperature, solar radiation, resultant wind speed and direction) were obtained from EPA's AIRS database (USEPA 2002) or directly from the TCEQ. Daily total rainfall data at the Deer Park monitoring site was obtained from the National Climatic Data Center website (NOAA 2003b). This additional environmental data was obtained only for the FRM speciation sites (Figure 3.1c).

There are a number of concerns regarding how accurate and representative the FRM measurements are. Among the greatest concerns are negative sampling artifacts, particularly for ammonium nitrate, and positive artifacts, particularly due to semi-volatile hydrocarbons and water adsorbing onto filters. The potential for positive and negative artifacts raises some questions about whether the FRM accurately characterizes PM<sub>2.5</sub> present in the atmosphere. Of most concern to this research are sampling artifacts for OC and EC.

It is widely accepted that quartz filters used to collect PM<sub>2.5</sub> adsorb organic vapors that contribute to measured particulate OC concentrations. The positive artifact introduced by this sorption can vary considerably depending on OC loading, sampling time and ambient conditions of the sampled air (see Turpin et al. 2000). In addition, the equilibrium between semi-volatile species in the gas and particle phase may change during sampling, for example, due to the pressure drop across the filter or changes in the composition of incoming air. This can result in a negative artifact as organic matter evaporates from the collected particles. It is difficult to estimate the net effect of these two (and perhaps other)

important sampling artifacts, and in this work it is assumed that they do not invalidate our conclusions. However, in interpreting absolute OC concentrations, the possibility of sampling artifacts should be considered.

It is also worth mentioning that concentrations of EC are dependent on the specific thermal-optical analysis method used. The method used to analyze these samples (Birch and Cary 1996; NIOSH 1996, 1998) differs from another common protocol (Chow et al. 1993) used widely over the past decade to analyze for OC and EC. Although both protocols predict similar total carbon concentrations, the former method predicts more OC and less EC than the latter from the same sample (Chow et al. 2001). As a result, caution must be taken when comparing OC and EC concentrations (and estimated primary and secondary OC) or OC/EC ratios between this analysis and that in other studies.

The TEOM data also have artifacts that must be considered. The TEOM sampler measures a heated air stream (50°C for the samples reported here). TEOM mass averaged over 24-hours tends to be less than the FRM samples due to volatilization of water and other volatile components. It is difficult to estimate volatile losses of organic carbon mass; however, it is expected that some volatile species will evaporate from TEOM samples when heated.

Despite limitations to accuracy, FRM and TEOM methods provide the most extensive database on PM<sub>2.5</sub> mass and speciation broadly available over multiple sites in Southeast Texas. In addition these methods are widely used by regulatory agencies to monitor PM<sub>2.5</sub> throughout the U.S. FRM and TEOM data are used in this research to develop a conceptual model for attributing PM<sub>2.5</sub>

sources in Southeast Texas and to develop an empirical model for predicting total SOA concentrations. Conceptual model results are presented in the first section of the Results (section 4.1); the methodology used to develop the empirical model for SOA is presented in the next section.

### **3.2 Development of SOA Empirical Model for Southeast Texas**

The development of the empirical model for SOA makes use of the FRM speciation data collected by the TCEQ and the EC tracer method described in the Literature Review (section 2.4). The EC tracer method involves reducing a dataset of OC and EC measurements to include only those measurements with no expected secondary organic carbon. The remaining OC and EC concentrations are used to form an expression for primary OC as a function of EC. In this analysis, this expression is of the form:

$$(OC)_{\text{primary}} = a*EC + b \quad (2.10)$$

This expression accounts for both types of primary OC:  $OC_1 (= a*EC)$ , primary OC associated with EC and  $OC_2 (=b)$  is primary OC that is not associated with EC. Secondary OC is calculated as the difference of total OC and primary OC. As discussed in the Literature Review, SOA mass concentrations are typically assumed to be 1.2-1.4 times secondary OC concentrations to account for the non-carbon mass associated with the organic compounds. This factor may be as high as 2.1, however, depending on the age and compositions of the particulate

matter. It was chosen to not speculate in this research on the relative amount of carbon to non-carbon mass in secondary organic compounds. The results of this analysis will be presented in terms of organic carbon mass concentrations, and organic carbon will be used as an indicator of SOA. The reader should recognize that concentrations of primary and secondary organic aerosol may be 1.2 – 2.1 times the organic carbon concentrations.

The analysis presented in this paper is concerned with seasonal patterns of primary and secondary OC, thus monitoring sites that are included in the analysis must contain one or more full years of PM<sub>2.5</sub> speciation data. Furthermore, for valid comparison among sites, data for each site are limited to a range of dates that are common to all sites. The sites, site descriptions, and sampling periods for this analysis are listed in Table 3.1. Note that six of nine sites are analyzed for the two-year period from 8/15/2000 through 8/15/2002. Channelview and Mauriceville are analyzed only for the last half of that period; HRM-3 is analyzed only for the first half of that period. The analysis periods for these three sites are limited by data availability. Site locations are shown in Figure 3.1c.

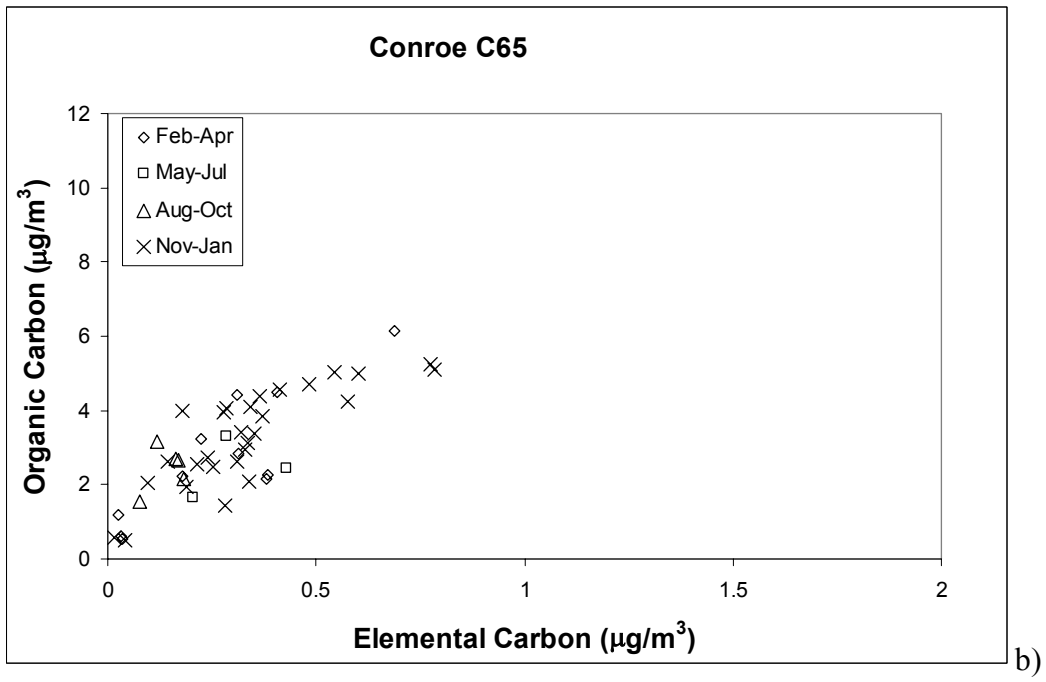
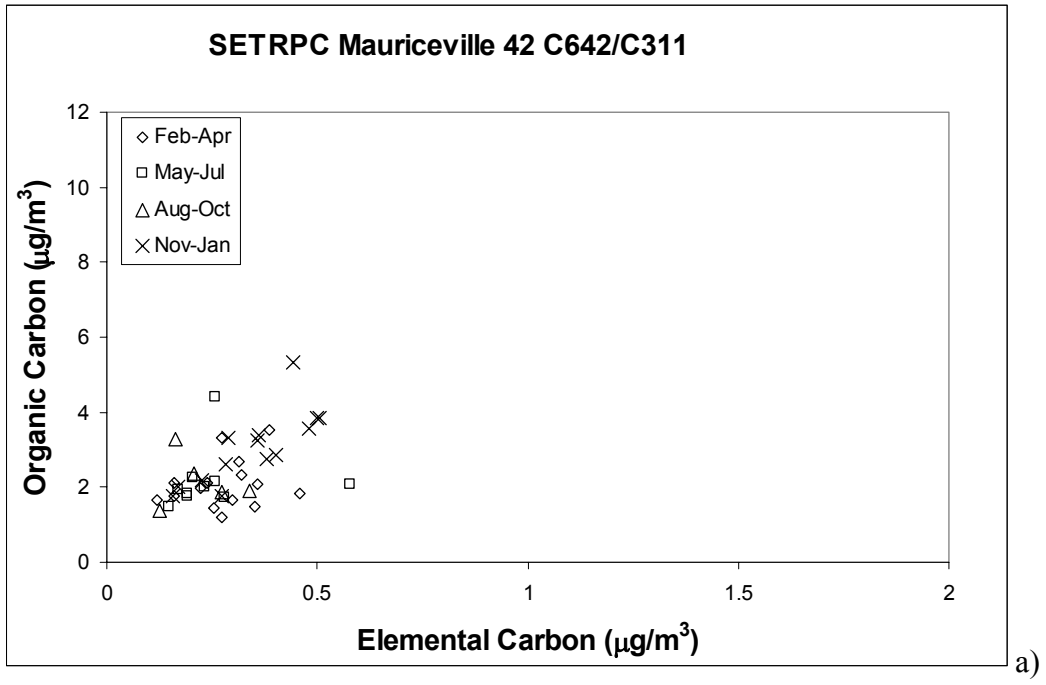
Table 3.1: PM<sub>2.5</sub> speciation sites in Southeast Texas included in this analysis. Each site had valid PM<sub>2.5</sub> speciation data and ozone data for one or two full year periods. ‘C’ numbers in the site names refer to Texas Continuous Air Monitoring Station (CAMS) IDs. A short name for each site is indicated in bold. Sites with only one year of data in the analysis are denoted by (1).

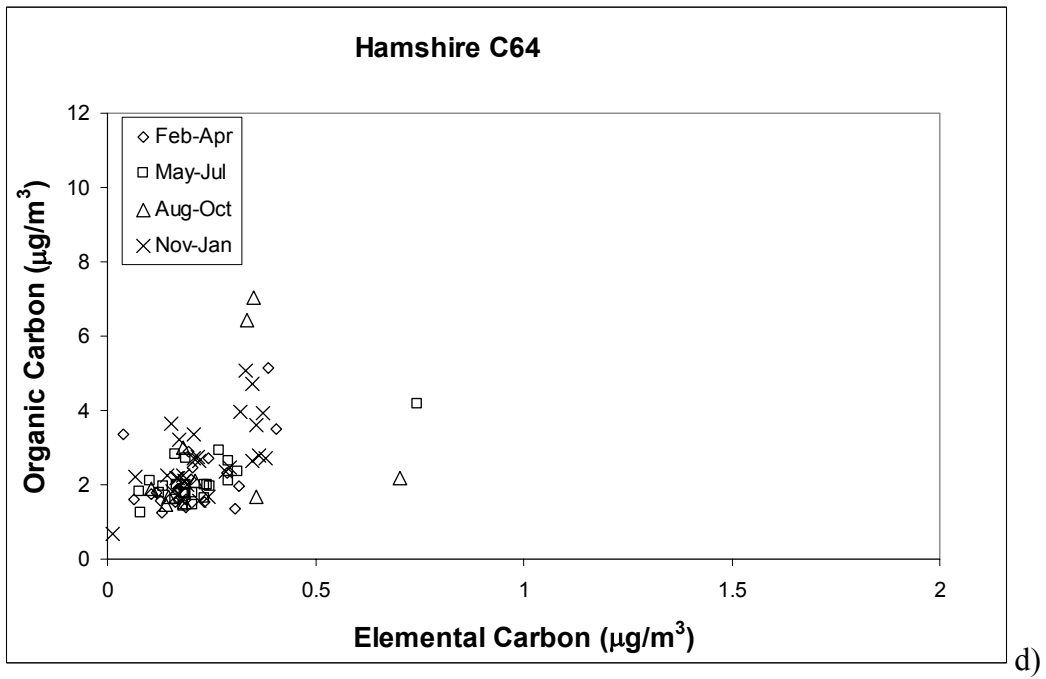
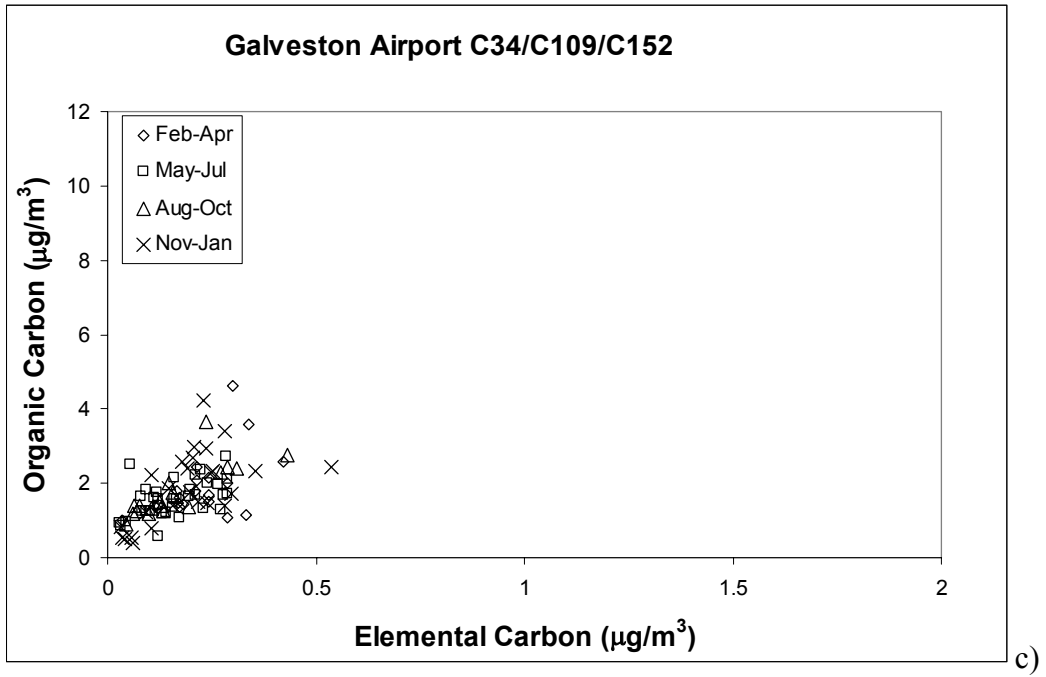
<b>Site name</b>	<b>Data range</b>	<b>Setting/surroundings</b>
<b>Channelview</b> C15/C115	8/15/2001 – 8/15/2002 (1)	Urban/industrial
<b>Conroe</b> C65	8/15/2000 – 8/15/2002	Rural/remote
<b>Galveston</b> Airport C34/C109/C152	8/15/2000 – 8/15/2002	Coastal/remote
<b>Hamshire</b> C64	8/15/2000 – 8/15/2002	Rural/remote
Houston <b>Aldine</b> C8/C108/C150	8/15/2000 – 8/15/2002	Urban/commercial,residential
Houston <b>Bayland Park</b> C53/C146/C181	8/15/2000 – 8/15/2002	Urban/commercial,residential
Houston <b>Deer Park</b> 2 C35/139	8/15/2000 – 8/15/2002	Non-urban/industrial
<b>HRM-3</b> Haden Road C603/C114	8/15/2000 – 8/15/2001 (1)	Urban/industrial
SETRPC <b>Mauriceville</b> 42 C642/C311	8/15/2001 – 8/15/2002 (1)	Rural/remote

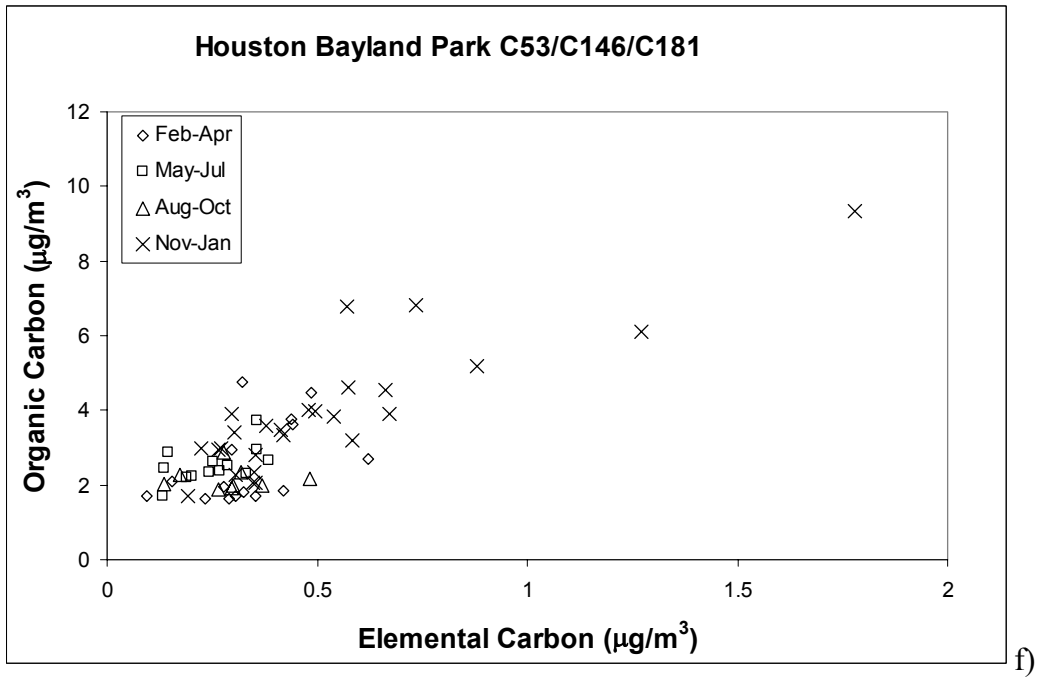
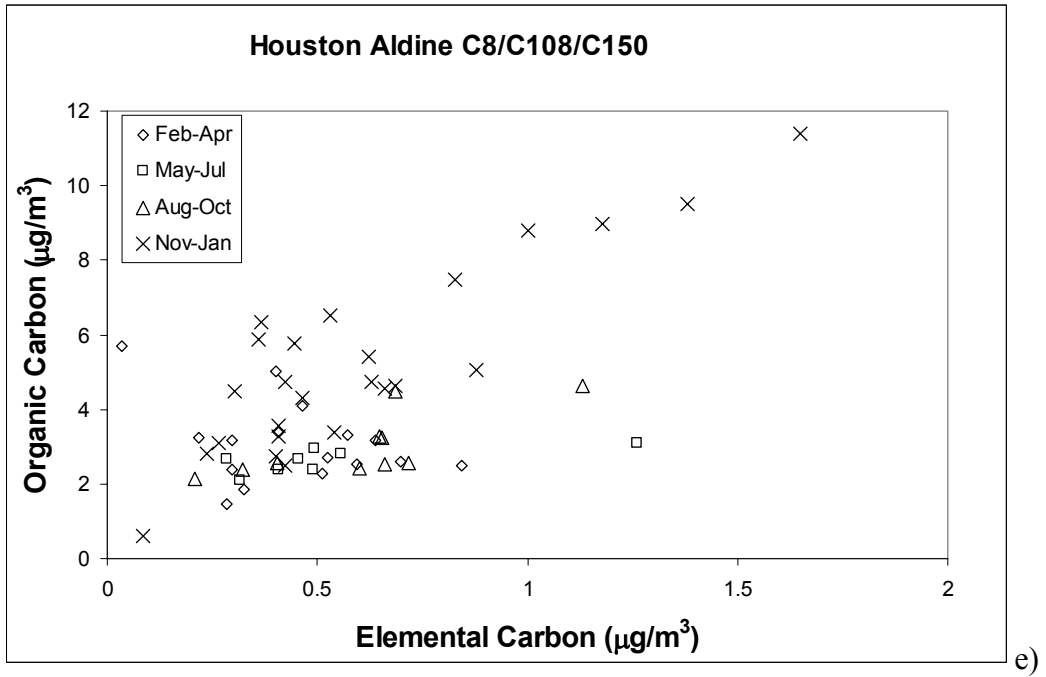
The first step in the estimation of primary OC is to isolate days when no secondary OC is expected. Maximum daily ozone is used as the indicator for photochemical activity and hence secondary OC. For each site, the data set of OC and EC concentrations is successively reduced based on maximum daily ozone concentrations observed at the site. Data sets are constructed that only contain data for days with maximum hourly-averaged ozone concentrations, at the site of interest, of less than 100 ppb, less than 80 ppb, less than 60 ppb, less than 40 ppb, less than 30 ppb and less than 25 ppb. For each data set, the OC to EC relationship, defined by Equation 2.3.2, is determined using least squares regression. The slope of the regression, at each site, steadily decreases with successive reductions to the maximum ozone concentrations allowed. The decreasing slope is consistent with reducing the number of data points with high

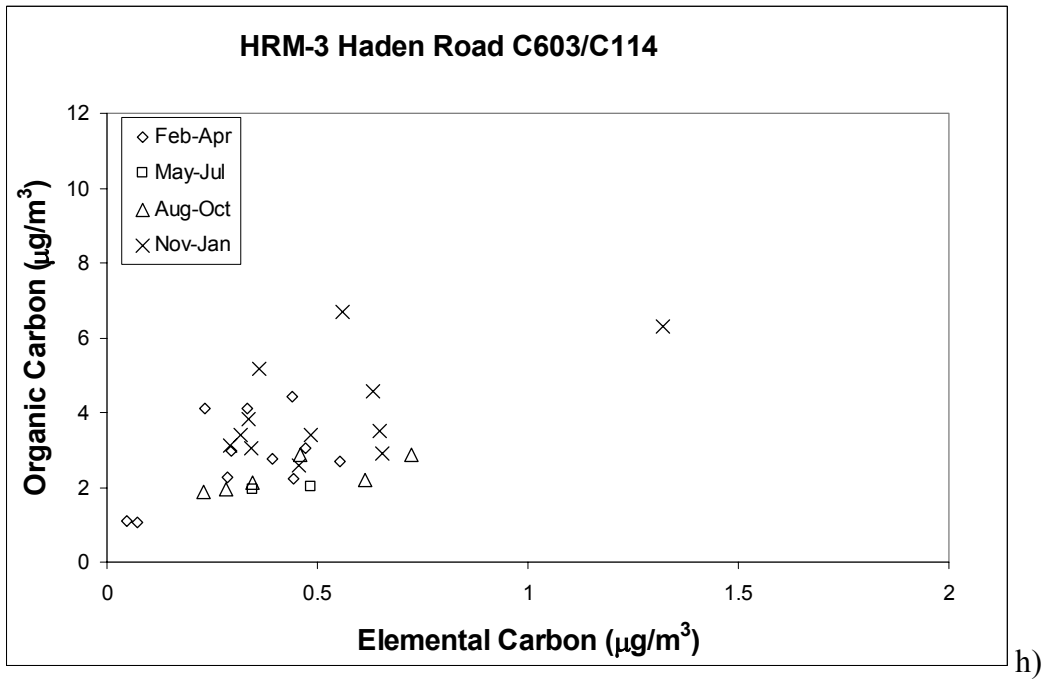
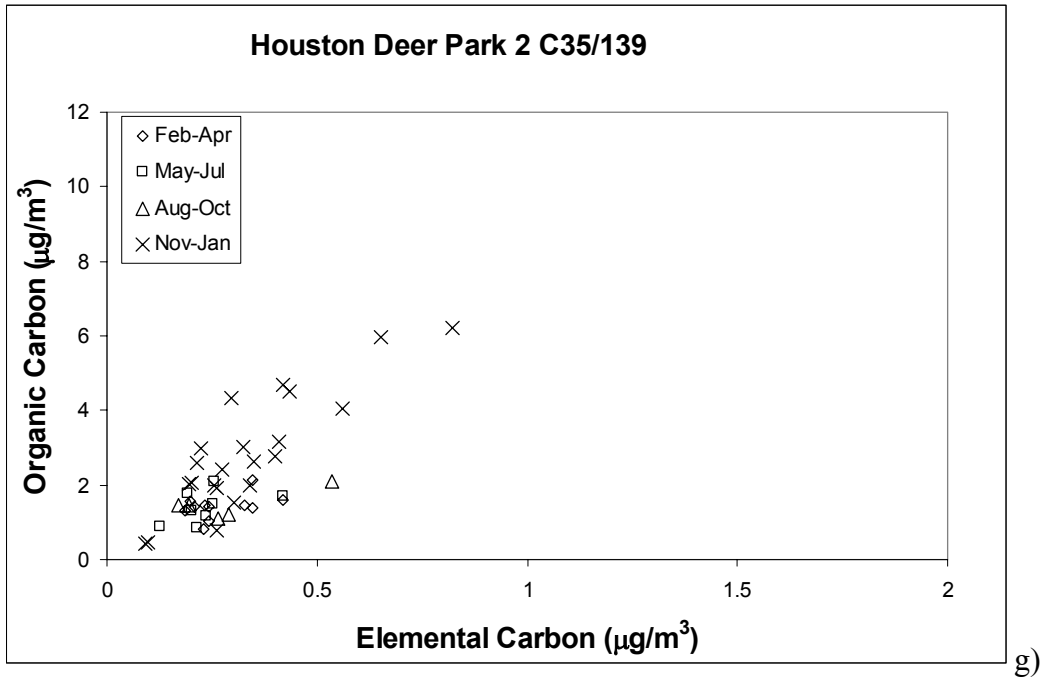
secondary OC. At very low maximum ozone concentrations (30 and 25 ppb), however, this trend reversed and the slope of OC to EC increases at most sites. The reason for this increase is not entirely clear. Reducing the data set to days with maximum ozone concentrations less than 30 ppb may leave too few data pairs for a meaningful regression. Therefore, to establish expressions for mean daily OC primary as a function of EC, the data for days with maximum ozone concentrations less than 40 ppb is used.

Figure 3.2a through 3.2i below show scatter plots of OC to EC from this dataset (maximum ozone concentrations less than 40 ppb) for all sites. The Figures show the seasonality of the data. The data from the urban/industrial sites have higher absolute OC and EC concentrations than at remote sites. Most of the high OC and EC concentrations occur in the November to January and February to April periods.









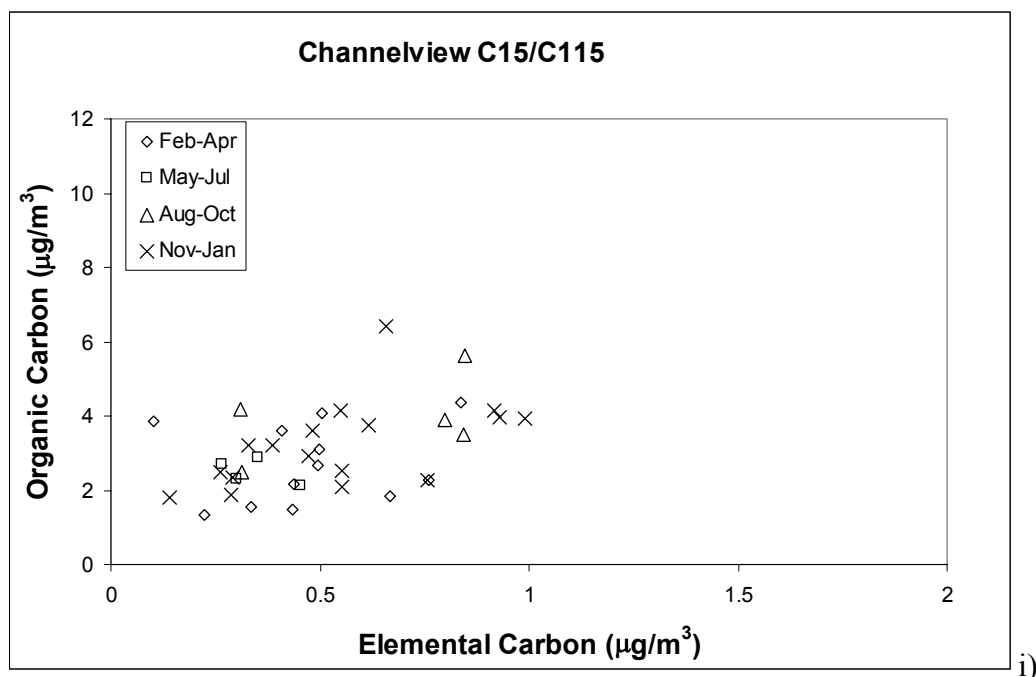


Figure 3.2: Scatterplot of OC and EC concentrations for all measurements on days with maximum ozone concentrations less than 40 ppb a)Mauriceville b)Conroe c)Galveston d)Hamshire e)Aldine f)Bayland Park g)Deer Park h)HRM-3 i)Channelview. Data points are divided into one of four seasons: Feb-Apr, May-Jul, Aug-Oct and Nov-Jan.

Figure 3.2 clearly shows variability in a linear model fit through data at any of the sites. Day to day variability in the relative amounts of primary OC and EC is expected as a result of daily variation in the mix of pollutants that influence a site, which in turn is a result of daily variation in meteorology. The model for primary OC should reflect average conditions; however, the model should not include variability due to extreme events that have a significant influence on the relationship between primary OC and EC. There may be several reasons for such extreme events. For this analysis, the following three arguments are used to

eliminate extreme events and further reduce the dataset to give a better representation of mean primary OC and EC.

1. Previous research has indicated that biomass burning, both locally and regionally, can significantly influence  $PM_{2.5}$  concentrations in Southeast Texas (Walk et al. 1999; Fraser et al. 2002). Furthermore, the ratio of OC to EC is typically higher in biomass burning emissions than from other sources, such as motor vehicle emissions (Seinfeld and Pandis 1998; Khalil and Rasmussen 2003). The OC/EC ratios from burning, however, vary widely depending on, for example, wood type and combustion temperature. It is assumed that large regional fires are irregular, and their contribution should not be included in the primary OC model. Besides OC to EC ratio, potassium (K) is a known marker for biomass burning (Seinfeld and Pandis 1998; Khalil and Rasmussen 2003). The 90th percentile of K/  $PM_{2.5}$  concentration ratio is calculated from the original full dataset for each site. This 90th percentile was between 0.009 – 0.012 at different sites. All days with K/  $PM_{2.5}$  ratios greater than the 90th percentile for their site are removed from the data set used to establish the primary OC to EC relationship.

2. Data with very high  $NO_x$  concentrations are removed from the dataset used to establish the primary OC to EC relationship. High  $NO_x$  concentrations on days with maximum ozone concentrations smaller than 40 ppb may be indicative of extensive ozone scavenging. The 90th percentile of average daily  $NO_x$  concentration at each day is calculated from the original full dataset for each site. This is between 12 – 50 ppb among sites. All days with average  $NO_x$

concentrations greater than the 90th percentile for their site are removed from the data set used to establish the primary OC to EC relationship.

3. Finally, there could be any number of reasons for extreme events that may alter the ratio of primary OC to EC that are not understood or not apparent from these data. Extreme events are indicated by high ratios of  $OC_1/EC$ . High ratios of total primary OC/EC, or  $(OC_1 + OC_2)/EC$ , are not necessarily representative of extreme events, since total primary OC/EC will be high when  $OC_1$  is low relative to  $OC_2$ . For each site,  $OC_2$  is calculated as the intercept of the linear regression of OC and EC on days with maximum ozone less than 40 ppb. (The intercept remained relatively constant at each site irrespective of the maximum daily ozone concentrations of the days included in the regression).  $OC_1$  for each day is then estimated as the difference between total OC and  $OC_2$ , and  $OC_1/EC$  is calculated for each day. The 90th percentile of the ratio of  $OC_1/EC$  is calculated for each site. This is between 4.3 - 10.4 among sites. All days with  $OC_1/EC$  greater than the 90th percentile for their site are removed from the data set used to establish the primary OC to EC relationship.

An additional issue to be considered is whether the OC-EC relationship will change, as relative source strengths change, from season to season. If wind directions vary significantly from season to season, then the mix of sources that influence a site, and the OC-EC relationship, will change with the season. Figure 3.3 shows a weighted frequency distribution of wind direction at the Deer Park site for three periods: November-February, March-June and July-October. The y-axis shows the product of frequency of hourly resultant wind direction and mean

resultant wind speed for each wind direction. This product of wind speed and frequency accounts for both the probability that transport is from a particular direction and also the potential magnitude of the transport. The metric deemphasizes stagnation events and emphasizes data from days with significant advection.

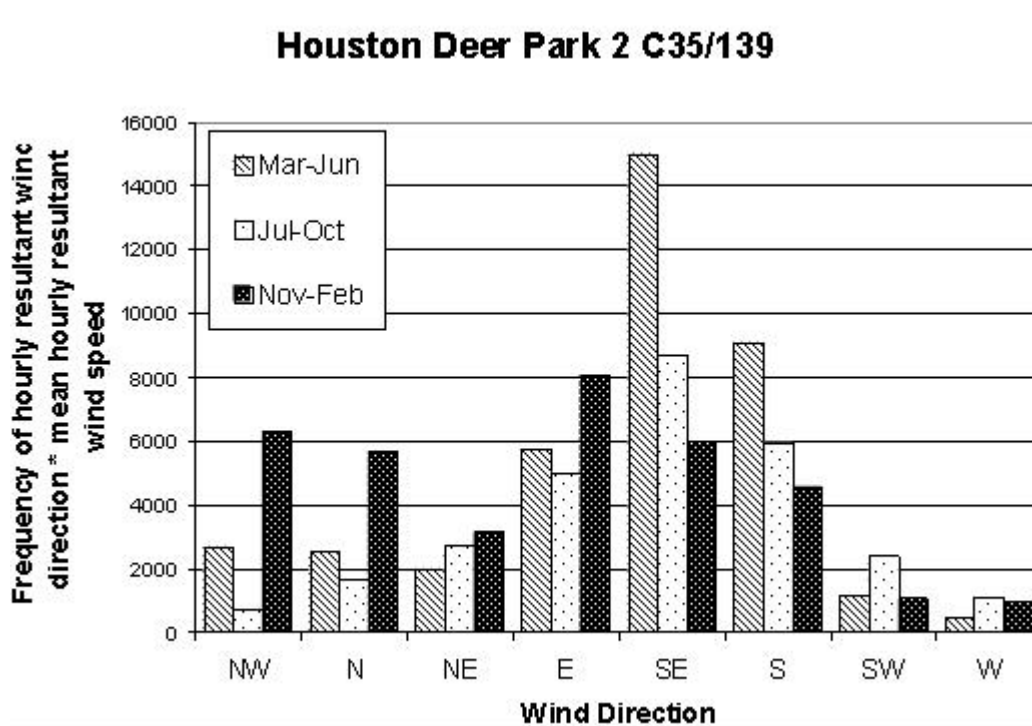


Figure 3.3: Product of frequency of hourly resultant wind direction and mean resultant wind speed for each wind direction at the Deer Park site. Data is shown separately for the November-February, March-June and July-October period.

A feature that is common among monitoring sites is that there is a significant Northwest/North/Northeast wind component between November and February. The remaining months are dominated by winds from the South/Southeast at all sites. As a result, separate relationships between primary

OC and EC are sought during November-February and during March-October at each site.

After applying the reductions described above to the dataset, least-squares linear regressions were performed for each site to estimate  $OC_2$  and  $OC_1/EC$ . The regression was performed separately for the November–February period and the March–October period. The number of OC–EC data that were used for the regression compared to the total number of data points is shown in Figure 3.4.

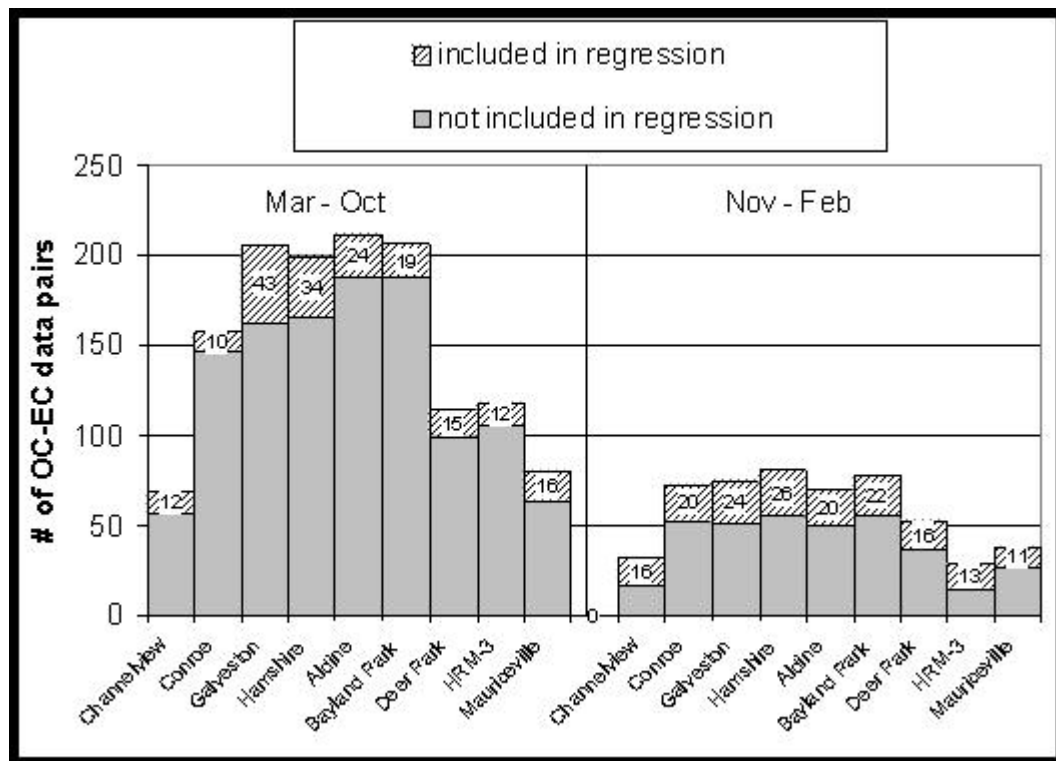
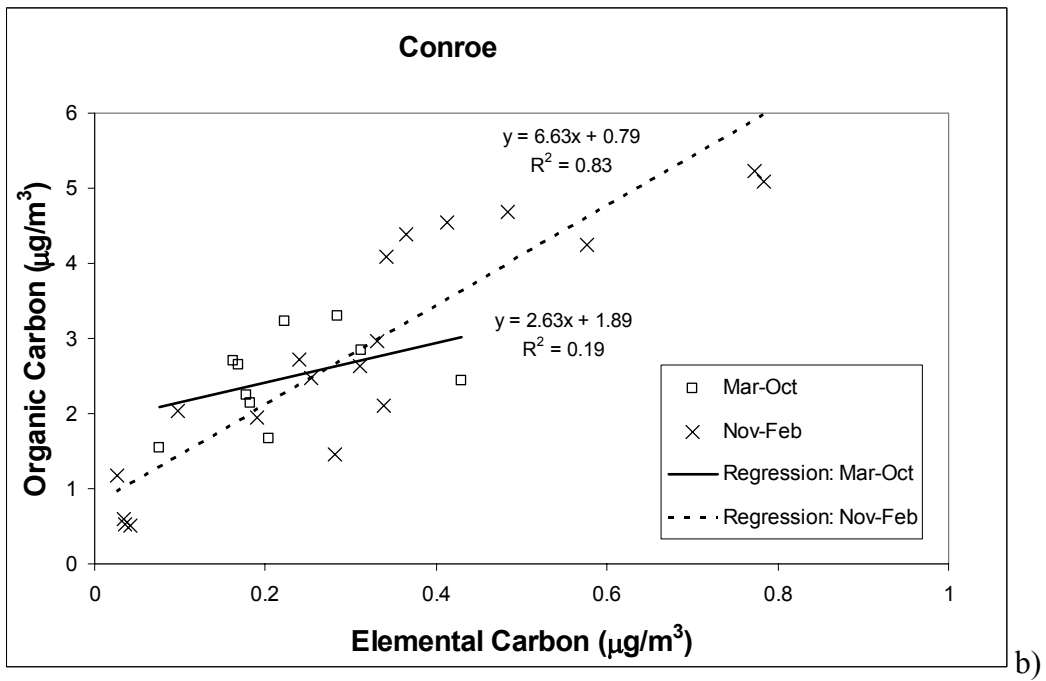
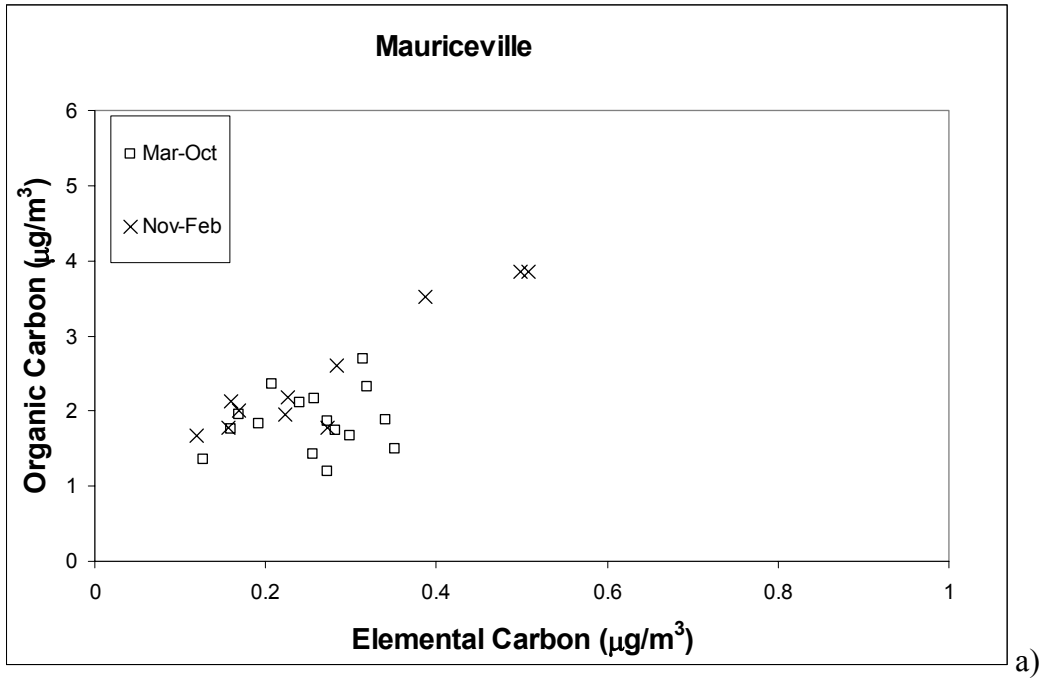
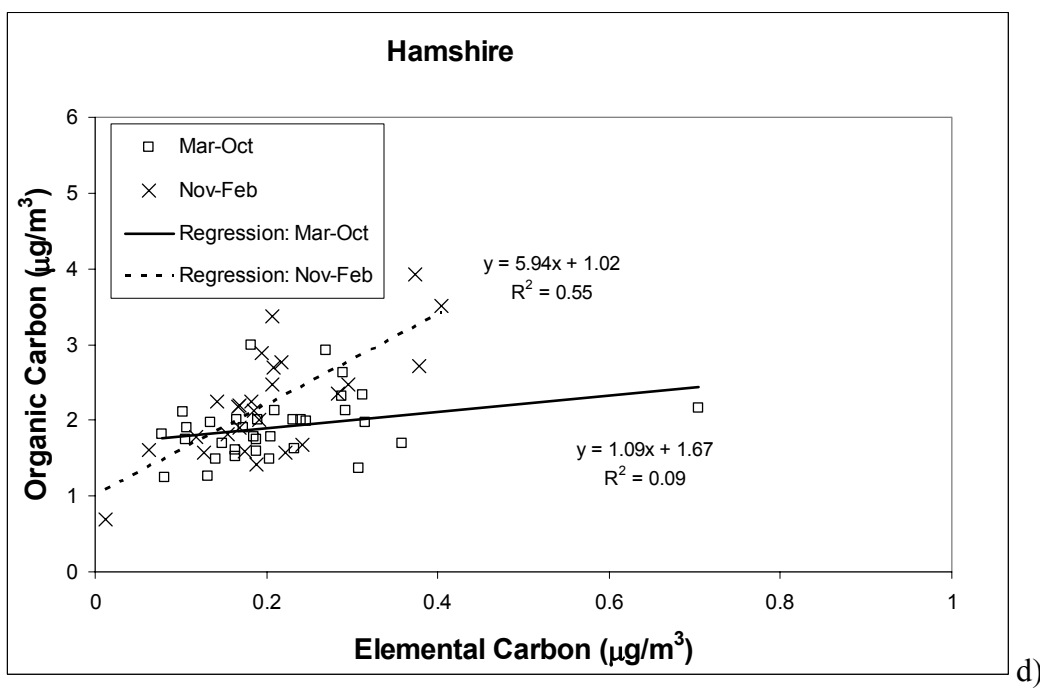
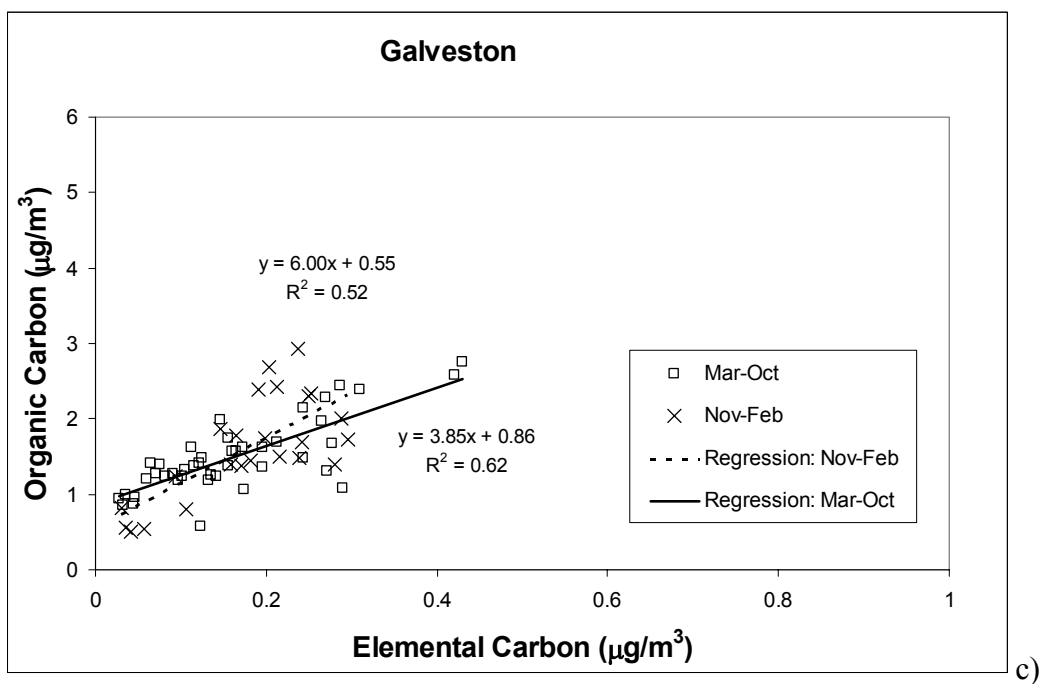


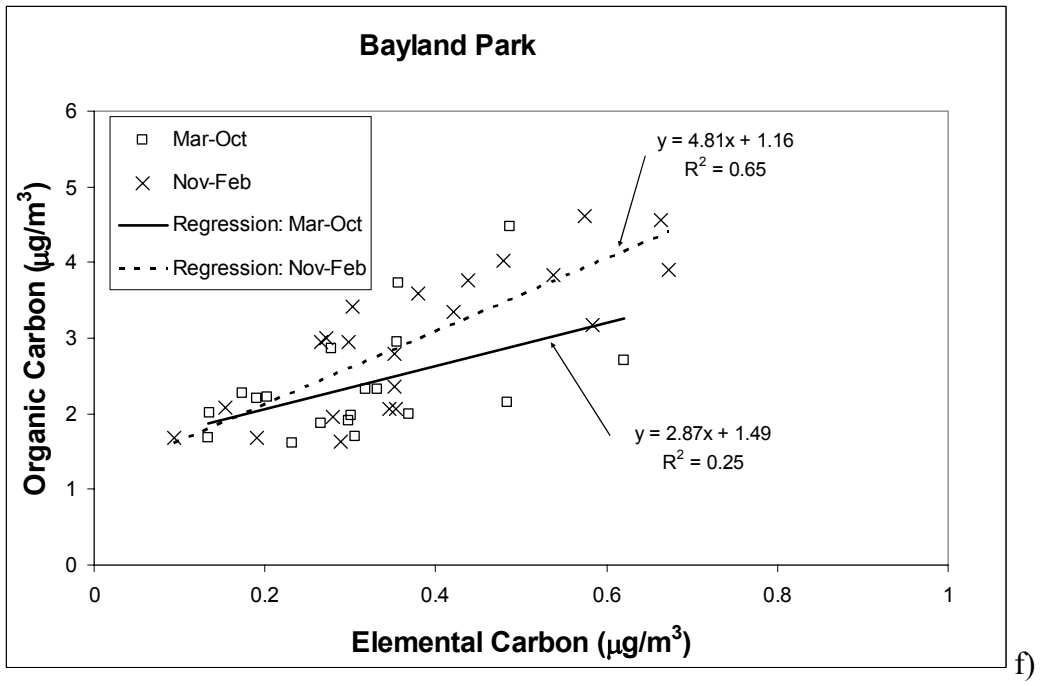
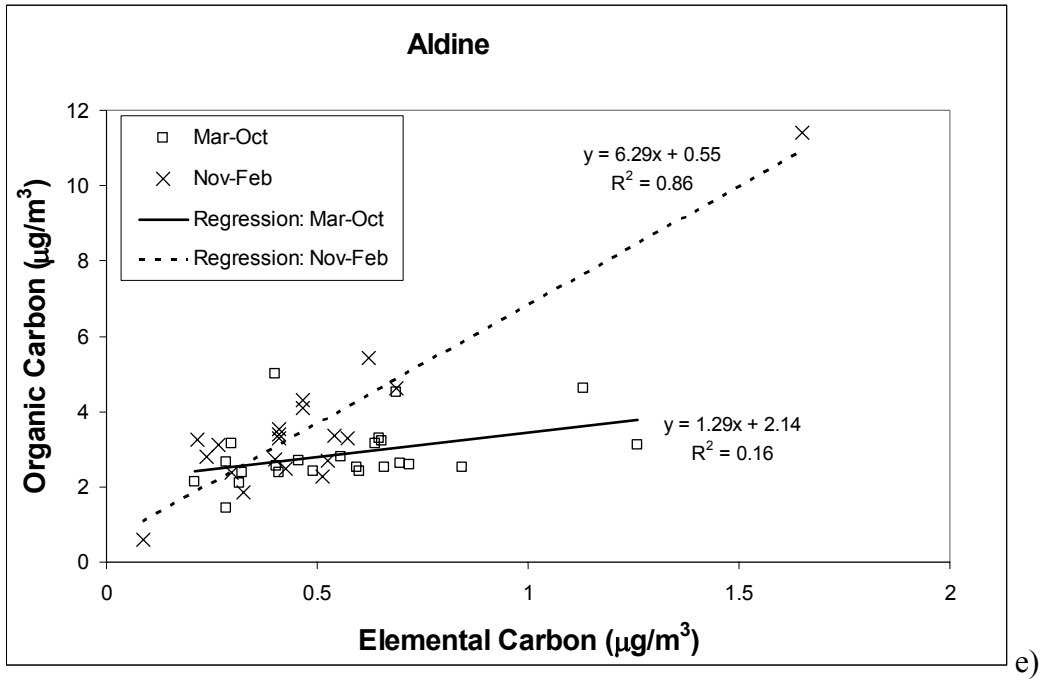
Figure 3.4. Number of OC-EC data points used in the regression estimates (in parenthesis) by site and season. Total numbers of data points in the dataset are indicated by the height of each column.

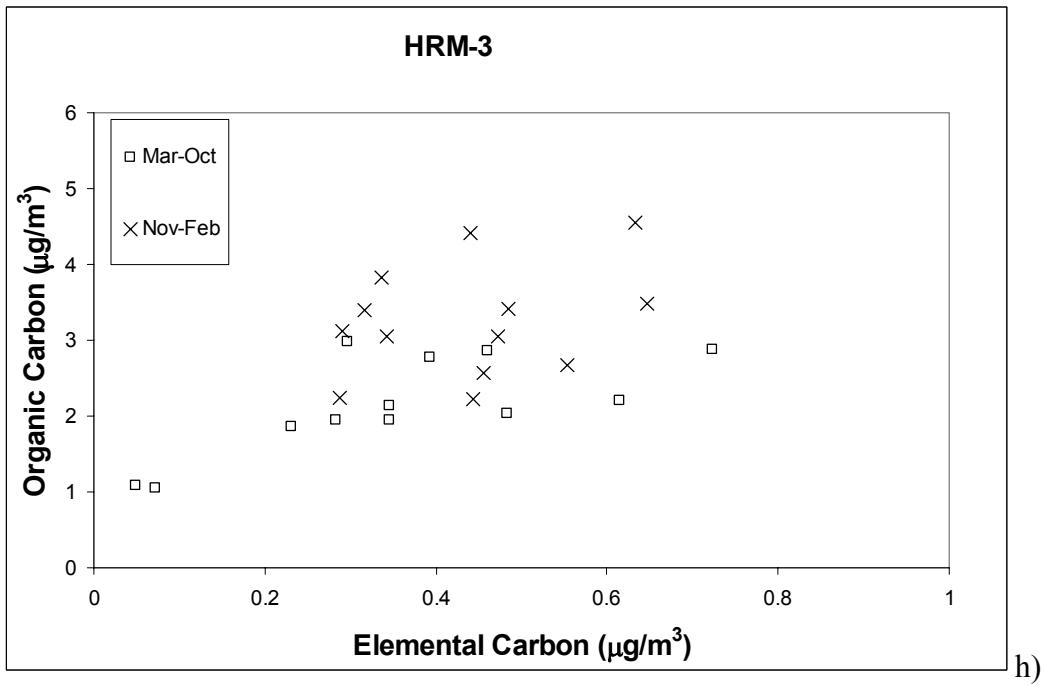
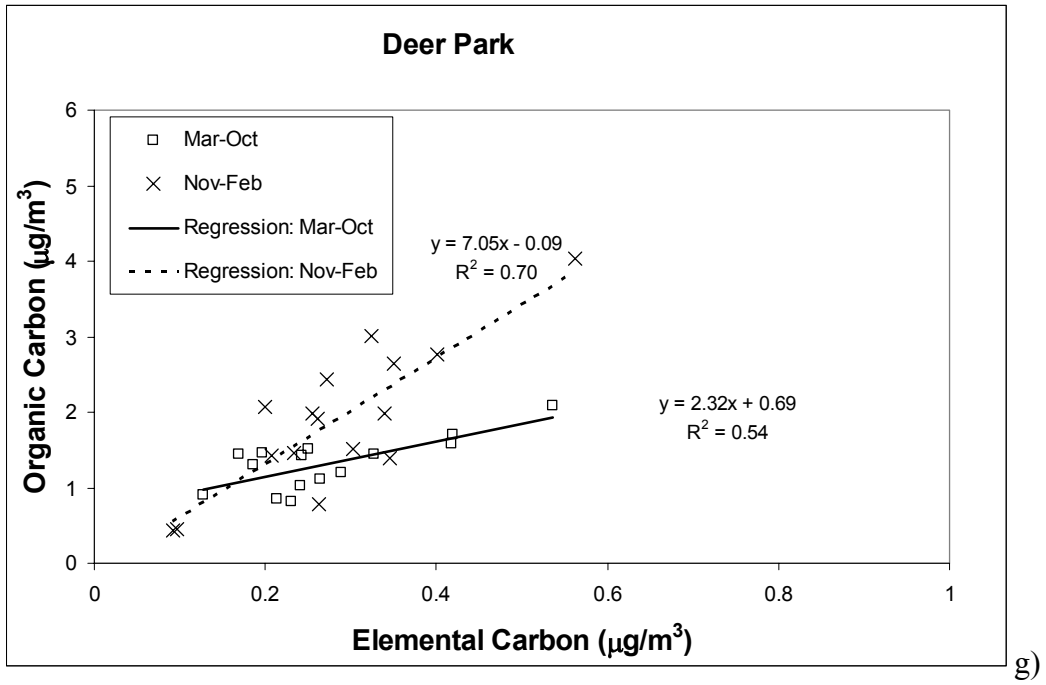
Regression results are presented in Table 3.2. An F statistic is calculated as the ratio of mean regression sum of squares to mean residual sum of squares and is used to test the significance of the regression by comparing it to values in standard tables for the F distribution at the 90% confidence level, i.e. whether the linear relationship is a better explanation of dependence of OC on EC compared to no relationship at all. The regression is not found to be significant for three of nine sites in the March-October period and one site in the November-February period, and these are not included in Table 3.2. The sites where the regression is not significant are those that include only one year of data (except Conroe); these sites have the fewest data.

The Conroe monitoring site is located to the north of urban/industrial Houston and is immediately surrounded primarily by biogenic emission sources. Conroe was of interest in this study because it provided a contrast to the other monitoring locations, which are closer to anthropogenic sources. The regression for Conroe during the March-October period was significant at the 80% confidence level, but not at the 90% level, which was the criteria used for all other sites; nevertheless, data for Conroe was included in the analysis since it is an important location and since this site had two full years of data. The OC and EC concentrations that were used in the final regressions are plotted by site in Figure 3.5a through Figure 3.5i.









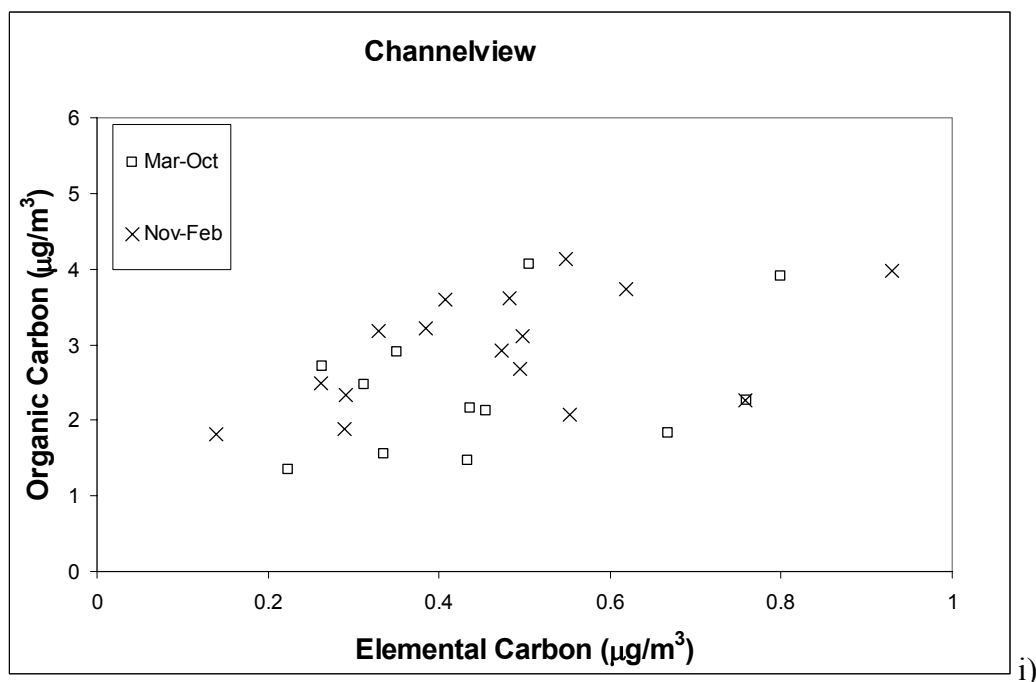


Figure 3.5: Scatterplot of OC and EC concentrations for all measurements used in the final regression (max ozone less than 40ppb and extreme events removed). a)Mauriceville b)Conroe c)Galveston d)Hamshire e)Aldine f)Bayland Park g)Deer Park h)HRM-3 i)Channelview. Regression equations are shown for the sites with two full years of data.

The six sites in Table 3.2 with significant regressions in both periods have higher slopes ( $OC_1/EC$ ) in the November-February period than in the March-October period. These six sites also all have lower intercepts ( $OC_2$ ) in November-February compared to March-October. The variation in slopes and intercepts by season suggests that there is seasonality to the relationship between primary OC and EC and this is likely due to a different mix of sources influencing these sites. This mix could be a result of emissions from different source regions, or seasonal differences in emission composition or strengths.

It should also be noted that the regression for all sites was poorer during the March-October period, compared to the November-February period. The  $R^2$  parameter for the least-squares regression was between 0.1 and 0.6 at sites with significant regressions during the March-October period. The  $R^2$  parameter was between 0.5 and 0.9 at sites with significant regressions during the November-February period. The low  $R^2$  parameters during March-October may be a result of including days with either significant secondary organic carbon or unusual primary source signatures.

Table 3.2: Regression results for the set of OC and EC measurements on days assumed to have no secondary OC and to be representative of primary OC and EC at the Southeast Texas monitoring sites. The slope represents OC<sub>1</sub>/EC and the intercept represents OC<sub>2</sub>. Italics indicate the standard error of each estimate. The data are not shown wherever the regression was not significant at the 90% confidence level, except for the Conroe site during Mar-Oct (shaded). The regression was significant at the 80% confidence level for this site/period, and the site was included because of its importance to the study.

Site	Mar - Oct		Nov - Feb	
	Slope +/-	Intercept +/-	Slope +/-	Intercept +/-
Channelview C15/C115			1.90 <i>0.89</i>	2.06 <i>0.45</i>
Conroe C65	2.63 <i>1.92</i>	1.89 <i>0.46</i>	6.63 <i>0.71</i>	0.79 <i>0.29</i>
Galveston Airport C34/C109/C152	3.85 <i>0.47</i>	0.86 <i>0.09</i>	6.00 <i>1.24</i>	0.55 <i>0.24</i>
Hamshire C64	1.09 <i>0.61</i>	1.67 <i>0.15</i>	5.94 <i>1.09</i>	1.02 <i>0.24</i>
Houston Aldine C8/C108/C150	1.29 <i>0.62</i>	2.14 <i>0.38</i>	6.29 <i>0.59</i>	0.55 <i>0.34</i>
Houston Bayland Park C53/C146/C181	2.87 <i>1.21</i>	1.49 <i>0.40</i>	4.81 <i>0.79</i>	1.16 <i>0.32</i>
Houston Deer Park 2 C35/139	2.32 <i>0.59</i>	0.69 <i>0.17</i>	7.05 <i>1.23</i>	0.00 <i>0.37</i>
HRM-3 Haden Road C603/C114	2.33 <i>0.73</i>	1.31 <i>0.30</i>		
SETRPC Mauriceville 42 C642/C311			5.88 <i>0.70</i>	0.88 <i>0.21</i>

The slope and intercept estimates are used to calculate primary OC for all dates in the original dataset excluding dates with non-zero rainfall at Deer Park, with K/ PM<sub>2.5</sub> ratios above the 90th percentile for that site and with mean daily NO<sub>x</sub> concentrations above the 90th percentile for that site. In addition, primary OC is not estimated for all dates/sites with maximum ozone concentrations less than 40 ppb that have OC<sub>1</sub>/EC ratios in the top 10 percent for their site. These

data are not analyzed since they are excluded from the data that are used to estimate the regression parameters. Secondary OC is estimated using Equation 2.10 and the primary OC estimates. These estimates of primary and secondary OC are referred to as the regression primary OC and regression secondary OC respectively. Figure 3.6 shows the number of data points (days) for which SOC concentrations were calculated by site and season.

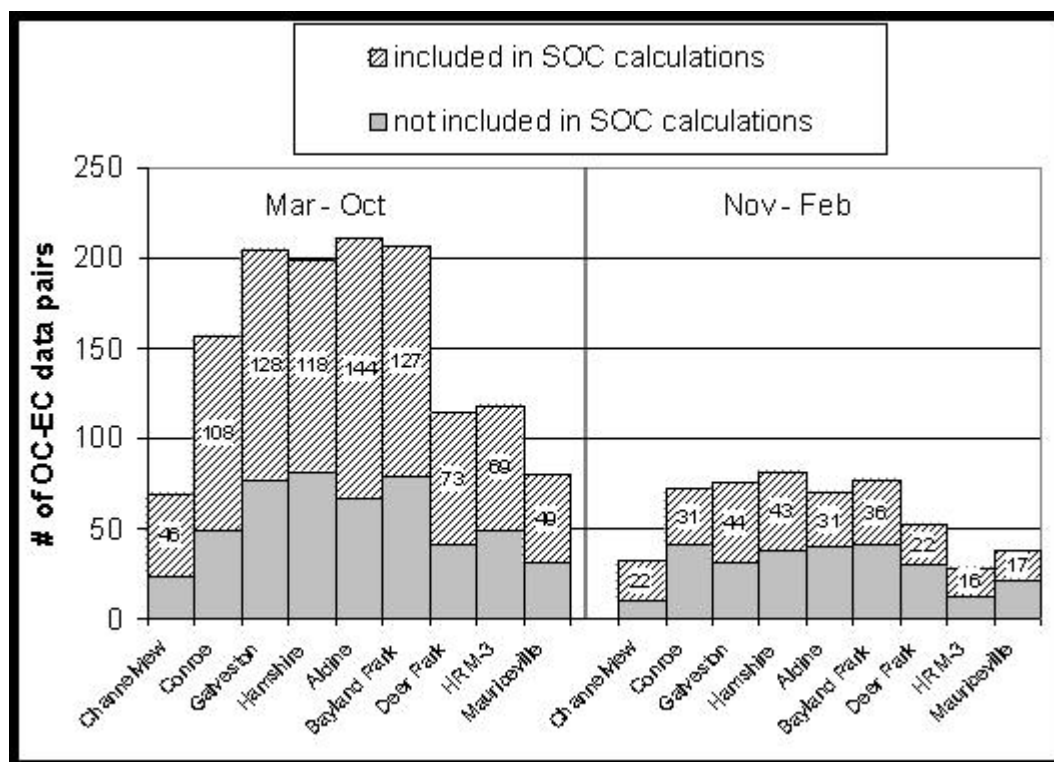


Figure 3.6. Number of data points (days) for which SOC concentrations were calculated (in parenthesis) by site and season. Total numbers of data points in the dataset are indicated by the height of each column.

For the various sites, 60% - 80% of regression secondary OC estimates fall between  $-1$  and  $1 \mu\text{g}/\text{m}^3$ , and 30%-50% of the estimates are less than zero.

Negative estimates are a result of over-predicting the primary OC. Occasional over prediction is expected due to day-to-day variability in the relationship between primary OC and EC. The variability in primary OC also comes inevitably from using 24-hour integrated samples, given that source signatures at a given location can vary considerably during a 24-hour period. However, since some days in the dataset used to establish the regression parameters may still have secondary OC (i.e. since these days had maximum ozone concentrations up to 40 ppb), a lower bound on primary OC is used to calculate an upper bound on secondary OC for each day. A lower bound on primary OC is calculated by subtracting the standard error of the slope from the slope and by subtracting the standard error of the intercept from the intercept, for site and period. The upper bound secondary OC estimate is then the difference between total OC and the lower bound primary OC:

$$OC_{\text{primary\_low}} = EC * (\text{slope} - (\text{std. error})) + (\text{intercept} - (\text{std. error})) \quad (3.1)$$

$$OC_{\text{secondary\_high}} = OC - OC_{\text{primary\_low}} \quad (3.2)$$

The percentage of upper bound secondary OC estimates less than zero is now 5%-20% among sites, which is considered acceptable for purposes of this analysis. When predicted primary OC is estimated to be greater than total OC, primary OC is set equal to total OC and secondary OC is set equal to zero. Since these corrections are made to account for potential over-prediction of the primary

OC, absolute concentrations of primary and secondary OC on a given day will have some bias. The data are however useful for comparing mean primary and secondary OC estimates and for performing qualitative comparisons between sites and seasons.

The estimates of primary and secondary OC are presented and discussed in the Results chapter (section 4.2). These are presented by site and month and using both the original regression parameters and the lower bound regression parameters. A limitation to this method is the use of 24 hour integrated samples. SOA may vary considerably during the day and this diurnal variation is ‘averaged’ when a sample is taken over a 24 period. However, to date, there are no existing OC or EC measurements from shorter time periods at Southeast Texas sites. The methods presented here give a best estimate of the contribution of SOA to daily average  $PM_{2.5}$ .

## **4.0 Results-Part 1: PM<sub>2.5</sub> Conceptual Model and SOA Empirical Model**

### **4.1 Conceptual Model of PM<sub>2.5</sub> in Southeast Texas**

This section presents data that form a conceptual model for attribution of sources of PM<sub>2.5</sub> in Southeast Texas. A conceptual model is useful in answering questions such as:

- What are PM<sub>2.5</sub> concentrations relative to health based standards?
- How do PM<sub>2.5</sub> concentrations vary seasonally, spatially and diurnally?
- What is the composition of PM<sub>2.5</sub> and how does this composition vary seasonally and spatially?

In order to address these questions, data in this section are presented in four subsections: FRM mass analysis, TEOM mass analysis, spatial distribution of FRM mass and FRM speciation analysis.

#### ***FRM Mass Analysis***

Since annual statistics among monitoring sites are important, sites are included only if they were active for entire year-long periods. Ten monitoring sites were active for the entire two-year period beginning January 1st, 2000 and ending December 31st, 2001. The first four columns in Table 4.1 show mean, standard deviation, maximum and number of FRM mass concentrations for these ten sites. The last four columns show the same statistics for these same ten sites

and an additional five sites for the one-year period beginning January 1st, 2001 and ending December 31st, 2001. (The additional five sites were not active for the entire 2000-2001 two-year period). Note that the collection frequency for FRM samples is typically every third day but some sites' samples are collected every day. Not all sites reported in Table 4.1 have the same number of samples for the same time period because invalid data were excluded.

The monitoring sites in Table 4.1 are located over a large geographic area, in a wide range of settings ranging from industrial and urban to rural and remote, yet daily average fine particulate matter concentrations are remarkably consistent among sites in Southeast Texas. Annual means of FRM mass concentrations are 10 - 14  $\mu\text{g}/\text{m}^3$  (the Annual National Ambient Air Quality Standard is 15  $\mu\text{g}/\text{m}^3$ ). Maximum daily FRM mass concentrations are 30 - 50  $\mu\text{g}/\text{m}^3$  (the Daily National Ambient Air Quality Standard is 65  $\mu\text{g}/\text{m}^3$ ). Although not shown in Table 4.1 (it was outside of the 2001 one-year period), there was a maximum daily FRM mass concentration as high as 127.2  $\mu\text{g}/\text{m}^3$  at Thomas Jefferson School, on September 3rd, 2000. The site with the highest annual mean FRM mass concentration in this dataset is the Clinton site which is in the heavily industrialized Houston Ship Channel area. The location of the highest annual mean is consistent with the early monitoring study findings (Tropp et al. 1998). Note that a site must be active for three consecutive years for valid comparison to the NAAQS. The statistics in Table 4.1 characterize either a one or two year period, so these data should not be used to determine the attainment status of any monitoring site for  $\text{PM}_{2.5}$ . The data do suggest, however, that annual mean FRM mass in Southeast Texas is close to

the annual NAAQS of 15  $\mu\text{g}/\text{m}^3$  and tends to be higher at monitoring sites near the urban and industrial core of Houston (Clinton, Channelview, Baytown).

Table 4.1 : Mean, standard deviation, maximum and number of FRM mass concentrations for the January 1st, 2000-December 31st, 2001 period and for the January 1st, 2001-December 31st, 2001 period. Each monitoring site was active for the entire period under which it is listed.

Site	Period: 1/1/2000 -12/31/2001				Period: 1/1/2001-12/31/2001			
	Mean	Std Dev	Max	n	Mean	Std Dev	Max	n
Clinton C403/C113/C304	14.0	5.7	45.2	605	13.8	6.2	45.2	311
Channelview C15/C115	13.1	5.9	38.4	355	12.9	6.5	34.5	116
Baytown C148	12.8	6.9	53.7	199	12.7	7.6	53.7	118
Houston Aldine C8/C108/C150					12.5	6.5	44.0	135
Thomas Jefferson School C303					11.4	6.0	42.3	349
West Orange C9/C141					11.3	5.9	35.1	124
Conroe C65	12.1	6.0	38.5	205	11.1	5.9	38.5	91
Hamshire C64					10.8	5.6	33.2	149
Bayland Park C53/C146/C181					10.4	5.3	30.2	129
Houston Deer Park 2 C35/139	12.0	6.0	42.8	208	10.4	5.1	29.3	81
Texas City C100	11.8	6.3	44.5	210	11.4	6.1	32.7	113
Houston Monroe C406	11.2	5.6	34.4	212	11.1	6.2	34.4	111
Calder Drive	10.8	5.7	46.8	200	10.2	4.8	30.7	102
Houston Croquet C409	10.8	5.3	43.3	219	10.4	5.1	32.9	120
Clute C11	10.2	4.9	36.9	186	10.2	4.9	36.9	112
Galveston Airport C34/C109/C152					9.9	5.5	31.1	151

The remainder of the FRM analysis in this section is limited to the ten sites that were active during the entire two-year 2000-2001 period. Figure 4.1 shows mean FRM mass concentrations by month for all sites. Also shown is mean FRM mass concentrations by month for Clinton and Clute. The Clinton site is located in the Houston Ship Channel and has the largest 2-year mean FRM mass concentration. Clute is a rural receptor site and has the lowest 2-year mean FRM mass concentration. There is a seasonal as well as a spatial homogeneity to the concentrations. While there may be subtle increases in fine particulate matter concentrations in the late fall and spring, the values are otherwise fairly consistent over the year and from site to site. A t-test was used to test the difference between

a monthly mean at a given site and the two-year mean for that site. This test was performed for each site, for each month. Seven of ten sites had December means that were significantly lower than their two-year mean at the 95% confidence level. Five of ten sites had November means that were significantly higher than their two-year mean at the 95% confidence level. Aside from these instances, there was not a statistically significant difference between monthly mean and overall mean FRM mass concentration at any site. It is difficult to conclude whether the variability in December (lower than normal) and November (higher than normal) are real, given the relatively short dataset. However it is apparent that mean FRM mass concentrations in Southeast Texas show little seasonality in this dataset.

While average concentrations show seasonal and spatial homogeneity, the extreme values of FRM mass concentrations show more variability. Figure 4.2 shows the monthly variation of the maximum FRM mass concentration over all sites. Also shown are the maximum FRM mass concentrations for Clinton and Clute. The Figure shows that maximum FRM mass concentrations tend to be higher in the late fall. Several monitoring sites also show high maximum FRM mass concentrations in the month of April. Maximum FRM mass concentrations show more seasonal variation than mean FRM mass concentrations at all sites.

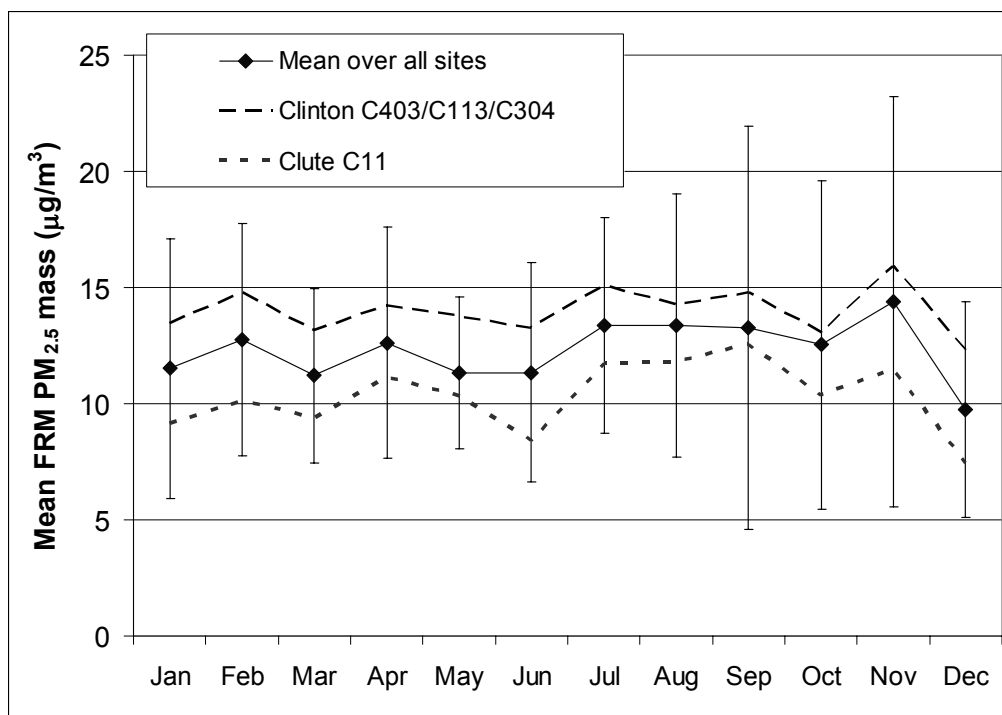


Figure 4.1. Monthly variations in mean FRM mass concentrations. The data points show mean FRM mass concentrations over all sites that were active during the entire two-year 2000-2001 period. Bars show one standard deviation for all data in that month, i.e. both intersite and intrasite variability. Also shown are the mean FRM mass concentrations for Clinton and Clute (no bars shown for these individual sites).

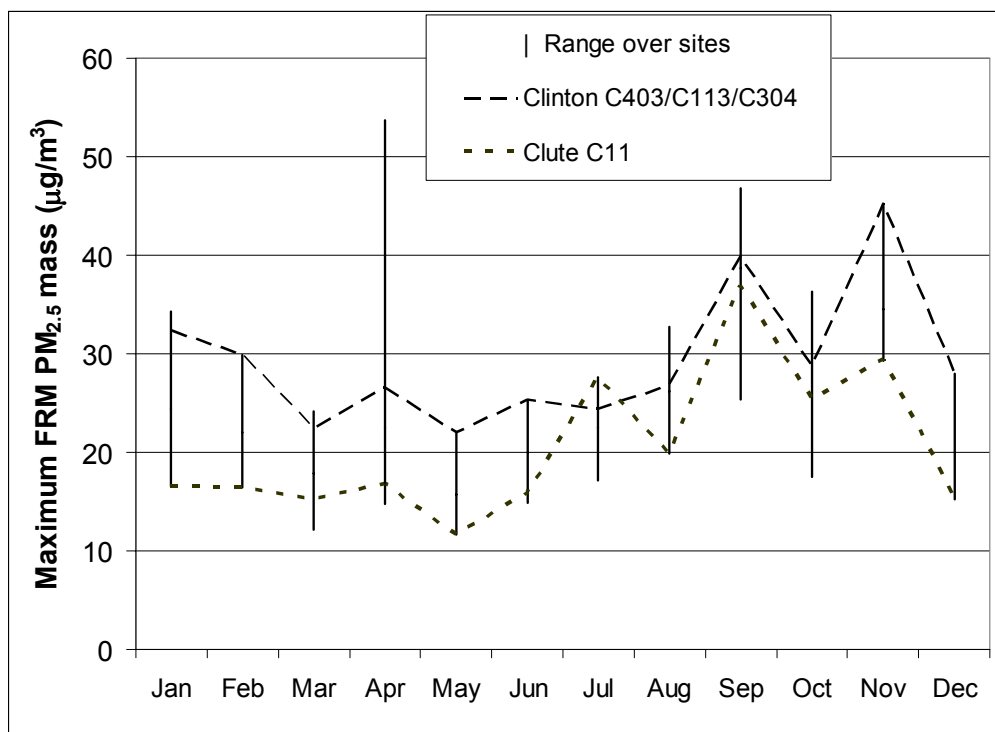


Figure 4.2. Monthly variations in maximum FRM mass concentrations. The vertical bars show the range between the lowest and highest maximum over all sites that were active during the entire two-year 2000-2001 period. Also shown are the maximum FRM mass concentrations for Clinton and Clute.

### ***TEOM Mass Analysis***

Many of the TEOM monitoring sites in Figure 3.1b began collecting data in February 2000. All TEOM analysis presented in this section is limited to the sites that were active during the entire two-year period beginning March 1st, 2000 and ending February 28th, 2002. This allows the use of two years of data for all sites in the analysis. These sites are Channelview, Conroe, Galveston, Hamshire, Deer Park 2 and Houston East. During this period, no site had less than 96% data completeness for any individual hour of the day. TEOM data provide valuable

information on diurnal variability in  $PM_{2.5}$  mass concentrations; however, as noted earlier, TEOM samplers result in different estimates of  $PM_{2.5}$  mass than FRM samplers. Figure 4.3 is a scatter plot of mean daily (24-hour average) TEOM mass concentrations to FRM mass concentrations for all date and site combinations where both 24 hours of valid TEOM data and a valid FRM mass concentration were available. The scatter plot shows that TEOM mass estimates tend to be lower than FRM filter based mass but that, at least in these data, the two measurements are generally consistent.

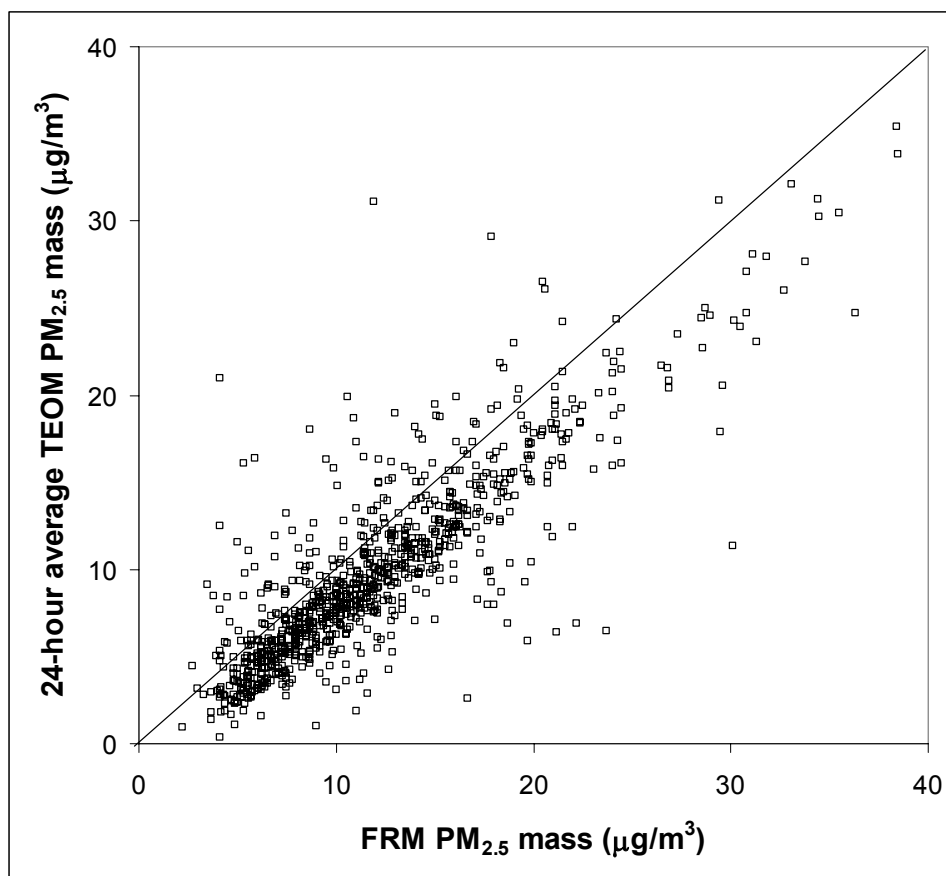


Figure 4.3. Mean daily TEOM mass (24-hour average) vs. FRM mass for all site/date combinations with 24 valid hourly TEOM mass concentrations and concurrent FRM mass concentrations. The data are limited to sites that were active during the entire March 2000 – February 2002 period.

Figure 4.4 shows the mean diurnal pattern of TEOM mass concentrations from hourly-averaged TEOM data. The mean for each hour is taken over all sites and dates. Also shown are the mean diurnal patterns for Houston East and Hamshire, which have the highest mean for any hour and lowest mean for any hour respectively. Similar to the FRM mass data, mean diurnal patterns are

remarkably similar for monitoring sites in very different settings and far removed from each other.

The most prominent feature of this diurnal pattern is the pronounced morning peak. This feature is present in the mean diurnal patterns of each individual site and in each individual month during the two-year period. Furthermore, the morning peak is independent of day of week and may occur between 5:00 am and 9:00 am. The 7:00 am mean TEOM mass concentration in Figure 4.4 is significantly different from the overall mean TEOM mass concentrations (all sites, all hours) at the 95% confidence level. Several hypotheses have been put forward to explain the morning maximum, including a strong traffic source, low mixing heights, and bursts of photochemical activity associated with sunrise. In evaluating these hypotheses, it should be noted that the morning maximum is observed at both rural and urban sites, sites close to roadways and far from roadways, and sites near the coast and inland (see Figure 3.1b for site locations).

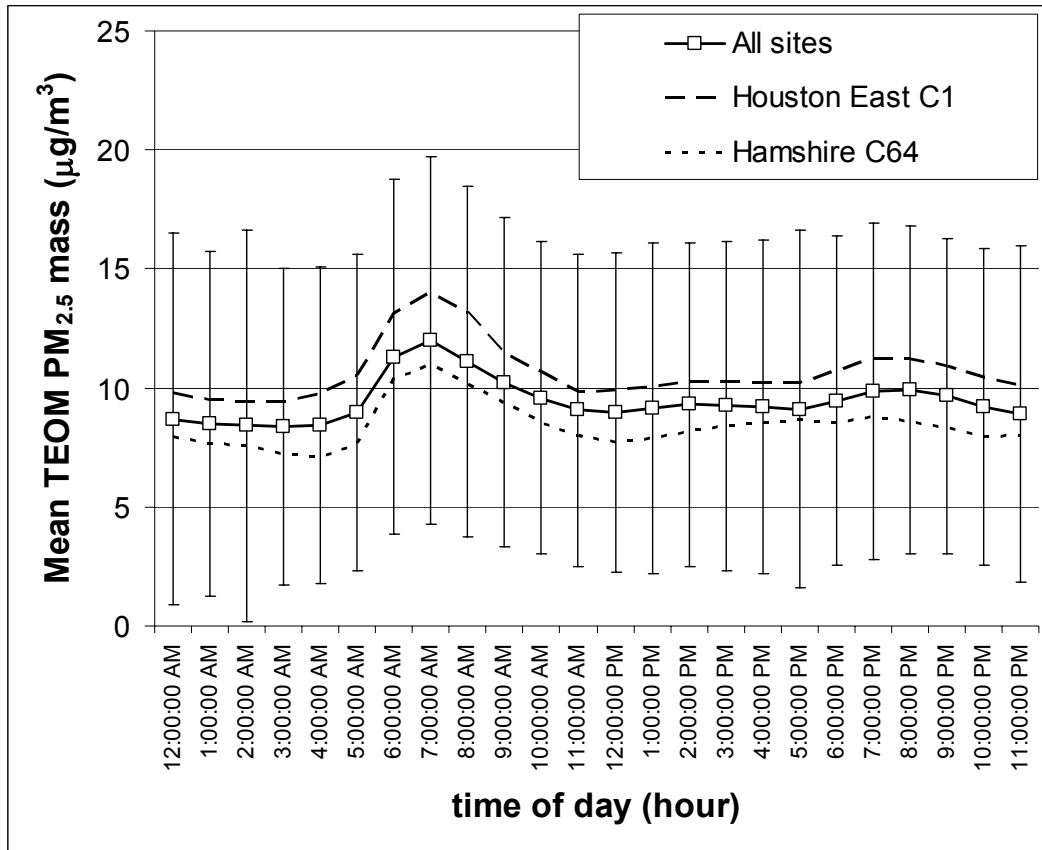


Figure 4.4. Mean diurnal pattern of TEOM mass concentrations from hourly-averaged TEOM data. The mean for each hour is taken over all sites and dates. The data are limited to sites that were active during the entire March 2000 – February 2002 period. Bars show one standard deviation for all data in that hour, i.e. both intersite and intrasite variability. Also shown are the mean diurnal patterns for Houston East and Hamshire (no bars shown for these individual sites).

Examination of mean diurnal patterns for individual sites and months also show an occasional secondary maximum that occurs in late afternoon and early evening that is less pronounced than the morning maximum. If the analysis of the diurnal data is just restricted to days with high mass concentrations (FRM

mass > 25  $\mu\text{g}/\text{m}^3$ ), the morning maximum is relatively weaker and the afternoon maximum is relatively stronger, but both are still present.

During the July to October period, when ozone concentrations are highest in Southeast Texas, mean diurnal  $\text{PM}_{2.5}$  patterns are generally similar to those in Figure 4.4. The afternoon secondary maximum is most prominent in the months of August and September at all sites, notably at the Conroe site, which is a downwind rural site. This may reflect a contribution from biogenic secondary organic aerosol as suggested by Lemire et al. (2002). However, this may also be a result of transport of SOA from upwind urban and industrial areas. Figure 4.5 shows mean diurnal  $\text{PM}_{2.5}$  and ozone patterns at Conroe for all days when maximum ozone is greater than 80 ppb at Conroe and for all days when maximum ozone is less than 80 ppb at Conroe (the choice of 80 ppb is arbitrary and is meant to separate high ozone days from low ozone days). Figure 4.5 provides further evidence that a fraction of the  $\text{PM}_{2.5}$  at Conroe is associated with photochemical activity and is likely SOA.

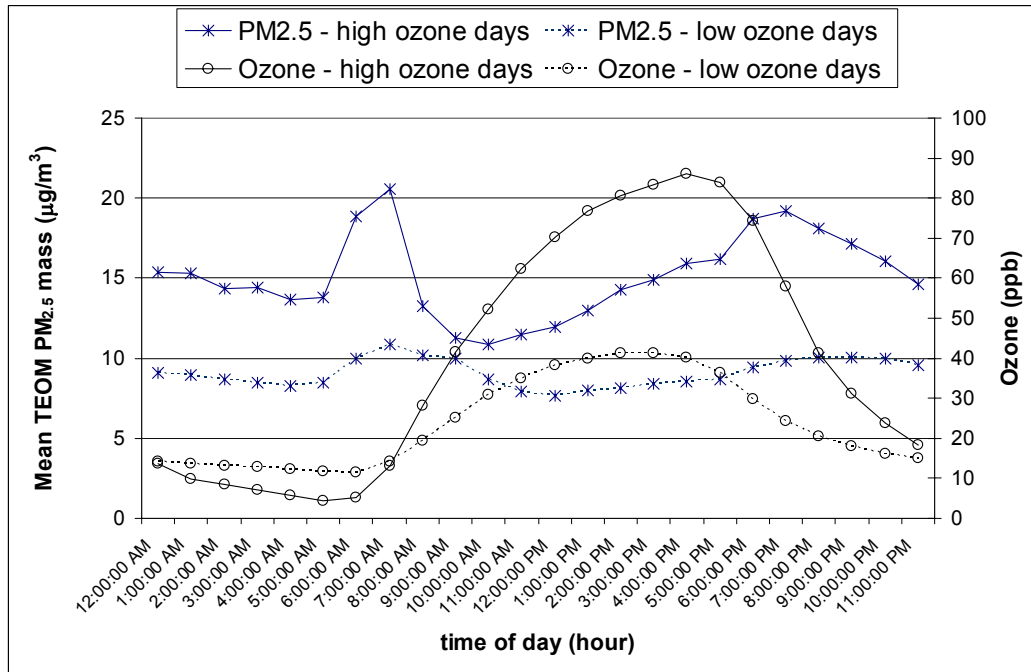


Figure 4.5. Mean diurnal patterns of PM<sub>2.5</sub> and ozone at the Conroe site on days when maximum ozone is greater than 80 ppb at Conroe (high ozone days) and on days when maximum ozone is less than 80 ppb at Conroe (low ozone days). The data are limited to the entire March 2000 – February 2002 period.

Aside from slight variations in the strength of the afternoon secondary PM<sub>2.5</sub> maximum at some sites, mean diurnal patterns suggest that, on average, PM<sub>2.5</sub> mass concentrations are spatially homogeneous throughout Southeast Texas. However, if data from individual days are examined, there are a number of instances when localized, high hourly TEOM mass concentrations are observed. The highest single-hour TEOM mass concentration in this dataset was 301 µg/m<sup>3</sup> at Hamshire, on October 13th, 2000, 2:00 am. High hourly TEOM mass events

are summarized using the two histograms in Figures 4.6a and Figure 4.6b. Figure 4.6a shows the frequency distribution of mean hourly TEOM mass concentrations (24- hour averaged) when maximum hourly TEOM mass exceeds  $40 \mu\text{g}/\text{m}^3$ . The analysis was limited to dates with 24 hours of valid TEOM mass concentrations. Figure 4.6a shows that on days with maximum hourly  $\text{PM}_{2.5}$  mass greater than  $40 \mu\text{g}/\text{m}^3$ , mean hourly concentrations tend to be above  $15 \mu\text{g}/\text{m}^3$  (or potentially higher if measured with an FRM sampler). These events are thus not only important from an acute exposure perspective, but also in determining compliance with the annual NAAQS. Note also that in this particular dataset, there are no 24-hour averaged TEOM mass concentrations that exceed the daily NAAQS for  $\text{PM}_{2.5}$ .

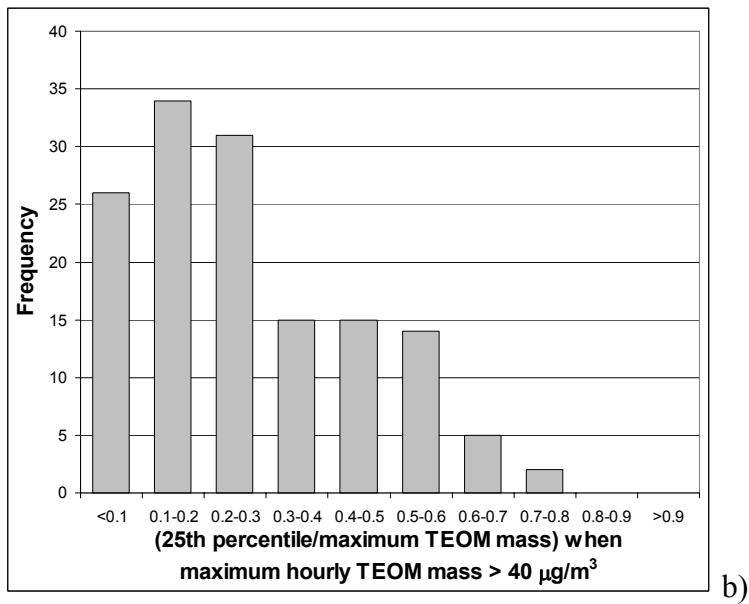
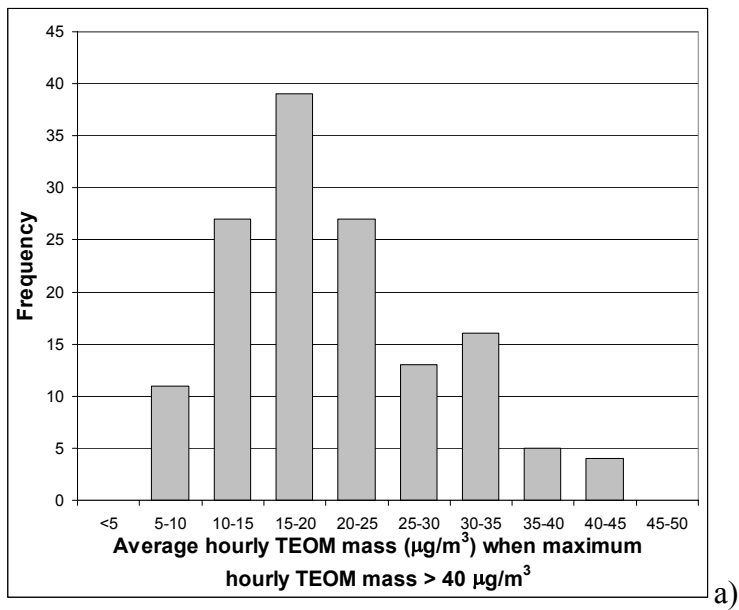


Figure 4.6. a) Frequency of mean hourly TEOM mass concentration (24 hour averaged) when the maximum hourly TEOM mass on that day exceeds 40 µg/m³. b) Frequency of the ratio of 25th percentile hourly TEOM mass to maximum hourly TEOM mass on days when the maximum hourly TEOM mass exceeds 40 µg/m³. The analysis was limited to dates with 24 hours of valid TEOM mass concentrations.

Figure 4.6b shows the frequency distribution of the ratio of 25th percentile hourly TEOM mass to maximum hourly TEOM mass when the maximum hourly TEOM mass exceeds  $40 \mu\text{g}/\text{m}^3$ . The analysis was limited to dates with 24 hours of valid TEOM mass concentrations. The [25th percentile hourly TEOM mass / maximum hourly TEOM mass] ratio is a measure of the daily variation in hourly average TEOM mass at a given location on a given day. A low ratio represents a large difference in daily maximum and 25th percentile values and is used here to represent days when short-lived  $\text{PM}_{2.5}$  episodes may occur. Figure 4.6b suggests that unusually high hourly  $\text{PM}_{2.5}$  mass events tend to be relatively short-lived.

#### ***Spatial distribution of FRM mass***

The local versus regional nature of events with high  $\text{PM}_{2.5}$  concentrations can be characterized by examining the spatial variation of FRM mass concentrations on a given day. Figure 4.7a shows the ratio of 25th percentile FRM mass (over all sites) to the FRM mass at the site with the highest concentration for that day, plotted versus maximum FRM mass for the day. The 25th percentile and maximum are taken over all the monitoring sites on a given day with at least 5 valid FRM mass measurements. A high value of this ratio indicates that at least 75% of monitors were recording similar concentrations. A low value of this ratio indicates large spatial variation in FRM mass. Figure 4.7b shows the distribution of values of the [25th percentile FRM mass / maximum FRM mass] ratio. The data in Figures 4.7a and 4.7b suggest that on many days with high FRM mass concentrations ( $>15 \mu\text{g}/\text{m}^3$ ), roughly equal numbers of days have values above 0.7

and below 0.5. This suggests that both regional and localized events occur frequently and are important in determining compliance with the NAAQS.

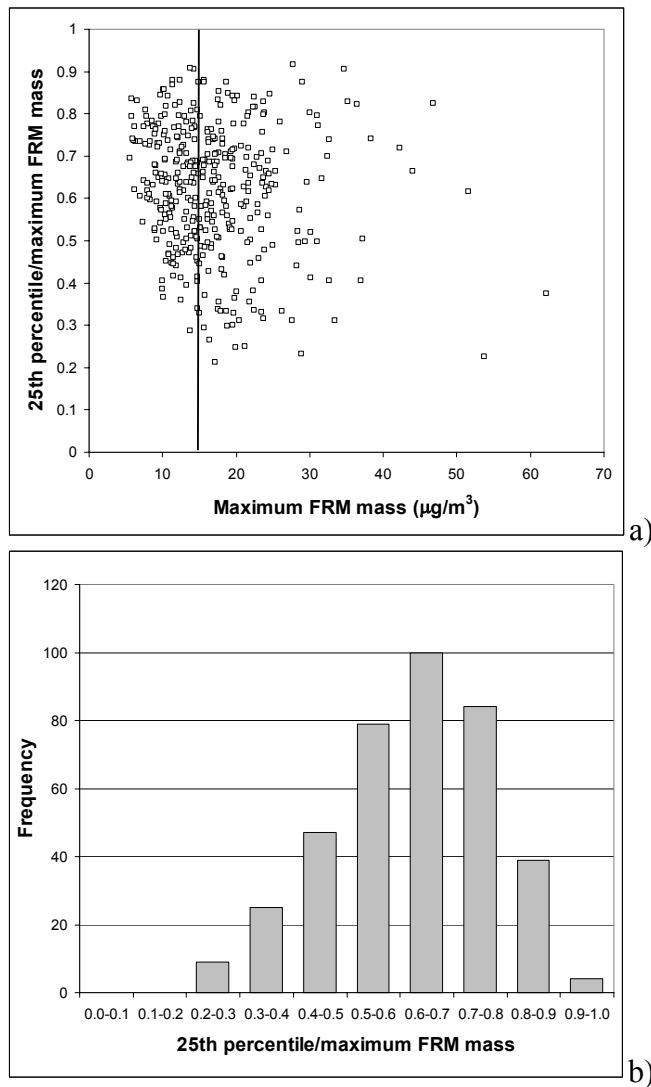


Figure 4.7. a) Ratio of 25th percentile FRM mass to maximum FRM mass, versus maximum FRM mass for a given day. The 25th percentile and maximum are taken over all the monitoring sites on a given day with at least 5 valid FRM mass measurements. b) Distribution of the values of the ratio of 25th percentile FRM mass to maximum FRM mass.

Further insight into the frequency of local versus regional PM<sub>2.5</sub> events can be gained by plotting air parcel back trajectories. Forty-eight hour back trajectories starting at midday on the day of interest in the Houston Ship Channel area were simulated using the HYSPLIT model (HYSPLIT4, 1997) for two subsets of data. The first subset includes dates where maximum FRM concentration is greater than 20 µg/m<sup>3</sup> and where the ratio on the y-axis of Figure 4.7a is greater than 0.7. These dates are expected to be regional PM<sub>2.5</sub> events since there is little spatial variation in FRM mass. These trajectories are shown in Figure 4.8. The second subset includes dates where maximum FRM mass concentration is greater than 20 µg/m<sup>3</sup> and where the ratio on the y-axis in Figure 4.7a is less than 0.5. These dates are expected to be local PM<sub>2.5</sub> events since there is large spatial variation in FRM mass. These trajectories are shown in Figure 4.9. When FRM mass tends to be high and spatially homogeneous in Southeast Texas, synoptic scale winds, as predicted by 48 hour back trajectories, tend to come from the east or northeast. This suggests that high levels of background PM<sub>2.5</sub> are advected into Southeast Texas from the eastern half of North America. In contrast, when FRM mass is high but the stations recording high mass concentrations are isolated, suggesting local source contributions, synoptic scale winds may come from any direction and preferentially come from the South-Southeast.

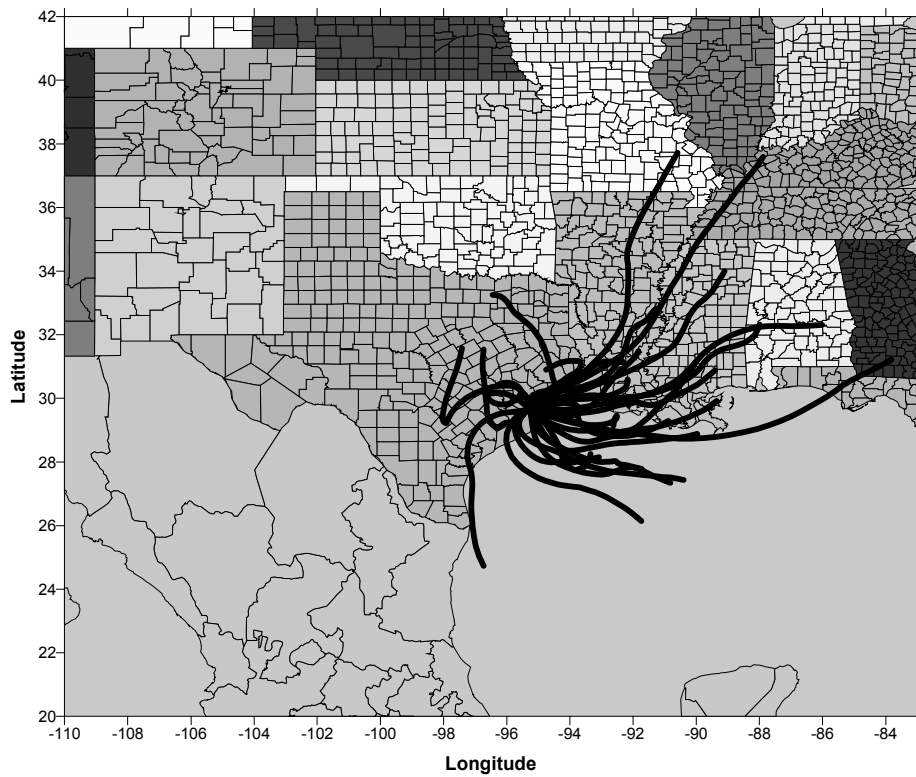


Figure 4.8. Forty-eight hour back trajectories calculated using the HYSPLIT model, for days when maximum FRM concentration observed in the region was greater than  $20 \mu\text{g}/\text{m}^3$  and all monitors recorded relatively high concentrations (regional events).

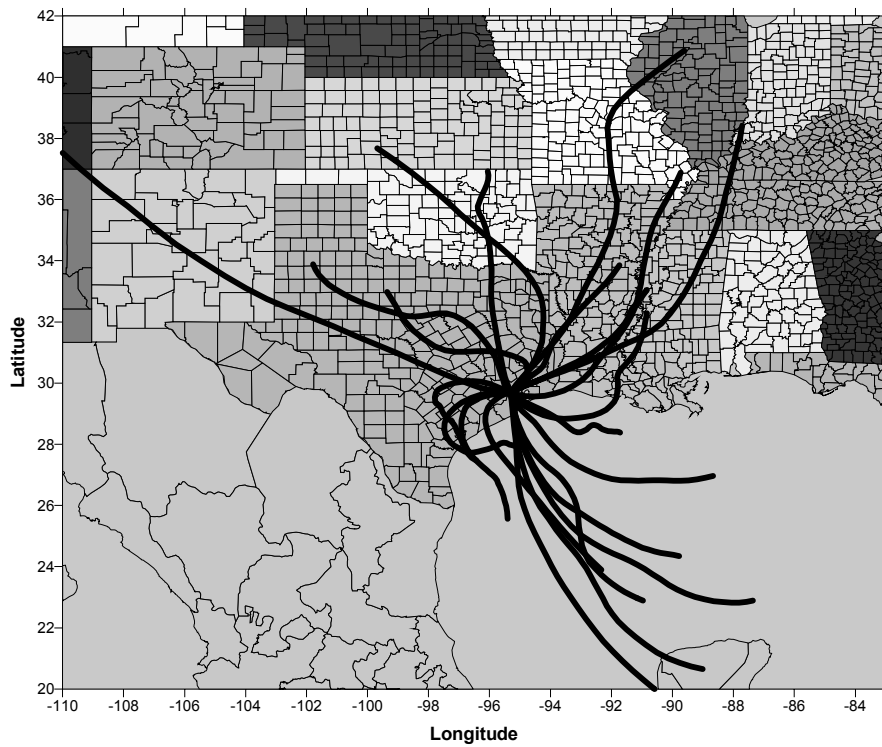


Figure 4.9: Forty-eight hour back trajectories calculated using the HYSPLIT model, for days when maximum FRM concentration observed in the region are greater than  $20 \mu\text{g}/\text{m}^3$  and at least some monitors recorded low mass concentrations (local events)

Air advected into Southeast Texas from the Gulf of Mexico is expected to have a lower background level of  $\text{PM}_{2.5}$  than air from the continent. Although there is a clear directional preference to the trajectories in Figure 4.8, there are also a higher number of shorter trajectories compared to Figure 4.9. If short trajectories are indicative of lower wind speeds, this may indicate region-wide accumulation of  $\text{PM}_{2.5}$  pollutants. These trajectories and the data in Figures 4.7a and 4.7b do suggest, however, that both regional and local sources are important contributors to  $\text{PM}_{2.5}$  pollution in Southeast Texas.

### ***FRM composition analysis***

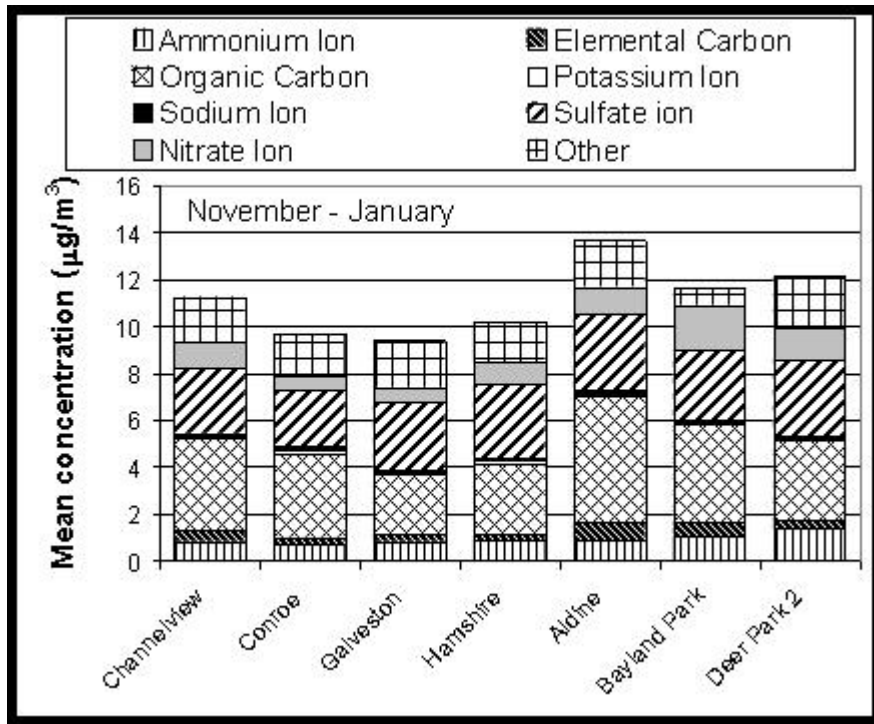
Further insight into the sources of fine particulate matter requires an examination of particle composition. Many of the speciation sites for PM<sub>2.5</sub> began collecting data in August 2000. All speciation analysis presented in this section is limited to the sites that were active during the entire two-year period beginning September 1st, 2000 and ending August 31st, 2002. This allows the use of two years of data for all sites in the speciation analysis, similar to the FRM mass and TEOM mass analysis. These sites are Channelview, Conroe, Galveston, Hamshire, Aldine, Bayland Park and Deer Park 2.

Mean component concentrations (+/- standard deviation) over all sites and dates are: ammonium ion 0.97 +/- 0.82 µg/m<sup>3</sup>, elemental carbon 0.37 +/- 0.25 µg/m<sup>3</sup>, organic carbon 3.32 +/- 2.07 µg/m<sup>3</sup>, potassium ion 0.07 +/- 0.15 µg/m<sup>3</sup>, sodium ion 0.17 +/- 0.16 µg/m<sup>3</sup>, sulfate ion 3.54 +/- 2.43 µg/m<sup>3</sup>, nitrate ion 0.62 +/- 0.70 µg/m<sup>3</sup>. The mean total PM<sub>2.5</sub> mass over this same dataset is 11.22 +/- 6.39 µg/m<sup>3</sup>. This is consistent with average composition found in the study by Tropp et al. (1998).

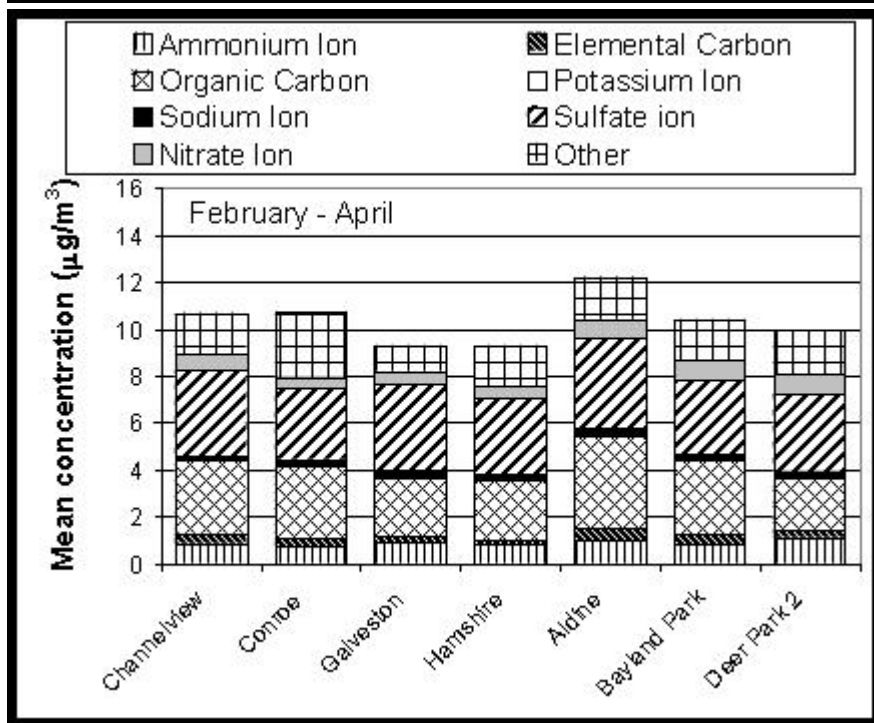
Figures 4.10a-d shows the mean concentrations of the major components of the 24-hour averaged PM<sub>2.5</sub> by site and season, where season is classified into periods of February-April, May-July, August-October or November-January. The difference between the sum of the mean component concentrations and the mean total mass concentration is classified as 'other', such that the total height of each column in Figure 4.10 equals the mean total PM<sub>2.5</sub> mass concentration for that site and season. In reality, the 'other' category represents the sum of all chemical

components that are not explicitly included in the Figure 4.10. Note that organic carbon is not adjusted to account for the non-carbon mass associated with the organic matter. The relative amount of organic mass to organic carbon mass is a source of some debate, but is typically assigned a value of 1.2-1.6 (Seinfeld and Pandis 1998). In this analysis, non-carbon organic matter is assumed to be included in the 'other' category. It is also important to note that estimates of total mass from a filter sample may not add up to the sum of the individual component masses due to various sampling and analyses artifacts. These differences are also included in the 'other' category.

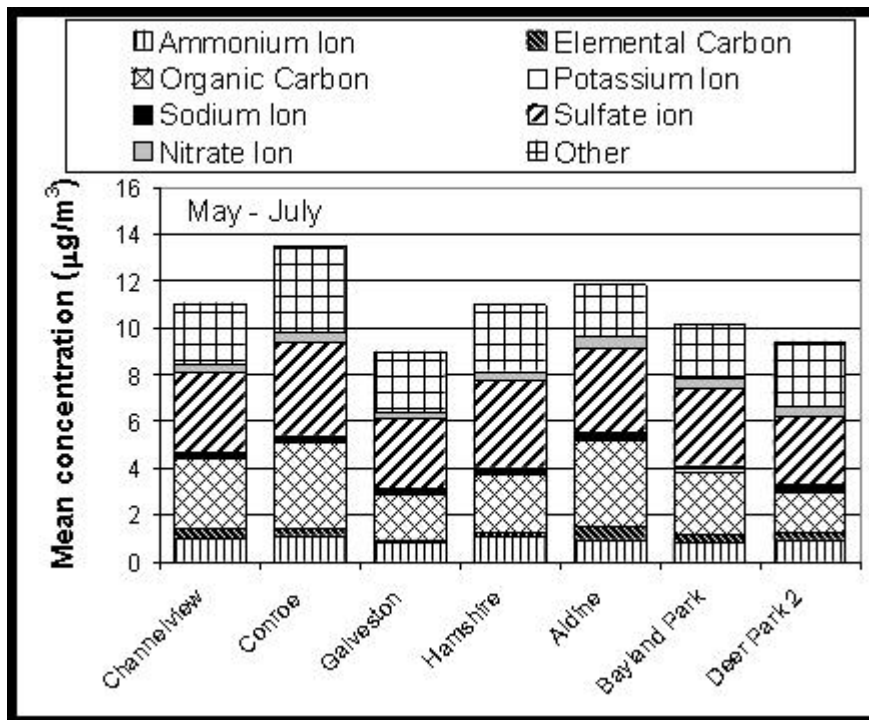
Figure 4.10 shows that, similar to the FRM mass and TEOM mass data, the bulk composition is generally similar between sites in very different settings and far removed from each other. The relative amounts of the major components to total mass also do not vary considerably by season. Bulk composition was also calculated for the subset of data when FRM mass is greater than  $25 \mu\text{g}/\text{m}^3$ . In this case, the bulk composition is nearly identical by site to the bulk composition shown in Figure 4.10. This suggests that  $\text{PM}_{2.5}$  composition, on average, is independent of total  $\text{PM}_{2.5}$  mass and does not vary significantly over the year. Once again, however, while average compositions show seasonal and spatial homogeneity, individual days can show great variability from mean values.



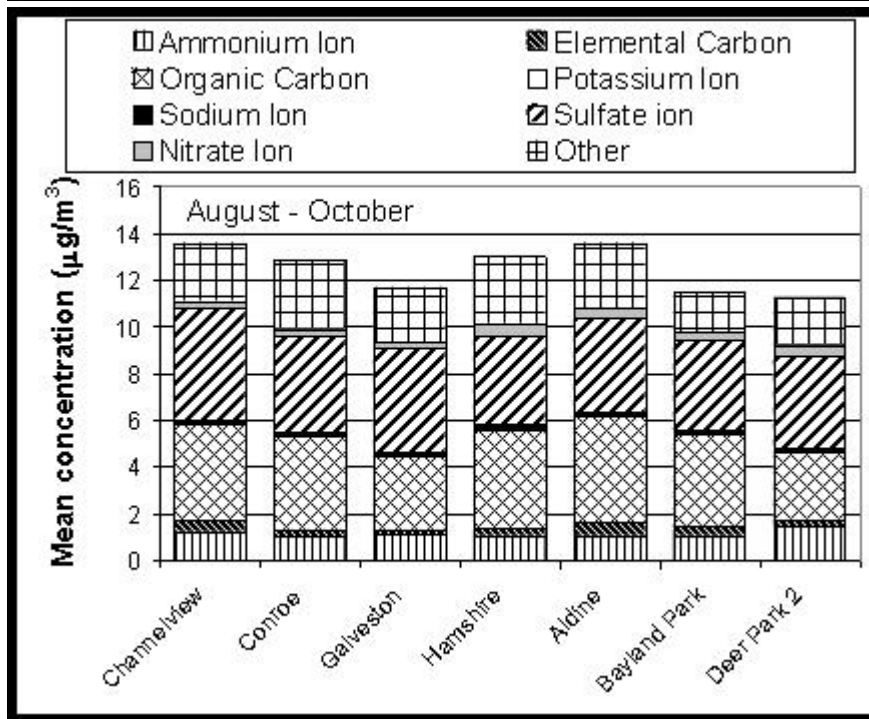
a)



b)



c)



d)

Figure 4.10. (Preceding Pages) Mean composition of PM<sub>2.5</sub> during a) November-January, b) February-April, c) May-July and d) August-October. The difference between the sum of the major component concentrations and the total mass concentration is classified as ‘other’, such that the total height of each column equals the mean total PM<sub>2.5</sub> mass concentration for that site and season. Data are limited to the sites that were active during the entire two-year period beginning September 1st, 2000 and ending August 31st, 2002.

Sulfate and organic carbon are the two largest contributors by mass to PM<sub>2.5</sub> at all sites, in all seasons. On average, sulfate accounts for approximately 32% of fine particulate mass, and while this fraction is variable on a daily basis, sulfate fractions do not dramatically increase or decrease with FRM mass concentrations in this data set. Mean sulfate mass by month tends to be higher in fall and spring and this seasonality is slightly stronger than that of the mean FRM mass. On average, organic carbon accounts for approximately 31% of fine particulate mass. As with sulfate, organic carbon fractions do not dramatically increase or decrease with FRM mass concentrations. Organic carbon concentrations have a stronger seasonality than FRM mass, with the highest concentrations in the late fall.

A cation-anion balance, based on the chemical composition data, can be used to assess the overall acidity of the particulate matter samples. Since nitrate mass in Southeast Texas is low, it is expected that the majority of the ammonium neutralizes sulfate to form either ammonium sulfate ((NH<sub>4</sub>)<sub>2</sub>SO<sub>4</sub>) or ammonium bisulfate (NH<sub>4</sub>HSO<sub>4</sub>). Assuming all sulfate is present as SO<sub>4</sub><sup>2-</sup> and converting to microequivalents per cubic meter, the mean charge balance ratio of ammonium to sulfate is 0.72 +/- 0.27 (standard deviation). This ratio is taken over all dates/sites with valid ammonium and sulfate concentrations and is limited to the sites that

were active during the entire two-year period beginning September 1st, 2000 and ending August 31st, 2002. The ratio suggests that on average the ammonium is entirely taken up in neutralizing sulfate. The excess sulfate may be neutralized by other cations or may make the aerosol acidic. Sodium from sea salt may be important as an additional cation in Southeast Texas given the proximity to the coast. To assess the significance of sodium cations in the charge balance, the ratio of [ammonium + sodium] to sulfate was calculated. Note there are fewer valid sodium concentrations in the dataset, so the ratio of ammonium to sulfate is recalculated using only dates/sites with valid ammonium, sulfate and sodium concentrations. The ammonium to sulfate ratio becomes 0.85 +/- 0.17. If sodium is added to the calculation, the [ammonium + sodium] to sulfate ratio increases to 0.99 +/- 0.17. If the only source of sodium cation is sea salt, then the data also suggest that chloride displacement by sulfate occurs to a significant extent.

The data presented in this section suggests that PM<sub>2.5</sub> is close to violating the NAAQS in Southeast Texas. Furthermore, PM<sub>2.5</sub> mass concentrations and diurnal patterns, and PM<sub>2.5</sub> composition are relatively consistent from site to site and from season to season. Analysis also suggests that both regional and local sources are important in determining PM<sub>2.5</sub> concentrations. Although this analysis is limited to two years, it is the most extensive analysis of PM<sub>2.5</sub> in the area to date. The most important finding for this research is that organic carbon is consistently one of the two largest mass components of PM<sub>2.5</sub> (tied with sulfate). The following sections will present results on the relative importance of primary and secondary OC to PM<sub>2.5</sub> in Southeast Texas.

## 4.2 SOA Empirical model

Results in the previous section indicate that OC is one of the largest fractions of  $PM_{2.5}$  at all sites and during all seasons in Southeast Texas. The data presented in this section quantify the relative amounts of primary vs. secondary OC in Southeast Texas. This section is organized into four sub-sections: seasonal and spatial trends in EC and total OC, seasonal and spatial trends in primary and secondary OC, secondary OC and ozone scatter plots, and estimates of secondary and primary OC during the TXAQS modeling episode. Finally a brief section summarizes the main findings of the  $PM_{2.5}$  data analysis.

### *Seasonal and spatial trends in total OC and EC.*

Before presenting the model for primary and secondary OC, it is useful to examine seasonal and spatial trends in total OC and EC. This analysis was limited to the six speciation sites in Table 3.2 with data over the full two-year period of 8/15/2000 to 8/15/2002. Table 4.2 shows mean OC, EC and fractions of OC and EC of total PM mass for each site. The data in Table 4.2 suggest that although mean OC and EC concentrations can vary by site, the contribution of each to  $PM_{2.5}$  mass is on average spatially homogeneous. Note that the highest mean OC and EC concentrations occur at Aldine, which is an urban site that is influenced by local primary emissions from nearby roadways and residences. The lowest mean OC and EC occur at Galveston, a coastal site removed from the major urban and industrial centers of Houston. Note also that the rural sites of Hamshire and

Conroe have higher mean OC concentrations than the industrial Deer Park monitoring site. The higher OC at the rural sites may indicate a contribution from secondary OC in photochemically aged air parcels.

Table 4.2: Mean OC, EC and fractions of OC and EC in total PM<sub>2.5</sub> for six sites in Southeast Texas. Means are taken over the two-year period 8/15/2000 through 8/15/2002.

Site	Organic Carbon (OC) $\mu\text{g}/\text{m}^3$		Elemental Carbon (EC) $\mu\text{g}/\text{m}^3$		OC/( PM <sub>2.5</sub> mass)		EC/( PM <sub>2.5</sub> mass)	
	mean	std dev	mean	std dev	mean	std dev	mean	std dev
Conroe	3.62	<i>1.76</i>	0.32	<i>0.19</i>	0.33	<i>0.14</i>	0.04	<i>0.06</i>
Galveston	2.43	<i>1.62</i>	0.23	<i>0.14</i>	0.26	<i>0.11</i>	0.03	<i>0.03</i>
Hamshire	3.10	<i>2.13</i>	0.26	<i>0.19</i>	0.29	<i>0.10</i>	0.03	<i>0.01</i>
Aldine	4.33	<i>2.18</i>	0.57	<i>0.32</i>	0.33	<i>0.11</i>	0.05	<i>0.07</i>
Bayland Prk	3.51	<i>1.97</i>	0.42	<i>0.25</i>	0.33	<i>0.11</i>	0.04	<i>0.02</i>
Deer Park	2.56	<i>1.80</i>	0.32	<i>0.15</i>	0.24	<i>0.10</i>	0.04	<i>0.03</i>

Seasonal fluctuations in OC and EC are shown in Figure 4.11. The top portion of the Figure shows mean OC concentration by month over all sites and at Aldine and Galveston, the sites with the highest and lowest average concentrations. The seasonal pattern for monthly mean OC is similar at all monitoring sites. The highest monthly mean concentration for each site occurs between September and December and this maximum is significantly different from the overall mean at each site (using a t-test between monthly mean and overall mean at the 95% confidence level). The bottom portion of Figure 4.11 shows mean EC concentration by month over all sites and at Aldine and Galveston.

As with OC, the seasonal variations in monthly mean EC concentrations are very similar from site to site. Highest monthly mean EC concentrations occur in November at every site except Hamshire (October) and are significantly different from the overall mean EC concentration at each site (using a t-test between monthly mean and overall mean at the 95% confidence level). Seasonal variations in monthly mean ratios of OC/ PM<sub>2.5</sub> and EC/ PM<sub>2.5</sub> are less pronounced than those for OC and EC concentrations. Monthly mean OC/ PM<sub>2.5</sub> is significantly higher between September and December than the overall mean OC/ PM<sub>2.5</sub> at all sites (using a t-test between monthly mean and overall mean at the 95% confidence level). Monthly mean EC/ PM<sub>2.5</sub> ratios were highest between September and April; however, the highest monthly mean EC/ PM<sub>2.5</sub> at most sites is not significantly different from the overall mean.

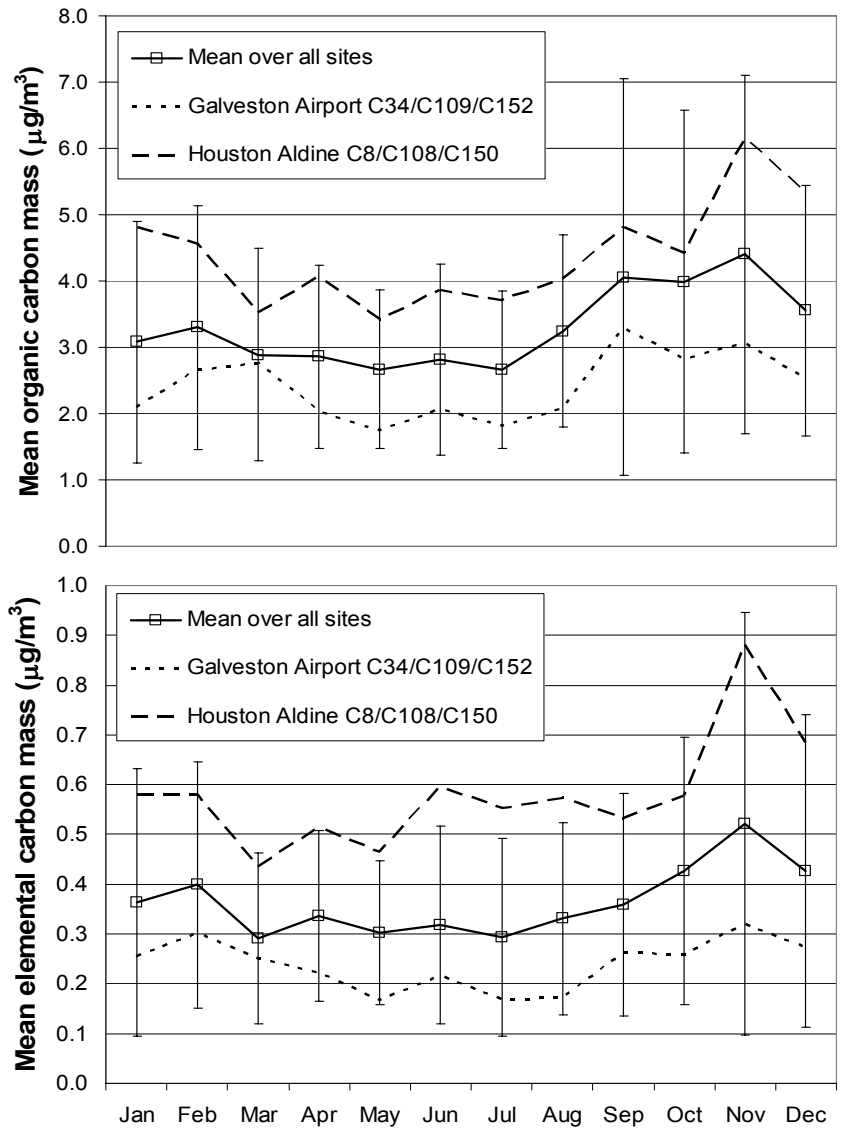


Figure 4.11: Monthly mean OC (top) and EC (bottom) concentrations over all six monitoring sites with valid data for the two-year 8/15/2000 – 8/15/2002 period. Error bars represent one standard deviation from the mean over all sites, i.e. showing inter- and intra-site variability. Monthly mean OC and EC are also shown for both Aldine and Galveston which recorded the highest and lowest overall mean OC and EC respectively. There are no error bars reported for these sites.

### ***SOA empirical model results***

The methods to develop the SOA empirical model (section 3.2) were used to estimate primary and secondary OC. Table 4.3 shows monthly mean primary OC by site, both the regression primary OC and the lower bound primary OC. Table 4.4 shows monthly mean secondary OC by site, both the regression secondary OC and upper bound secondary OC. Figure 4.12 shows mean monthly, regression secondary OC and regression primary OC. (i.e. Figure 4.12 shows graphically the same data that is in Tables 4.3a and 4.4a.) Figure 4.13 shows mean monthly, upper bound secondary OC and lower bound primary OC. (i.e. Figure 4.13 shows graphically the same data that is in Tables 4.3b and 4.4b.) These two figures show data for the five sites that had significant regressions for the full dataset, and for the Conroe site. The regression equation for the Conroe site in March-October was significant at the 80% confidence level; however, this site was included because it represents a location with significant local biogenic emissions and is useful for comparing to urban/industrial sites. The regression equations for all other data shown in Figures 4.12 and 4.13 were significant at 90% confidence level or greater, including Conroe during the November-January period.

With the exception of Galveston, highest primary OC tends to occur in the winter months, which is also the season when concentrations of other primary pollutants, such as NO<sub>x</sub> and CO, are highest in Southeast Texas. Higher primary OC might be due to seasonal variations in emissions composition or strengths from certain sources. The higher primary OC at Aldine, Bayland Park and Deer

Park are consistent with these sites being closer to primary sources compared to Hamshire and Galveston. The higher primary OC in winter is also consistent with higher EC seen in the winter months.

Primary OC, averaged over a year period, is clearly a larger fraction of OC than secondary OC in this dataset. Secondary OC is highest in September, and roughly equivalent to primary OC concentrations for this month when considering upper-bound concentrations. September is at the height of the ozone season in Southeast Texas and this is consistent with photochemical activity that would lead to secondary OC formation. As with primary OC, monthly mean secondary OC maxima are higher at sites closer to emissions sources (Aldine, Bayland Park, Deer Park) compared to remote locations (Galveston, Hamshire). This suggests that anthropogenic emissions may be important secondary OC precursors. The exception to this is the rural Conroe site, which has a monthly maximum secondary OC concentration equivalent to the urban/industrial sites. The increased mean total OC seen in fall and early winter (see previous section 4.2.1) is probably a result of both primary and secondary OC. This analysis does suggest that both primary and secondary OC are important to fine PM concentrations in Southeast Texas.

Table 4.3. Mean **primary** OC by month. a) Regression primary OC. b) Lower bound primary OC. Italics indicate the standard deviation of each estimate. Data for which the initial regression was not valid are not included. Bold numbers indicate the month with the highest mean primary OC for that site (only for sites when all months of data are available).

a)

Site	Jan	Feb	Mar	Apr	May	Jun	Jul	Aug	Sep	Oct	Nov	Dec
Channelview	2.96 <i>0.52</i>	2.95 <i>0.31</i>									2.99 <i>1.16</i>	2.54 <i>0.50</i>
Conroe	2.77 <i>1.13</i>	2.54 <i>1.90</i>									3.90 <i>1.97</i>	3.13 <i>1.47</i>
Galveston	1.55 <i>0.55</i>	<b>2.14</b> <i>0.80</i>	1.54 <i>0.23</i>	1.56 <i>0.43</i>	1.01 <i>0.22</i>	1.65 <i>0.27</i>	1.46 <i>0.38</i>	1.53 <i>0.31</i>	1.94 <i>0.84</i>	1.88 <i>0.51</i>	2.07 <i>1.44</i>	1.70 <i>0.66</i>
Hamshire	2.26 <i>0.51</i>	2.02 <i>0.74</i>	1.73 <i>0.23</i>	1.78 <i>0.23</i>	1.86 <i>0.21</i>	1.79 <i>0.24</i>	1.84 <i>0.17</i>	1.94 <i>0.22</i>	1.95 <i>0.18</i>	1.94 <i>0.10</i>	<b>2.41</b> <i>0.57</i>	1.94 <i>0.58</i>
Aldine	<b>4.72</b> <i>4.46</i>	3.21 <i>1.06</i>	2.39 <i>0.55</i>	2.74 <i>0.39</i>	2.65 <i>0.27</i>	2.88 <i>0.34</i>	2.89 <i>0.32</i>	2.85 <i>0.24</i>	2.68 <i>0.32</i>	2.80 <i>0.64</i>	4.36 <i>2.82</i>	3.18 <i>0.73</i>
Bayland Park	2.78 <i>0.73</i>	2.34 <i>0.56</i>	2.23 <i>0.46</i>	2.53 <i>0.63</i>	2.35 <i>0.43</i>	2.39 <i>0.46</i>	2.25 <i>0.32</i>	2.38 <i>0.44</i>	2.65 <i>0.66</i>	2.69 <i>0.55</i>	<b>3.74</b> <i>1.73</i>	3.09 <i>0.86</i>
Deer Park 2	1.83 <i>1.10</i>	1.56 <i>0.26</i>	1.26 <i>0.15</i>	1.18 <i>0.23</i>	1.20 <i>0.15</i>	1.28 <i>0.23</i>	1.36 <i>0.37</i>	1.35 <i>0.20</i>	1.46 <i>0.52</i>	1.57 <i>0.28</i>	<b>3.86</b> <i>1.81</i>	1.88 <i>0.89</i>
HRM-3			2.26 <i>0.24</i>	2.13 <i>0.74</i>	2.16 <i>0.26</i>	2.66 <i>0.67</i>	2.49 <i>0.33</i>	2.62 <i>0.32</i>	2.55 <i>0.51</i>	2.50 <i>0.15</i>		
Mauriceville	2.06 <i>0.42</i>	2.55 <i>0.88</i>									3.61 <i>1.23</i>	2.81 <i>0.98</i>

b)

Site	Jan	Feb	Mar	Apr	May	Jun	Jul	Aug	Sep	Oct	Nov	Dec
Channelview	2.18 <i>0.21</i>	2.11 <i>0.15</i>									2.26 <i>0.48</i>	1.98 <i>0.15</i>
Conroe	2.50 <i>1.15</i>	2.14 <i>1.61</i>									3.32 <i>1.77</i>	2.72 <i>1.40</i>
Galveston	1.25 <i>0.42</i>	1.71 <i>0.67</i>	1.41 <i>0.19</i>	1.41 <i>0.35</i>	0.97 <i>0.22</i>	1.48 <i>0.23</i>	1.33 <i>0.32</i>	1.37 <i>0.27</i>	<b>1.74</b> <i>0.73</i>	1.67 <i>0.44</i>	1.61 <i>1.09</i>	1.33 <i>0.52</i>
Hamshire	1.93 <i>0.35</i>	1.72 <i>0.53</i>	1.56 <i>0.11</i>	1.58 <i>0.13</i>	1.63 <i>0.07</i>	1.59 <i>0.13</i>	1.61 <i>0.07</i>	1.67 <i>0.10</i>	1.65 <i>0.08</i>	1.64 <i>0.04</i>	<b>2.03</b> <i>0.41</i>	1.67 <i>0.52</i>
Aldine	<b>4.21</b> <i>3.88</i>	2.86 <i>0.92</i>	1.95 <i>0.37</i>	2.08 <i>0.20</i>	2.06 <i>0.08</i>	2.15 <i>0.16</i>	2.17 <i>0.19</i>	2.13 <i>0.12</i>	2.08 <i>0.13</i>	2.08 <i>0.40</i>	3.86 <i>2.51</i>	2.75 <i>0.65</i>
Bayland Park	2.39 <i>0.57</i>	1.99 <i>0.51</i>	1.61 <i>0.17</i>	1.83 <i>0.27</i>	1.71 <i>0.17</i>	1.64 <i>0.23</i>	1.53 <i>0.18</i>	1.63 <i>0.24</i>	1.80 <i>0.37</i>	1.81 <i>0.29</i>	<b>3.14</b> <i>1.40</i>	2.60 <i>0.72</i>
Deer Park 2	1.29 <i>0.80</i>	1.14 <i>0.27</i>	0.94 <i>0.12</i>	0.93 <i>0.14</i>	0.93 <i>0.07</i>	0.97 <i>0.15</i>	1.09 <i>0.22</i>	1.02 <i>0.13</i>	1.12 <i>0.37</i>	1.17 <i>0.21</i>	<b>3.12</b> <i>1.36</i>	1.22 <i>0.68</i>
HRM-3			1.67 <i>0.16</i>	1.64 <i>0.42</i>	1.63 <i>0.17</i>	2.01 <i>0.42</i>	1.86 <i>0.24</i>	1.91 <i>0.22</i>	1.89 <i>0.35</i>	1.83 <i>0.11</i>		
Mauriceville	1.82 <i>0.30</i>	2.17 <i>0.75</i>									3.08 <i>1.08</i>	2.43 <i>0.81</i>

Table 4.4: Mean **secondary** OC by month. a) Regression secondary OC. b) Upper bound secondary OC. Italics indicate the standard deviation of each estimate. Data for which the initial regression was not valid are not included. Bold numbers indicate the month with the highest mean secondary OC for that site (only for sites when all months of data are available).

a)

Site	Jan	Feb	Mar	Apr	May	Jun	Jul	Aug	Sep	Oct	Nov	Dec
Channelview	0.39 <i>0.42</i>	0.78 <i>1.43</i>									2.83 <i>3.87</i>	0.19 <i>0.26</i>
Conroe	0.13 <i>0.36</i>	0.52 <i>0.60</i>									1.31 <i>1.54</i>	0.68 <i>0.85</i>
Galveston	0.21 <i>0.31</i>	0.52 <i>0.83</i>	0.74 <i>0.70</i>	0.37 <i>0.55</i>	0.19 <i>0.40</i>	0.36 <i>0.50</i>	0.24 <i>0.29</i>	0.64 <i>0.84</i>	<b>1.88</b> <i>2.35</i>	0.87 <i>0.92</i>	0.78 <i>1.15</i>	0.18 <i>0.31</i>
Hamshire	0.22 <i>0.28</i>	0.31 <i>0.75</i>	1.09 <i>1.92</i>	0.36 <i>0.59</i>	0.58 <i>0.73</i>	0.64 <i>1.03</i>	0.68 <i>0.98</i>	1.36 <i>1.37</i>	<b>1.64</b> <i>1.11</i>	1.31 <i>1.08</i>	0.54 <i>0.76</i>	0.18 <i>0.39</i>
Aldine	0.12 <i>0.23</i>	0.26 <i>0.45</i>	0.86 <i>1.23</i>	1.03 <i>0.92</i>	0.71 <i>0.79</i>	1.01 <i>0.96</i>	0.85 <i>0.59</i>	1.18 <i>0.97</i>	<b>2.38</b> <i>2.71</i>	2.16 <i>2.07</i>	0.56 <i>1.19</i>	0.47 <i>0.43</i>
Bayland Park	0.24 <i>0.33</i>	0.37 <i>0.59</i>	0.62 <i>0.61</i>	0.83 <i>0.95</i>	0.32 <i>0.50</i>	0.64 <i>1.03</i>	0.55 <i>1.01</i>	1.02 <i>1.12</i>	<b>2.28</b> <i>3.63</i>	1.03 <i>1.11</i>	0.73 <i>1.18</i>	0.30 <i>0.31</i>
Deer Park 2	0.23 <i>0.30</i>	0.36 <i>0.59</i>	0.97 <i>1.03</i>	0.53 <i>0.65</i>	0.40 <i>0.58</i>	0.35 <i>0.81</i>	0.47 <i>0.68</i>	1.72 <i>1.38</i>	<b>3.08</b> <i>4.75</i>	1.61 <i>1.92</i>	0.81 <i>1.40</i>	0.12 <i>0.22</i>
HRM-3			1.31 <i>0.76</i>	1.02 <i>0.81</i>	0.52 <i>0.88</i>	0.87 <i>0.95</i>	0.20 <i>0.23</i>	1.10 <i>1.23</i>	<b>1.46</b> <i>1.22</i>	2.48 <i>2.10</i>		
Mauriceville	0.06 <i>0.07</i>	0.81 <i>1.02</i>									1.04 <i>0.91</i>	0.01 <i>0.02</i>

b)

Site	Jan	Feb	Mar	Apr	May	Jun	Jul	Aug	Sep	Oct	Nov	Dec
Channelview	1.17 <i>0.68</i>	1.62 <i>1.58</i>									3.57 <i>4.53</i>	0.76 <i>0.61</i>
Conroe	0.40 <i>0.53</i>	0.92 <i>0.85</i>									1.89 <i>1.70</i>	1.09 <i>1.03</i>
Galveston	0.50 <i>0.50</i>	0.95 <i>0.99</i>	0.88 <i>0.76</i>	0.52 <i>0.60</i>	0.23 <i>0.44</i>	0.53 <i>0.51</i>	0.37 <i>0.34</i>	0.80 <i>0.87</i>	<b>2.08</b> <i>2.46</i>	1.09 <i>0.96</i>	1.24 <i>1.44</i>	0.56 <i>0.47</i>
Hamshire	0.56 <i>0.46</i>	0.61 <i>0.89</i>	1.25 <i>1.99</i>	0.56 <i>0.65</i>	0.82 <i>0.83</i>	0.85 <i>1.09</i>	0.91 <i>1.02</i>	1.63 <i>1.46</i>	<b>1.94</b> <i>1.20</i>	1.60 <i>1.09</i>	0.92 <i>0.95</i>	0.45 <i>0.52</i>
Aldine	0.63 <i>0.80</i>	0.61 <i>0.66</i>	1.30 <i>1.42</i>	1.70 <i>1.02</i>	1.30 <i>0.94</i>	1.74 <i>1.05</i>	1.56 <i>0.68</i>	1.90 <i>0.99</i>	<b>2.99</b> <i>2.86</i>	2.87 <i>2.18</i>	1.06 <i>1.37</i>	0.90 <i>0.66</i>
Bayland Park	0.62 <i>0.58</i>	0.71 <i>0.76</i>	1.23 <i>0.86</i>	1.53 <i>1.27</i>	0.96 <i>0.73</i>	1.39 <i>1.18</i>	1.27 <i>1.01</i>	1.77 <i>1.22</i>	<b>3.13</b> <i>3.89</i>	1.91 <i>1.26</i>	1.34 <i>1.41</i>	0.79 <i>0.53</i>
Deer Park 2	0.77 <i>0.57</i>	0.79 <i>0.82</i>	1.29 <i>1.05</i>	0.77 <i>0.73</i>	0.67 <i>0.64</i>	0.66 <i>0.83</i>	0.74 <i>0.84</i>	2.04 <i>1.44</i>	<b>3.42</b> <i>4.90</i>	2.01 <i>1.96</i>	1.55 <i>1.92</i>	0.77 <i>0.33</i>
HRM-3			1.91 <i>0.72</i>	1.52 <i>1.10</i>	1.05 <i>0.94</i>	1.51 <i>1.15</i>	0.84 <i>0.27</i>	1.81 <i>1.24</i>	<b>2.12</b> <i>1.32</i>	3.15 <i>2.15</i>		
Mauriceville	0.31 <i>0.27</i>	1.19 <i>1.13</i>									1.57 <i>1.07</i>	0.39 <i>0.19</i>

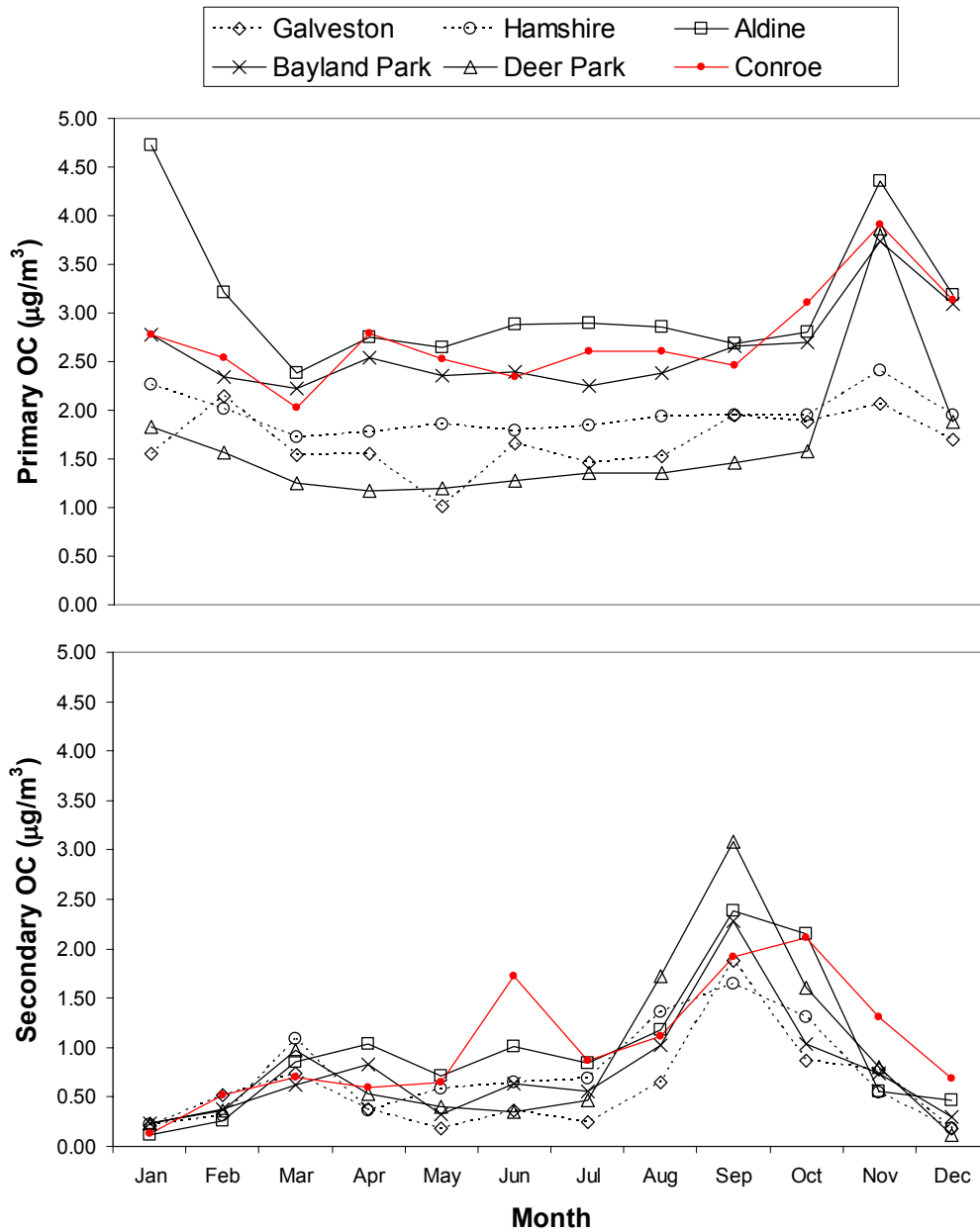


Figure 4.12. **Regression** mean monthly primary OC (top) and **regression** mean monthly secondary OC (bottom). This is the same data that is presented in Tables 4.3a and 4.4a.

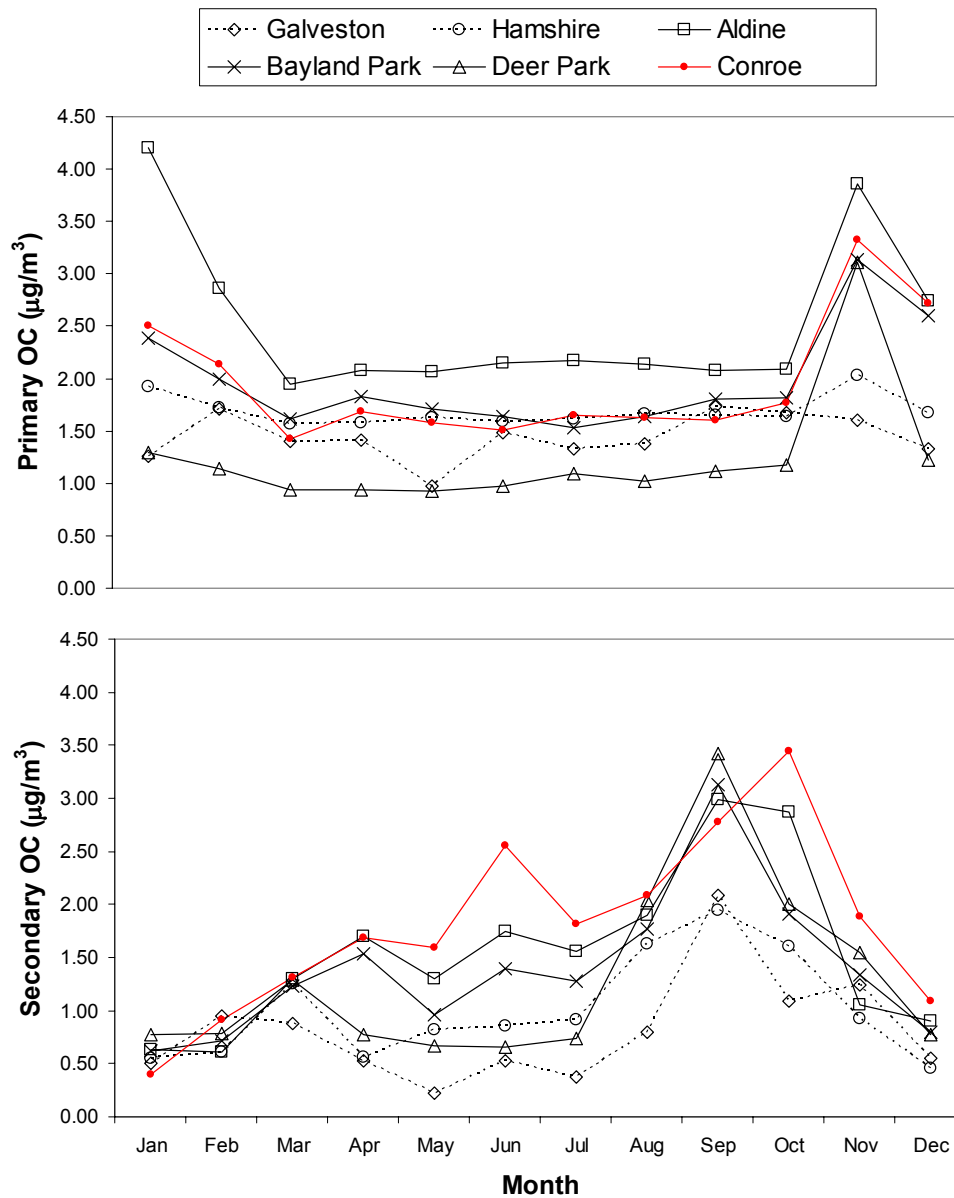


Figure 4.13. **Lower-bound** mean monthly primary OC (top) and **upper-bound** mean monthly secondary OC (bottom). This is the same data that is presented in Tables 4.3b and 4.4b.

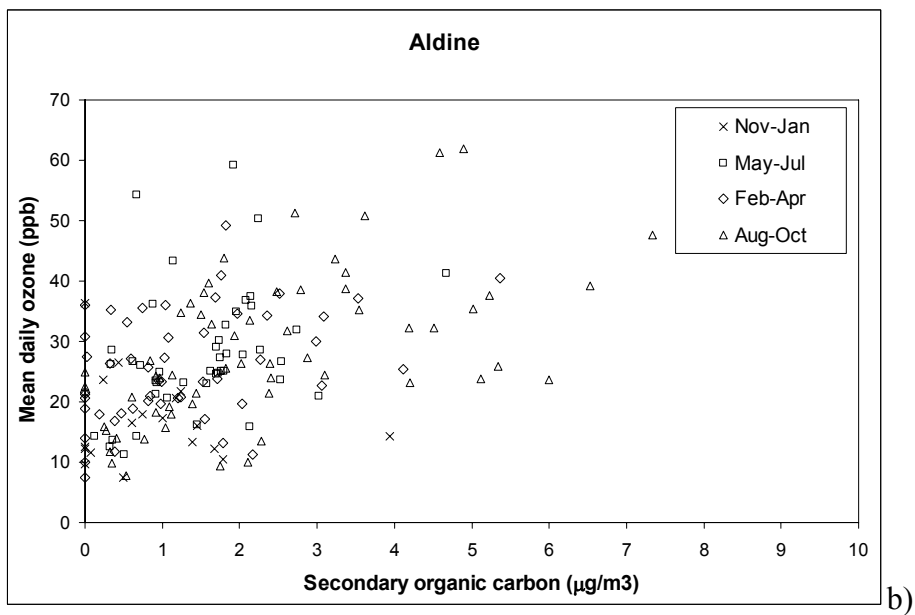
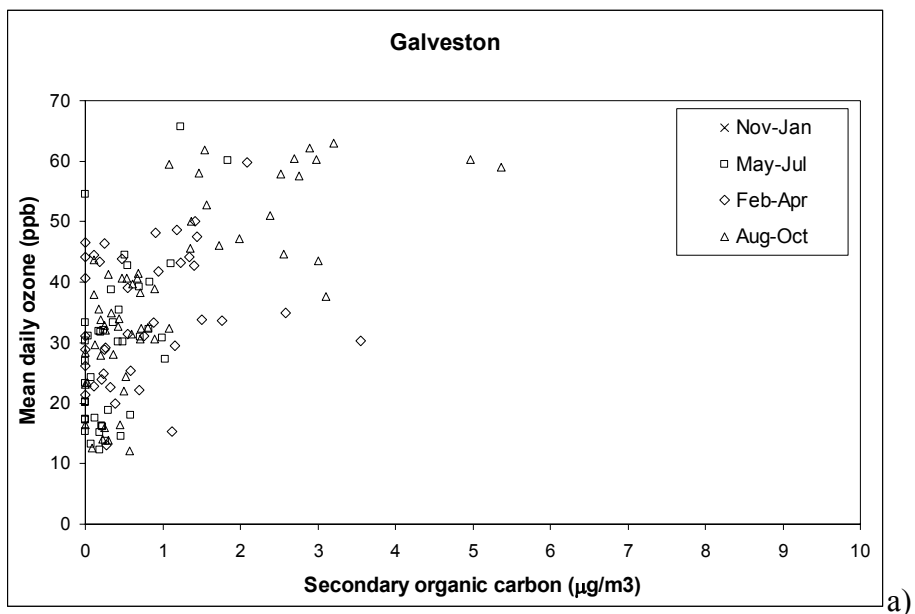
The percentage of primary OC in fine PM is between 13 +/- 9% at Deer Park and 23 +/- 29% at Aldine (using lower bound primary OC). The percentage of secondary OC in fine PM is between 8 +/- 12% at Galveston and 14 +/- 29% at Aldine (using upper bound secondary OC). It should be noted that the amounts of secondary OC relative to primary OC in these 24-hour integrated samples is high compared to other studies. In previous studies, researchers found that secondary OC could be a high fraction of total OC, but this was mainly during short periods (2-6 hours), and primary OC typically dominated total OC over 24-hour periods (Turpin and Huntzicker 1995; Strader et al. 1999; Lim and Turpin 2002).

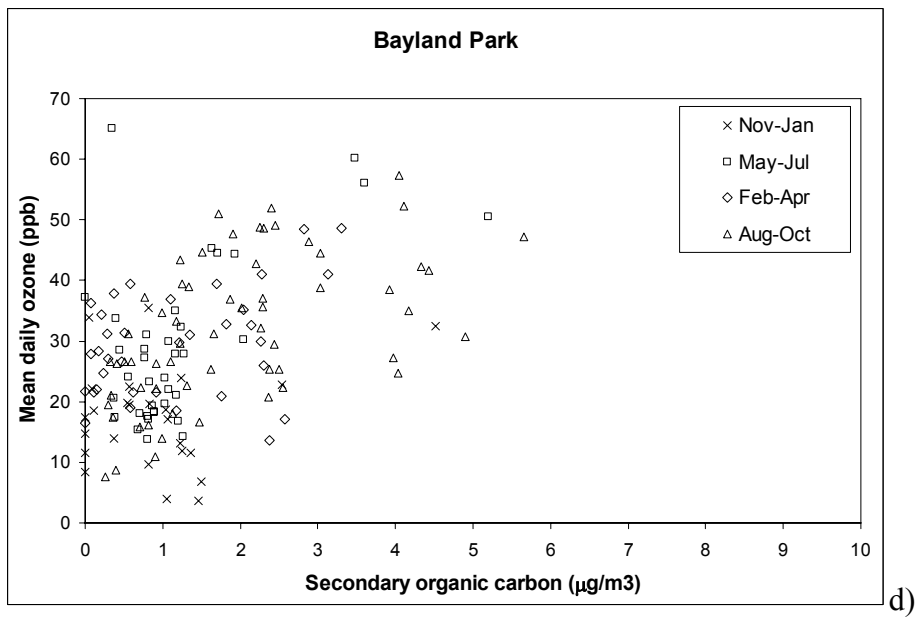
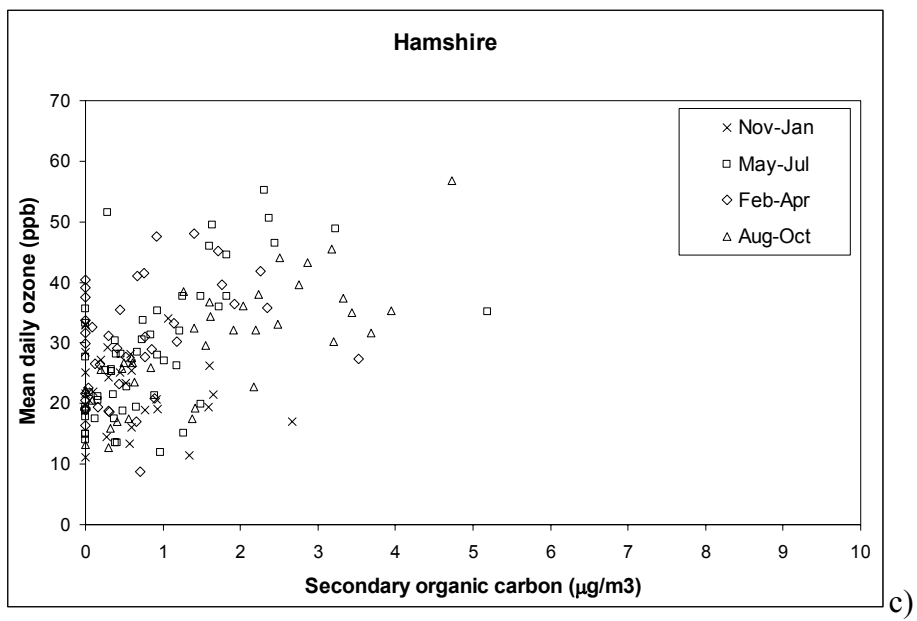
There is a degree of uncertainty in these estimates and, as mentioned earlier, they are used here as a first approximation of spatial and seasonal variations in primary and secondary OC. However, the data do provide evidence that secondary OC is an important fraction of 24-hour integrated PM<sub>2.5</sub> mass concentrations. Secondary OC can be as much as primary OC during certain times of the year, and thus secondary OC is important for determining attainment of the NAAQS for PM<sub>2.5</sub> in Southeast Texas.

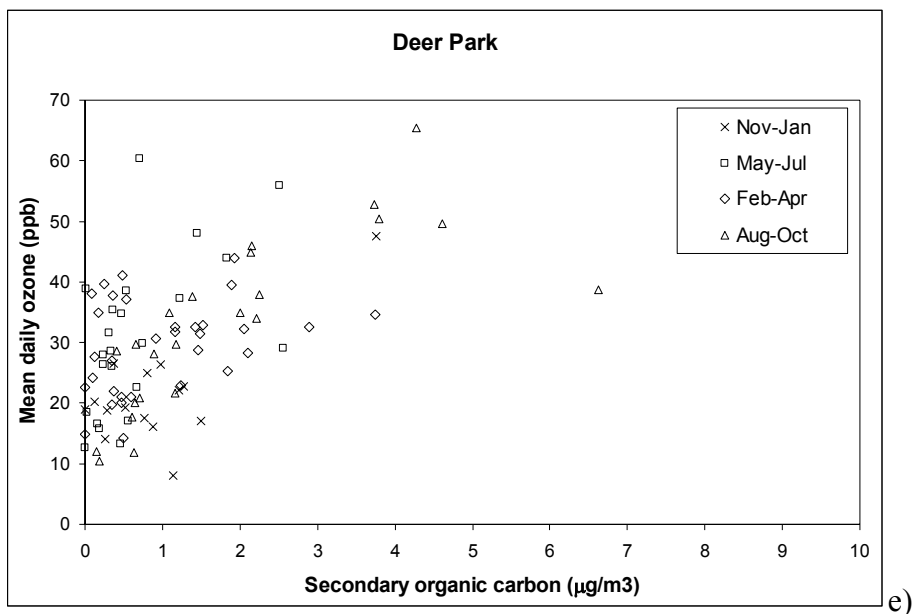
### ***Secondary OC and ground-level ozone.***

Ground-level ozone is assumed to be an indicator of secondary organic aerosol. Figure 4.14a through 4.14f show scatter plots of mean daily ozone concentration versus predicted upper bound secondary organic carbon. The data is shown only for sites that had valid regression data for all 12 months and Conroe, and the data are categorized by season. At all sites, high secondary OC

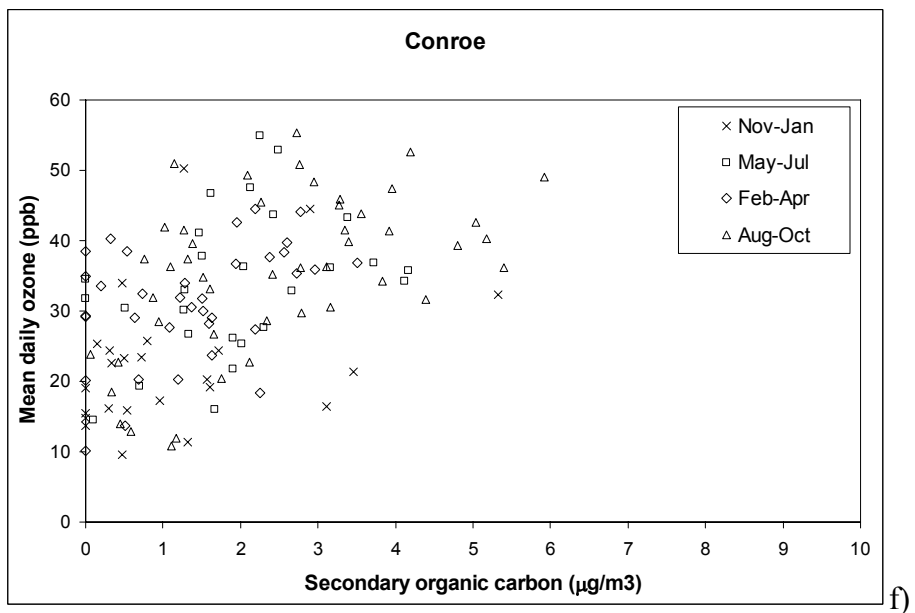
concentrations ( $> 3 \mu\text{g}/\text{m}^3$ ) tend to be associated with high mean daily ozone concentrations, and the majority of these days are in the August – October period. However, the converse is not true, i.e. there are several days of high mean daily ozone concentrations with low secondary OC concentrations ( $<3 \mu\text{g}/\text{m}^3$ ). A possible explanation is that the high ozone concentrations on these days are associated with elevated emissions of ethylene, propylene, and other light olefins, which have been observed in the Houston area (NOAA 2003c). Such precursors would not be expected to lead directly to secondary organic aerosol. Nonetheless, it is encouraging that the regression model tends to predict higher secondary OC concentrations when mean daily ozone is high given that ozone and SOA formation processes are coupled.







e)

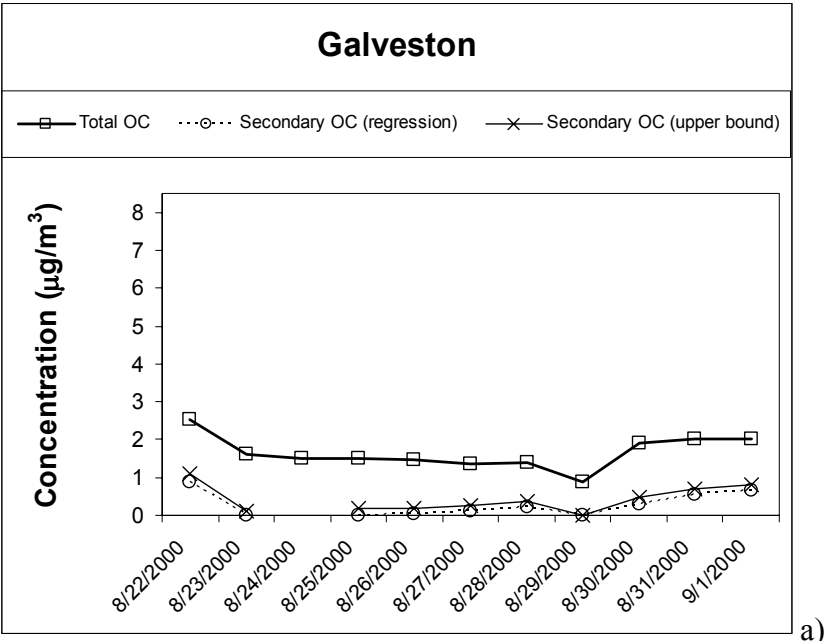


f)

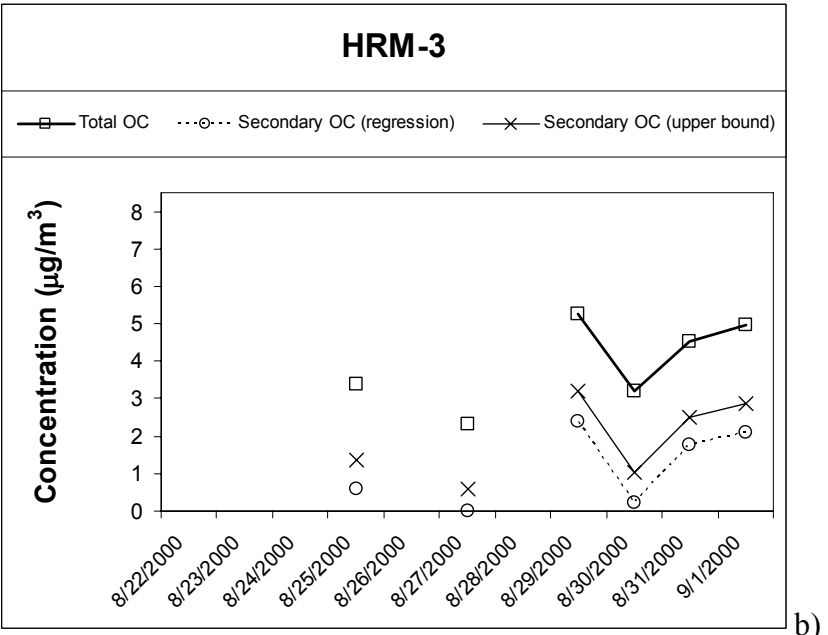
Figure 4.14: Scatter plot of mean daily ozone concentration vs. predicted secondary organic carbon at the same site and date. a)Galveston, b)Aldine, c)Hamshire, d)Bayland Park, e) Deer Park and f) Conroe.

### ***Primary and Secondary OC during TXAQS 2000***

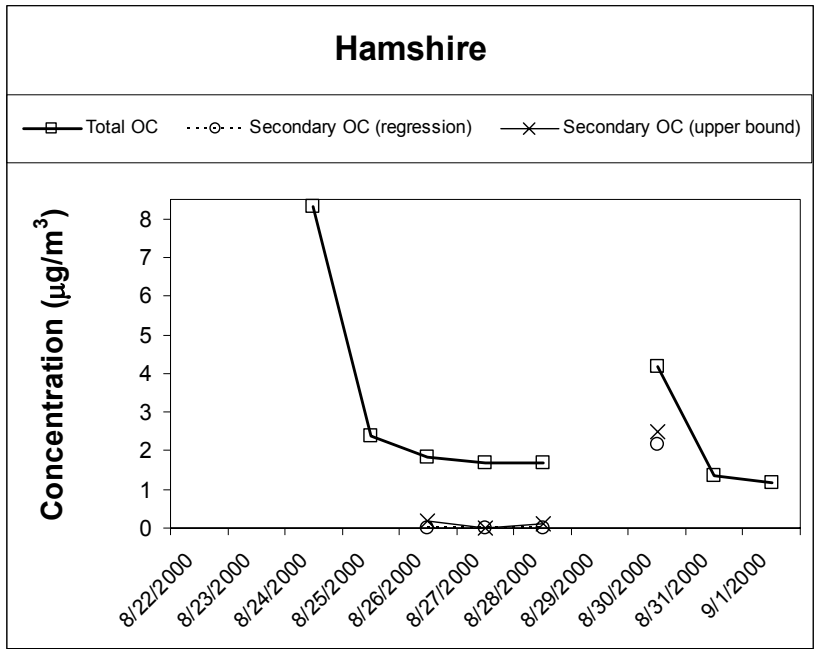
This final sub-section presents total and secondary OC estimates during the August 22<sup>nd</sup> through Sep 1<sup>st</sup>, 2000 period. This ten-day period is the episode used for photochemical grid modeling by the State of Texas (and SOA modeling in this research), and this episode falls during the TXAQS study. Figures 4.15 a through 4.15 f show measured total OC and predicted secondary SOC (both regression and upper bound) for each site with valid data for this period.



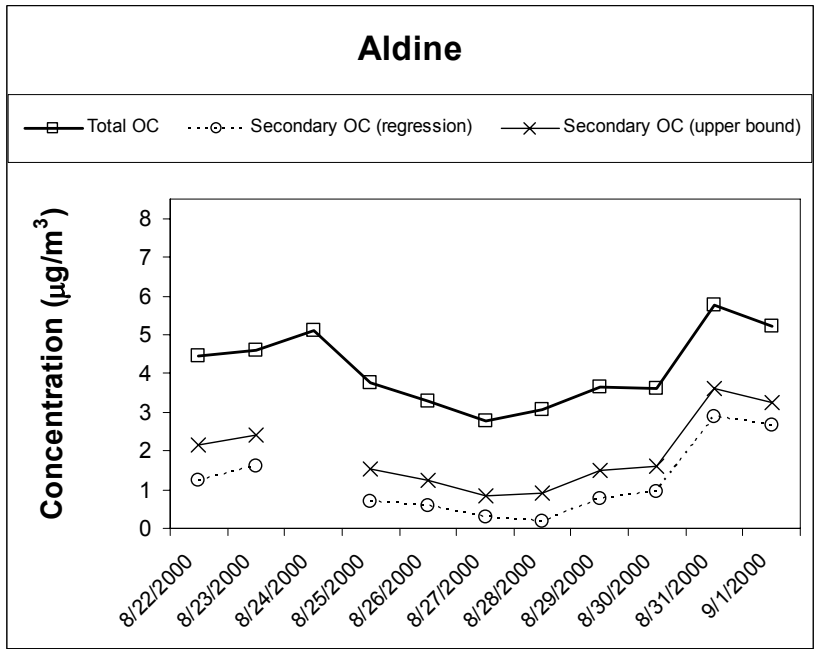
a)



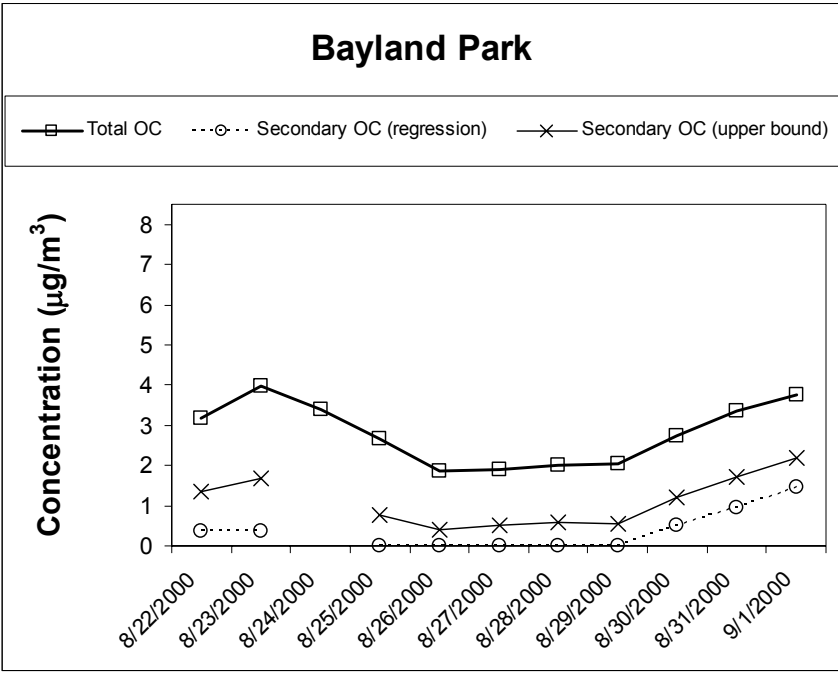
b)



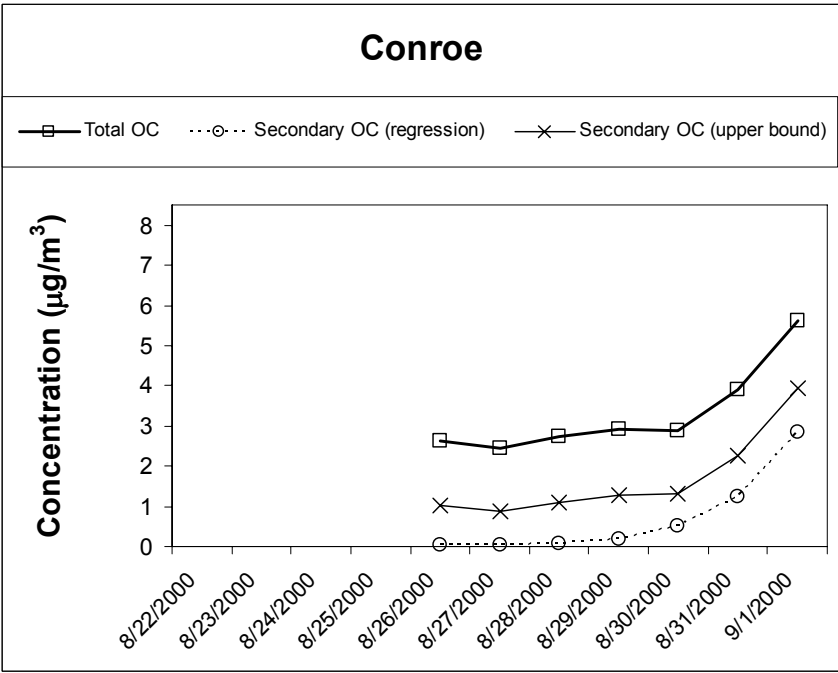
c)



d)



e)



f)

Figure 4.15 (Preceding pages) Measured total OC and predicted secondary OC (both regression and upper-bound) at all sites with valid data during this period a) Galveston, b) HRM-3, c) Hamshire, d) Aldine, e) Bayland Park and f) Conroe. Note some days have valid total OC and no secondary OC because these were excluded from the regression based on one of the arguments given in section 3.2.

The data in Figures 4.15 a-f show that OC was higher at the beginning and end of the episode and that the fraction that was secondary was higher during these events at all sites. These high OC events are common to all sites. Modeling results should reflect higher absolute secondary OC throughout the Southeast Texas area during the beginning and end of the episode.

## **5.0 Methods-Part 2: Modeling SOA formation in a Grid Model**

This chapter describes the methodology used to model the chemistry and gas/particle partitioning of SOA species in Southeast Texas. The approach taken in this research was to modify an existing photochemical grid model to include the capability of simulating SOA formation. The two major modifications made to the grid model were: inclusion of flexible, user-defined chemical mechanism, and addition of an independent module to predict SOA formation. The modified grid model is used to simulate an historical air pollution episode, and unique emissions inputs to the model were required to simulate SOA formation. Finally, the modified grid model was applied in a number of ways to test the sensitivity of SOA formation to input parameters and model formulation.

The chapter is divided into six sections: Episode Selection, Chemical Mechanism Development, Emissions Inventory Development, Performance Evaluation, SOA Model Development, and finally Model Application.

### **5.1 Episode Selection**

Photochemical grid models simulate horizontal and vertical pollutant transport, emissions, deposition and gas-phase chemistry. These models have been under continual development for over 30 years and several different grid model programs are readily available. Models that are used for regulatory purposes tend to be well-scrutinized and rigorously evaluated for both scientific accuracy and numerical stability, and these models are considered to represent the

state of the science. The grid model chosen for this research was the one used by the state of Texas for regulatory modeling of ground-level ozone: CAMx, (Comprehensive Air Quality Model with Extensions) version 3.10 (referred to as CAMx31). CAMx31 is available for free at (<http://www.camx.com>).

The development of a modeling episode is an enormous undertaking and broadly involves the preparation of model inputs and the evaluation of model results for accuracy (also called the performance evaluation). This research made use of a modeling episode that was developed (and continues to be under development) by the Texas Commission on Environmental Quality (TCEQ). This episode focused on the Southeast Texas area including Houston-Galveston and Beaumont-Port Arthur (HGBPA), and covered the 10-day August 23, 2000 through September 1, 2000 period. The tri-nested modeling domain is shown in Figure 5.1 and consists of a large “Regional” domain at 36km resolution, an “East Texas” domain at 12km resolution, and a “HGBPA” domain at 4km resolution.

This episode was significant for air pollution in Southeast Texas because it coincided with two major field studies in the area: Texas Air Quality Study 2000 (TEXAQS2000) and the intensive sampling period of GC-ARCH (Houston Supersite for PM). As a result, these studies provided a rigorous set of ambient measurements with which to validate model performance. The episode is referred to as the TXAQS episode. The reader is referred to the following two URL’s where numerous documents and technical reports can be accessed that describe the TXAQS episode development in detail (these links were accessed on 9/12/2003):

[http://www.tnrcc.state.tx.us/air/aqp/airquality\\_photomod.html#section4](http://www.tnrcc.state.tx.us/air/aqp/airquality_photomod.html#section4)

[http://www.tnrcc.state.tx.us/air/aqp/airquality\\_contracts.html#section3](http://www.tnrcc.state.tx.us/air/aqp/airquality_contracts.html#section3)

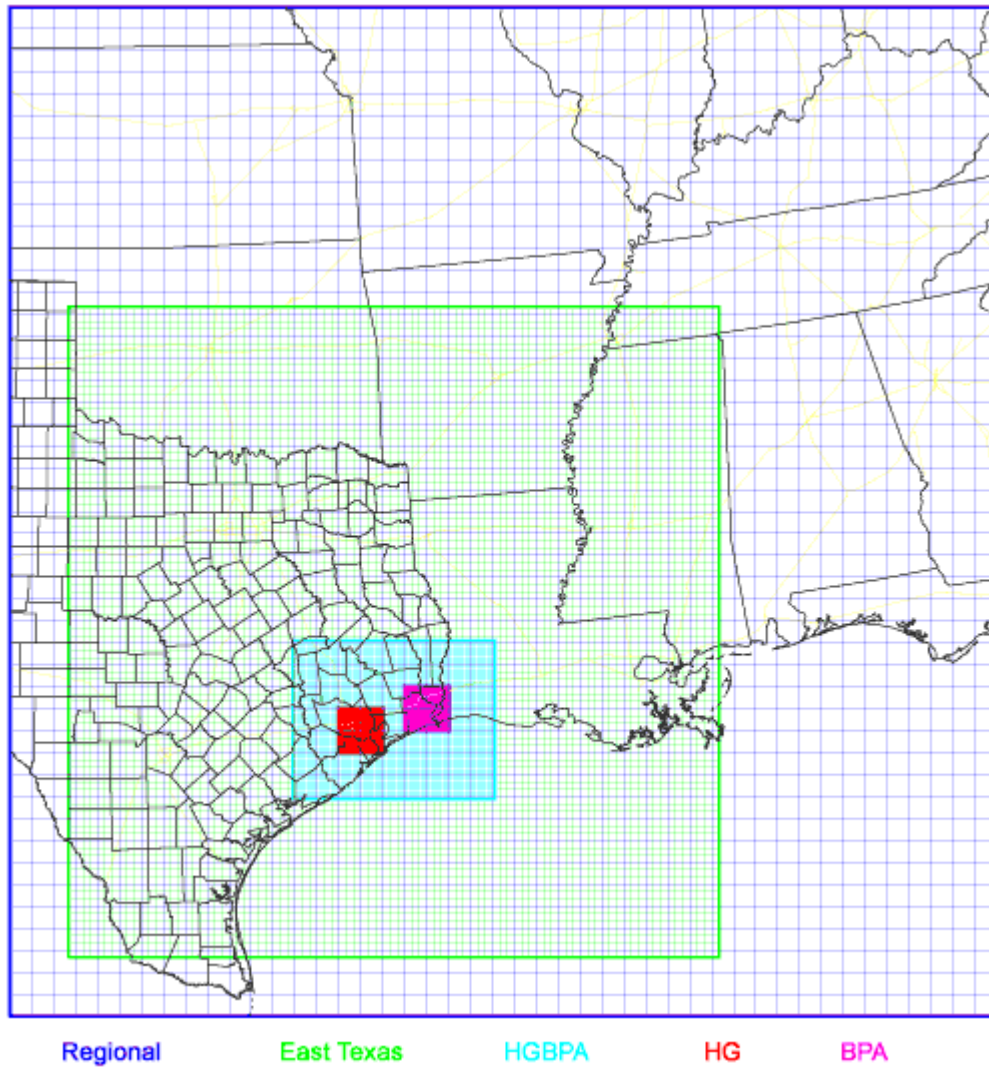


Figure 5.1: TXAQS episode modeling domain. The three largest grids were the primary modeling domains (Regional, East Texas and HGBPA). The two smallest 2km grids (HG and BPA) were not considered in this research. (This figure was obtained from the TCEQ).

The TCEQ and subcontractors developed CAMx31 model inputs for the TXAQS episode. Continual improvements were made to base case model inputs to improve model performance, and the TCEQ provided the public with model inputs at certain stages of development. The modeling in this research used inputs based on “Base Case 4a with 70% adjustment to the planetary boundary layer height”. As discussed in later sections, new sets of model species were used in this work, and, as a result, the emissions, boundary and initial condition inputs used in this work were developed separately. All other model inputs were obtained from the TCEQ and are summarized in Table 5.1.

Table 5.1. Input files for modeling the TXAQS modeling episode with CAMx version 3.10.

<b>input</b>	<b>grid</b>	<b>file</b>	<b>source</b>
albedo/haze/ozone	all	camx_aho.20000822-20000901.reg_36km+etx_12km+hgbpa_04km	2
wind	36km	camx_wind.2000MMDD.reg_36km.02FEB27_GRID2	1
height/pressure	36km	camx_zp.2000MMDD.reg_36km.02FEB27_GRID2	1
vertical diffusivity	36km	camx_kv.2000MMDD.reg_36km.02FEB27_GRID2.070pbl	1
temperature	36km	camx_temp.2000MMDD.reg_36km.02FEB27_GRID2	1
landuse	36km	camx_landuse.reg_36km.environ	2
cloud cover*	36km	camx_cloud.2000MMDD.reg_36km.02FEB27_GRID2	1
rainfall*	36km	camx_rain.2000MMDD.reg_36km.02FEB27_GRID2	1
water vapor*	36km	camx_hum.2000MMDD.reg_36km.02FEB27_GRID2	1
wind	12km	camx_wind.2000MMDD.etx_12km.02FEB28_GRID3	1
height/pressure	12km	camx_zp.2000MMDD.etx_12km.02FEB28_GRID3	1
vertical diffusivity	12km	camx_kv.2000MMDD.etx_12km.02FEB28_GRID3.070pbl	1
temperature	12km	camx_temp.2000MMDD.etx_12km.02FEB28_GRID3	1
landuse	12km	camx_landuse.etx_12km.environ	2
wind	4km	camx_wind.2000MMDD.hgbpa_04km.02AUG04_GRID4	1
height/pressure	4km	camx_zp.2000MMDD.hgbpa_04km.02AUG04_GRID4	1
vertical diffusivity	4km	camx_kv.2000MMDD.hgbpa_04km.02AUG04_GRID4.070pbl	1
temperature	4km	camx_temp.2000MMDD.hgbpa_04km.02AUG04_GRID4	1
landuse	4km	camx_landuse.hgbpa_04km	2

1: From TCEQ. Originally in archives: CAMxMet\_2000AUG\_20021107.#.tar.gz which were downloaded from <ftp.tnrc.state.tx.us/pub/OEPAA/TAD/Modeling/HGMCR/CAMx/input>.

2: From TCEQ. Originally in archive: CAMxOther\_2000AUG\_20020327.tar.gz which was downloaded from <ftp.tnrc.state.tx.us/pub/OEPAA/TAD/Modeling/HGMCR/CAMx/input>.

\*: Only input for 36km grid resolution and interpolated to finer resolution grids.

The TXAQS episode was developed by the TCEQ for purposes of modeling ground-level ozone concentrations in Southeast Texas. The episode is used here as a case for testing the SOA formation model developed in this work.

## **5.2 Chemical Mechanism Development**

The chemical mechanism is the mathematical representation of the model species and reactions that are used to represent the thousands of actual gas species and reactions that occur in the atmosphere. This mechanism is solved numerically by the grid model according to a certain numerical scheme (also called the solver). The solution of the chemical mechanism is typically the most computationally demanding part of the simulation, and so existing mechanisms balance accuracy with computational efficiency.

Each chemical mechanism consists of a set of base reactions involving organic and inorganic species that are represented explicitly in the model. This base mechanism is similar from mechanism to mechanism since these reactions are critical to accurate solution of the photochemistry. The remaining organic compounds that participate in atmospheric reactions are not treated explicitly but are 'lumped' into a reduced set of surrogate species. Different mechanisms differ primarily in the representation of lumped organic compounds.

A widely used chemical mechanism for regulatory modeling is Carbon Bond IV (CB4) (Gery et al. 1989) which lumps organic gases based on their

structure, more specifically bond types. For example, one mole of propene would be equivalent to one mol of PAR (paraffin bond) and one mole of OLE (olefin bond) in CB4. CB4 is efficient because of a relatively small number of model species to be solved (25 species, 20 radical species), and as a result is used widely for regulatory modeling. CB4 lumped model species, however, represent structural parts of molecules. SOA formation is highly dependent on individual molecules and especially their molecular weights, information that is not retained in the CB4 mechanism; CB4 is not suited for modeling SOA.

The Statewide Air Pollution Research Center (SAPRC) model (Carter 1990, 1995) is a chemical mechanism that uses a lumped molecule approach and is considered to be one of the most chemically up to date mechanisms available for modeling atmospheric photochemical reactions. Reactions, reaction rates and model species are updated often (leading to different versions of the SAPRC mechanism, most recently SAPRC99), and this mechanism is available for free as a software package that allows the user to control lumping of organic compounds and perform box-model simulations. SAPRC99 software allows organic compounds to be treated either explicitly or lumped into appropriate groups. This is ideal for modeling SOA since important SOA precursors can be treated explicitly in the mechanism, or precursors with similar SOA formation mechanisms can be lumped together.

SAPRC99 was chosen as the chemical mechanism on which to base SOA prediction in this research. SAPRC99 is available at (<http://pah.cert.ucr.edu/~carter/SAPRC99.htm>). The SAPRC99 software was used

to create two custom mechanisms with important SOA precursors treated explicitly and other organic compounds lumped appropriately. Once a SAPRC99 mechanism is created, i.e. once all explicit and lumped species have been decided upon, the SAPRC99 software generates source code that, when compiled, numerically solves for the concentrations of all species.

A current limitation of most available grid models is that chemical mechanisms are hard-coded into the grid model and they cannot be altered without major code modifications. In this research, CAMx31 and SAPRC99 software were modified to allow SAPRC99-generated mechanism code to be ‘plugged’ into CAMx31 and used for 3D simulations. The modifications were completed such that any mechanism developed with SAPRC99 software could theoretically be used in CAMx31. This was a major accomplishment of this research and the task was not trivial. The software modifications are presented in detail in Appendix B. The Appendix also contains more information about the SAPRC99 software and how the solver is used in CAMx31 to solve the chemical mechanisms. This ‘flexible mechanism’ tool will hopefully be used in future research to overcome the limitation of fixed mechanisms in photochemical grid models. The remainder of this section will discuss the custom mechanisms used for this research.

Formation of secondary organic aerosol is suspected to come from a number of precursors, but has been found to come predominantly from mono- and sesqui-terpenes, aromatics and high molecular weight alkanes and alkenes. Constant yield ( $d[\text{SOA}]/d[\text{HC}]$ ) data can be found for numerous individual gases

in these categories; however, as the understanding of SOA formation has evolved, experimental data on aerosol formation has been primarily focused on aromatics (strictly anthropogenic) and monoterpenes (dominantly biogenic). Previous studies have shown aromatics and monoterpenes to be primarily responsible for SOA formation near urban areas, and these two groups were the focus of this research. A comprehensive estimate of SOA formation from all precursors was not possible, simply due to lack of compound specific SOA formation data. It should be noted that some SOA formation was expected from compound groups other than aromatics and monoterpenes, and these groups should be included in similar analyses when data become available.

Two new chemical mechanisms were developed for this research: s99soa and s99soa2. Both new mechanisms had the same base reactions as the standard fixed parameter version of SAPRC99 (referred to here as s99), which is described in detail in SAPRC99 documentation (Carter 2000). The aromatics and monoterpenes were lumped differently in s99soa and s99soa2 compared to s99. In addition, stoichiometric parameters and rate constants for lumped VOC categories (olefins, alkanes, aromatics and monoterpenes) were based on a Texas anthropogenic emissions profile, and were different from the parameters and constants in s99. S99soa and s99soa2 differ from each other only in that the aromatic reaction mechanisms are more detailed in s99soa2. The remainder of this section describes the unique features of the s99soa and s99soa2 mechanisms.

All monoterpenes are lumped into one model species (TERP) in s99; however, this is not appropriate for SOA modeling. Previous research has shown

that aerosol formation differs significantly from monoterpene to monoterpene (Hoffmann et al. 1997; Griffin et al. 1999). As a result, these five monoterpenes were treated explicitly (unlumped) in the s99soa/s99soa2 mechanisms. SAPRC99 software includes individual reaction mechanisms for the five monoterpenes:  $\alpha$ -pinene,  $\beta$ -pinene,  $\Delta^3$ -carene, sabinene, and d-limonene. As explained in the next section, biogenic emissions were estimated for fourteen monoterpenes in the modeling domain; however, reaction data is only available for the five listed above, and furthermore these five monoterpenes make up the bulk of the biogenic monoterpenes emissions in the area of interest. These five monoterpenes are expected to account for the vast majority of SOA from monoterpene precursors.

Aromatic precursors are assumed to produce aerosol via oxidation by the OH radical. The SAPRC99 software includes reaction mechanisms for 21 individual aromatic species, which are used to represent the reaction mechanics of ~200 emitted aromatic compounds. The original s99 lumps all aromatics into two model species: low- and high-OH reactivity aromatics (ARO1 and ARO2), classified as compounds with  $k_{OH}$  less and greater than  $2 \times 10^4 \text{ ppm}^{-1} \text{ min}^{-1}$  respectively. Once again, however, it is desirable to have separate model species for compounds with different aerosol forming characteristics.

The work of Odum et al. (Odum et al. 1996; Odum et al. 1997a) provided evidence that many common aromatics could be put into distinct two groups, high- and low-SOA yield aromatics. The authors distinguish these groups broadly as aromatics with two or more methyl substituents (low-yield aromatics), and one or fewer methyl substituents or one or fewer ethyl substituents (high yield

aromatics). In addition, a few experiments with p-ethyl toluene and diethyl benzene produced high aerosol yields. These criteria were used to classify all emitted aromatic compounds. Compounds that could not be classified with the above criteria were considered here to be ‘no-yield’ aromatics; aerosol formation data simply does not exist for these compounds, despite the fact that some may produce SOA. Aromatics in s99soa/s99soa2 were categorized separately as high-SOA, low-SOA, or no-SOA yield aromatics, and each category was split into high vs. low reactivity aromatics, for a total of six lumped aromatic model species. No aromatic compounds in the emissions inventory, however, fell into the low-yield, low-OH reactivity category, and so there were five lumped aromatic model species. The lumping of emitted aromatic compounds into these categories is discussed with the emissions processing in the next section. Table 5.2 below shows estimated daily aromatic emissions in Texas for each of the aromatic model categories. The Table shows that SOA formation is accounted for from the majority of aromatic emissions.

Table 5.2: Estimated aromatic emissions from all anthropogenic sources in Texas in each yield/reactivity category. These estimates were made with emissions data listed in Appendix A and speciation profiles listed in Table 5.7.

<b>Aromatic category</b>	<b>Texas anthropogenic emissions typical day tons (%)</b>
High SOA yield, low reactivity	265.9 (55.1)
Low SOA yield, high reactivity	141.4 (29.3)
High SOA yield, high reactivity	41.4 (8.6)
No SOA yield, high reactivity	23.5 (4.9)
No SOA yield, low reactivity	10.0 (2.1)

One of the applications of the modified grid model was to test the sensitivity of SOA formation to the way SOA precursor reactions are represented

in the chemical mechanism. This was accomplished by representing aromatic reactions by more detailed mechanisms compared to what is used in s99.

Dechapanya et al. (2003a) developed new reaction mechanisms for 15 of the 21 aromatic compounds that had explicit reaction mechanisms in the SAPRC99 software. (The other 6 explicit aromatics were not considered because they are assumed to not produce SOA precursors, i.e. they are considered no-yield aromatics). These mechanisms were developed specifically to give a better mechanistic representation of aromatic reactions to form condensable products. The explicit aromatic reactions included with the original SAPRC99 software were developed to give an accurate representation of gas phase chemistry, not pathways that lead to condensable products. The latter pathways are more realistically represented by a series/parallel reaction mechanism (Dechapanya et al. 2003a), as illustrated in Figure 5.2. In addition, Dechapanya et al (2003a) estimated the partitioning coefficients for aromatic-condensable products from data in the literature. The use of these new reaction mechanisms to create lumped aromatic model species led to the s99soa2 mechanism, which differs from s99soa. S99soa uses original SAPRC99 reaction mechanisms to create lumped aromatic model species.

In summary, s99soa/s99soa2 contain all base mechanisms reactions that are in s99 (see Carter (2000) for details and for model species). All lumped model species in s99soa and s99soa2 are the same as in s99, except there are five instead of two lumped aromatics, and five monoterpenes are represented explicitly rather than lumped. Additionally, s99soa2 contained extra intermediate

model species (aerosol precursors) and reaction products (condensable products), corresponding to updated aromatic reaction mechanisms (see Dechapanya et al. (2003a) for details). All model species that are used to represent emitted VOCs in s99soa and s99soa2 are listed in Table 5.3. Appendix E contains the .rxn SAPRC input files for both the s99soa and s99soa2 mechanisms. The .rxn files are used to create the source code for the model mechanism, and these files list all reactions, rate constants and stoichiometric coefficients in the mechanisms.

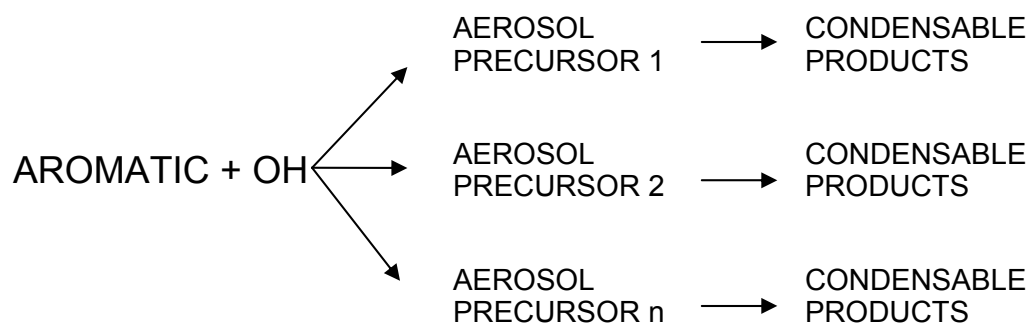


Figure 5.2: Illustration of series/parallel nature of aromatic reactions to form condensable organic compounds.

Table 5.3. List of model species in s99soa and s99soa2 mechanisms that represent VOC compounds in the emissions inventory. Some descriptions taken from SAPRC documentation (Carter 2000).

Model Species	Represents
CH4	methane (explicit)
ETHE	ethylene (explicit)
ISOP	isoprene (explicit)
ACET	acetone (explicit)
HCHO	formaldehyde (explicit)
PHEN	phenol (explicit)
MEOH	methanol (explicit)
GLY	glyoxal (explicit)**
MGLY	methyl glyoxal and other higher $\alpha$ -dicarbonyl aldehydes**

BACL	biacetyl and other $\alpha$ -dicarbonyl ketones**
CCHO	acetaldehyde and glycolaldehyde
RCHO	lumped C3+ aldehydes
MEK	slow reacting ketones
PROD	fast reacting ketones
CRES	cresols
BALD	aromatic aldehydes
METH	methacrolein and acrolein
ISPD	unsaturated aldehydes other than METHACRO
MVK	unsaturated ketones
ALK1*	alkanes and other non-aromatics that react with OH and with $2 \times 10^2 < k_{OH} < 5 \times 10^2 \text{ ppm}^{-1} \text{ min}^{-1}$
ALK2*	alkanes and other non-aromatics that react with OH and with $5 \times 10^2 < k_{OH} < 2.5 \times 10^3 \text{ ppm}^{-1} \text{ min}^{-1}$
ALK3*	alkanes and other non-aromatics that react with OH and with $2.5 \times 10^3 < k_{OH} < 5 \times 10^3 \text{ ppm}^{-1} \text{ min}^{-1}$
ALK4*	alkanes and other non-aromatics that react with OH and with $5 \times 10^3 < k_{OH} < 1 \times 10^4 \text{ ppm}^{-1} \text{ min}^{-1}$
ALK5*	alkanes and other non-aromatics that react with OH and with $1 \times 10^4 < k_{OH} \text{ ppm}^{-1} \text{ min}^{-1}$
AR1H*	high-SOA yield aromatics with $k_{OH} < 2 \times 10^4 \text{ ppm}^{-1} \text{ min}^{-1}$
AR2H*	high-SOA yield aromatics with $k_{OH} > 2 \times 10^4 \text{ ppm}^{-1} \text{ min}^{-1}$
AR2L*	low-SOA yield aromatics with $k_{OH} > 2 \times 10^4 \text{ ppm}^{-1} \text{ min}^{-1}$
AR1N*	no-SOA yield aromatics with $k_{OH} < 2 \times 10^4 \text{ ppm}^{-1} \text{ min}^{-1}$
AR2N*	no-SOA yield aromatics with $k_{OH} > 2 \times 10^4 \text{ ppm}^{-1} \text{ min}^{-1}$
OLE1*	alkenes other than ethylene with $k_{OH} < 7 \times 10^4 \text{ ppm}^{-1} \text{ min}^{-1}$
OLE2*	alkenes other than ethylene with $k_{OH} > 7 \times 10^4 \text{ ppm}^{-1} \text{ min}^{-1}$
APIN	$\alpha$ -pinene (explicit)
BPIN	$\beta$ -pinene (explicit)
DCAR	$\Delta^3$ -carene (explicit)
SABI	sabinene (explicit)
DLIM	d-limonene (explicit)
TERP*	all other monoterpenes not treated explicitly

\* lumped model species whose rate parameters and reaction stoichiometry are determined by weighted lumping methods.

\*\* GLY,MGLY and BACL are primarily reaction products, but some emitted compounds are lumped to these species

An important step in developing the chemical mechanisms in SAPRC99 software is to determine the rate constants and product stoichiometric coefficients for lumped model species (i.e. determine the lumped parameters). A lumped species represents different compounds, in different amounts, and each has different reaction rate constants and product stoichiometry. Some lumped groups such as RCHO and MEK simply use a constant set of parameters, and all compounds lumped into these groups use these parameters, no matter what the simulation conditions. For lumped groups with a more variable composition (ALK1-ALK5, OLE1, OLE2, ARO1, ARO2), it is more appropriate to use a weighted average of the parameters of the compounds that make up the lumped group. For grid model applications, these parameters must be determined prior to running the grid model and they remain fixed throughout the simulation, hence the 'fixed parameter' designation.

The developers of SAPRC99 recommend using a typical mixture of VOC compounds, and weighting lumped parameters by the concentrations of each compound in this composition. The original s99 uses average VOC concentrations from urban atmospheres in the U.S. (Carter 2000). In this research, a Texas anthropogenic VOC emissions profile was generated to determine lumped model species parameters. This profile was created using emissions data and speciation profiles summarized in the next section (one exception is that mobile source emissions in the Houston area were speciated using profiles from SPECIATE3.2

and the TCEQ, not from the Washburn Tunnel Study). There were 633 separate VOC compounds and mixtures in the anthropogenic emissions. Table 5.4 shows the top 30 compounds emitted by area, mobile and point sources. Table 5.5 shows the top 90 compounds emitted from all anthropogenic sources in Texas. The composition profile by compound was converted to a composition profile in SAPRC99 notation using a tool called emitdb.xls (See Appendix C, SAPRC99 notation refers to SAPRC99 Detailed Model Species categories). SAPRC99 software was then used to determine the parameters for lumped model species.

Table 5.4. Speciated Texas anthropogenic emissions from area/offroad mobile, onroad mobile, and point sources. (% by mass)

<b>Area/Offroad Sources (total 1985 tons/day)</b>		<b>Onroad Sources (total 967 tons/day)</b>		<b>Point Sources (total 482 tons/day)</b>	
<b>COMPOUND</b>	<b>%</b>	<b>COMPOUND</b>	<b>%</b>	<b>COMPOUND</b>	<b>%</b>
METHANE	12.75%	N-BUTANE	9.83%	PROPANE	10.88%
N-BUTYL ALCOHOL	9.52%	METHANE	8.86%	METHYL ALCOHOL	7.36%
TOLUENE	5.89%	UNIDENTIFIED	7.67%	N-BUTANE	6.05%
N-BUTANE	5.53%	ISOPENTANE	6.48%	HEXANE	4.70%
ISOPENTANE	4.84%	TOLUENE	4.76%	ETHYLENE	4.68%
UNIDENTIFIED	2.14%	ETHYLENE	3.94%	PROPENE	4.66%
PROPANE	1.95%	N-PENTANE	2.88%	ISOBUTANE	4.19%
N-PENTANE	1.89%	1,2,4-TRIMETHYLBENZENE	2.27%	ISOMERS OF PENTANE	3.46%
ETHANE	1.88%	P-XYLENE	2.21%	TOLUENE	3.45%
ISOMERS OF HEXANE	1.78%	2,2,4-TRIMETHYLPENTANE	1.81%	FORMALDEHYDE	2.98%
N-DODECANE	1.58%	2-METHYLPENTANE	1.77%	BENZENE	2.88%
ISOMERS OF HEPTANE	1.54%	1,3,5-TRIMETHYLBENZENE	1.75%	ISOMERS OF XYLENE	2.33%
HEPTANE	1.53%	C10 AROMATIC	1.74%	METHYLETHYL KETONE	2.18%
ETHYLENE	1.48%	ISOBUTANE	1.72%	TERPENES,UNSPECIFIED	2.05%
ISOMERS OF XYLENE	1.43%	O-XYLENE	1.50%	ISOPENTANE	1.98%
BENZENE	1.27%	1,3-BUTADIENE	1.46%	N-PENTANE	1.55%
PERCHLOROETHENE	1.23%	BENZENE	1.40%	ISOPROPYL ALCOHOL	1.49%
ISOMERS OF OCTANE	1.15%	ETHANE	1.29%	METHYL-T-BUTYL ETHER	1.47%
C7 CYCLOPARAFFINS	1.10%	2,3-DIMETHYLPENTANE	1.23%	STYRENE	1.43%
NAPHTHA	1.09%	CYCLOHEXANE	1.21%	METHANE	1.32%
2-METHYLPENTANE	0.96%	PROPENE	1.13%	HEPTANE	1.25%
METHYLNAPHTHALENES	0.93%	3-METHYLPENTANE	1.07%	ETHYL ALCOHOL	1.15%
ISOBUTANE	0.90%	2-METHYLDECANE	0.98%	1,3-BUTADIENE	0.98%
N-BUTYLACETATE	0.89%	2,3,3-TRIMETHYLPENTANE	0.97%	ISOMERS OF BUTENE	0.97%
C2 ALKYLINDAN	0.88%	3-METHYLHEXANE	0.97%	CYCLOHEXANE	0.92%
MINERAL SPIRITS	0.86%	1-METHYL-3-ETHYLBENZENE	0.93%	ACETYLENE	0.90%
O-XYLENE	0.84%	ACETYLENE	0.90%	M-XYLENE	0.85%
ISOMERS OF PENTANE	0.81%	HEXANE	0.89%	CARBONYL SULFIDE	0.80%
2,4-DIMETHYLHEXANE	0.81%	BUTENE	0.89%	ETHYLBENZENE	0.75%
N-UNDECANE	0.81%	2-METHYL-2-BUTENE	0.87%	A-PINENE	0.73%

Table 5.5. Speciated Texas anthropogenic VOC emissions, from all sources. The list continues from column to column. (% by mass)

<b>All Anthropogenic Sources (total 3434 tons/day)</b>					
<b>COMPOUND</b>	<b>%</b>	<b>COMPOUND</b>	<b>%</b>	<b>COMPOUND</b>	<b>%</b>
METHANE	10.05%	C10 AROMATIC	0.71%	2,3,3-TRIMETHYLPENTANE	0.40%
N-BUTANE	6.81%	ISOMERS OF OCTANE	0.69%	2,3-DIMETHYLBUTANE	0.40%
N-BUTYL ALCOHOL	5.59%	CYCLOHEXANE	0.67%	1-METHYL-3-ETHYLBENZENE	0.38%
TOLUENE	5.23%	N-UNDECANE	0.65%	C7 ALKYL BENZENE	0.37%
ISOPENTANE	4.90%	3-METHYLPENTANE	0.65%	2,4-DIMETHYLPENTANE	0.36%
UNIDENTIFIED	3.40%	C7 CYCLOPARAFFINS	0.64%	METHYLENE BROMIDE	0.33%
PROPANE	2.81%	NAPHTHA	0.63%	C2 ALKYL NAPHTHALENE	0.33%
ETHYLENE	2.62%	2,4-DIMETHYLHEXANE	0.63%	TRANS-2-BUTENE	0.31%
N-PENTANE	2.12%	ACETYLENE	0.60%	TERPENES, UNSPECIFIED	0.29%
ISOBUTANE	1.60%	2-METHYL-2-BUTENE	0.60%	1-PENTENE	0.29%
BENZENE	1.53%	METHYLNAPHTHALENES	0.58%	CIS-2-BUTENE	0.28%
ETHANE	1.53%	C16 BRANCHED ALKANE	0.55%	ACETONE	0.28%
HEXANE	1.33%	2,3-DIMETHYLPENTANE	0.54%	ETHYL ACETATE	0.27%
HEPTANE	1.24%	N-BUTYLACETATE	0.54%	ISOPROPYL ALCOHOL	0.27%
PROPENE	1.19%	C2 ALKYLINDAN	0.51%	1,2,3-TRIMETHYLBENZENE	0.27%
ISOMERS OF XYLENE	1.15%	MINERAL SPIRITS	0.50%	2,5-DIMETHYLHEPTANE	0.27%
2-METHYLPENTANE	1.09%	ETHYLBENZENE	0.49%	CIS-2-PENTENE	0.26%
ISOMERS OF HEXANE	1.07%	BUTENE	0.48%	ACETALDEHYDE	0.26%
METHYL ALCOHOL	1.04%	TRANS-2-PENTENE	0.46%	3,4-DIMETHYLOCTANE	0.26%
1,2,4-TRIMETHYLBENZENE	1.01%	METHYLCYCLOHEXANE	0.46%	TRIMETHYLDECENE	0.26%
N-DODECANE	0.98%	ISOMERS OF DODECANE	0.46%	2,2-DIMETHYLBUTANE	0.25%
O-XYLENE	0.96%	3-METHYLHEXANE	0.45%	M-XYLENE AND P-XYLENE	0.25%
ISOMERS OF PENTANE	0.96%	METHYLCYCLOPENTANE	0.44%	N-DECANE	0.24%
P-XYLENE	0.93%	1,1,1-TRICHLOROETHANE	0.43%	DIMETHYLCYCLOHEXANE	0.24%
1,3-BUTADIENE	0.89%	TRIMETHYLBENZENE	0.43%	STYRENE	0.23%
ISOMERS OF HEPTANE	0.89%	NAPHTHALENE	0.41%	OCTANE	0.22%
FORMALDEHYDE	0.89%	METHYLETHYL KETONE	0.41%	1,2-DIETHYLBENZENE	0.22%
2,2,4-TRIMETHYLPENTANE	0.79%	TRICHLOROETHYLENE	0.41%	ETHYL ALCOHOL	0.22%
1,3,5-TRIMETHYLBENZENE	0.74%	2-METHYLDECANE	0.40%	M-DIETHYLBENZENE	0.22%
PERCHLOROETHYLENE	0.71%	BUTYL CELLOSOLVE	0.40%	METHYL-T-BUTYL ETHER	0.21%

As noted earlier, approximately 200 aromatic compounds were recognized by SAPRC99 and these are mapped to 21 aromatics that have detailed reaction

mechanisms. Mapping should not be confused with lumping. Mapping refers to simply assigning one compound the reaction parameters, i.e. rate constants and reaction product stoichiometry, of another compound. Mapping is necessary since explicit reaction mechanisms simply do not exist for all VOC compounds. Mapping is also practical since many types of VOC's (such as aromatics) have similar reaction mechanisms. Lumping refers to creating a surrogate (lumped) species whose reaction parameters are a weighted combination of the reaction parameters of all the compounds in the group. After aromatics in the composition file have been mapped to one of the 21 explicit species, SAPRC99 lumps the explicit species into model species based on kOH.

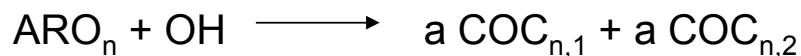
There were a few instances when both a high-SOA and a low-SOA yield aromatic compound in the composition profile were mapped to the same explicit aromatic, yet they need to be lumped into separate model species. As a result, mapping could not be done with a single composition file since compounds in different SOA-yield groups were assigned to the same explicit compound and SAPRC99 would not know which lumped group this mapped compound belongs to. To overcome this, three separate composition files were created for high-yield, low-yield and no-yield SOA compounds, and the mapping and lumping was done separately for each composition file. In this way a high-yield and a low-yield compound could be represented by the same explicit species to determine its reaction mechanics, yet they would end up in separate lumped groups.

A final complication arose when lumping the expanded aromatic mechanisms, which have additional model species for intermediate aerosol

precursors (APRs) and condensable organic carbon (COC) reaction products. (Note that COC is synonymous with SVOC, semi-volatile organic compound, in this work.) Lumping rate constants and product stoichiometry for intermediate reaction products is not straightforward because there is no way to determine what the relative composition of these compounds will be. Nevertheless, Dechapanya et al (2003b) describe a method to lump parameters for these intermediate precursors and reaction products using weighting methods that account for the reactivity of the intermediate and reacted amount of aromatic precursor. Two lumped precursors are created per lumped aromatic model species, and two lumped condensable products are created per lumped intermediate, as shown in Figure 5.3. There are three lumped aromatic species in s99soa2 that produce SOA: high-yield low-reactivity (AR1H), high-yield high-reactivity (AR2H) and low-yield high-reactivity (AR2L). Three lumped species result in a total of six lumped aerosol precursors and 12 lumped condensable species.

The lumping of *aromatic* compounds is the same for s99soa and s99soa2, i.e. emissions weighted average parameters based on the Texas anthropogenic profile. The lumping of *aerosol precursor* and *condensable product* parameters follows exactly the weighting methods described by Dechapanya et al, but uses the Texas anthropogenic emissions profile for relative composition. The lumping methods described by Dechapanya et al (2003b) cannot be done automatically by SAPRC99 software, so lumped parameters were calculated using Microsoft Excel. These lumped parameters are given in Table 5.6.

a) s99soa representation of condensable OC (COC) formation



b) s99soa2 representation of condensable OC (COC) formation

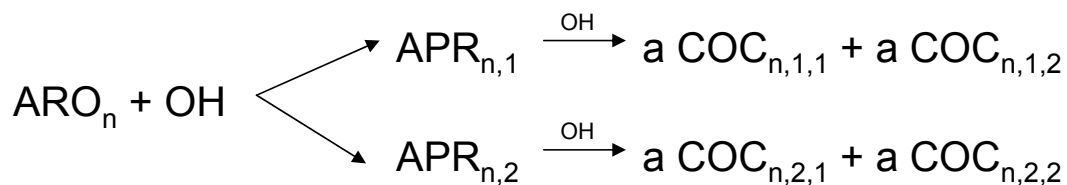


Figure 5.3. Illustration of aromatic-SOA formation in a) s99soa and b) s99soa2 (Dechapanya et al. 2003b). ARO represents a lumped aromatic species. APR represents intermediate aerosol precursors. COC represents condensable (or semi-volatile) organic compounds.

Table 5.6 Lumped mechanism parameters for intermediate model species (APR) and condensable reaction products (COC) in the s99soa2 mechanism. Parameters were derived using spreadsheet calculations and using the Texas anthropogenic emissions profile.

ARO name	APR			COC			
	name	kOH cm <sup>3</sup> /molec-s	MW g/mol	name	a	MW g/mol	Kom
AR1H	APH1	7.1 e-12	85.5	SVH1	0.25	164.5	0.01801
				SVH2	0.75	118.5	0.001392
	APH3	18.5 e-12	100.4	SVH3	0.25	179.4	0.016617
				SVH4	0.75	133.4	0.001251
AR2H	APH2	9.23 e-12	98.2	SVH5	0.25	177.2	0.004442
				SVH6	0.75	131.2	0.000383
	APH4	22.2 e-12	108.4	SVH7	0.25	187.4	0.004513
				SVH8	0.75	141.4	0.000387
AR2L	APL2	9.56 e-12	96.1	SVL5	0.25	175.1	0.004415
				SVL6	0.75	129.1	0.000341
	APL4	30.07 e-12	109.7	SVL7	0.25	188.7	0.004839
				SVL8	0.75	142.7	0.000274

\* Note there is no AR1L because no emitted aromatic compounds fall into this category

This section described the development of two new chemical mechanisms to model SOA formation: s99soa and s99soa2. Both were based on the original fixed parameter version of SAPRC99, except they included explicit (unlumped) representations of five monoterpenes and separate lumped categories for high-, low- and no-yield aromatics. In addition, s99soa2 had additional aerosol precursor reactions and model species, which are formed by high- and low-SOA yield aromatic species. These mechanisms were used in a modified version of CAMx31 to model SOA formation, which in turn requires the emissions to be represented using the model species of the mechanism. The next section describes the development of emissions inventories for the s99soa/s99soa model species.

### **5.3 Emissions Inventory development**

There are four major emissions categories in air quality modeling: point sources, on-road mobile sources, area sources (which include off-road mobile sources) and biogenic sources. Standard emissions inventories (EI) are collected typically as total VOC, NO<sub>x</sub> and CO emissions (SO<sub>2</sub>, NH<sub>3</sub> and primary PM may also be collected for PM modeling). Furthermore this raw data is usually available as annual or 24-hour ‘typical day’ emissions and reported for large geographic areas, for example, entire counties. Grid models require speciated VOCs (into species represented by the chemical mechanism), at hourly intervals and for each grid cell. As a result, the three main steps involved in emissions processing are 1) speciation of total VOC emissions to model species, 2) allocation of daily or

annual emissions to each hour of the modeling episode, and 3) allocation of emissions to the modeling grid cells.

The TCEQ has assembled raw emissions data for purposes of modeling the TXAQS episode. Ideally, raw emissions data from all categories would be determined for each specific episode day; however, developing emissions inventories is an enormous undertaking and often the best available emissions are from previous years. Emissions may be adjusted during the emissions processing if they are thought to be substantially different from emissions during the modeling episode. In contrast, raw emission data for some important sources are often collected or estimated for specific days or even hours, for example, biogenic emissions are highly temperature dependent and are determined specific to each hour in the modeling episode.

Anthropogenic emissions were processed into model ready format using the Emissions Preprocessor System 2.0 (EPS2) which is a series of FORTRAN-77 programs originally designed by the U.S. Environmental Protection Agency and Systems Application International. (EPS2 is no longer available via the Internet from the E.P.A.) The EPS2 that was used in this research has been enhanced (updated, patched etc.) extensively compared to the original release. This code was compiled and run on the UNIX-based workstations at the Center for Energy and Environmental Resources at the University of Texas at Austin.

Biogenic emissions data were processed into model ready format using the Global Biosphere Emissions and Interactions System version 2.2 (GLOBEIS) which is a Microsoft Access based application developed by ENVIRON

International and the National Center for Atmospheric Research (NCAR). GLOBEIS 2.2 is available for free at [www.globeis.com](http://www.globeis.com). GLOBEIS estimates biogenic emissions using land use and meteorology data that is specific to the modeling domain and episode. As discussed later, GLOBEIS version 2.2 was modified for this research.

Both GLOBEIS and EPS2 require significant user experience and the reader is referred to the EPS2 and GLOBEIS User's Manuals for details on using these programs. This chapter will focus on the way these programs were used to develop emissions inventories for SOA modeling. The detail presented here is meant to allow someone who is familiar with GLOBEIS or EPS2 to reproduce the emissions inventories created for SOA modeling. The next two sub-sections describe the processing of the anthropogenic and biogenic emissions respectively. Note that the s99soa and s99soa2 mechanisms share the same model species for emitted VOC compounds, so the same emissions were used for both mechanisms (they will be referred to as s99soa emissions). The emissions for the TXAQS episode were also processed into s99 mechanism species (the standard fixed parameter version of SAPRC99). Although this mechanism was not used in this research, the SAPRC99 mechanism is regarded as one of the most up-to-date mechanisms for gas-phase chemistry. These emissions were processed so they could be used in future research with this important modeling episode. The development of a SAPRC99 modeling inventory for the modeling domain was a major accomplishment of this research.

### ***Anthropogenic emissions processing***

The majority of the work in processing the emissions inventory for the TXAQS episode involved organization and quality assurance of the files necessary to run EPS2. The details of this routine processing, and sources and descriptions of the EI files are presented in Appendix A for all anthropogenic sources.

The TCEQ has processed emissions for the TXAQS episode and has developed the inputs that are needed to accomplish chemical, temporal and spatial allocation. Temporal and spatial allocation of the emissions in this research is done with inputs provided by TCEQ (see Appendix A for references). The TCEQ, however, speciates the emissions to CB4 species because this is the chemical mechanism used for regulatory modeling. Since this research used the new s99soa mechanism used for regulatory modeling. Since this research used the new s99soa mechanism, the emissions were speciated to s99soa species. Note that even though only the chemical speciation was of interest in this research, the temporal and spatial allocation of emissions needed to be repeated. In essence the entire emissions inventory was reprocessed from raw emissions data into model ready format. The chemical speciation step was the most important part of the emissions processing for this research and is discussed below.

Raw VOC emissions data that is input to EPS2 is in units of mass of total VOC. EPS2 speciates total VOC emissions into model species using splitfactors, which are multiplicative factors for converting mass of VOC to moles of model species. One set of splitfactors (one for each model species) is unique to each emissions source or category. A set of splitfactors is created in two steps: 1)

speciating total VOC emissions to individual organic compounds (speciation profile), and 2) representing these compounds as model species. It is important to distinguish splitfactors from speciation profiles: a speciation profile refers to the mass fractions of individual organic compounds that make up total VOC emissions from a particular source. The objectives here are to create splitfactors for the new s99soa mechanism and to establish a methodology to create splitfactors for any new chemical mechanism.

The first step to creating splitfactors was to gather speciation profiles for all emissions categories (sources), and to gather data on which profiles are assigned to which categories. The sources of speciation profiles and assignments for each emissions group are summarized in Table 5.7 below (note that each emissions group can have thousands of individual sources, and thus thousands of different speciation profiles). Many emissions inventories are speciated using a standard set of speciation profiles that are adequate, but that are outdated or that are not region-specific. A unique feature of this modeling study is that all Texas point sources, and motor vehicles in the Southeast Texas area have unique speciation profiles, which increases the accuracy of the inventory.

The TCEQ has collected detailed speciation profiles from all major point sources in Texas and compiled a compound specific emissions inventory. These data and associated documentation can be found at:

[http://www.tnrc.state.tx.us/air/aqp/airquality\\_photomod.html#ei3a](http://www.tnrc.state.tx.us/air/aqp/airquality_photomod.html#ei3a)

In addition, an emissions measurement study in a vehicular tunnel during the TXAQS time period provided motor vehicle emission speciation that is specific to the area. The tunnel study data and report can be found at:

[ftp://narsto.esd.ornl.gov/pub/EPA\\_Supersites/houston/WASHBURN\\_TUNNEL](ftp://narsto.esd.ornl.gov/pub/EPA_Supersites/houston/WASHBURN_TUNNEL)

Both links above were accessed on 10/01/2003.

Table 5.7: Sources of speciation profiles for different emissions groups

<b>Group</b>	<b>Profiles (source)</b>	<b>Assignment file (source)</b>
Mobile sources (outside HG )	SPECIATE 3.2 (5)	chmprf.xref.voc.v0598.98May05.x_tra.a1 (1)
Mobile sources (inside HG)	Washburn Tunnel Study (6)	chmprf.xref.voc.links.UT (3)
Area sources (4km grid)	SPECIATE 3.2 and TCEQ (7)	scc-voc.prf.voc.xref.08Jan02.area.strip (2)
Area sources (36km&12km)	SPECIATE 3.2 and TCEQ (7)	chmprf.xref.voc.v0598.98May05.x_tra.a1 (1)
Point sources (outside TX)	SPECIATE 3.2 (5)	xref.voc.hg2000.pt.all (4)
Point sources (inside TX)	TCEQ point source database (8)	xref.voc.hg2000.pt.all (4)
Point sources (Special Inventory)	TCEQ point source database (2)	xref.voc.hg2000.pt.all (4)

1: From the 'Texas near non-attainment area' (txna) modeling projects. Residing on CEER systems on disk: /aacogl (Spring 2003) and originally from ENVIRON under contract to the University of Texas at Austin.

2: From TCEQ. Directly obtained from a staff member via email or file transfer ftp site.

3: These link processing files are slightly modified files that were originally in the archive: mobile6.2000.hga\_8county.eps2x\_input\_files.tar which was downloaded from (<ftp://tnrcc.state.tx.us/pub/OEPAA/TAD/Modeling/HGAQSE/Modeling/EI>). chmprf.xref.voc.links.UT is the same as chmprf.xref.voc.MV\_hstn\_upd.m6 except the labels of the speciation profiles are different.

4: From TCEQ. Directly obtained from a staff member via file transfer ftp site. This file was originally in an archive called EPSbase4a.tar.

5: Available online: [www.epa.gov/ttn/chief/software/speciate/index.html](http://www.epa.gov/ttn/chief/software/speciate/index.html).

6: Available online: [narsto.esd.ornl.gov/pub/EPA\\_Supersites/houston/WASHBURN\\_TUNNEL](http://narsto.esd.ornl.gov/pub/EPA_Supersites/houston/WASHBURN_TUNNEL).

7: All SPECIATE3.2 profiles had 4-digit labels less than 9000. The TCEQ provided some additional speciation profiles with labels greater than 9000 and with non-numeric labels, e.g. D410.

8: From TCEQ. Available online: [ftp://tnrcc.state.tx.us/pub/OEPAA/TAD/Modeling/HGAQSE/Modeling/EI/HGMCR\\_Point\\_Source\\_Speciation\\_Profiles\\_20030707.zip](ftp://tnrcc.state.tx.us/pub/OEPAA/TAD/Modeling/HGAQSE/Modeling/EI/HGMCR_Point_Source_Speciation_Profiles_20030707.zip)

After all speciation profiles were gathered and appropriate assignments had been made for each emissions category, the second step was to convert the profiles (mass of organic compounds and mixtures) to splitfactors (moles of model species per unit mass). Generally, this involves ‘mapping’ or assigning the organic compounds to model species, and converting mass of compound to moles of model species. Speciation profiles may also contain components that are mixtures of organic compounds. In this case, these first must be split into individual compounds before being assigned to a model species. One important consideration is that classifications or identifiers used for the organic compounds/mixtures can be different depending on the source of the information. For example, the SPECIATE3.2 (see reference in Table 5.7) profiles denote propene as “PROPE”, whereas Texas speciation profiles use the 5-digit code “43205”. There are thousands of organic compounds and mixtures in speciation profiles, and there are thousands of unique speciation profiles; therefore lumping to model species must be automated. This research made use of a tool, emitdb.xls, which was developed by the same researchers that developed SAPRC and was available at (<ftp://ftp.cert.ucr.edu/pub/carter/emitdb/emitdb.xls>). Emitdb.xls was modified and used in this research to create splitfactors for the new mechanism. These modifications are presented in detail in Appendix C.

There are five lumped aromatic groups in the s99soa mechanism: low-reactivity/high-SOA yield (AR1H), high-reactivity/high-SOA yield (AR2H), high-reactivity/low-SOA yield (AR2L), low-reactivity/no-SOA yield (AR1N) and high-reactivity/no-SOA yield (AR2N). The aromatics were classified into SOA-

yield groups according to criteria discussed in the previous section; they were classified into reactivity groups based on whether kOH was less or greater than  $2 \times 10^4 \text{ ppm}^{-1} \text{ min}^{-1}$  (low or high reactivity respectively). Table 5.8 below lists all possible aromatic compounds included in emitdb.xls and shows their assigned yield and reactivity category. Assignments to SOA-yield categories were based on broad criteria from limited experimental data, and this is clearly an area where improvements can be made when better data becomes available. Table 5.2 shows the total aromatic emissions for Texas for each category. The majority of emitted aromatics fall into the high- or low- yield categories, and so SOA formation is accounted for from the majority of aromatic emissions.

Table 5.8 All aromatic compounds in emitdb.xls and that are found in speciation profiles. Also shown is their assigned yield classification.

UniqueID (CAS number)	Description	SOA yield	OH reactivity
C100-41-4	ethylbenzene	high	low
C103-65-1	n-propylbenzene	high	low
C104-51-8	n-butylbenzene	high	low
C1077-16-3	n-hexylbenzene	high	low
C1078-71-3	heptyl benzene	high	low
C108-88-3	toluene	high	low
C1196-58-3	3-phenylpentane	high	low
C135-98-8	(1-methylpropyl)benzene (sec-butyl benzene)	high	low
C29316-05-0	s-pentylbenzene	high	low
C538-68-1	n-pentylbenzene	high	low
C538-93-2	(2-methylpropyl)benzene	high	low
C71-43-2	benzene	high	low
C98-06-6	t-butylbenzene	high	low
C98-82-8	cumene (isopropyl benzene)	high	low
C13632-95-6	1,3-diethyl-2-methyl Benzene	high	high
C13732-80-4	1,2-diethyl-4-methylbenzene	high	high
C1758-85-6	1,3-diethyl-4-methyl benzene	high	high

C2050-24-0	1,3-diethyl-5-methyl benzene	high	high
C100-18-5	1,2-isodipropylbenzene	high	high
C100451-97-6	1-methyl-2,4-dipropyl benzene	high	high
C102-25-0	1,3,5-triethylbenzene	high	high
C105-05-5	1,4-diethylbenzene (para)	high	high
C1074-17-5	1-methyl-2n-propylbenzene	high	high
C1074-43-7	1-methyl-3n-propylbenzene	high	high
C1074-55-1	1-methyl-4n-propylbenzene	high	high
C1074-92-6	1-methyl-2-tert-butylbenzene	high	high
C126028-51-1	1-butyl-3-ethyl benzene	high	high
C135-01-3	1,2-diethylbenzene (ortho)	high	high
C141-93-5	1,3-diethylbenzene (meta)	high	high
C1595-04-6	1-methyl-3-butylbenzene	high	high
C1595-11-5	1-methyl-2-n-butylbenzene	high	high
C16021-20-8	1-ethyl-2-propylbenzene	high	high
C17171-72-1	m-dipropyl benzene	high	high
C18970-44-0	1-ethyl-2-isopropylbenzene	high	high
C26573-16-0	ethyl isopropyl benzene	high	high
C27138-21-2	trans-1-butyl-2-methylbenzene	high	high
C4218-48-8	1-ethyl-4-isopropylbenzene	high	high
C527-84-4	1-methyl-2-isopropylbenzene	high	high
C535-77-3	1-methyl-3-isopropylbenzene	high	high
C577-55-9	1,4-isodipropylbenzene	high	high
C611-14-3	o-ethyltoluene	high	high
C620-14-4	m-ethyltoluene	high	high
C622-96-8	p-ethyltoluene	high	high
C7364-19-4	trans-1-butyl-4-ethylbenzene	high	high
C877-44-1	1,2,4-triethylbenzene	high	high
C98-51-1	1-methyl-4-t-butylbenzene	high	high
C99-62-7	1,3-isodipropylbenzene	high	high
C99-87-6	1-methyl-4-isopropylbenzene	high	high
S2-91120	1-methyl-4-n-pentylbenzene	high	high
S2-99064	1-methyl-4-isobutylbenzene	high	high
C106-42-3	p-xylene	low	high
C108-38-3	m-xylene	low	high
C108-67-8	1,3,5-trimethylbenzene	low	high
C17059-44-8	1,2-dimethyl-3-propyl benzene	low	high
C17059-45-9	1,3-dimethyl-2-propyl benzene	low	high
C1758-88-9	1,4-dimethyl-2-ethylbenzene	low	high
C17851-27-3	1-ethyl-2,4,5-trimethyl benzene	low	high
C18262-85-6	1-ethyl-2,3,5-trimethyl benzene	low	high

C25321-29-3	dimethyl, isopropyl benzene	low	high
C2870-04-4	1,3-dimethyl-2-ethylbenzene	low	high
C3042-50-0	1,4-dimethyl-2-propyl Benzene	low	high
C31366-00-4	1,2,3-trimethyl-5-ethyl Benzene	low	high
C3982-64-7	1,3-dimethyl-5-propylbenzene	low	high
C3982-66-9	1,2-dimethyl-4-propyl benzene	low	high
C3982-67-0	2-ethyl-1,3,5-trimethyl benzene	low	high
C4706-89-2	1,3-dimethyl-4-isopropylbenzene	low	high
C488-23-3	1,2,3,4-tetramethylbenzene	low	high
C526-73-8	1,2,3-trimethylbenzene	low	high
C527-53-7	1,2,3,5-tetramethylbenzene	low	high
C61827-85-8	2,4-dimethyl-1-propyl benzene	low	high
C61827-86-9	1,2,3-trimethyl-4-ethylbenzene	low	high
C61827-87-0	2-ethyl-1,3,4-trimethyl benzene	low	high
C700-12-9	pentamethylbenzene	low	high
C874-41-9	1,3-dimethyl-4-ethylbenzene	low	high
C933-98-2	1,2-dimethyl-3-ethylbenzene	low	high
C934-74-7	1,3-dimethyl-5-ethylbenzene	low	high
C934-80-5	1,2-dimethyl-4-ethylbenzene	low	high
C95-47-6	o-xylene	low	high
C95-63-6	1,2,4-trimethylbenzene	low	high
C95-93-2	1,2,4,5-tetramethylbenzene	low	high
C98-19-1	1-(1,1-dimethylethyl)-3,5-dimethylbenzene	low	high
C100-21-0	terephthalic acid (p-benzenedicarboxylic acid)	no	low
C100-44-7	benzyl chloride	no	low
C100-51-6	benzyl alcohol	no	low
C100-61-8	4-methylaniline	no	low
C101-77-9	4,4-methylene dianiline	no	low
C101-90-6	diglycidyl resorcinol ether [dgre]	no	low
C103-29-7	diphenyl ethane [bibenzyl]	no	low
C103-71-9	phenyl isocyanate	no	low
C103-82-2	Phenylacetic Acid	no	low
C103-90-2	acetaminophen	no	low
C106-46-7	p-dichlorobenzene	no	low
C108-90-7	chlorobenzene	no	low
C109201-63-0	butyl isopropyl phthalate	no	low
C110-02-1	Thiophene	no	low
C110-86-1	pyridine	no	low
C119-36-8	methyl salicylate (an ester)	no	low
C120-32-1	chlorophene	no	low
C120-61-6	dimethylterephthalate	no	low

C121-14-2	2,4-Dinitrotoluene	no	low
C122-70-3	benzylcarbinyl propionate	no	low
C122-99-6	2-phenoxyethanol	no	low
C131-11-3	dimethyl phthalate	no	low
C131-16-8	dipropyl phthalate	no	low
C1331-14-2	2,2-dichloronitroaniline	no	low
C133753-32-9	trans-1-phenylbutene	no	low
C136-60-7	n-butyl benzoate	no	low
C140-11-4	benzyl acetate	no	low
C15232-92-5	3-pentylcyclohexane	no	low
C1817-73-8	bromodinitroaniline [2,4-dinitro-6-bromoaniline]	no	low
C27129-87-9	3,5-Dimethylbenzyl alcohol	no	low
C4169-04-4	propylene glycol phenyl ether (2-phenoxy-1-propanol)	no	low
C475-38-7	5,8-dihydroxy-1,4-Naphthalenedione	no	low
C541-73-1	1,3-dichlorobenzene [m-dichlorobenzene]	no	low
C584-48-5	bromodinitrobenzene	no	low
C605-02-7	1-Phenylnaphthalene	no	low
C619-04-5	3,4-dimethylbenzoic acid	no	low
C62-53-3	aniline [aminobenzene]	no	low
C643-93-6	3-methyl biphenyl	no	low
C65-85-0	benzoic acid	no	low
C768-56-9	4-phenyl-1-butene	no	low
C84-74-2	dibutyl phthalate	no	low
C85-44-9	phthalic anhydride	no	low
C88-04-0	4-chloro-3,5-xyleneol	no	low
C88-72-2	2-nitrotoluene	no	low
C92-52-4	biphenyl [phenyl benzene]	no	low
C93-58-3	methyl benzoate	no	low
C95-16-9	benzothiazole	no	low
C95-49-8	o-chlorotoluene	no	low
C95-50-1	o-dichlorobenzene	no	low
C98-00-0	furfuryl alcohol	no	low
C98-01-1	2-furfural	no	low
C98-08-8	Benzotrifluoride	no	low
C98-86-2	acetophenone (Phenyl methyl ketone)	no	low
C98-88-4	Benzoyl chloride	no	low
C98-95-3	nitrobenzene	no	low
S1-45230	di(ethylphenyl)ethane	no	low
S2-99377	ethyl-phenyl-phenyl-ethane	no	low
C1075-22-5	5,6-dimethyl-2,3,dihydro-1-h-indenes	no	high
C110-00-9	furan	no	high

C119-64-2	tetralin	no	high
C120-12-7	anthracene	no	high
C129-00-0	pyrene	no	high
C1321-67-1	naphthol	no	high
C132-64-9	dibenzofuran	no	high
C1556-99-6	4-methyl fluorene	no	high
C1685-82-1	4,6-dimethyl-2,3,dihydro-1-h-indenes	no	high
C1685-83-2	4,5-dimethyl-2,3,dihydro-1-h-indenes	no	high
C1705-85-7	6-Methylchrysene	no	high
C1730-37-6	1-methyl-9h-fluorene	no	high
C195-19-7	benzo(c)phenanthrene	no	high
C201-06-9	acephenanthrylene	no	high
C203-12-3	benzo[ghi]fluoranthene	no	high
C206-44-0	fluoranthene	no	high
C208-96-8	acenaphthylene	no	high
C218-01-9	chrysene	no	high
C2245-38-7	2,3,5-trimethylnaphthalene	no	high
C23339-05-1	7-methylfluoranthenes	no	high
C2531-84-2	2-methylphenanthrene	no	high
C27208-37-3	cyclopenta[cd]pyrene	no	high
C2765-18-6	1-propyl naphthalene	no	high
C29036-25-7	methylindene	no	high
C3208-16-0	2-ethyl furan	no	high
C33484-76-3	1,2,3-trimethyl indan	no	high
C39292-53-0	methyldihydronaphthalene	no	high
C496-11-7	indan	no	high
C53563-67-0	Dimethyl Indan	no	high
C54340-88-4	2,3-dihydro-1,5,7-trimethyl-1h-indene	no	high
C56147-63-8	2-ethylindan	no	high
C56-55-3	benzo(a)anthracene	no	high
C571-58-4	1,4-dimethylnaphthalene	no	high
C573-98-8	1,2-dimethyl naphthalene	no	high
C581-40-8	2,3-dimethylnaphthalene	no	high
C581-42-0	2,6-dimethyl naphthalene	no	high
C6111-78-0	11-Methylbenz[a]anthracene	no	high
C613-12-7	2-methylanthracene	no	high
C6232-48-0	4,5-dihydroacephenanthrylene	no	high
C641-48-5	1,2-Dihydroaceanthrylene	no	high
C652-04-0	2-Methyl-3,4-benzphenanthrene	no	high
C66291-35-8	1-ethylanthracene	no	high
C66291-36-9	4-Ethylphenanthrene	no	high

C66610-91-1	2,3-diethylnaphthalene	no	high
C6682-71-9	4,7-dimethyl-2,3-dihydro-1-h-indenes	no	high
C70063-93-3	1,2-dimethylindene	no	high
C767-58-8	1-methyl indan	no	high
C824-22-6	4-methylindan	no	high
C824-63-5	2-methylindan	no	high
C832-69-9	1-methylphenanthrene	no	high
C832-71-3	3-methylphenanthrene	no	high
C83-32-9	acenaphthene	no	high
C84-65-1	9,10-anthraquinone	no	high
C85-01-8	phenanthrene	no	high
C86-73-7	fluorene	no	high
C874-35-1	5-methylindan	no	high
C87-44-5	caryophyllene	no	high
C879-12-9	1,2,3-trimethyl naphthalene	no	high
C883-20-5	9-methylphenanthrene	no	high
C90-12-0	1-methyl naphthalene	no	high
C91-20-3	naphthalene	no	high
C91-57-6	2-methylnaphthalene	no	high
C93-04-9	2-methoxy-naphthalene	no	high
C939-27-5	2-ethylnaphthalene	no	high
C95-13-6	indene	no	high

Splitfactors were created for all anthropogenic speciation profiles using the modified emitdb.xls, and the emissions were ready to be processed through EPS2. One limitation of EPS2 is that it is recommended to not process more than 30 model species. The s99soa and s99 mechanisms have 46 and 40 emission model species respectively. To overcome this limitation, EPS2 was processed twice for each emissions file: in one process the total VOC emissions were split into half of the model species, in the other process the emissions were split into the other half of the model species. Each set of splitfactors was divided into two, creating two files, each with half the model species. In addition, two sets of EPS2 userin files were created, each with half the model species. In this way EPS2 could be used to process an inventory with any number of model species, as long

as each process used less than thirty model species in the splitfactor and userin files. Note that a set of split factors for a particular source need not add up to 1.0 for the CHMSPL module, i.e. the total VOC inputs to CHMSPL may be partially split to model species during the EPS2 process, and therefore it is feasible to divide splitfactor files into multiple sets.

Each emissions category uses a label to identify the set of splitfactors that are assigned to it. The assignment of a splitfactor set is listed in a cross reference file. The original EPS2 only recognizes splitfactors label up to five-digits. There are over 9000 individual speciation profiles for Texas point sources (and thus over 9000 splitfactors), and the TCEQ developed a nomenclature system for these profiles that uses 14-digit labels. An alternate version of CHMSPL that recognized 14-digit splitfactor labels was obtained from the TCEQ and this was used for the point source emissions processing.

### ***Biogenic emissions processing***

Biogenic emissions for the TXAQS episode were processed using the Global Biosphere Emissions and Interactions System (GLOBEIS) version 2.2, which is available at ([www.globeis.com](http://www.globeis.com)). GLOBEIS is a Microsoft Access based program that calculates emissions of isoprene, NO, total monoterpenes and ‘other’ VOC’s. GLOBEIS requires gridded landuse and temperature data as inputs. In addition, cloud-cover or photo-synthetic active radiation (PAR) in each grid cell can be included. A built-in data base contains the leaf mass density of tree species

that are found in each landuse category, and emissions factors of isoprene, NO, total monoterpenes and ‘other’ VOC’s for each tree species.

Two modifications were necessary to GLOBEIS to estimate biogenic emissions for s99 and the s99soa mechanism. First, the program was modified to calculate emissions for s99 and s99soa/s99soa2 model species, in addition to CB4 model species. This was done to allow the user to choose a mechanism at run time. Second, the program was modified to calculate emissions from 14 individual monoterpene compounds. Total monoterpene emissions estimates were speciated into the 14 compounds by tree species using monoterpene speciation data from Geron et al. (2000). The result was the most detailed emissions model for biogenic monoterpenes in Southeast Texas to date. The s99soa mechanism considers only 5 monoterpenes explicitly, and so emissions of the remaining 9 were lumped into an ‘other terpene’ category. Both GLOBEIS modifications are described in detail in Appendix D.

### ***SOA precursor emissions summary***

The processing of emissions to new chemical mechanisms was challenging because most emissions processing software is intended to produce CB4 model species. As described above, multiple programs were modified or developed to allow emissions to be processed to new model species. These tools, along with the modified grid model, are intended to help future researchers overcome the limitation of fixed chemical mechanisms. This section concludes by presenting the emissions of SOA precursors for a single day in the modeling

episode. Table 5.9 shows emissions of aromatics and monoterpene model species in the entire 4km HGBPA modeling domain, in the 11-county HGBPA area, and in the SOA-formation subdomain. (The SOA-formation subdomain is the area within which SOA formation rates were calculated and is described in section 5.5). As can be seen, biogenic monoterpenes dominate these emissions and it is expected that these will contribute greatly to SOA formation in the area. The SOA formation model is described in the section 5.5.

Table 5.9. Emissions of SOA precursors input to the TXAQS episode on August 31<sup>st</sup>, 2000. (AR1H: high-SOA yield/low-reactivity aromatics. AR2H: high-SOA yield/high-reactivity aromatics. AR2L: low-SOA yield/high-reactivity aromatics) Units are in tons/day

<b>tons/day</b>	<b>AR1H</b>	<b>AR2H</b>	<b>AR2L</b>	<b><math>\alpha</math>-pinene</b>	<b><math>\beta</math>-pinene</b>	<b>sabinene</b>	<b><math>\Delta^3</math>-carene</b>	<b>limonene</b>	<b>other terpenes</b>
<b>4-km HGBPA modeling domain</b>									
Low-level anthropogenic	78.6	10.1	51.5	2.8	1.8	0.1	0.1	0.4	0.2
Elevated anthropogenic	3.4	0.1	1.4	0.5	0.3	0.0	0.0	0.1	0.0
Biogenic	0.0	0.0	0.0	699.2	373.6	9.3	58.8	139.8	118.1
<b>Total</b>	<b>82.0</b>	<b>10.2</b>	<b>52.9</b>	<b>702.5</b>	<b>375.8</b>	<b>9.4</b>	<b>58.9</b>	<b>140.3</b>	<b>118.3</b>
<b>11-county Houston-Galveston, Beaumont Port-Arthur Area</b>									
Low-level anthropogenic	63.3	7.8	39.4	0.3	0.2	0.0	0.0	0.1	0.0
Elevated anthropogenic	1.9	0.0	0.7	0.2	0.1	0.0	0.0	0.0	0.0
Biogenic	0.0	0.0	0.0	258.1	136.2	2.8	20.0	53.0	37.8
<b>Total</b>	<b>65.2</b>	<b>7.8</b>	<b>40.0</b>	<b>258.6</b>	<b>136.6</b>	<b>2.8</b>	<b>20.0</b>	<b>53.1</b>	<b>37.8</b>
<b>SOA formation subdomain (limit of Kriging interpolation)</b>									
Low-level anthropogenic	50.3	6.1	30.9	0.3	0.2	0.0	0.0	0.1	0.0
Elevated anthropogenic	2.7*	0.0	0.9*	0.1	0.1	0.0	0.0	0.0	0.0
Biogenic	0.0	0.0	0.0	187.6	100.1	1.8	14.2	38.3	26.0
<b>Total</b>	<b>53.0</b>	<b>6.1</b>	<b>31.7</b>	<b>188.0</b>	<b>100.4</b>	<b>1.8</b>	<b>14.2</b>	<b>38.3</b>	<b>26.0</b>

\* Note that the elevated aromatic emissions are greater in the SOA subdomain than in the 11-county area, despite the fact that the SOA subdomain is smaller. The additional emissions are from offshore sources which were included in the SOA subdomain but fall outside of the borders of the 11 counties.

#### 5.4 TXAQS Episode Model Performance

The previous sections described the development of a chemical mechanism for modeling SOA formation in Southeast Texas, and the development of emissions inventories of the mechanism's species for the TXAQS episode. The primary objective of this research was to model SOA formation and these results are presented in the next chapter. Before presenting the results, however, it is useful to evaluate the overall performance of the model. Photochemical grid models are evaluated by comparing modeled versus measured concentrations. A full statistical performance evaluation of the TXAQS episode went beyond the scope of this research; however, this section presents a general comparison of modeled vs. measured ground-level ozone concentrations during important episode days. These comparisons were relevant since many of the reactive intermediates important in ozone formation are also important in SOA formation.

Model performance was examined by looking at sets of ozone concentration isopleths for modeled and measured ozone, at 2pm, 4pm, 6pm and 8pm on Aug 28<sup>th</sup> through Aug 31<sup>st</sup>, 2000. Model concentration isopleths were created in PAVE from the base case modeling results with the s99soa mechanism. Measured concentrations isopleths were available online from the TCEQ ([http://www.tnrec.state.tx.us/cgi-bin/monops/ozone\\_animation](http://www.tnrec.state.tx.us/cgi-bin/monops/ozone_animation)). This site was accessed on Nov 1<sup>st</sup>, 2003. Measured concentration isopleths reflect spatially interpolated ambient measurements. Note that spatial interpolation is most accurate where monitoring site density is highest, namely in the urban/industrial

areas of Houston and not, for example, in the areas between Houston and Beaumont. Concentration isopleths for each episode day are presented separately in Figures 5.4 through 5.7.

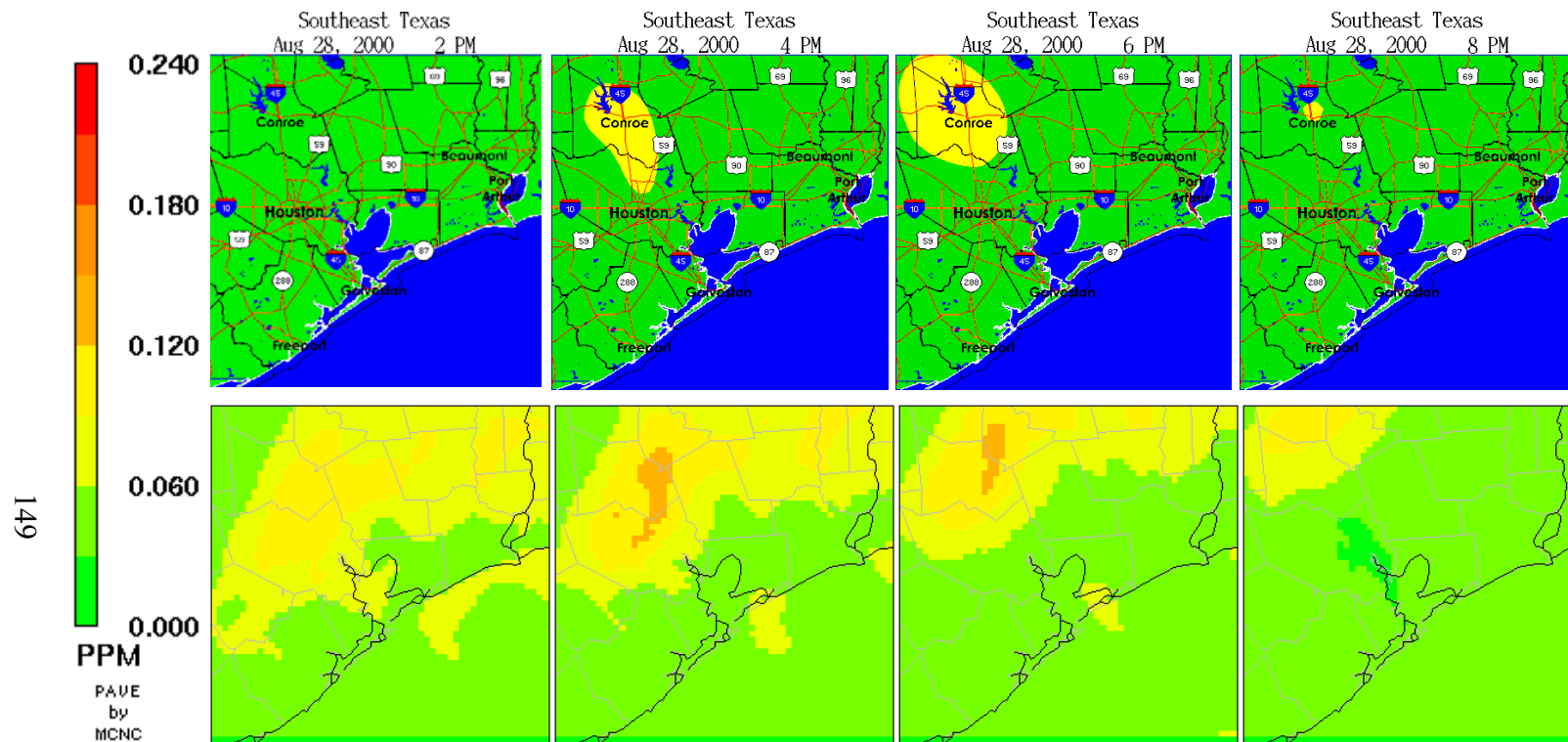


Figure 5.4. Monitored (top row) and modeled (bottom row) ozone concentrations on Aug 28<sup>th</sup>, 2000 at 2pm, 4pm, 6pm and 8pm.

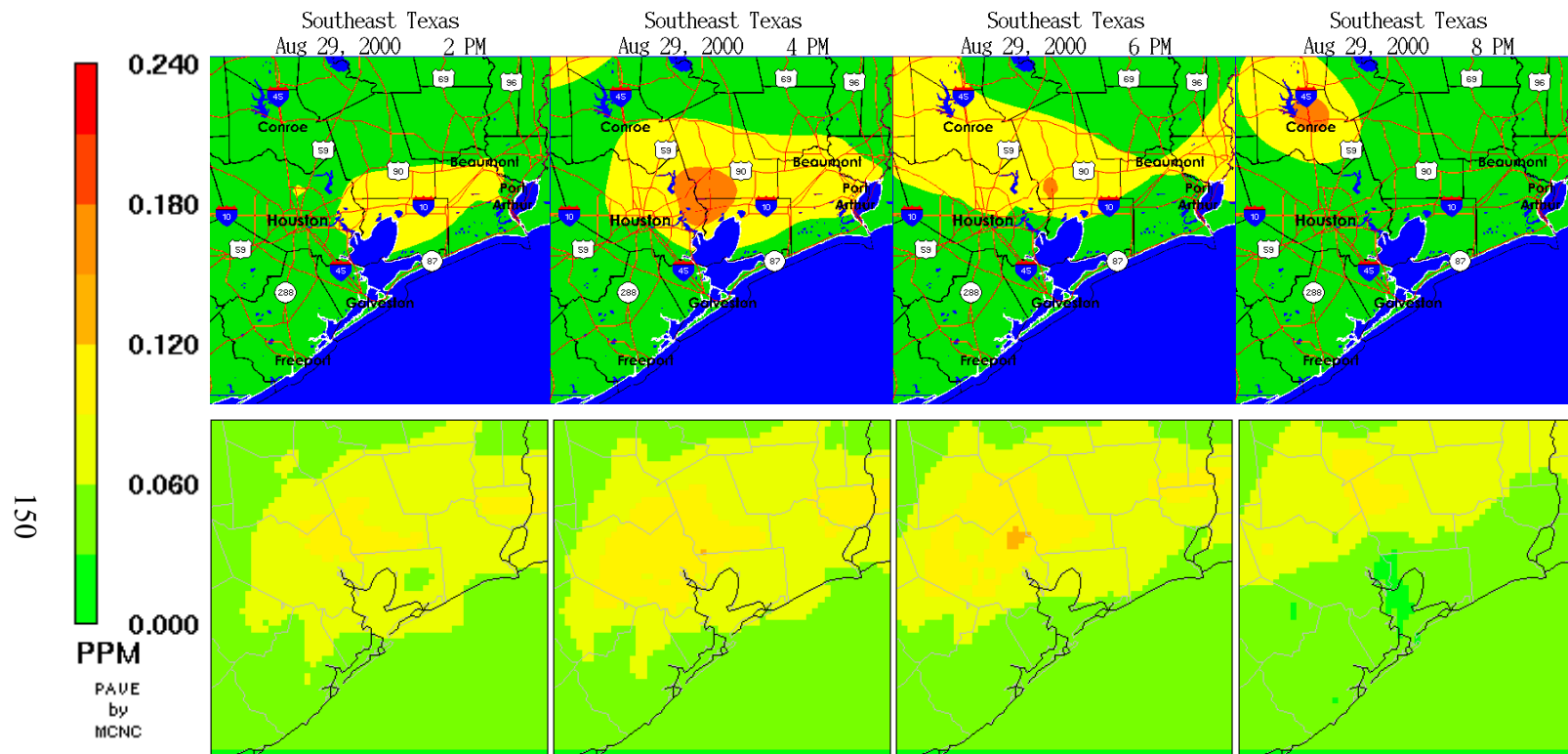


Figure 5.5. Monitored (top row) and modeled (bottom row) ozone concentrations on Aug 29<sup>th</sup>, 2000 at 2pm, 4pm, 6pm and 8pm.

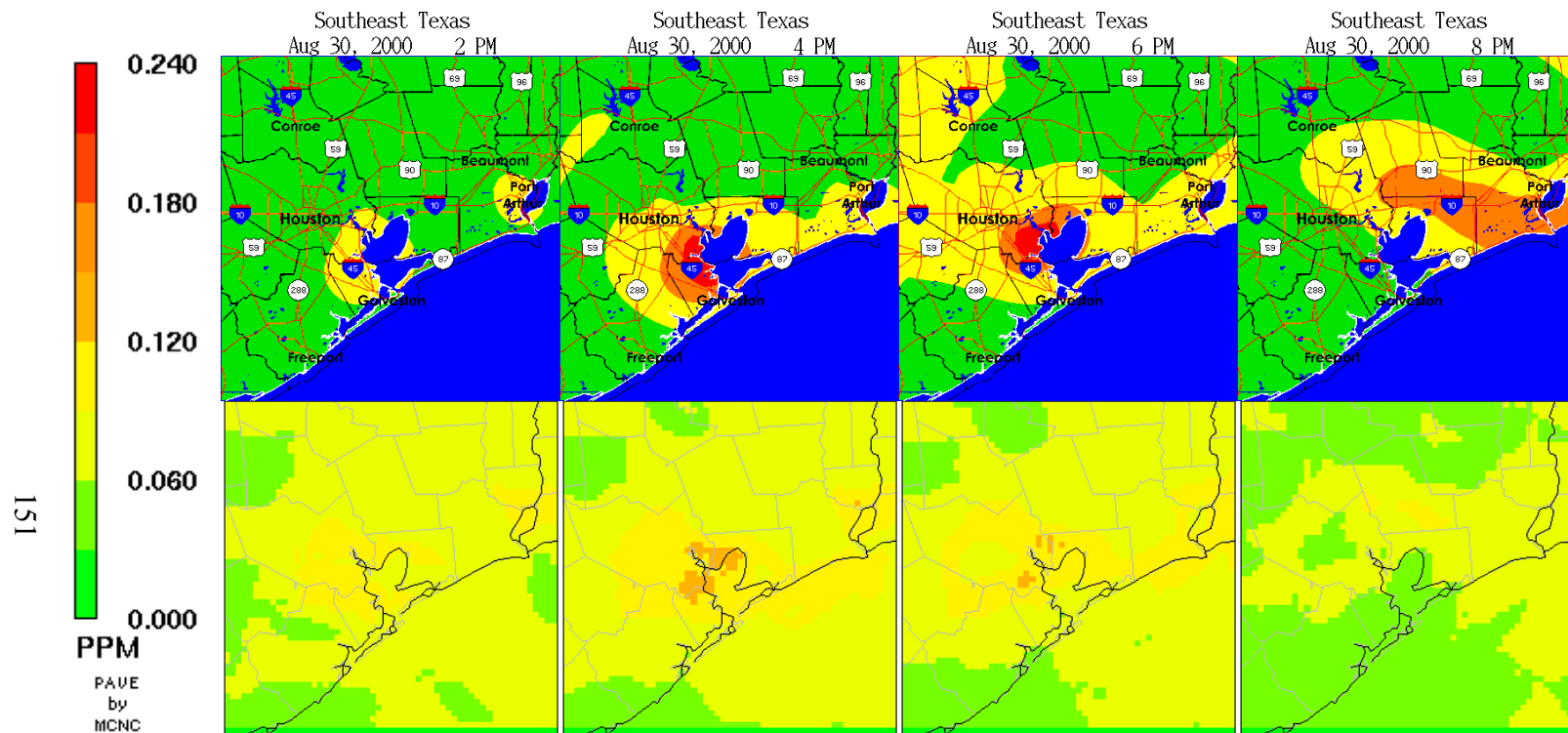


Figure 5.6. Monitored (top row) and modeled (bottom row) ozone concentrations on Aug 30<sup>th</sup>, 2000 at 2pm, 4pm, 6pm and 8pm.

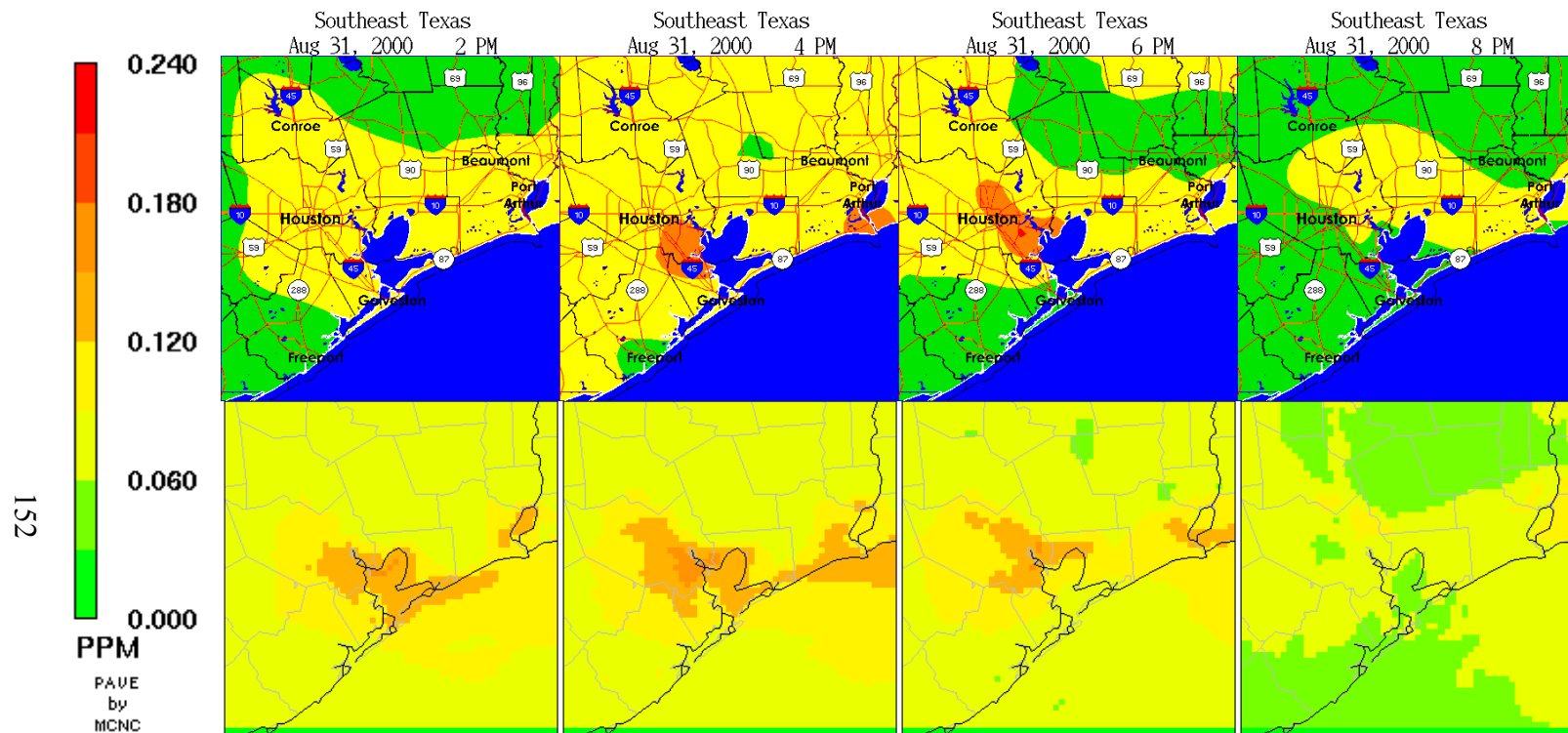


Figure 5.7. Monitored (top row) and modeled (bottom row) ozone concentrations on Aug 31<sup>st</sup>, 2000 at 2pm, 4pm, 6pm and 8pm.

The features of each episode day are described in brief below:

**August 28<sup>th</sup>, 2000:** A characteristic feature on this day is that the urban/industrial plume travels north/northeast from urban Houston. The model is predicting this northerly flow well, both spatially and temporally; however, maximum ozone concentrations are over-predicted within this plume by the model.

**August 29<sup>th</sup>, 2000:** In contrast to the 28<sup>th</sup>, the model is under-predicting maximum ozone concentrations on Aug 29<sup>th</sup>. Once again, however, the model is predicting the gradual north/northeast flow of ozone, created around midday, in the urban and industrial areas of Houston and Beaumont. The model seems to be capturing the spatial extent of ozone above 0.06 ppm very well on this day.

**August 30<sup>th</sup>, 2000:** Elevated ozone remained fairly stagnant near the industrial areas of Houston on the 30<sup>th</sup>, and the ozone plume developed and stayed over Galveston Bay. The model shows a larger spatial extent of ozone pollution early in the day, compared to monitored ozone, but under-predicts maximum concentrations later in the day. The model does predict the spatial extent of elevated ozone concentrations and the gradual movement of elevated ozone in the evening towards Beaumont-Port Arthur.

**August 31<sup>st</sup>, 2000:** Similar to August 30<sup>th</sup>, another stagnant ozone plume developed over urban/industrial Houston, and this was predicted very well by the model. In addition, the model predicted the temporal patterns and regional distribution of ozone well.

The SOA formation results presented in the next chapter are presented for these key episode days. In general, this qualitative analysis showed that this episode is predicting the spatial/temporal distribution of the photochemistry well. There was a significant under-prediction of ozone on August 30<sup>th</sup>. Some research provided compelling evidence that emissions inventories used in the modeling did not have sufficient light olefins, and these emissions were responsible for increasing maximum ozone concentrations significantly in industrial plumes (see NOAA (2003c)). It is expected that improvements will be made to the emissions inventory and these should be incorporated into base case modeling as they become available. This modeling episode was sufficient for the purpose of this research, which was to predict spatial and temporal patterns in SOA formation and investigate the relative importance of SOA precursors.

## **5.5 SOA Model Development**

The first major step of the methodology to include an SOA model into CAMx31 was to become familiar with the structure and functionality of the 100+ FORTRAN routines that make up CAMx31. This familiarization was a necessary step in planning the modifications for this research. There were two major modifications made to CAMx31: addition of a flexible, user-defined chemical mechanism and addition of an independent module to predict SOA. The first modification is explained in detail in Appendix B. The second will be described in this section.

As discussed in the Literature Review, it is not yet possible to model total SOA formation due to lack of detailed reaction data from many SOA precursors and partitioning data from SVOC reaction products. This research is a first approximation of which *known* precursors and precursor reactions are contributing to SOA formation in SE Texas. Many data needs must be filled before a true, comprehensive SOA model can be implemented. Based on previous studies, however, the precursors considered here probably account for the large majority of SOA formation.

The model for SOA formation used in this research is the gas/particle partitioning yield coefficient first proposed by Odum et al. (Odum et al. 1996):

$$Y = \frac{\Delta SOA}{\Delta HC} = \sum_i Y_i = M_o \sum_i \left( \frac{\alpha_i K_{om,i}}{1 + K_{om,i} M_o} \right) \quad (2.8)$$

*Summation over i condensable reaction products from a single precursor.  $K_{om}$  refers to a partitioning coefficient to organic matter (om), and will be referred to simply as K from here on. Partitioning of condensable organic compounds is assumed to occur predominantly to organic matter in the particle phase.*

The work of Odum et al. and Griffin et al. (Odum et al. 1997a; Griffin et al. 1999) assumed two, hypothetical, condensable reaction products per SOA precursor ( $i=2$ ). Rearranging equation 2.8 gives the increase in SOA from the reaction of a single precursor producing two condensable reaction products:

$$\Delta SOA = \Delta HC * Y = \Delta HC * M_o \left( \frac{\alpha_1 K_1}{1 + K_1 M_o} + \frac{\alpha_2 K_2}{1 + K_2 M_o} \right) \quad (2.8)$$

Both Odum et al. and Griffin et al. reacted a number of important aromatic and monoterpene SOA precursors in smog chambers, and derived  $\alpha_1, \alpha_2, K_1, K_2$  by fitting Equation 2.8 to curves of Y versus  $M_o$  for each individual precursor. Aromatics are assumed to be oxidized exclusively by the OH radical; however, monoterpenes can be oxidized by  $O_3$  and the OH and  $NO_3$  radicals. In addition, different oxidation pathways produce different aerosol yields (Hoffmann et al. 1997; Griffin et al. 1999). The reactions of monoterpenes with different oxidants are represented separately in the chemical mechanism, and so it is desirable to predict SOA formation separately from these different pathways. This in turn requires yield parameters ( $\alpha_1, \alpha_2, K_1, K_2$ ) to describe the yield of monoterpenes from different reaction pathways.

Griffin et al (1999) conducted monoterpene oxidation experiments under three conditions: in sunlight with  $NO_x$  (photo-oxidation experiments), in the dark with  $NO_3$ , and in the dark with  $O_3$ . The latter two conditions were used to derive yield parameters that describe aerosol formation from  $NO_3$  and  $O_3$  oxidation respectively. The photo-oxidation experiments lead to aerosol formation from OH,  $NO_3$  and  $O_3$  oxidation pathways. Griffin et al used a SAPRC97 mechanism to model their photo-oxidation experiments, and, using yield data from the separate  $O_3$  and  $NO_3$  experiments, were able to derive what fraction of monoterpene reacted via which pathway. Aerosol yields from OH oxidation were

calculated in this research from data provided in the reference, and assuming that aerosol yields from individual reactants were additive in photo-oxidation experiments. Finally, Microsoft Excel Solver was used to find the best fit of Equation 2.8 and to give yield parameters for OH oxidation. The most significant assumption made here was that aerosol formation in a single oxidant system is the same as in a multiple oxidant system, which may be a gross simplification. Using the full photo-oxidation yield parameters to describe SOA formation from a single pathway would give an over-estimate, so this method gives an approximation to aerosol yields from the monoterpene-OH reactions. All yield parameter data are summarized in Table 5.10.

Table 5.10 Yield parameter data for four-parameter yield model.

Compound	oxidant	$\alpha_1$	$\alpha_2$	$K_1$	$K_2$	T (K)	Ref
high-yield aromatics	OH	0.038	0.167	0.042	0.0014	307	1
low-yield aromatics	OH	0.071	0.138	0.053	0.0019	308	1
$\alpha$ -pinene*	photo***	0.038	0.326	0.171	0.004	315	2
	O <sub>3</sub>	0.125	0.102	0.088	0.0788	307	2
$\beta$ -pinene	OH	0.0983	0.9900	0.0010	0.0010	315	calculated
	photo***	0.13	0.406	0.044	0.0049	313	2
	O <sub>3</sub>	0.026	0.485	0.195	0.003	308	2
sabinene	NO <sub>3</sub>	1	0.00	0.0163	0.00	307	2
	OH	0.1759	0.0012	0.0352	0.0010	313	calculated
	photo***	0.067	0.399	0.258	0.0038	313	2
d-limonene**	O <sub>3</sub>	0.037	0.239	0.819	0.0001	308	2
	NO <sub>3</sub>	1	0.00	0.0115	0.00	309	2
	OH	0.0681	0.4954	0.3130	0.0024	313	calculated
$\Delta^3$ -carene	photo***	0.054	0.517	0.043	0.0042	312	2
	O <sub>3</sub>	0.128	0.068	0.337	0.0036	308	2
	NO <sub>3</sub>	0.743	0.257	0.0088	0.0091	309	2
d-limonene**	OH	0.1239	0.0838	0.0150	0.0150	312	calculated
	photo***	0.239	0.363	0.055	0.0053	312	2

	OH	0.239	0.363	0.055	0.0053	312	2
--	----	-------	-------	-------	--------	-----	---

1. (Odum et al. 1997a)

2. (Griffin et al. 1999)

\* There is no yield data provided for the reaction of  $\alpha$ -pinene with  $\text{NO}_3$ .

\*\* d-limonene is assumed to react exclusively with the OH radical in photo-oxidation experiments.

\*\*\* Photo-oxidation experiments in the presence of  $\text{NO}_x$ . All three of OH radical,  $\text{O}_3$  and  $\text{NO}_3$  radical are possible oxidants.

The yields of SOA can be adjusted via the partitioning coefficients  $K$  to account for the temperature difference between model simulations and smog chamber experiments (Sheehan and Bowman 2001):

$$\frac{K}{K^*} = \frac{T}{T^*} \frac{P_{vap}^*}{P_{vap}} = \frac{T}{T^*} \exp\left[\frac{\Delta H_{vap}}{R} \left(\frac{1}{T} - \frac{1}{T^*}\right)\right] \quad (4.1)$$

\* smog chamber conditions

$R$  is the universal gas constant

$\Delta H_{vap}$  is the latent heat of vaporization.

Equation 4.1 was used to adjust all  $K$  values in Table 5.10 using the actual temperature in the model grid cell. A constant value for  $\Delta H_{vap}$  of 17.0 kcal/mol was chosen for all condensable products, following an example in the literature (Sheehan and Bowman 2001). Although  $\Delta H_{vap}$  is different for individual SVOC reaction products, the mean value of 17.0 is considered acceptable here. The value of  $\Delta H_{vap}$  itself can vary slightly with temperature; however, this is not considered.

The mass of reacted precursor ( $\Delta HC$ ) is readily available from the chemistry solver in CAMx31, which leaves only  $M_o$  to be determined in Equation 2.8. Data analysis shows that ambient organic carbon (OC) in SE Texas is mostly

primary, and it is reasonable to assume that this primary organic carbon will act as absorbing medium for condensable reaction products. Ideally, all emissions, transport and removal of primary organic carbon are accounted for in a grid model; however, a major limitation to modeling OC is the lack of primary OC emissions inventories. There is currently no primary OC inventory compiled for the modeling domain. The common approach to modeling SOA is to make 'rough' approximations of primary OC emissions or to assume that secondary OC partitions only to a solution of secondary reaction products, thus ignoring primary OC as partitioning medium. Both of these approaches can introduce unacceptable uncertainty in predicting SOA, and a different approach is taken in this research.

The Mo concentrations in this research were estimated from ambient data that was specific to the modeling episode, i.e. the data presented in Chapter 4. It was assumed that the total amount of organic carbon in PM<sub>2.5</sub> was a good estimate of total Mo. The PM<sub>2.5</sub> monitoring network in SE Texas is fairly extensive and estimates of total OC (i.e. Mo) are obtained by interpolating ambient measurements of OC to model grid cells within a domain bounded by the SE Texas area PM monitoring sites. The Kriging interpolation method was chosen for the interpolation and implemented using Surfer version 7.02 (Point Kriging, linear variogram, slope=1, no drift). Although there is uncertainty associated with interpolation in general, this method gives a more reliable estimate of Mo compared to a model based on emissions of primary OC, simply because the uncertainty associated with estimating emissions from thousands of sources is avoided.

There are many different interpolation methods, and the relative advantages and disadvantages of each went beyond the scope of this research. The objective here was to estimate Mo based on the dense network of ambient data, and the Kriging method sufficed for this purpose. Interpolated Mo concentrations were limited to within the boundaries of the local monitoring network, or roughly the area shown in Figure 3.1c. Figure 5.8 shows the size of this subdomain, and shows interpolated Mo concentrations for one hour in the modeling episode. There are a number of points that should be made regarding the use of interpolated Mo fields.

The first point is that FRM samples are 24-hour integrated filter samples. The chemistry solver in CAMx31 solves species reactions on the order of minutes. It is desirable to solve for SOA formation at a high temporal resolution, and so it is desirable to account for temporal variability of Mo. The PM analysis in Chapter 4 provided evidence that OC is a consistent fraction of PM in SE Texas, and it was assumed that OC and total PM mass correlate well throughout the day. Hourly-averaged TEOM measurements of total PM mass were also interpolated to each model grid cell within the same subdomain as the interpolated Mo fields (using the same interpolation methods reported above). The relative amount of hourly PM mass to daily PM mass was used as an indicator of hourly OC mass to daily OC mass, and this was used to estimate hourly OC mass in each grid cell, at each hour of the modeling episode.

## Total Organic Carbon (Mo)

August 31st, 2000, 6 pm  
From FRM data and Kriging interpolation

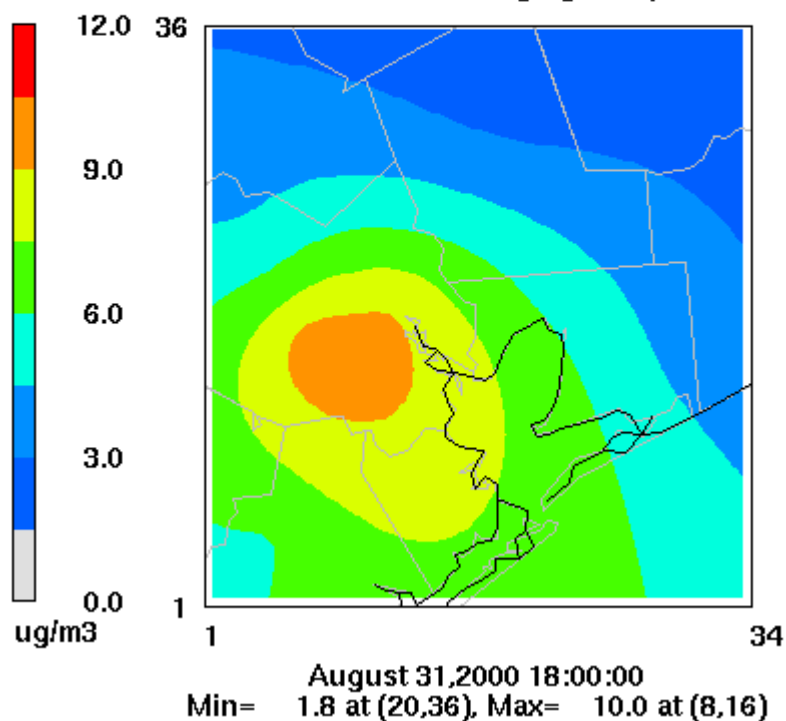


Figure 5.8. Interpolated Mo concentrations for August 31<sup>st</sup>, 2000, 6 pm.

The second point is that Mo is both primary and secondary, but the fraction of each is unknown. (Note that the fractions of primary and secondary OC were estimated at each monitoring site in Chapter 4 using the empirical SOA model; however, this estimate was limited to days when the regression was significant, and data was not available for all sites and episode days) The advantage of using ambient OC (Mo) was that it could be directly applied to

Equation 2.8 to calculate yield of SOA concentration (SOA formation). The initial amount of SOA, however, is not known at each time step, and thus a total SOA concentration could not be calculated. Despite this limitation, the methods used here gave reasonable estimates of SOA formation, because the large uncertainty involved in developing a PM emissions inventory was not a factor.

Grid models have the capability of modeling atmospheric processes in multiple vertical layers. It was assumed that the interpolated Mo fields represented OC concentrations throughout the mixed layer, and SOA formation was calculated in all vertical layers under the mixing height for each time step. The layer corresponding to the top of the mixed layer was determined externally from the vertical diffusivity ( $K_v$ ) fields, which are inputs to CAMx31, using a program called metpave (available at [www.camx.com](http://www.camx.com)). Metpave determined the planetary boundary layer (PBL) height in each grid cell from the vertical profile of  $K_v$ . Metpave was modified slightly for this research to output the layer number of the PBL (instead of height) and to print results to a text file (rather than UAM format binary file).

As described above, a model for SOA in the framework of gas/particle partitioning yields was added to CAMx31 to predict the total mass of SOA formed under the PBL for reactions of aromatics and monoterpenes. Although not comprehensive, the model includes the aromatics and monoterpene precursors that are expected to be the most significant SOA producing compounds. (See section 5.3 for details on which aromatic and monoterpene precursors are included). The model uses interpolated fields of actual Mo concentrations,

externally calculated estimates of PBL height, and yield parameter data that can be corrected to account for the effect of temperature on gas/particle partitioning. There are thus three model inputs for the SOA model: a text file with interpolated Mo fields (2D), a text file with PBL layer fields (2D), and a text file with yield parameter information for chemical reactions that lead to SOA formation (SOA parameters file). The implementation of the model in CAMx31 is described next.

The SOA model was added to the CAMx31 by both adding and modifying existing subroutines. It should be noted that the SOA model was added to the CAMx31 code that had already been modified to solve SAPRC99 generated mechanisms. In addition, the SOA model is an option, and CAMx31 maintains its original capabilities if the SOA option is not selected. There is an additional flag in the CAMx.in file indicating whether the SOA model is to be used. If the flag is set to TRUE, CAMx31 expects the names of the three new input files listed above, and opens an extra output file with a .soa extension. The SOA output file gives grams of SOA formed, for each hour, for each SOA precursor reaction indicated in the yield parameter input file. This output file is a UAM format AVERAGE file, the same format as the standard CAMx31 output file with gas phase concentrations. The formats of the SOA parameters file, the Mo fields file and the PBL fields file are shown in Tables 5.11, 5.12 and 5.13 respectively. Note that the size of the Mo field determines the size of the subdomain for SOA calculations; however, the PBL field must be the same size as the fine grid in which the SOA subdomain is found. The modifications and additions to the CAMx31 source code for the SOA formation model are listed in Table 5.14.

Table 5.11. Format of SOA parameters input file.

Line #	Description
1	The number of SOA species (= number of reaction pathways considered to produce SOA)
repeat lines 2 through 5 for each SOA species:	
2	Name of SOA species
3	Name of SOA precursor (must be a model species)
4	Name of reactant for this precursor (must be a model species)
5	Molecular weight of SOA precursor, reaction number of reaction pathway (must be the reaction of the precursor and reactant listed above), $\alpha_1$ , $\alpha_2$ , $K_1$ , $K_2$ , reference temperature for parameters, $\Delta H_{\text{vap}}$ for the adjustment of K values. [comma delimited]

Table 5.12. Format of Mo fields file.

Line #	Description
1	x-coordinate of lower left corner of Mo field (must be in the same coordinate system as the model domain) in meters
2	y-coordinate of lower left corner of Mo field (must be in the same coordinate system as the model domain) in meters
3	number of columns in Mo field
4	number of rows in Mo field
5	grid cell size in meters
repeat the following information 24 times, once per hour:	
6	hour for the Mo information to follow
7+ (# rows)	Mo value for each column in $\mu\text{g}/\text{m}^3$ [space delimited]

Table 5.13. Format of PBL layer fields file.

Line #	Description
1	x-coordinate of lower left corner of PBL field (must be in the same as model fine grid) in meters
2	y-coordinate of lower left corner of PBL field (must be in the same as model fine grid) in meters
3	number of columns in PBL field (must be in the same as model fine

	grid)
4	number of rows in PBL field (must be in the same as model fine grid)
5	grid cell size in meters (must be in the same as model fine grid)
repeat the following information 24 times, once per hour:	
6	hour for the PBL information to follow
7+ (# rows)	PBL value for each column. The value indicates the vertical modeling layer above which is the top of the PBL [space delimited]

Table 5.14. Modifications and additions to the CAMx31 source code for the SOA formation model.

Subroutine	Function	Modifications/Description
startup.f	Reads CAMx.in file and calls routines to read in information files (chemparam etc.)	Added a read and message for SOA flag. If SOA=TRUE, call SOAprep.
openfiles.f	Opens file units for input and output data	If SOA=TRUE, open an output file with .soa extension, and open SOA parameters file, Mo fields file, and PBL fields file.
SOAprep.f (New. Called by startup.f)	Reads SOA parameters file, Mo fields file, PBL fields file. Performs checks and fills arrays.	<ul style="list-style-type: none"> <li>• Maps precursor and reactant names to model species #'s.</li> <li>• Prints SOA parameter information to .out file.</li> <li>• Determines what fine grid the SOA subdomain is in based on cell size.</li> <li>• Determines where SOA subdomain is located.</li> <li>• Sets SOA formation arrays to zero.</li> <li>• Writes header information to SOA output file.</li> </ul>
chemdriv.f	Sets up the solver for the chemical mechanism. Loops over grid cells.	Passed in the length of the grid cell to calculate cell volume. Additionally pass to utieh.f: the end hour of the current time step, the cell volume, and a conversion factor for converting between ppm and mol units.
chemrxn.f	Calls chemdriv.f for the appropriate grid.	Pass the cell length for the appropriate grid to chemdriv.f.
utieh.f	This is the solver	<ul style="list-style-type: none"> <li>• Passed in cell volume, current time</li> </ul>

	routine to solve the SAPRC99 generated mechanism. If SOA = TRUE, this is where the SOA formation is calculated.	<p>step and factor to convert between ppm and mol units</p> <ul style="list-style-type: none"> <li>• Declared several new local variables for SOA calculations</li> <li>• If SOA is true and this grid cell is within the Mo field and under the PBL top, then: <ul style="list-style-type: none"> <li>• After the gas species are solved, calculate the <math>\Delta HC</math> for each SOA precursor and pathway.</li> <li>• Make sure the reacted precursor does not result in concentration lower than the lower bound; if so adjust the <math>\Delta HC</math> accordingly. Do a weighted adjustment over multiple reactions (oxidants) if necessary.</li> <li>• Convert <math>\Delta HC</math> to <math>\mu g/m^3</math>. Adjust K values to account for grid cell temperature.</li> <li>• Calculate <math>\Delta SOA</math> using yield equation and appropriate Mo for that grid cell and hour.</li> <li>• Convert <math>\Delta SOA</math> to grams, and keep a running total for that hour.</li> </ul> </li> </ul>
CAMx.f	Main simulation routine.	If SOA=TRUE, call new routine wrtsoa.f at the end of each hour.
wrtsoa.f (New. Called by CAMx.f)	Writes SOA output	Writes the hourly total SOA formation in the SOA subdomain to the .soa output file. This is done at the end of each model hour. Also writes out the Mo fields to the same file.
utchem.com	Include file with arrays and parameters for new mechanism and SOA model.	Added several new global variables for modeling SOA formation, and stored them in three new common blocks: soavarr, soavarc, and soavari.

One application of the modified grid model involved using a mechanism with expanded aromatic reaction mechanisms, the s99soa2 mechanism. In the

s99soa2 mechanism, condensable reaction products were assumed to come from reactions of intermediate aerosol precursors, rather than parent aromatic compounds. The SOA model can easily be applied for this purpose by providing  $\alpha_1$ ,  $\alpha_2$ ,  $K_1$ ,  $K_2$  for aerosol precursor reactions, i.e.  $\alpha_1$  and  $\alpha_2$  now give the mass of condensable product produced per mass of *aerosol precursor* reacted. Alpha values were derived from reaction product stoichiometry and the ratio of molecular weights of condensable product (COC) to aerosol precursor (APR):

$$\alpha = a \frac{MW_{COC}}{MW_{APR}} \quad (5.2)$$

*a* is the stoichiometric coefficient of COC product from APR

As described in a previous section, stoichiometric coefficients, partitioning coefficients and molecular weights for lumped aerosol precursors and condensable products were calculated, and these are listed in Table 5.15 below.

Table 5.15 Yield parameter data for lumped intermediate model species using the four-parameter yield model.

<b>Compound</b>	<b>oxidant</b>	$\alpha_1$	$\alpha_2$	$K_1$	$K_2$
APH1	OH	0.481	1.040	0.01801	0.001392
APH2	OH	0.451	1.002	0.004442	0.000383
APH3	OH	0.447	0.997	0.016617	0.001251
APH4	OH	0.432	0.978	0.004513	0.000387
APL2	OH	0.456	1.008	0.004415	0.000341
APL4	OH	0.430	0.976	0.004839	0.000274

1 Lumped K a and MW from Table 5.5.

2 K values estimated by Dechapanya et al from literature on SOA yield experiments

## 5.5 Model Applications

The previous section described the development of a SOA formation model that was included in CAMx31. This model took into account the gas/particle partitioning nature of SOA formation by treating aerosol yields as a function of mass of absorbing medium and temperature. Although not comprehensive, the model was used for the SOA precursors that are thought to contribute most significantly to SOA. This section describes the model simulations that were performed.

The most important application of the model was the simulation of base case SOA formation in the urban and industrial areas of Southeast Texas, using the s99soa mechanism. Few grid model simulations of SOA have been performed in any airshed, and the base case results contribute greatly to characterization of SOA formation in general. Four important questions were addressed when analyzing the base case model run:

1. What are the relative contributions of the different SOA formation pathways to SOA formation?
2. What is the temporal pattern of SOA formation from these pathways in this area?
3. What is the spatial distribution of SOA formation in this area?
4. How does spatial and temporal SOA formation relate to  $PM_{2.5}$  concentrations in this area?

The primary objective of this research was to develop a model for SOA formation and apply it to the Southeast Texas area. The model was developed to be robust and allow user's to make changes to both the chemical mechanism and SOA formation parameters. The model was applied here in a number of ways to explore the sensitivity of SOA formation to various inputs and parameters. The sensitivity simulations can be divided into four types: sensitivity to reaction mechanisms, sensitivity to Mo concentrations, sensitivity to SOA precursor emissions, and sensitivity to ozone precursor emissions. All simulations and their descriptions are listed in Table 5.16 below. The sensitivity simulations were performed for the Aug 29<sup>th</sup>- Aug 31<sup>st</sup> 2000 period, since these were the days of interest and it was not practical to simulate the entire episode for each case. The only exception was the simulation with the s99soa2 chemical mechanism, which was performed for the entire Aug 22<sup>nd</sup> - Sep 1<sup>st</sup> 2000 episode. The initial conditions used to start sensitivity simulations, i.e. midnight concentrations on Aug 28<sup>th</sup>, were taken from the base case. Using base case initial conditions is not expected to have any effect on relative differences between base case and sensitivity simulations, especially on Aug 30<sup>th</sup> and Aug 31<sup>st</sup>, 2000.

Table 5.16. List of sensitivity simulations.

#	Description (%'s are relative to base case conditions)
<b>Reaction mechanism sensitivity:</b>	
1	s99soa2 mechanism was implemented with series/parallel reaction mechanisms for SOA formation from aromatic precursors.
<b>Mo concentration sensitivity:</b>	
1	200% Mo concentration in each grid cell
2	50% Mo concentration in each grid cell
3	Mo concentrations in each grid cell were set equal to the mean Mo concentration in the subdomain for that hour. Mo concentrations were homogenous throughout the domain.
<b>SOA precursor sensitivity:</b>	
1	200% biogenic monoterpene emissions throughout the domain
2	50% biogenic monoterpene emissions throughout the domain
3	200% aromatic emissions in the 11-county Houston Galveston Beaumont Port Arthur area.
4	50% aromatic emissions in the 11-county Houston-Galveston, Beaumont-Port Arthur area.
<b>Ozone precursor sensitivity:</b>	
1	200% anthropogenic NOx emissions in the 11-county Houston-Galveston, Beaumont-Port Arthur area.
2	50% anthropogenic NOx emissions in the 11-county Houston-Galveston, Beaumont-Port Arthur area.
3	10% anthropogenic NOx emissions in the 11-county Houston-Galveston, Beaumont-Port Arthur area.
4	200% anthropogenic light olefin emissions in the 11-county Houston-Galveston, Beaumont-Port Arthur area.
5	50% anthropogenic light olefin emissions in the 11-county Houston-Galveston, Beaumont-Port Arthur area.
6	10% anthropogenic light olefin emissions in the 11-county Houston-Galveston, Beaumont-Port Arthur area.

The first sensitivity simulation was a test on how the representation of aromatic formation mechanisms affected SOA formation rates. This was accomplished by running the base case conditions with the s99soa2 mechanism

which included expanded chemistry for the AR1H, AR2H and AR2L model species. Instead of considering  $\Delta HC$  from parent aromatics, the yield parameters were applied to  $\Delta HC$  from the intermediate aerosol precursors of each parent. SOA formation was compared between the base case with s99soa and s99soa2. This was an example of how the SOA grid model could be used to test theoretical assumptions on the chemistry of SOA formation.

The second type of sensitivity simulations tested the effect of varying Mo concentrations on SOA formation. This effect is not immediately apparent since Equation 2.8 has Mo terms in both the numerator and denominator. At certain levels of Mo, SOA formation may no longer be sensitive to this parameter. Two simulations were performed with Mo concentrations set to 50% and 200% of base case concentrations. Additionally a simulation was performed with Mo concentrations throughout the SOA-subdomain set equal to the domain-wide average Mo concentration for that hour. This was referred to as the homogeneous Mo simulation. PERL scripts were used to create ASCII sensitivity Mo concentration files based on the original base case Mo concentrations files.

The next set of sensitivity simulations involved varying emissions of SOA precursors. Two simulations were performed where biogenic monoterpene emissions were set equal to 50% and 200% of base case levels throughout the modeling domain. Biogenic sources are by far the biggest sources of monoterpenes (see Table 5.9) so this sensitivity simulation is effectively to all monoterpene emissions. This is not a practical emissions reduction strategy; however, it will provide valuable insight as to how important the biogenic

emissions are to the accurate prediction of SOA. Domain-wide variations in biogenic emissions were made by factoring the biogenic file while merging anthropogenic and biogenic model-ready emissions files together using MRGAUM, an EPS2 module.

Two more simulations were performed where aromatic emissions in the 11-county Houston-Galveston, Beaumont-Port Arthur (HGBPA) non-attainment area were set equal to 50% and 200% of base case levels. The emissions reductions were limited to this area to emulate a real emissions reduction strategy. The SOA subdomain is wholly within this area, and local SOA formation rates are expected to be determined predominantly by local emissions. Reduction of aromatic precursors may be an important strategy to reduce SOA and thus PM<sub>2.5</sub> concentrations. Variations in anthropogenic emissions were made directly to the model-ready emissions files using LOMASK and ELMASK, which were FORTRAN77 programs developed by the University of Texas. The sensitivity files were then merged with base case biogenics using MRGUAM, an EPS2 module.

The final set of sensitivity simulations involved varying ozone precursors. Non-SOA precursors such as NO<sub>x</sub> and light olefins (such as ethylene) contribute greatly to the photochemistry in the Southeast Texas area. These compounds are critical to formation of ground-level ozone in the area. Three simulations were performed with anthropogenic NO<sub>x</sub> emissions set at 200%, 50% and 10% of base case levels in the 11-county HGBPA non-attainment area. Variations in NO<sub>x</sub> concentrations can both decrease and increase ozone; these sensitivity simulations

tested whether NO<sub>x</sub> had a similar effect on SOA formation. Three more simulations were performed with anthropogenic light-olefins emissions set at 200%, 50% and 10% of base case levels in the 11-county HGBPA non-attainment area. Evidence exists that light-olefins contribute to high maximum ozone concentrations in industrial plumes in Houston (NOAA 2003c). The light-olefin sensitivity simulations were used to test whether SOA formation was sensitive to changes in ozone concentrations by way of changes in predominant ozone precursor emissions. Variations in anthropogenic emissions were made directly to the model-ready emissions files using LOMASK and ELMASK, which were FORTRAN77 programs developed by the University of Texas. The sensitivity files were then merged with base case biogenics using MRGUAM, an EPS2 module.

The next chapter presents the results of the base case SOA formation modeling and the sensitivity simulations described above.

## **6.0 Results – Part 2: Base Case Model Results and Sensitivity Applications**

This Chapter summarizes the results of the SOA grid model. The first section is devoted to analysis of base case model predictions of SOA formation in Southeast Texas. There are only a few photochemical grid model predictions of SOA formation in the literature today and none have examined Southeast Texas in detail, so these results contribute to the overall understanding of temporal distributions, spatial distributions and sources of SOA. The model predictions are compared to the limited ambient data on SOA for Southeast Texas. The second section shows results of model sensitivity studies and finally the third section summarizes the findings from the modeling and presents recommendations for future model applications.

Before presenting the model results it is important to point out that the modified grid model predicts only the hourly SOA formation rate in each grid cell, not ambient concentrations. Formation rates cannot be directly compared to SOA concentrations because other transport and loss processes have not been considered; however, there are two advantages to predicting formation rates. The first is that formation rates are predicted here without the need for emissions inventories of primary organic carbon, which might introduce considerable uncertainty to the results. The second advantage is that the model gives a direct indication of how local emissions contribute to SOA concentrations; chemical

reaction is the only process which produces SOA, and so formation rates show the temporal and spatial distribution of total SOA formation in the airshed.

SOA formation rates were calculated in units of total mass in the planetary boundary layer (PBL) per hour, since this is the mass that would contribute to concentrations of SOA in the mixed layer. Base case formation rates are also normalized by the volume of each grid column under the PBL giving SOA formation rate per unit volume. Formation rates in these units give another perspective on the contribution of local SOA formation to SOA concentrations.

## **6.1 Base Case Model Results**

The TXAQS episode covered the 8/22/2000-9/01/2000 period, with the first three days considered as model ‘spin-up’ days and not considered for analysis. The initial base case simulation predicted SOA concentrations for 8/25/2000 through 9/01/2000, but for purpose of this research the results are presented for the three-day period of 8/29/2000 to 8/31/2000. This period was chosen because SOA formation increased throughout the three days and the results were representative of results on other modeling days. In addition, 8/31/2000 experienced the highest ozone concentrations during the TXAQS episode. The base case results are presented in three sub-sections: Domain-wide SOA formation, Monitoring location SOA formation, and Evaluation of SOA formation.

### ***Domain-wide SOA formation.***

The totals in Table 6.1 demonstrate the relative importance of each reaction pathway to SOA formation in Southeast Texas. Time series of SOA formation in grams/hour in the subdomain are shown in Figure 6.1; only the aromatic pathways and the most significant  $\alpha$ -pinene,  $\beta$ -pinene and limonene pathways are shown in Figure 6.1 ( $\Delta^3$ -carene and sabinene pathways are omitted because they are relatively insignificant compared to the three other monoterpenes).

Table 6.1. Daily total formation of SOA in tons from each reaction pathway for 8/29/2000, 8/30/2000 and 8/31/2000. (HYA = high-yield aromatics, LYA = low-yield aromatics)

<b>Pathway</b>	<b>SOA formation (tons/day) in SOA formation subgrid</b>		
	<b>8/29/2000</b>	<b>8/30/2000</b>	<b>8/31/2000</b>
$\alpha$ -pinene + O <sub>3</sub>	1.2716	3.4901	4.8346
$\beta$ -pinene + OH	0.8198	1.3934	1.7692
$\beta$ -pinene + NO <sub>3</sub>	0.6469	1.0091	1.0743
limonene + OH	0.4981	0.7173	0.6788
LYA + OH	0.3583	0.2385	0.3130
$\alpha$ -pinene + OH	0.2801	0.4570	0.4900
HYA + OH	0.2205	0.1449	0.1844
$\Delta^3$ -carene + NO <sub>3</sub>	0.0892	0.1415	0.1497
$\Delta^3$ -carene + O <sub>3</sub>	0.0605	0.1479	0.2253
$\Delta^3$ -carene + OH	0.0536	0.0907	0.1082
$\beta$ -pinene + O <sub>3</sub>	0.0473	0.1449	0.2265
sabinene + OH	0.0233	0.0291	0.0318
sabinene + NO <sub>3</sub>	0.0156	0.0235	0.0240
sabinene + O <sub>3</sub>	0.0056	0.0107	0.0157

### SOA formation through individual reaction pathways

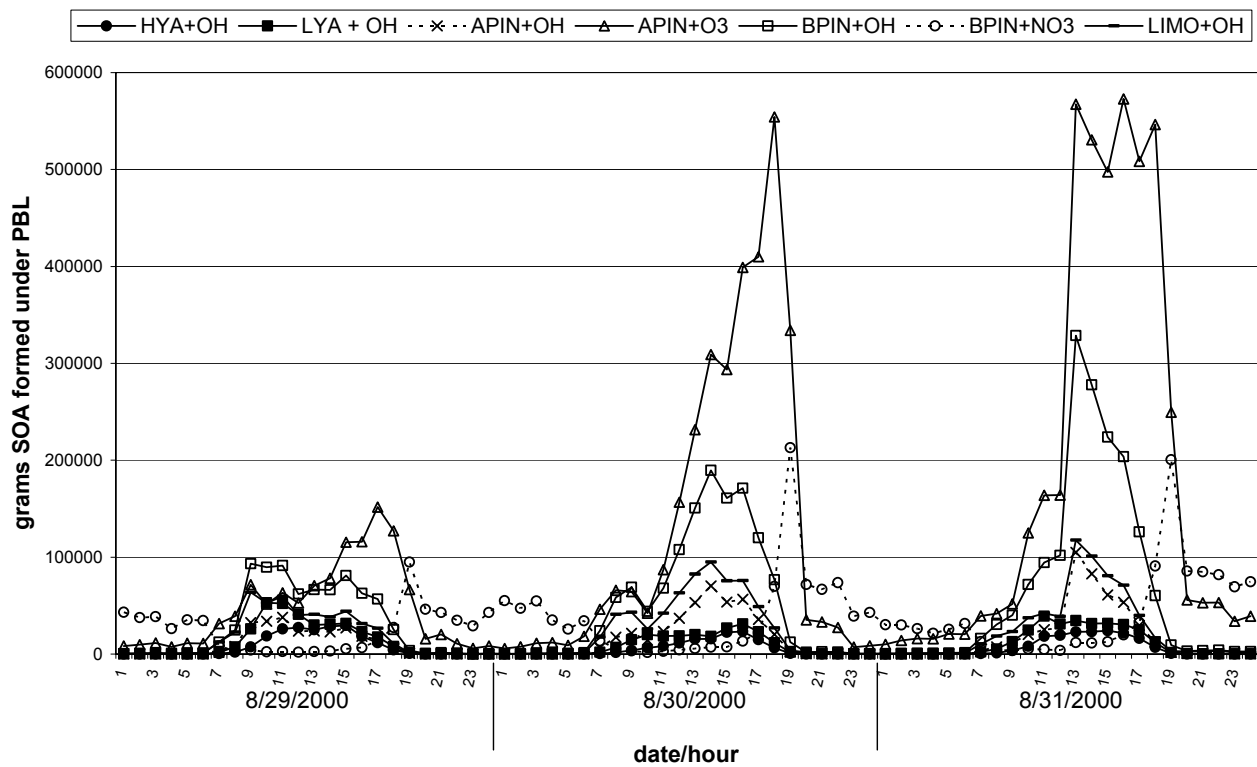


Figure 6.1. Time series of total SOA mass formed in the SOA-formation subdomain for the most significant formation pathways (top seven in Table 6.1).

The data in Table 6.1 and Figure 6.1 suggest that SOA formation via the oxidation of  $\alpha$ -pinene by ozone is a major contributor to ambient SOA levels in the area. This formation is linked to the diurnal cycle of ozone which tends to peak in late afternoon. To a lesser extent,  $\beta$ -pinene reactions with the OH and NO<sub>3</sub> radicals are also significant. There were no yield parameters available for the reactions of  $\alpha$ -pinene with the nitrate radical, and so this pathway was not considered in the model. The reaction of  $\alpha$ -pinene with nitrate showed insignificant aerosol formation in at least one study (Griffin et al. 1999); however, considering the importance of  $\alpha$ -pinene chemistry, this pathway should be considered in future modeling. There were also no partitioning parameters available for reactions of limonene with either the nitrate radical or ozone. Limonene-OH reactions form the fourth largest amount of SOA mass on all three episode days (see Table 6.1). Reactions of limonene with other oxidants may be significant pathways and should be considered in future model applications.

Figures 6.2 through 6.5 show the spatial distributions of SOA formation from aromatics with OH, from all five monoterpenes with OH, from all five monoterpenes with NO<sub>3</sub> and from all five monoterpenes with O<sub>3</sub> respectively. These are shown for 8/30/2000 for the SOA formation sub-domain. Figure 6.6 (Figure 3.1c from Chapter 3) is included again to show locations of monitoring stations in Southeast Texas, which will be referenced in the discussion to follow.

## SOA formation; aromatics w OH

daily grams formed under PBL  
8/30/2000

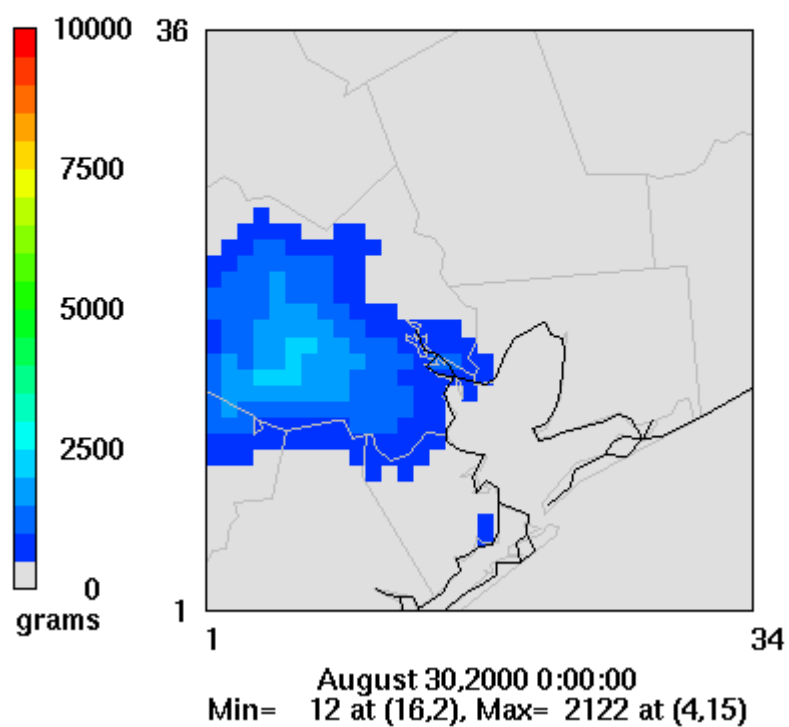


Figure 6.2. Daily SOA formation in grams under the PBL for reactions of aromatics with the hydroxyl radical. 8/30/2000.

## SOA formation; mterpenes with OH

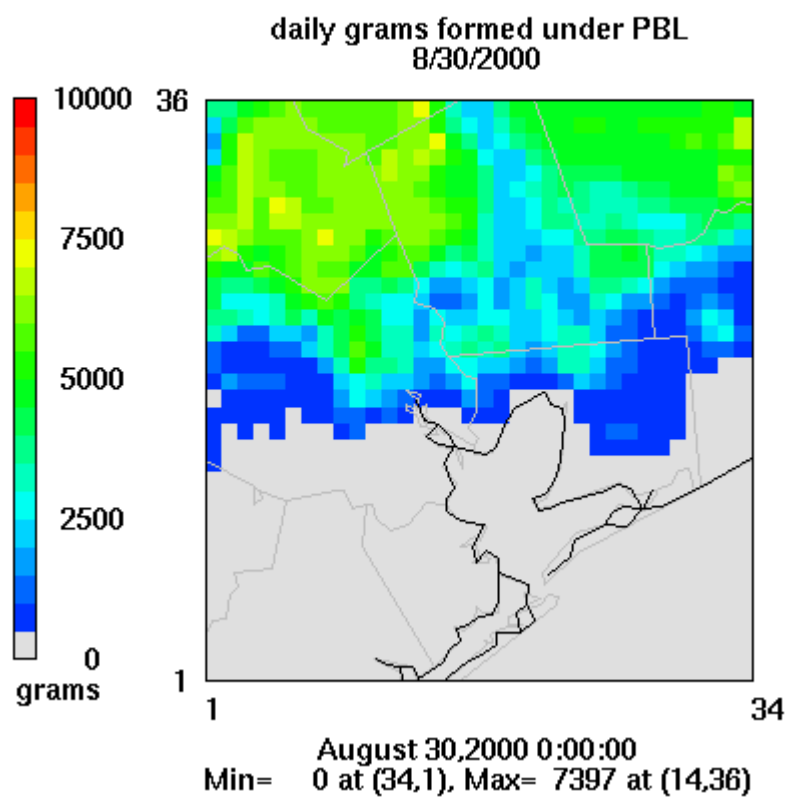


Figure 6.3. Daily SOA formation in grams under the PBL for reactions of monoterpenes with the hydroxyl radical. 8/30/2000.

## SOA formation; mterpenes with NO3

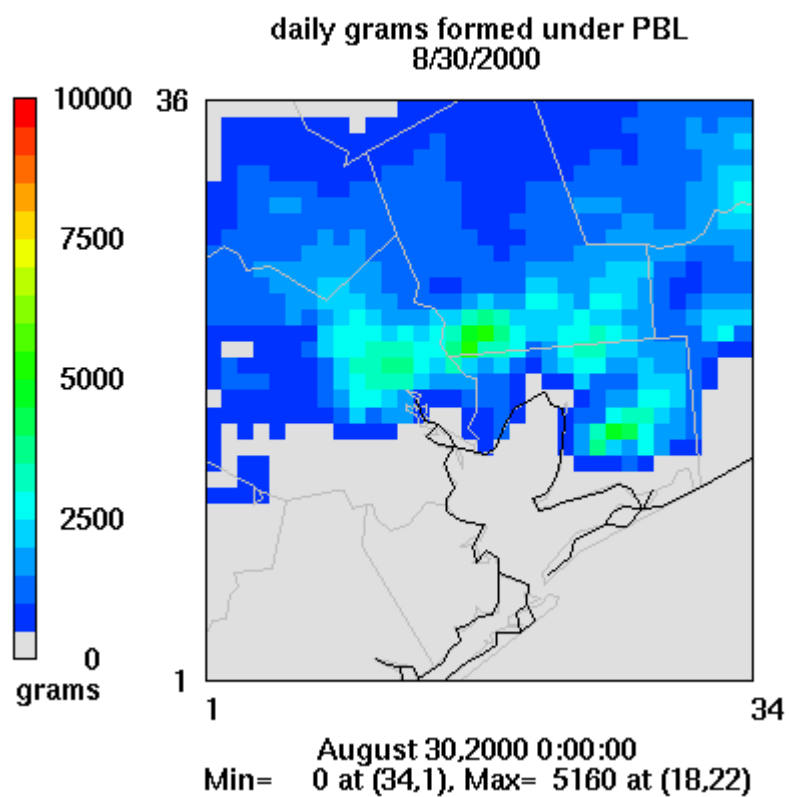


Figure 6.4. Daily SOA formation in grams under the PBL for reactions of monoterpenes with the nitrate radical. 8/30/2000.

## SOA formation; mterpenes with O3

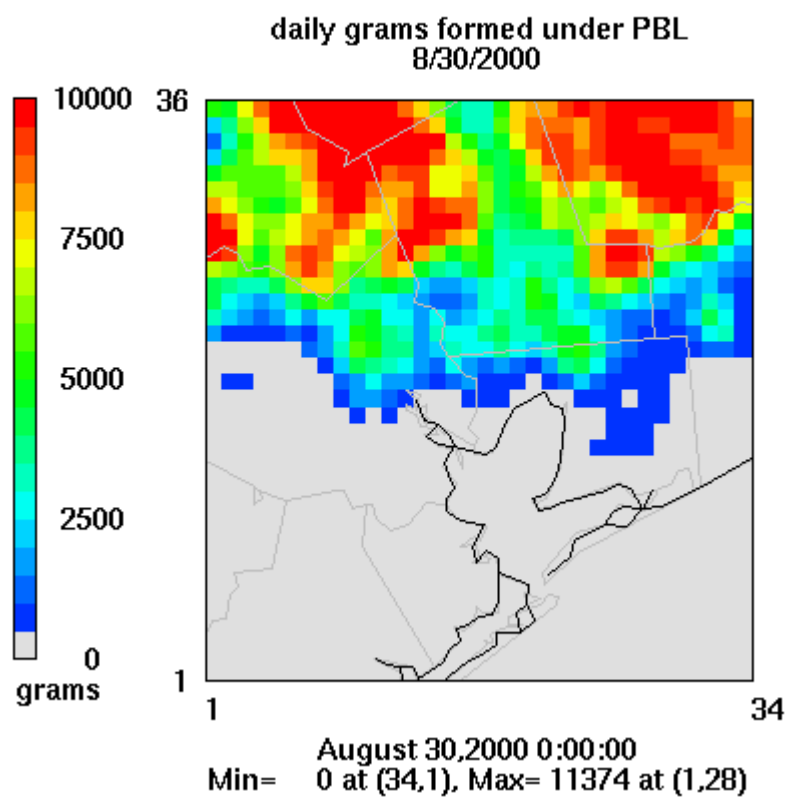


Figure 6.5. Daily SOA formation in grams under the PBL for reactions of monoterpenes with ozone. 8/30/2000



Figure 6.6. Locations of FRM speciation monitoring stations in Southeast Texas.

Figures 6.2 through 6.5 show that the reactions of monoterpenes with ozone contribute the most to SOA mass formation, and Figure 6.1 shows this is almost entirely  $\alpha$ -pinene. The SOA formation from monoterpene reactions is spatially very similar to the distribution of biogenic emissions. (See Appendix D, Figure D1 for the spatial distributions of individual monoterpene emissions). It is expected that monoterpene-SOA formation is spatially similar to biogenic monoterpene emissions, since these dominate the anthropogenic monoterpene emissions in the inventory (see Table 5.9). The notable exception to SOA formation occurring near emission sources is for the SOA formation via nitrate reactions, which occurs much closer to urban and industrial Harris County, at the edge of areas where biogenic emissions increase. This indicates that nitrate, formed in plumes near the urban and industrial centers, is reacting quickly with any monoterpenes in the atmosphere.

Figure 6.2 shows that SOA formation rates from aromatic precursors are lower than formation rates from monoterpene pathways; however, aromatic precursors lead to SOA formation over the urban center of Houston, which is where total PM<sub>2.5</sub> mass tends to be highest. From a regulatory standpoint, aromatic precursors may be important if they contribute to total PM<sub>2.5</sub> mass concentrations in the urban/industrial areas of Houston.

SOA formation rates in  $\mu\text{g}$  under the PBL were divided by the volume of each grid column, for each time step, to give formation rates normalized by volume i.e. in  $\mu\text{g}/\text{m}^3$  per hour in each grid column. The grid column volume was the grid cell length squared (4000 m x 4000 m), multiplied by the height of the PBL for that time step (Note this was done as a post processing step with a FORTRAN script written especially for this purpose; PBL heights were extracted from CAMx input files). Formation rates in  $\mu\text{g}/\text{m}^3\text{-hr}$  give a closer estimate of how much SOA is contributing to concentration increases in each cell; however caution should be taken to infer any information about absolute SOA concentrations since other gain and loss processes are not taken into account. Figure 6.7 shows time series of hourly SOA formation rates in  $\mu\text{g}/\text{m}^3\text{-hr}$ , averaged over all grid cells in the SOA formation sub-domain (also referred to as the mean-grid cell SOA formation rate).

Figure 6.7 shows that the relative importance of nitrate reactions is much greater when normalized by volume, and this is a result of nitrate reactions occurring under lower mixing heights. Strong SOA formation by ozone reactions occurs at similar times as formation by nitrate reactions, in the 7 pm to 10 pm

time period. The relative importance of ozone to nitrate reactions increased during this period when SOA formation was normalized by volume, indicating that SOA formation by ozone is generally occurring in locations with even lower mixing heights than SOA formation by nitrate. This is not unexpected since the mixing height changes both spatially and temporally. Note also that the relative importance of OH reactions is much less when SOA formation is normalized by volume. SOA formation by OH occurs mid-day when mixing heights are highest. The relative importance of SOA formation from aromatic precursors is less for this same reason.

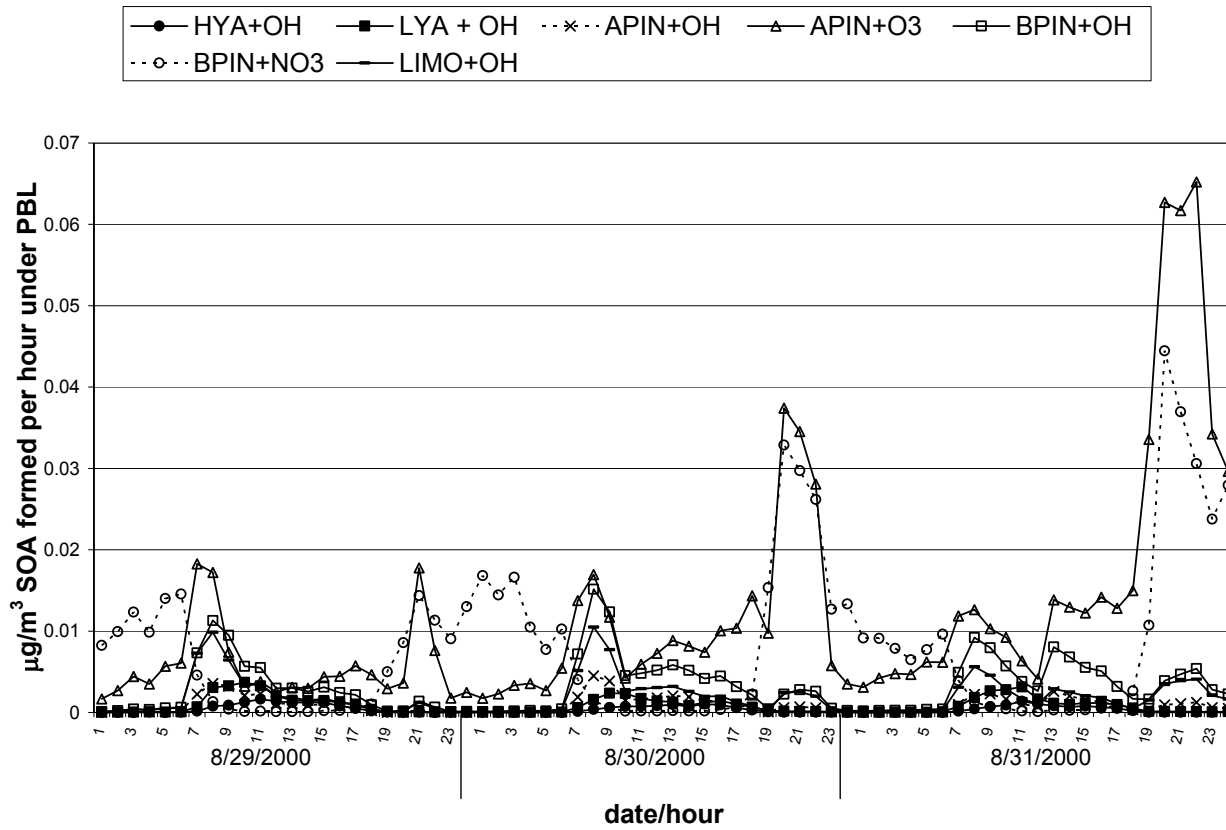


Figure 6.7. Mean-grid cell SOA formation rates in  $\mu\text{g}/\text{m}^3$ -hour in the SOA-formation subdomain. For each grid column, formation was normalized by volume under the PBL.

SOA formation in  $\mu\text{g}/\text{m}^3\text{-day}$  (i.e. summed over 24 hours) are shown in Figures 6.8 through 6.11, for aromatics with OH, all five monoterpenes with OH, all five monoterpenes with  $\text{NO}_3$ , and all five monoterpenes with  $\text{O}_3$  respectively. The spatial distributions of daily SOA mass formation per unit volume look very similar to those for daily SOA mass formation, i.e. similar to Figures 6.2 through 6.5. SOA formation is generally occurring in the same locations as precursor emissions with the exception of nitrate reactions with monoterpenes, which lead to SOA formation closer to urban and industrial areas of Houston. SOA mass formation per unit volume via ozone reactions is less intense in the north area of the sub-domain compared to absolute SOA mass formation. The high SOA mass formation via ozone reactions (Figure 6.5) is occurring when mixing heights are high.

## SOA formation; aromatics w OH

Aug 30, 2000

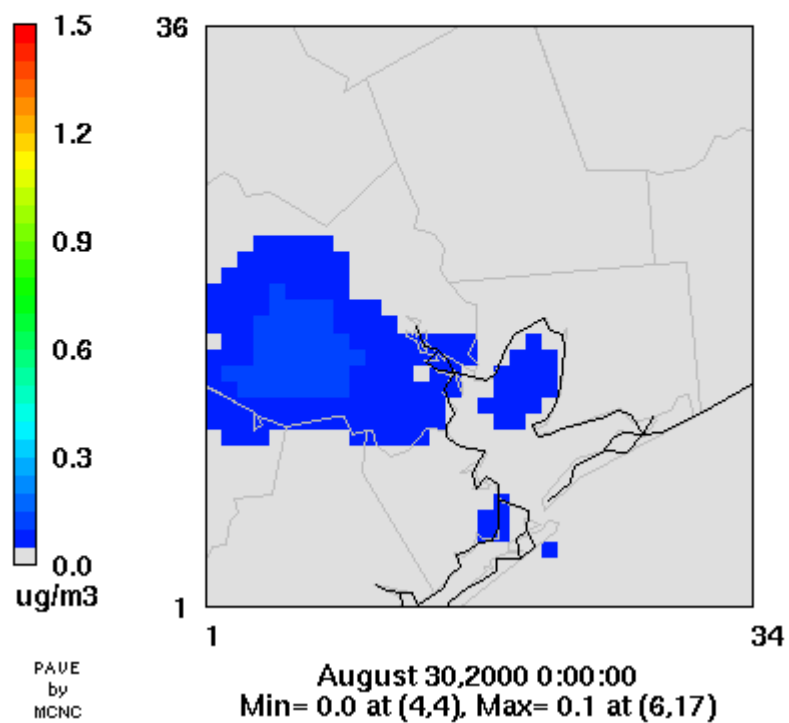


Figure 6.8. Daily SOA formation in  $\mu\text{g}/\text{m}^3$  under the PBL for reactions of aromatics with the hydroxyl radical. 8/30/2000.

# SOA formation; mterpenes w OH

Aug 30, 2000

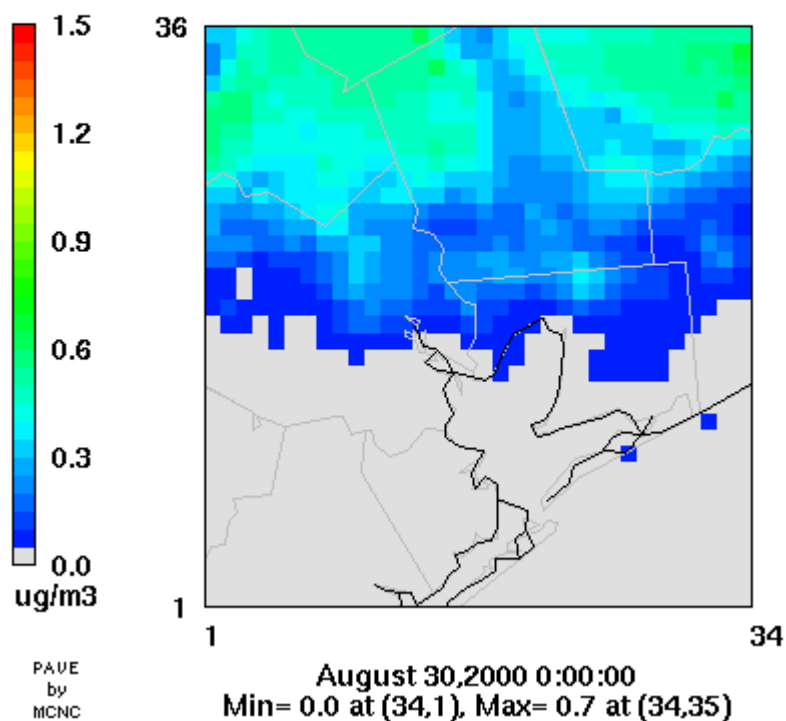


Figure 6.9. Daily SOA formation in  $\mu\text{g}/\text{m}^3$  under the PBL for reactions of monoterpenes with the hydroxyl radical. 8/30/2000.

## SOA formation; mterpenes w NO3

Aug 30, 2000

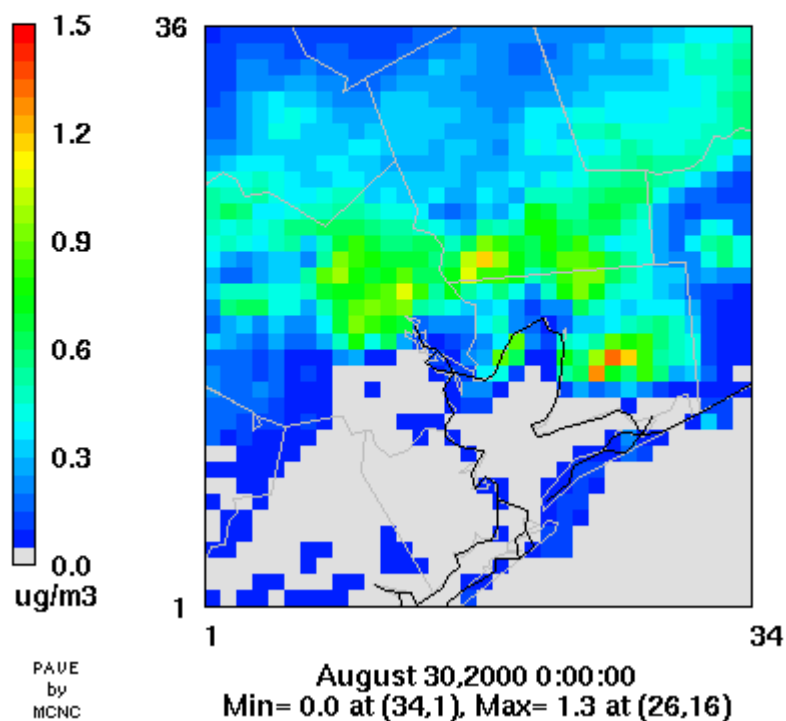


Figure 6.10. Daily SOA formation in  $\mu\text{g}/\text{m}^3$  under the PBL for reactions of monoterpenes with the nitrate radical. 8/30/2000.

## SOA formation; mterpenes w O3

Aug 30, 2000

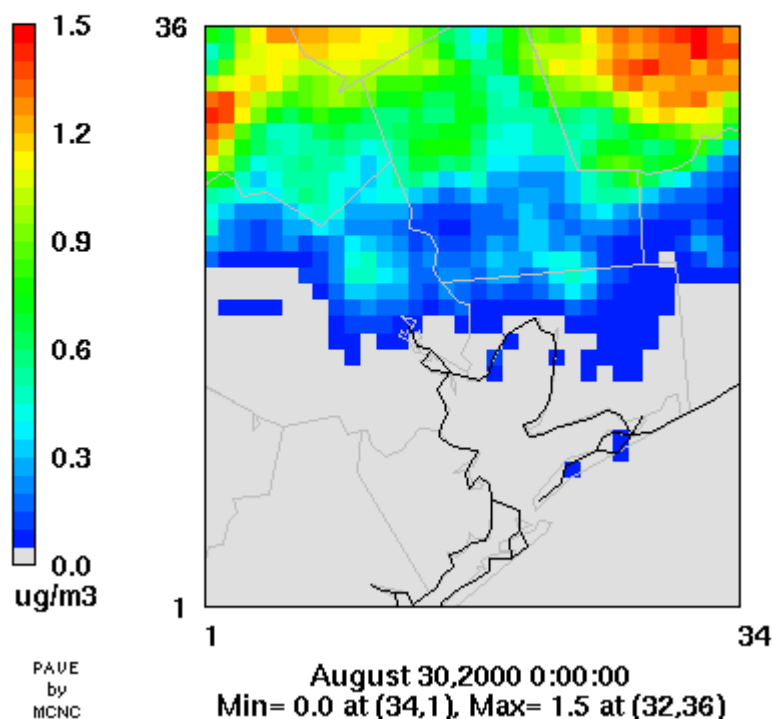


Figure 6.11. Daily SOA formation in  $\mu\text{g}/\text{m}^3$  under the PBL for reactions of monoterpenes with ozone. 8/30/2000.

### *Monitoring location SOA formation.*

The model for SOA formation implemented here (Equation 2.8) is a function of  $M_o$ ,  $\Delta\text{HC}$  (reacted precursor) and empirical constants ( $\alpha_1, \alpha_2, K_1, K_2$ ):

$$\Delta\text{SOA} = \Delta\text{HC} * Y = \Delta\text{HC} * M_o \left( \frac{\alpha_1 K_1}{1 + K_1 M_o} + \frac{\alpha_2 K_2}{1 + K_2 M_o} \right) \quad 2.8$$

Figures 6.12 through 6.15 show time series of SOA formation in  $\mu\text{g}/\text{m}^3\text{-hr}$  in four individual grid cells, which correspond to four monitoring locations in the sub-domain. The time series are shown for the grid cells containing the Conroe, Aldine, Galveston Island and Deer Park monitoring sites. These site locations are shown in Figure 6.6 above. Also shown in Figures 6.12 through 6.15 are estimated Mo concentrations at each location, which are used as input to Equation 2.8. Predicted SOA formation does not correlate well with Mo at any location, which suggests that the concentration of available absorption medium alone does not dictate temporal patterns of SOA formation. The spatial distribution of Mo is also not similar to the spatial distribution of SOA formation. It must be concluded that temporal and spatial patterns in SOA formation rates are greatly influenced by oxidation of precursors i.e.  $\Delta\text{HC}$  in Equation 2.8, as well as available Mo.

Note from Figure 6.12 and 6.13 respectively that SOA formation rates near the industrial Deer Park and coastal Galveston sites are low (at most  $\sim 0.03 \mu\text{g}/\text{m}^3$  per hour) compared to typical 24-hour averaged  $\text{PM}_{2.5}$  mass concentrations of  $10 - 15 \mu\text{g}/\text{m}^3$ . Furthermore local formation of SOA comes predominantly from aromatic precursors at these locations, especially near Deer Park which is closer to aromatic emissions sources. In contrast to Deer Park and Galveston, the Aldine and Conroe sites show much higher SOA formation rates (up to  $0.5 \mu\text{g}/\text{m}^3$  per hour) and these come predominantly from monoterpene-nitrate and monoterpene-ozone reactions. The higher local SOA formation rates at these locations are consistent with proximity of these locations to areas of higher biogenic emissions.

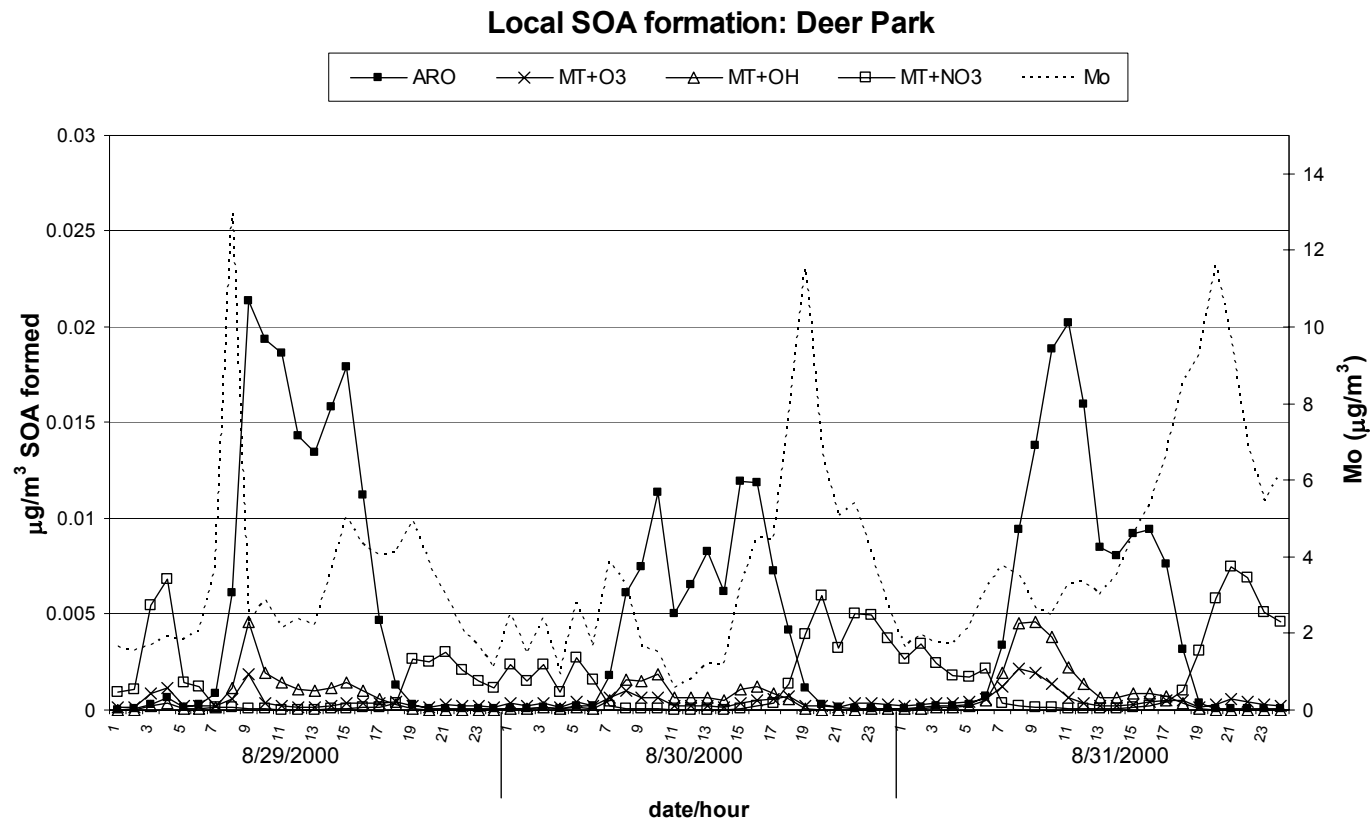


Figure 6.12. SOA formation rates in  $\mu\text{g}/\text{m}^3$ -hour, in the grid cell where the Deer Park monitoring station is located. The scale on the abscissa is at a maximum of  $0.03 \mu\text{g}/\text{m}^3$ .

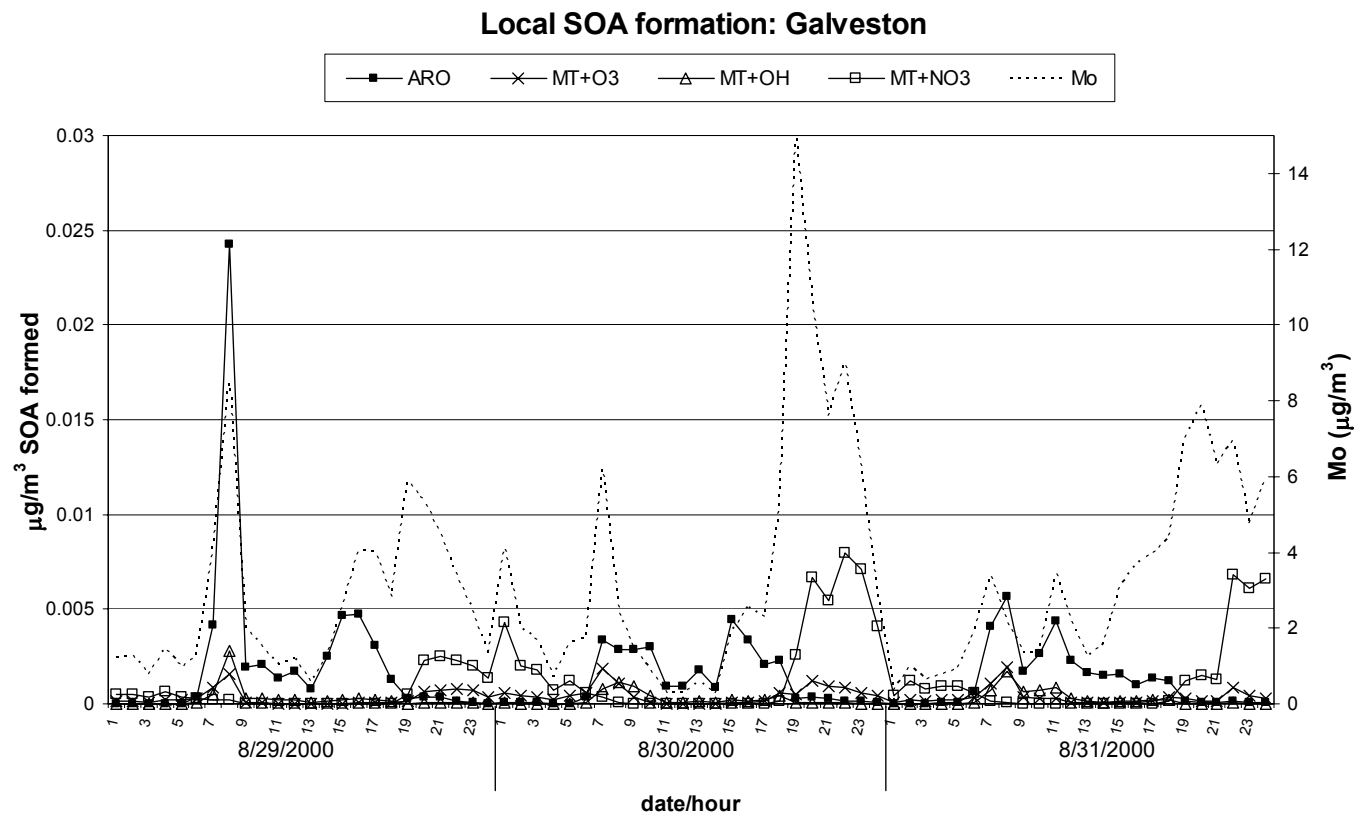


Figure 6.13. SOA formation rates in  $\mu\text{g}/\text{m}^3$ -hour, in the grid cell where the Galveston monitoring station is located. The scale on the abscissa is at a maximum of  $0.03 \mu\text{g}/\text{m}^3$ .

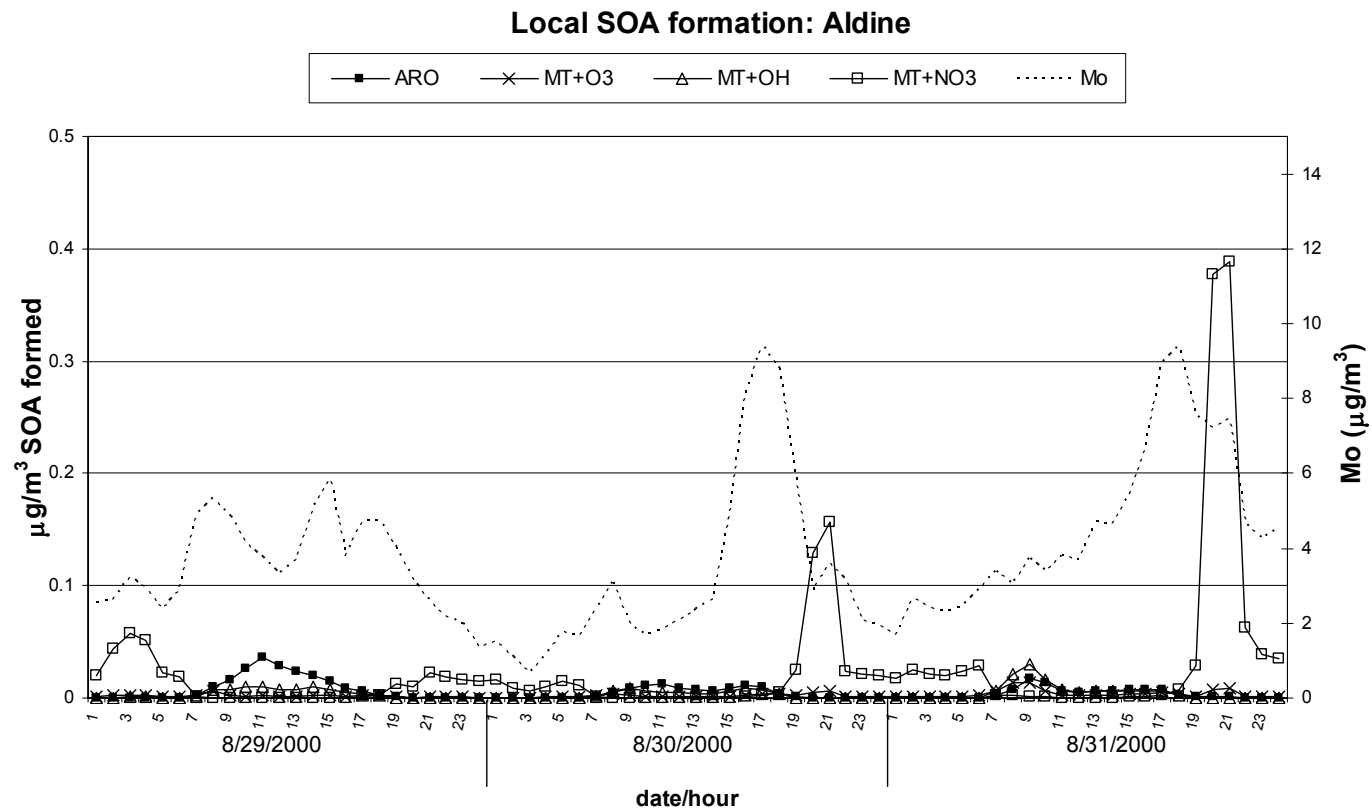


Figure 6.14. SOA formation rates in  $\mu\text{g}/\text{m}^3$ -hour, in the grid cell where the Aldine monitoring station is located. The scale on the abscissa is at a maximum of  $0.50 \mu\text{g}/\text{m}^3$ .

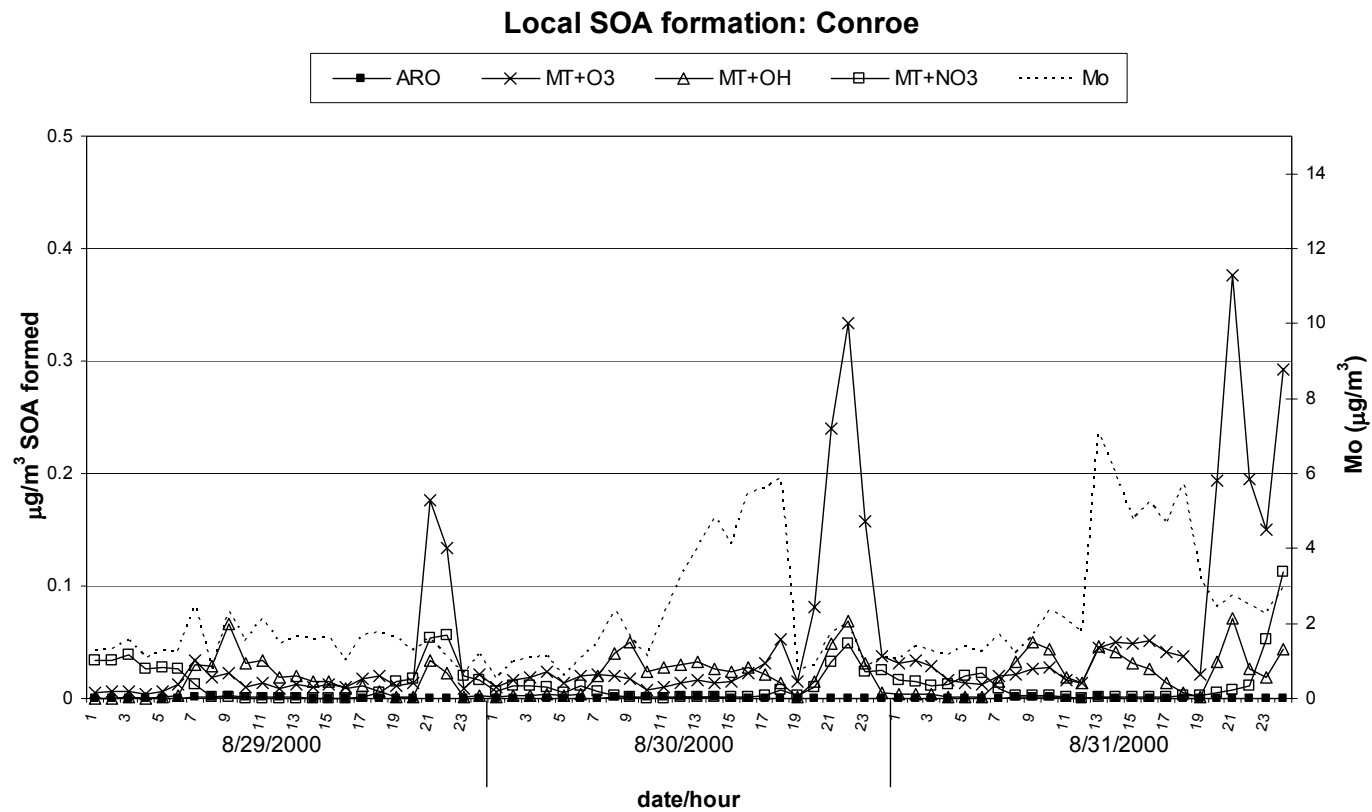


Figure 6.15. SOA formation rates in  $\mu\text{g}/\text{m}^3$ -hour, in the grid cell where the Conroe monitoring station is located. The scale on the abscissa is at a maximum of  $0.50 \mu\text{g}/\text{m}^3$ .

One important point to note is that hourly  $\text{PM}_{2.5}$  concentrations, which were used to calculate hourly  $\text{Mo}$  concentrations, were at their maximum in the late afternoon and evening at all site locations during this three day period. Although late-day maxima are not uncommon during the ozone season,  $\text{PM}_{2.5}$  concentrations averaged over seasons or years typically peak in the morning, as shown in Chapter 4. The diurnal pattern of  $\text{PM}_{2.5}$  is assumed here to be representative of this period.

#### ***SOA formation evaluation.***

The mean-grid cell SOA formation rate, summed over all pathways for Aug 31<sup>st</sup>, 2000 is  $\sim 1 \mu\text{g}/\text{m}^3$  per day. In other words, a hypothetical air parcel traveling through the sub-domain for 24 hours on Aug 31<sup>st</sup> would gain  $\sim 1 \mu\text{g}/\text{m}^3$  of SOA from local formation if it gained SOA mass each hour at the mean hourly formation rate over all grid cells. This parcel would gain  $\sim 6 \mu\text{g}/\text{m}^3$  of SOA from local formation, if it gained SOA mass each at hour at the maximum hourly formation rate over all grid cells (an impossible scenario since the parcel would need to jump to and from the grid cell with maximum formation rate at each hour). Since chemical reaction is the only SOA formation mechanism (it is not emitted), and large scale winds in August are from the south/southeast and presumably have little to no background SOA, it is reasonable to expect SOA concentrations in the local area to be on the same order of magnitude as integrated formation rates of SOA in the subdomain. Indeed, the empirical model for SOA presented in Chapter 4 predicts SOA concentrations at local sites between 1 and 3

$\mu\text{g}/\text{m}^3$ . It is very encouraging that this first attempt at predicting SOA formation shows such consistent results with concentrations derived from ambient data.

SOA concentrations that are inferred from formation rates should be interpreted with caution since the model does not account for SOA transport or loss processes. The mean local SOA formation of  $1 \mu\text{g}/\text{m}^3$  is based on the assumption of an air parcel remaining in the subdomain for a 24-hour period. Analysis of animated ozone concentrations shows that local urban plumes are generally advected out of the sub-domain in under 24 hours, even under light winds. Under stagnant conditions, however, an air parcel could reside in the subdomain for a period longer than 24 hours (e.g. at wind speeds of 1.5 m/s a parcel would not traverse the south-to-north distance of the sub-domain in 24 hours). There may also be background concentrations of SOA that are not insignificant. Predicted SOA concentrations from the SOA empirical model (Chapter 4) are slightly higher at most sites than what is reasonable to assume comes from local formation, and the difference is likely due to transport into the domain. A value of  $1 \mu\text{g}/\text{m}^3$  is taken to be reasonable order-of-magnitude estimate of the contribution of local source emissions to SOA concentrations in the SOA subdomain on a day with intense photochemical activity (as is August 31<sup>st</sup>). Higher wind speeds, less photochemical activity and loss processes of SOA would lower the contribution of local emissions to SOA concentrations.

It should be noted that mean daily SOA concentrations predicted by the SOA empirical model (Chapter 4) are as high at urban and industrial sites as at rural sites (on average and also on individual days during the TXAQS period).

This is interesting since formation rates are predicted by the grid model to be higher at rural locations where biogenic monoterpenes emissions are higher. The disparity raises some important questions as to the accuracy of predicted SOA formation rates.

The first question is whether there are other significant SOA precursors that have not been considered in this model. Aromatics and monoterpenes were found to be the most significant SOA precursors in Los Angeles, California (Grosjean and Seinfeld 1989; Pandis et al. 1992); however, there are other anthropogenic organic compounds that have been shown to have high aerosol yields (see reviews in Seinfeld and Pandis (1998); Jacobson et al. (2000)). The industrial emissions in Southeast Texas are unique, and there may be important SOA precursors were not included in SOA calculations, for example n-dodecane or naphthalene (Dechapanya et al. 2003c). On the other hand, there are biogenic precursors that have also not been considered, namely sesquiterpenes, which are known to have high aerosol yields, but whose emissions rates are uncertain. Sesquiterpene emissions in southeast Texas are distributed very similarly to isoprene (Vizueté et al. 2003) and they are not expected to contribute more SOA at urban/industrial sites than rural sites. Based on the body of available literature on SOA formation, however, aromatics and monoterpenes are assumed to be the dominant SOA precursors.

The second question raised by the spatial disparity of SOA concentrations vs. model-predicted formation rates is whether SOA formation is occurring via alternate physico-chemical mechanisms other than absorptive partitioning of low

volatility reaction products. Recent findings have shed light on the importance of heterogeneous reactions of high-volatility organic compounds on acidic aerosol surfaces resulting in formation of low-volatile particle phase organics (Jang et al. 2002). In other words, organic precursors that do not form low volatility gas-phase reaction products may form significant aerosol in the presence of an acid catalyst. Heterogeneous reactions may increase aerosol yields from biogenic as well as anthropogenic compounds. The chemistry behind these processes is only beginning to be understood, and this will need to be incorporated in a grid model as more data becomes available. If heterogeneous reactions were more significant near industrial sources, these reactions could account for additional aerosol detected from ambient measurements at these locations.

It is also important to note that the model used here is a simplified representation of condensable product formation and gas/particle partitioning. The mass yields of condensable products are represented by two fixed values, i.e.  $\alpha_1$  and  $\alpha_2$ , and gas/particle partitioning parameters are for hypothetical species, and do not take into account the interaction of condensable species with existing aerosol components. The smog chamber conditions under which the yield parameters were derived are likely very different from actual ambient conditions in Southeast Texas. Differences between actual and predicted yields might be greater or less in urban/industrial areas compared to biogenic areas. The limitations of using simplified SOA models are not clear; however, the four parameter yield model has represented smog chamber SOA formation remarkably well. In addition, it is not practical from a computational stand-point to include

multi-step reaction mechanisms for each SOA precursor into a grid model and to track individual aerosol components throughout the simulation. Simplified mechanisms for SOA are a necessity for including this pollutant in grid model applications.

The points discussed in the last three paragraphs are possible reasons why modeled SOA formation would not be accurate, and each point highlights a recommended area for improving the SOA model. The inaccuracies were identified assuming that the empirical model gave 'true' estimates of daily average SOA concentrations. As discussed in Chapter 3, however, FRM sampling and analysis methods also have uncertainties. In addition, the empirical model for the secondary fraction of OC is quite simple. It is possible that empirical estimates of SOA are over-estimated at urban/industrial sites compared to rural sites. Such uncertainties will only be assessed as better techniques become available to measure SOA. For now, the empirical model for SOA presented in this research is the best (and only) estimate of SOA concentrations in Southeast Texas. A number of other researchers have measured various aerosol properties in Southeast Texas from which spatial and temporal patterns of SOA can be inferred. The remainder of this section discusses these studies and presents a qualitative comparison to modeled SOA formation.

Brock et al. (2003) measured particle volume and number concentrations aboard an aircraft in industrial, urban and power plant plumes from the Houston area during the TXAQS period. Data were presented for Aug 27<sup>th</sup> and 28<sup>th</sup> 2000 when winds were southerly and distinct plumes could be detected advecting north

from urban and industrial Houston. There was a significant increase in particle number close to the plumes' origins and there was also a significant increase in particle volume further downwind of some plumes origins. Modeled SO<sub>2</sub> chemistry in the plumes showed that formation of ammonium sulfate accounted for particle volume increases, except in the ship channel (industrial) plume. The authors suggested that the additional particle volume in the ship channel plume was from heterogeneous reactions of organic gases on the acidic aerosol surface, in other words SOA from non-traditional precursors. Results from this research do not necessarily contradict that explanation but offer an additional explanation.

The ship channel plume was the only plume with elevated ozone on the days presented in the reference (Brock et al. 2003). Furthermore this observed ozone was at its highest downwind from the emissions sources, precisely where predicted biogenic emissions of monoterpenes become significant. The increased particle volume might be a result of ozone-monoterpene reactions and subsequent condensation of organic reaction products. The relative contribution of biogenic SOA to the observed particle volume increase is unknown and the high correlation between particle volume increase and SO<sub>2</sub> cannot be ignored. The observed particle volume increase north of Houston, however, is consistent with model results from this research that predict high SOA mass formation rates as ozone is advected north over areas of monoterpene emissions.

Lemire et al. (2002) present measurements of geologically modern carbon during TXAQS by measuring the ratio of <sup>14</sup>C/<sup>13</sup>C in filter samples of total PM<sub>2.5</sub> mass. The fraction of modern carbon is defined as the ratio of <sup>14</sup>C/<sup>13</sup>C of the

sample to  $^{14}\text{C}/^{13}\text{C}$  of a reference material of purely non-fossil fuel carbon. Modern carbon is expected to come from a limited number of sources including vegetative debris, secondary organic aerosol from biogenic precursors, primary organic carbon from biomass burning and primary organic carbon from meat cooking. The fraction of modern carbon (pMC) was calculated at two sites: Conroe (a rural site north of Houston surrounded by biogenic sources) and Aldine (an urban site influenced heavily by motor vehicle emissions and less heavily by biogenic sources). Results showed that the fraction of modern carbon correlated positively with the fraction of organic carbon in the samples. In other words as the relative amounts of OC to EC increased, the additional OC was not of fossil fuel origin (which excludes SOA from aromatics and other anthropogenic sources). Furthermore, the authors provide arguments that biomass burning, meat cooking and vegetative debris are not contributing significantly to the OC in the samples. The authors conclude that SOA in the samples at both sites is biogenic in origin and that there is a greater biogenic SOA contribution to the OC in samples measured at the Conroe site compared to the Aldine. Model results in this study confirm these findings and suggest that the SOA is from monoterpene oxidation.

Finally, airborne measurements of aerosol back-scatter as a function of height were made during the TXAQS period and data are available online (NOAA 2003a). A spatial analysis of these data showed that for the Aug 28<sup>th</sup> through Aug 31<sup>st</sup> period, the largest vertical cross sections of high aerosol back scatter occurred on Aug 28<sup>th</sup> in plumes that were situated north of Houston (flight paths on the other 3 days did not go very far north of urban Houston). The profiles probably

show the same urban/industrial plumes detected by measurements made by Brock et al. The vertical profile showed that the areas of intense back-scatter were high in the mixed layer, such that ground based monitors may not have measured high PM concentrations. SOA formation was calculated in this work as an average rate throughout the mixed layer, so vertical gradients of SOA formation were not available. An examination of model results showed little vertical variation of ozone concentrations in the mixed layer in the area of interest, which is an indication that the model is over-mixing pollutants vertically.

Regardless of the vertical variation in aerosol back-scatter, the particle volume concentrations measured by Brock et al are probably secondary PM, based on the fact that concentrations increase with downwind distance from source regions. The model results obtained in this research add an additional explanation for this secondary aerosol: oxidation of monoterpene emissions by ozone to form SOA.

## **6.2 Sensitivity Simulations Results**

The SOA grid model was used to test the sensitivity of SOA formation to various inputs and parameters, and the results of these simulations are presented in this section. The sensitivity simulations can be divided into four types: sensitivity to reaction mechanisms, sensitivity to Mo concentrations, sensitivity to SOA precursor emissions, and sensitivity to ozone precursor emissions. All simulations and their descriptions are listed in Table 6.2 below. The sensitivity simulations were performed for the Aug 29<sup>th</sup>- Aug 31<sup>st</sup> 2000 period, since these

were the days of interest and it was not practical to simulate the entire episode for each case. The only exception was the simulation with the s99soa2 chemical mechanism, which was performed for the entire Aug 22<sup>nd</sup> - Sep 1<sup>st</sup> 2000 episode. The initial conditions used to start sensitivity simulations, i.e. midnight concentrations on Aug 28<sup>th</sup>, were taken from the base case. Using base case initial conditions is not expected to have any effect on relative differences between base case and sensitivity simulations, especially on Aug 30<sup>th</sup> and Aug 31<sup>st</sup>, 2000.

Table 6.2. List of sensitivity simulations.

#	Description (%'s are relative to base case conditions)
<b>Reaction mechanism sensitivity:</b>	
1	s99soa2 mechanism was implemented with series/parallel reaction mechanisms for SOA formation from aromatic precursors.
<b>Mo concentration sensitivity:</b>	
1	200% Mo concentration in each grid cell
2	50% Mo concentration in each grid cell
3	Mo concentrations in each grid cell were set equal to the mean Mo concentration in the subdomain for that hour. Mo concentrations were homogenous throughout the domain.
<b>SOA precursor sensitivity:</b>	
1	200% biogenic monoterpene emissions throughout the domain
2	50% biogenic monoterpene emissions throughout the domain
3	200% aromatic emissions in the 11-county Houston Galveston Beaumont Port Arthur area.
4	50% aromatic emissions in the 11-county Houston-Galveston, Beaumont-Port Arthur area.
<b>Ozone precursor sensitivity:</b>	
1	200% anthropogenic NOx emissions in the 11-county Houston-Galveston, Beaumont-Port Arthur area.
2	50% anthropogenic NOx emissions in the 11-county Houston-Galveston, Beaumont-Port Arthur area.
3	10% anthropogenic NOx emissions in the 11-county Houston-Galveston, Beaumont-Port Arthur area.

4	200% anthropogenic light olefin emissions in the 11-county Houston-Galveston, Beaumont-Port Arthur area.
5	50% anthropogenic light olefin emissions in the 11-county Houston-Galveston, Beaumont-Port Arthur area.
6	10% anthropogenic light olefin emissions in the 11-county Houston-Galveston, Beaumont-Port Arthur area.

***Reaction Mechanism Sensitivity.***

The s99soa2 mechanism contained expanded mechanisms for aromatic reactions that produced condensable products. Figure 6.16 shows the mean-grid cell SOA formation rate per hour from high-SOA and low-SOA yield aromatics in the s99soa mechanism (original SAPRC aromatic mechanisms) and in the s99soa2 mechanism (expanded aromatic mechanisms Dechapanya et al. (2003a, b)). Figure 6.16 shows that, at all hours of the day, low-SOA yield aromatics form significantly less SOA per hour in the s99soa2 mechanism compared to s99soa. High-SOA yield aromatics form more SOA in the s99soa mechanism in the 7am – 11am period, but this reverses in late morning and the s99soa2 mechanism produces more SOA for the rest of the day. The daily formation rate of SOA from *total* aromatics throughout the subdomain is 40%-50% lower when using the s99soa2 mechanism, i.e. the net effect of using the expanded aromatic mechanisms is 40-50% less SOA formation in an average grid cell in the domain. Very similar results are obtained when considering aromatic-SOA formation at individual grid cells, namely the cells where the Conroe, Aldine, Galveston and Deer Park site are located, and results are similar from day to day. This suggests that using a different mechanism has a systematic effect on SOA formation rates.

Spatially, the differences between aromatic-SOA formation in *s99soa* and *s99soa2* occur where absolute aromatic-SOA formation rates are greatest: in urban and industrial Houston (see Figure 6.2). The change in aromatic reaction mechanisms had a negligible effect on monoterpene-SOA formation and a negligible effect on ground-level ozone concentrations. One interesting feature is that total aromatic-SOA formation occurs 3-4 hours later in the day when using *s99soa2*. The low-SOA yield aromatics (LYA) in the *s99soa* mechanism produced high SOA formation rates in the morning, but LYA SOA formation rates are much lower in the *s99soa2* mechanism. The high-SOA yield aromatic (HYA) formation rates are much stronger later in the day in *s99soa2* and they tend to form maximum SOA somewhat later compared to in *s99soa*. The overall result is a shift in the time of maximum SOA formation from aromatics.

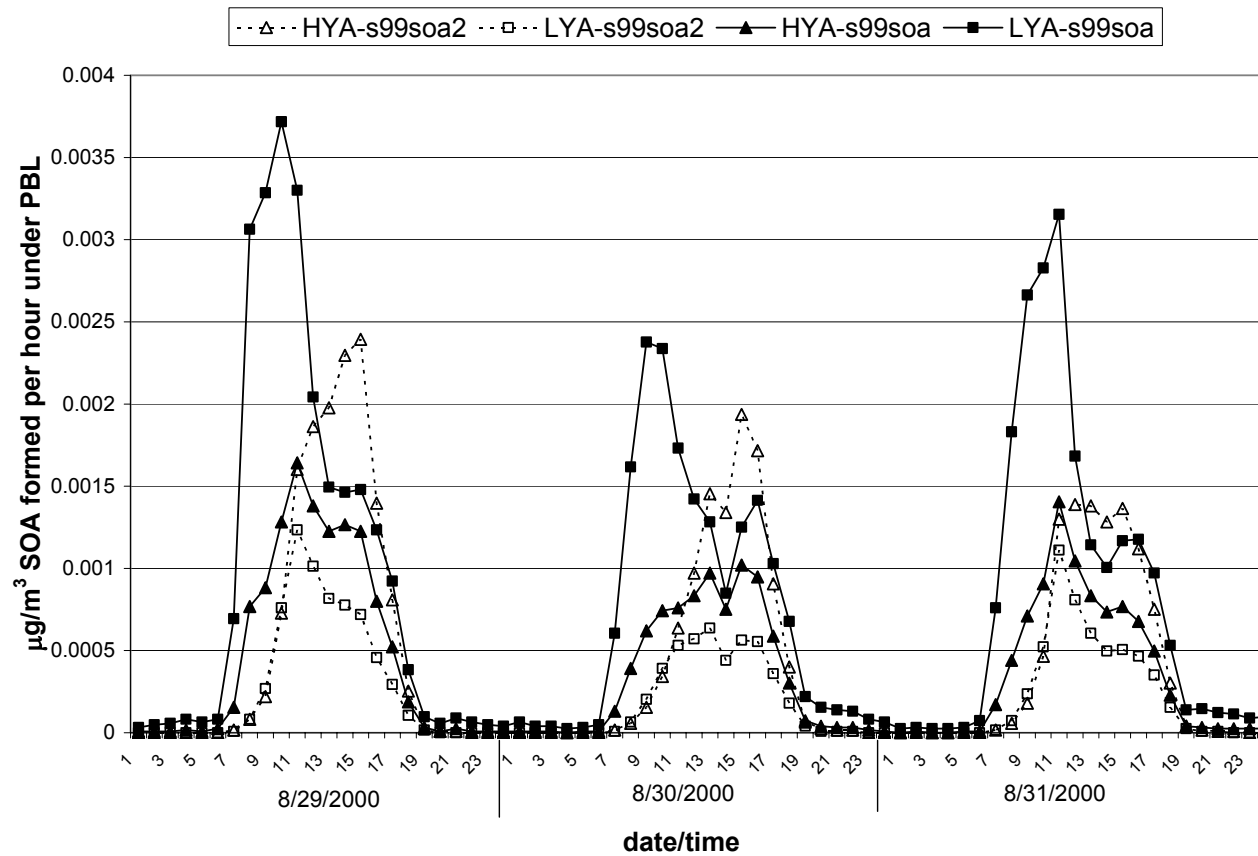


Figure 6.16. Aromatic SOA formation per hour, averaged over all grid cells in the SOA-formation subdomain. Solid lines show the s99soa mechanism, dashed lines show the s99soa2 mechanism.

The base case model results showed that aromatic-SOA formation rates were much less than monoterpene-SOA formation rates in the SOA subdomain as a whole. The differences in SOA formation between the original and expanded aromatic mechanisms are not that significant for predicting total SOA formation rates in this episode. The differences do, however, raise questions about the accuracy of assuming first generation condensable reaction products, which is inherently assumed in the original SOA model used here. The SOA grid model can (and is recommended to) be used to test the assumption of first generation condensable products from monoterpenes, particularly  $\alpha$ -pinene and  $\beta$ -pinene, using more detailed reaction mechanisms for these precursors.

***Mo concentration sensitivity.***

Three sensitivity simulations were performed to test the effect of Mo concentrations on SOA formation. Figure 6.17 shows the mean-grid cell daily SOA formation rate for the 200% Mo, 50% Mo and homogenous Mo simulations. The Figure shows SOA formation for Aug 30<sup>th</sup>, 2000 only. The sensitivity of base case SOA to the simulations is similar on all three episode days.

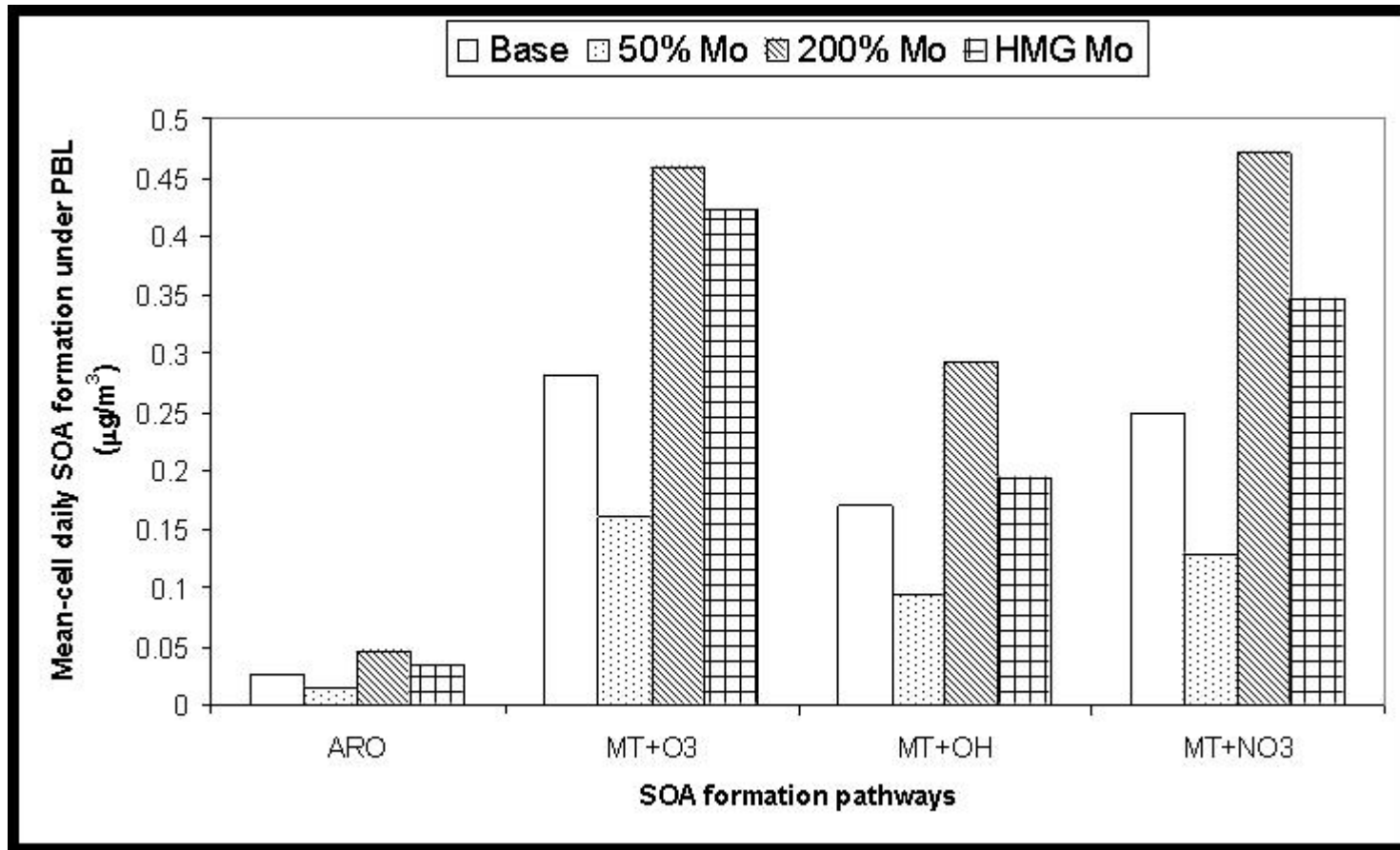


Figure 6.17. Mean-grid cell daily SOA formation rates for the base case, 200%, 50% and homogeneous Mo sensitivity simulations.

Homogeneous Mo throughout the subdomain, Aug 30th, 2000.  
 SOLID lines are BASE case. DASHED lines are SENSITIVITY case.

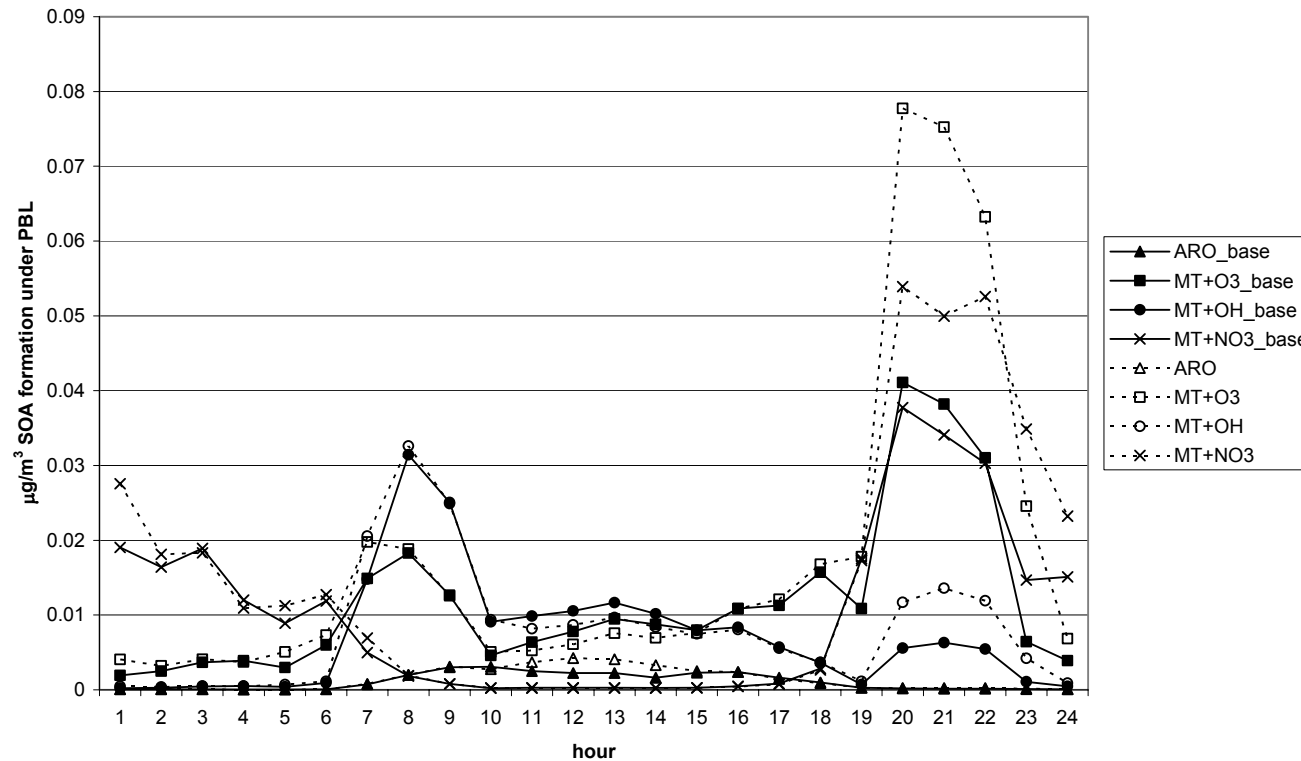


Figure 6.18. Mean-grid cell hourly SOA formation rates for the base case (solid lines) and the homogeneous Mo concentration case (dashed lines).

Figure 6.17 shows that mean-grid cell daily SOA formation rates are relatively proportional to Mo concentrations, within 50% - 200% of the base case conditions. The proportionality is consistent throughout the sub-domain and at all hours. In other words, the Mo terms in the denominators of Equation 2.8 are negligible with the partitioning parameters ( $K_1, K_2$ ) used in this research and within the range of Mo concentrations in Southeast Texas.

Setting Mo to be homogeneous throughout the domain leads to increases in mean-grid cell daily SOA formation, but this varies from hour to hour and throughout the domain. Figure 6.18 shows a time series of mean-grid cell SOA formation in both the base case and homogeneous Mo case. The largest SOA formation rates are sensitive to setting a homogeneous Mo, which highlights the importance of accurate spatial characterization of Mo concentrations. Mo concentrations are higher in the urban area of Houston and lower in the rural areas for most episode hours. In general, when Mo is made homogeneous, Mo concentrations in rural areas increase and Mo concentrations in urban areas decrease relative to base case. Increases in monoterpene-SOA formation rates in the rural areas occur to a much greater extent than decreases in aromatic-SOA formation rates in urban areas.

#### ***SOA precursor sensitivity.***

The sensitivity of SOA formation to precursor emissions was tested by varying biogenic monoterpene and anthropogenic aromatic emissions. Biogenic monoterpenes were varied to 200% and 50% of base case conditions throughout

the entire modeling domain (not just the SOA-subdomain). Aromatic emissions were varied to 200% and 50% of base case conditions in the 11-county Houston-Galveston, Beaumont-Port Arthur ozone non-attainment area. The aromatic emissions were reduced in this area to simulate a realistic emissions reduction scenario. Varying aromatic emissions domain wide is not expected to effect local SOA formation compared to varying emissions in the 11-county area, since local emissions are probably much higher than aromatics transported into the region.

Figure 6.19 shows the sensitivity of mean-grid cell daily SOA formation in both the biogenic monoterpene reduction and aromatic reduction simulations. In both cases, results relative to base case were consistent throughout the domain and at each hour. Figure 6.19 shows that, except for the monoterpene-NO<sub>3</sub> pathway, SOA formation is a fairly linear function of precursor emissions, within 50%-200% of base case conditions. The availability of precursor is limiting the formation of SOA. The monoterpene-NO<sub>3</sub> pathway results in ~40% more SOA formation when monoterpene emissions are doubled, and ~40% less SOA formation when monoterpene emissions are halved, which suggests that nitrate radical is limiting SOA formation at base case conditions. This is not unexpected since monoterpene-NO<sub>3</sub> reactions to form SOA occur at the very edge of the areas of biogenic emissions, suggesting that the oxidant, formed in the polluted urban/industrial areas, is quickly depleted by available monoterpene precursors.

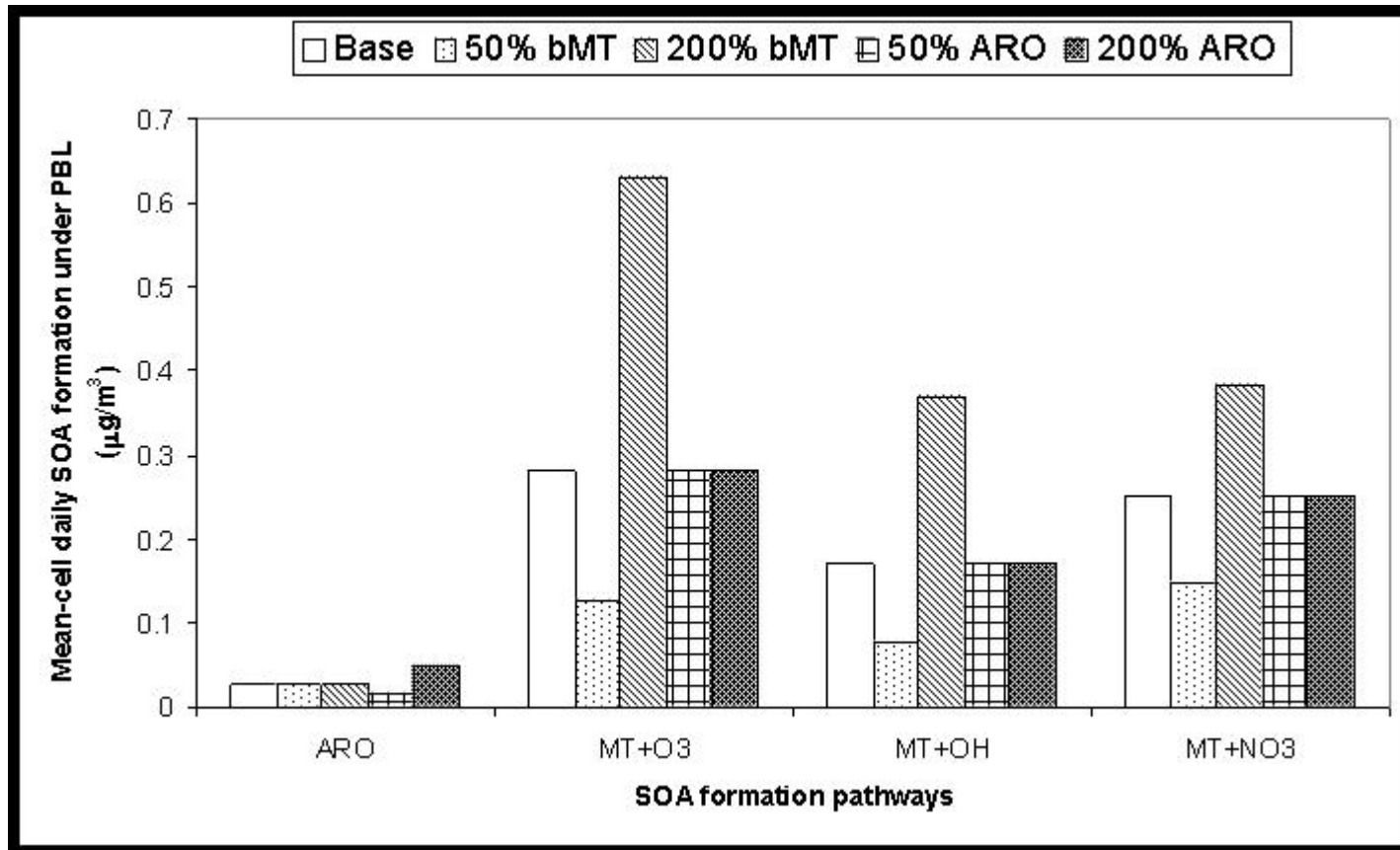


Figure 6.19. Mean-grid cell daily SOA formation rate in SOA-subdomain on Aug 30<sup>th</sup>, 2000. Results are shown for the base case and for the 50% and 200% biogenic monoterpene (bMT) emission reductions and the 50% and 200% aromatic (ARO) emissions reductions.

Monoterpene-SOA formation is not affected by changing aromatic emissions by 50% or 200%. Likewise, aromatic-SOA formation is not affected by changing biogenic monoterpene emissions. The fact that most of the SOA formation is occurring under precursor-limited conditions highlights the importance of having an accurate emissions inventory. Given their higher formation rates, the monoterpene emissions in particular should be critically evaluated for use in SOA models in Southeast Texas.

***Ozone precursor sensitivity.***

The final sets of sensitivity simulations involved varying anthropogenic emissions of ground-level ozone precursors, namely NO<sub>x</sub> and light-olefins. NO<sub>x</sub> emissions reductions typically have a dual effect: both reducing and increasing ozone concentrations. NO<sub>x</sub> emissions reductions are effective overall if ozone reductions occur where and when ozone concentrations are at a maxima. Light olefins are highly reactive compounds, such as propylene and ethylene, which are emitted in large quantities from industries in the Houston area. Some evidence exists that these compounds are responsible for producing hazardous concentrations of ozone near Houston (NOAA 2003b). Emissions reductions of ozone precursors will result in lower photochemical activity, lower oxidant concentrations, and thus lower SOA formation rates. Reducing oxidant concentrations is an important strategy to reduce SOA concentrations in Southeast Texas, since the results presented above indicate that precursor concentrations are predominantly biogenic.

Figure 6.20 shows mean-grid cell daily SOA formation rates for anthropogenic NO<sub>x</sub> emission sensitivity. The mean-cell daily formation rate is relatively insensitive to NO<sub>x</sub> emissions reductions. The mean-cell formation rates via hydroxyl radical oxidation vary little even at 10% of base case NO<sub>x</sub> emissions (i.e. 90% anthropogenic emissions reductions). Monoterpene-SOA formation via the nitrate radical is the pathway most affected by changes in NO<sub>x</sub> emissions. A 90% anthropogenic NO<sub>x</sub> emission reduction results in ~50% mean SOA formation from the monoterpene-NO<sub>3</sub> pathway. It is interesting that emitting twice as much anthropogenic NO<sub>x</sub> has a very slight effect on SOA formation in general. Finally, the mean-grid cell SOA formation from monoterpene-O<sub>3</sub> reactions shows a clear dis-benefit from reducing NO<sub>x</sub> emissions.

The mean-grid cell daily SOA formation is an indicator of the average effect of the sensitivity simulation throughout the domain and episode. In the case of NO<sub>x</sub> emissions variations, the sensitivity of SOA formation varies significantly throughout the domain. Spatial variations of this sensitivity are considered here for the 10% anthropogenic NO<sub>x</sub> emissions case. Figures 6.21a and 6.21b show spatial distributions of maximum ozone decreases at any hour and maximum ozone increase at any hour respectively on Aug 30<sup>th</sup>, when reducing anthropogenic NO<sub>x</sub> emissions by 90%. The ‘maximum-difference’ plots show that the NO<sub>x</sub> reduction can lead to significant ozone increases and decreases of similar magnitudes, but in different areas. The effect of NO<sub>x</sub> emissions reductions on daily SOA formation rates is shown in Figure 6.22a and 6.22b for the monoterpene-NO<sub>3</sub> and monoterpene-O<sub>3</sub> reactions respectively.

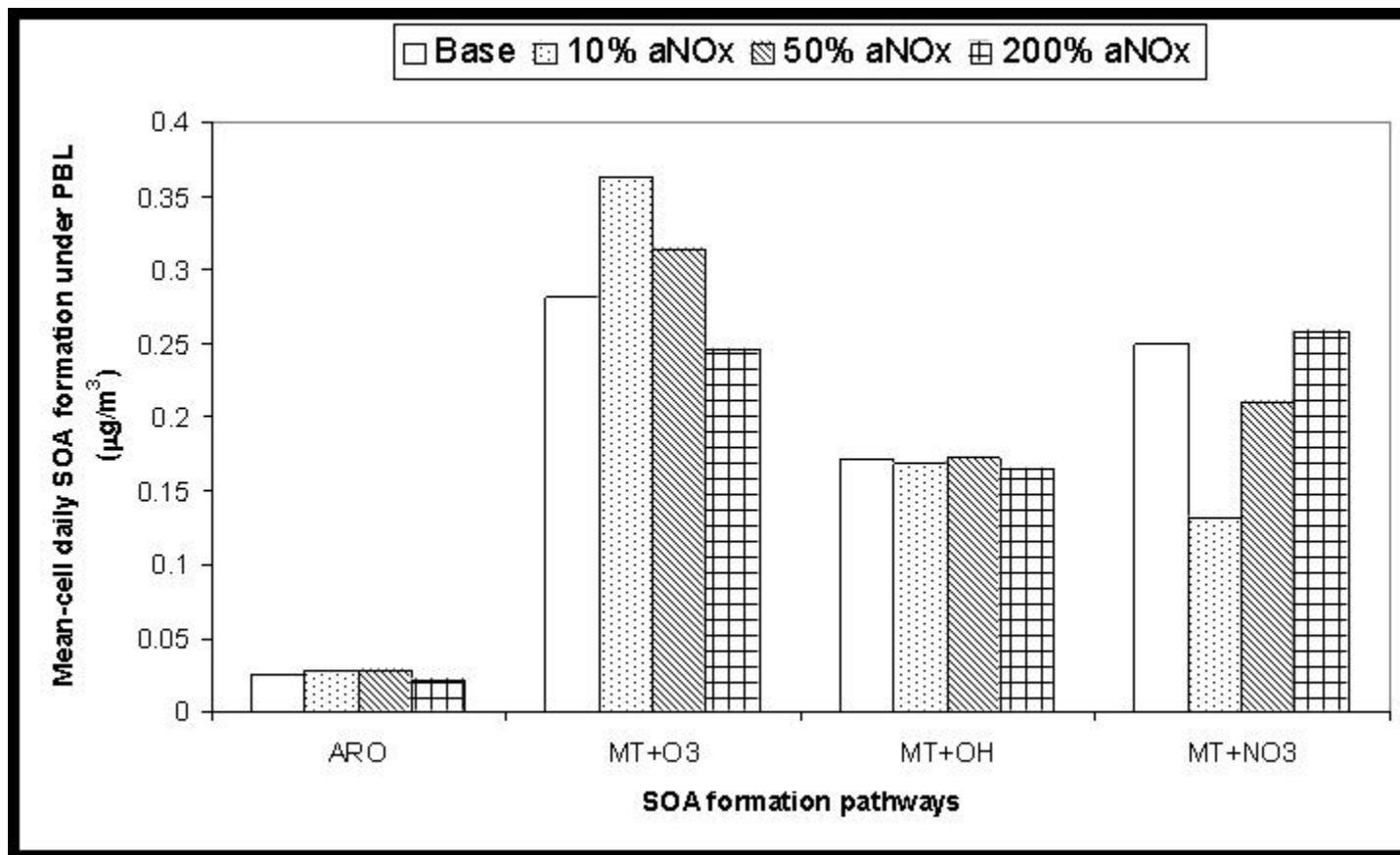


Figure 6.20. Mean-grid cell daily SOA formation rate in SOA-subdomain on Aug 30<sup>th</sup>, 2000. Results are shown for the base case and for the 10%, 50% and 200% anthropogenic NO<sub>x</sub> (aNO<sub>x</sub>) emissions reductions.

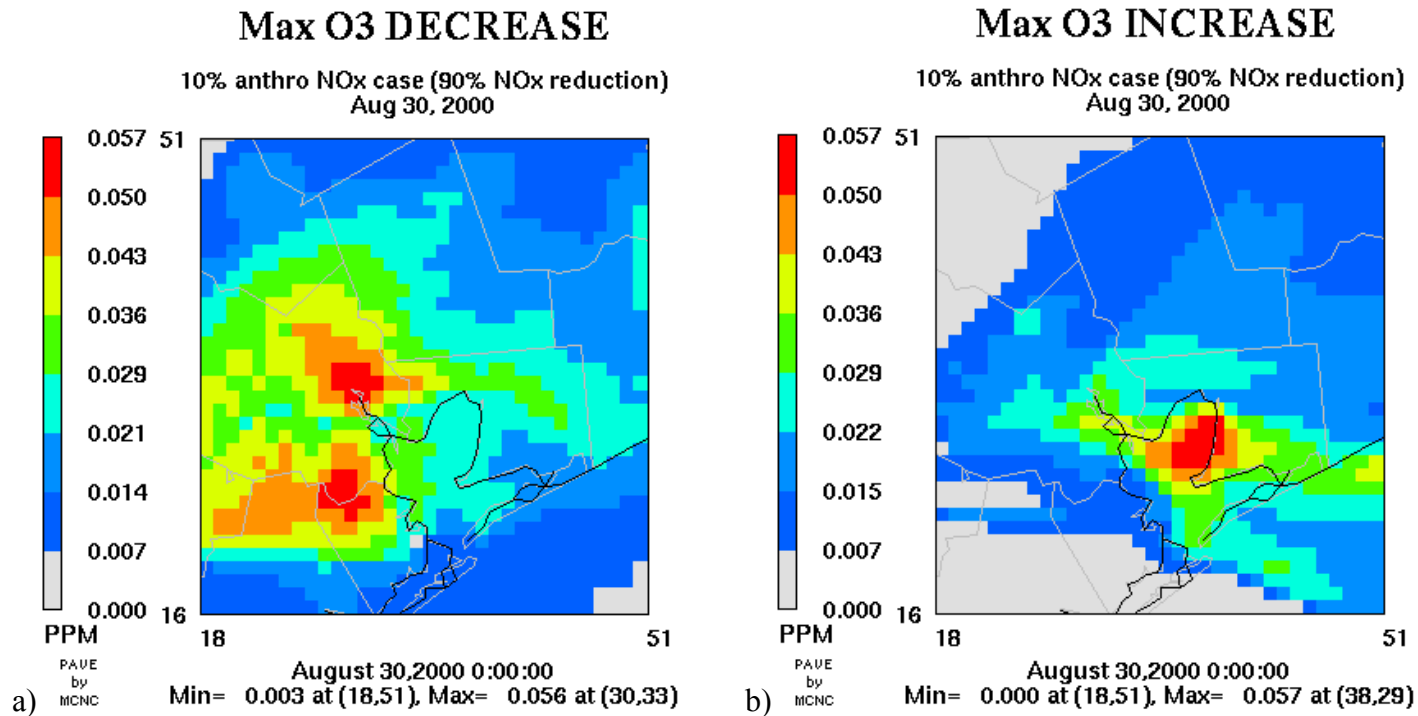


Figure 6.21. a) Maximum ozone decrease in each grid cell, and b) Maximum ozone increase in each cell (relative to base case) with 10% anthropogenic NO<sub>x</sub>, Aug 30, 2000.

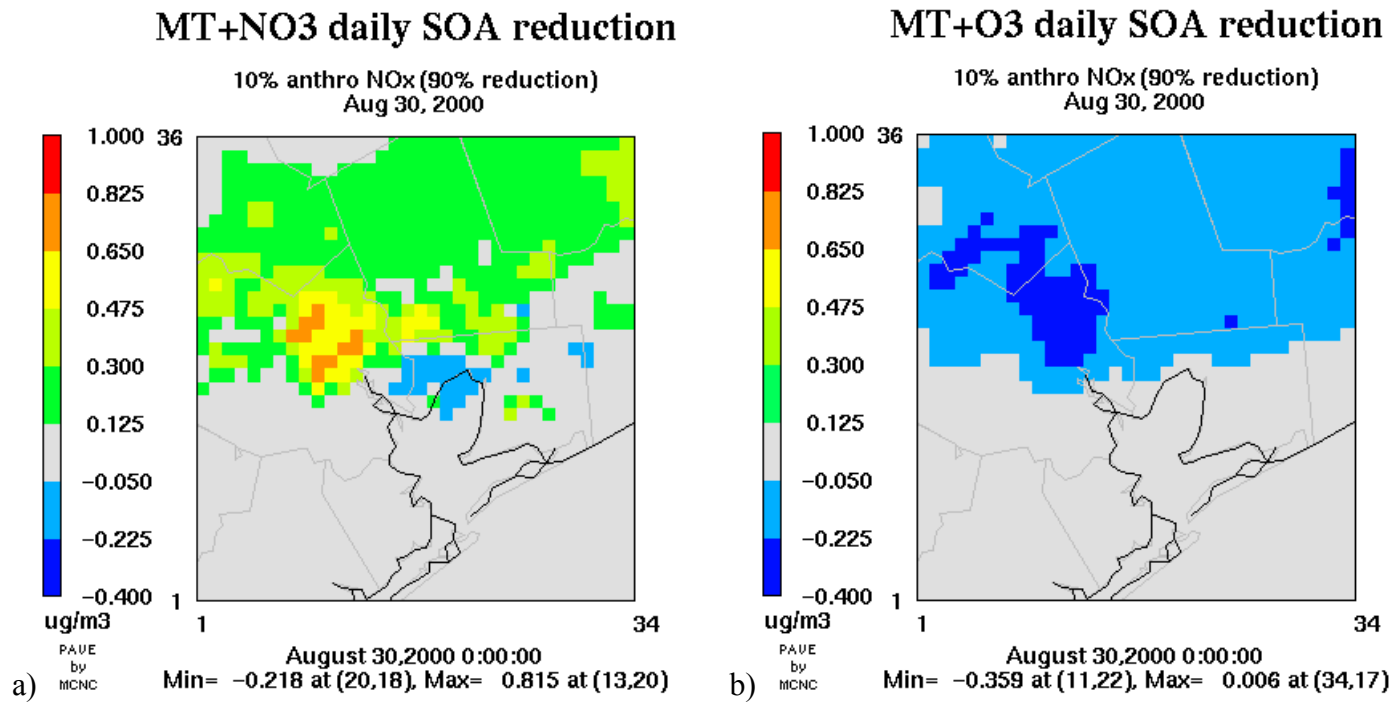


Figure 6.22. Reduction (relative to base case) in daily SOA formation with 10% anthropogenic NO<sub>x</sub> for a) monoterpene-NO<sub>3</sub> pathways and b) monoterpene-O<sub>3</sub> pathways. A negative 'reduction' means SOA formation increased relative to the base case.

Figures 6.22a and 6.22b show an interesting effect of NO<sub>x</sub> emissions reductions on SOA: monoterpene-O<sub>3</sub> reactions form more SOA while monoterpene-NO<sub>3</sub> reactions generally form less SOA when NO<sub>x</sub> emissions are reduced by 90%. Furthermore, SOA formation is mostly affected close to the urban and industrial areas, and not necessarily where biogenic emissions are high. The net effect of 90% NO<sub>x</sub> reductions on daily SOA formation from *all* reactions is shown in Figure 6.23.

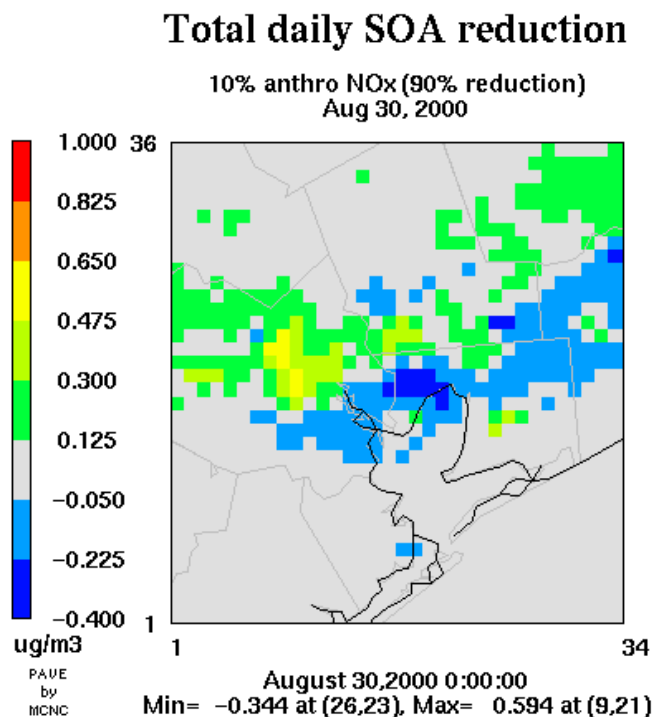


Figure 6.23. Reduction (relative to base case) in daily SOA formation with 10% anthropogenic NO<sub>x</sub> for all SOA formation reactions.

Figure 6.23 shows that substantial anthropogenic NO<sub>x</sub> emissions reductions lead to both SOA formation increases AND decreases in and near the

urban/industrial areas of Houston. The dual response of SOA formation is a result of opposite responses of monoterpene-NO<sub>3</sub> reactions and monoterpene-O<sub>3</sub> reactions. The effect of NO<sub>x</sub> reductions alone on SOA formation should be carefully considered because of the potential for SOA dis-benefits in areas where PM<sub>2.5</sub> concentrations are high.

The emissions of anthropogenic light-olefins were varied to 200%, 50% and 10% of the base case levels in the 11-county HGBPA non-attainment area. Figure 6.24 presents mean-cell daily SOA formation rates for the light-olefin sensitivity simulations. Variations in light-olefin emissions of 10%-200% of base case levels have a negligible effect on local SOA formation. Unlike NO<sub>x</sub> emission reductions, light-olefin emission reductions do not increase ground-level ozone concentrations. Figure 6.25a and 6.25b show the maximum decrease in ozone and the decrease in daily total SOA formation respectively in the 10% light-olefin case, relative to the base case. A 90% light-olefin emissions reduction results in minor ozone reductions (at most 11 ppb on this day), which results in minor SOA formation reductions (at most 0.01-0.02 μg/m<sup>3</sup>). Similar to NO<sub>x</sub> emissions reductions, however, the changes in SOA formation are occurring near the emissions reductions, which is where total PM<sub>2.5</sub> mass concentrations in Houston are highest.

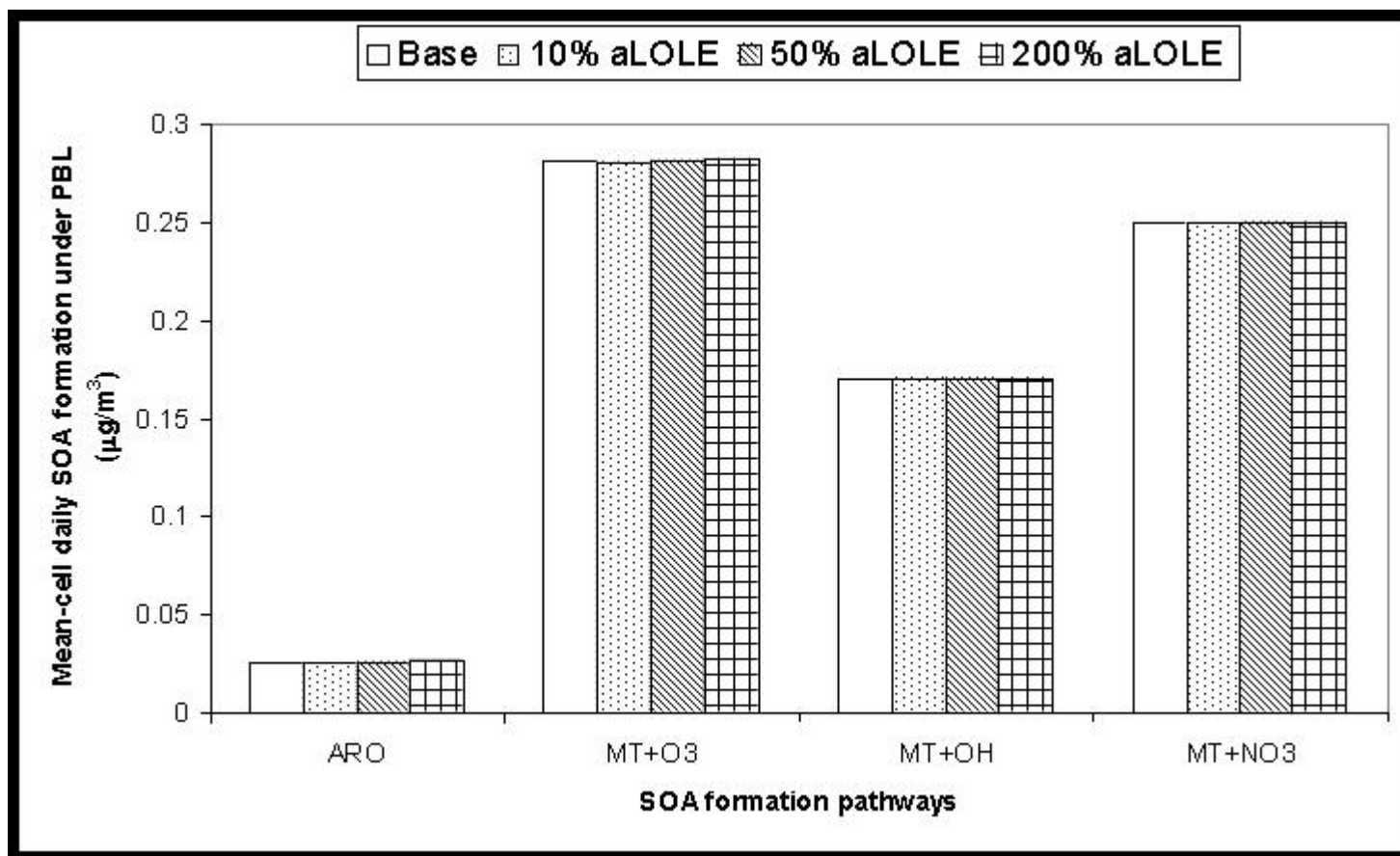


Figure 6.24. Mean-grid cell daily SOA formation rate in SOA-subdomain on Aug 30<sup>th</sup>, 2000. Results are shown for the base case and for the 10%, 50% and 200% anthropogenic light-olefin (aLOLE) emissions reductions.

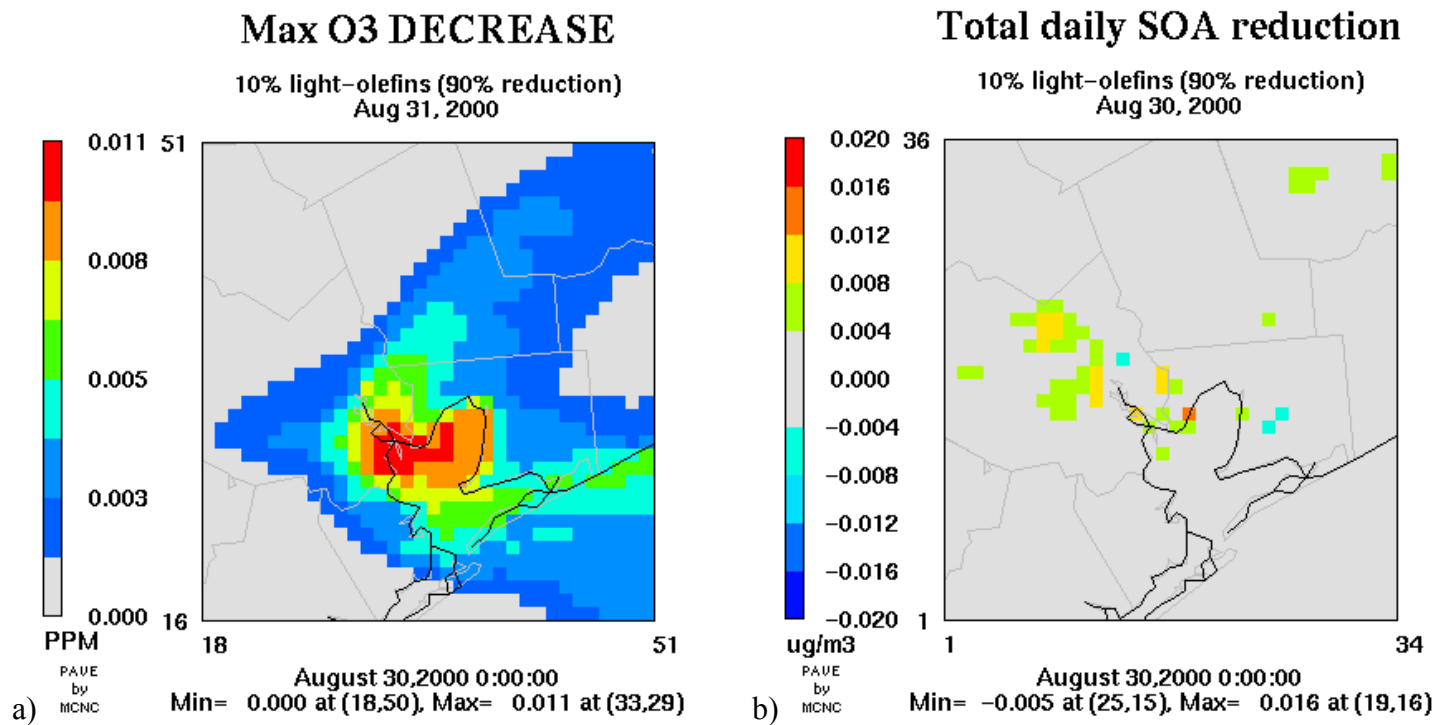


Figure 6.25. a) Maximum ozone decrease at any hour and b) reduction in daily total SOA formation rates for Aug 30, 2000, in the 10% anthropogenic light-olefin emissions case.

### 6.3 Chapter Summary.

Modeling results of SOA formation in Southeast Texas show that SOA is formed primarily via biogenic monoterpene oxidation. Aromatic SOA formation is, throughout the region, fairly low; however aromatics are the most significant SOA precursors in urban/industrial areas of Houston where mean PM<sub>2.5</sub> mass concentrations are highest. The highest rates of SOA formation are via  $\alpha$ -pinene reacting with ozone and  $\beta$ -pinene reacting with the nitrate radical and these pathways produce the most SOA per unit volume in the evening/night when mixing heights are lowest. Areas that have the highest SOA formation rates are located where biogenic emissions are highest: north of the urban Houston area.

Generally speaking, SOA is not a large fraction of total PM<sub>2.5</sub> mass in Southeast Texas. Organic carbon is for the most part primary; however, SOA formation rates can vary considerably from hour to hour, indicating that SOA concentrations might fluctuate throughout the day. This is consistent with estimated SOA concentrations in Los Angeles and Atlanta, where SOA is not a large fraction of 24-hour averaged OC concentrations, but can dominate OC for short time periods (Turpin and Huntzicker 1995; Lim and Turpin 2002).

A qualitative comparison of SOA formation rates to estimated SOA concentrations shows that modeled SOA formation accounts for much of the estimated SOA concentrations in Southeast Texas, although a true comparison will come if the model is improved to predict SOA concentrations and not just formation rates. The close agreement suggests that the compounds considered in this work, monoterpenes and aromatics, are important SOA precursors in the area.

This should be confirmed by considering other SOA precursors in the model when emissions and yield data become available for more compounds.

The results obtained here confirm or offer additional explanations for aerosol measurements in the area. Model results are not contrary to measured aerosol characteristics during this period, suggesting that current emissions inventories of SOA precursors are somewhat accurate, and that the simplified SOA model is sufficient to predict SOA. The model results show the importance of biogenic emissions in the region and the emissions inventories of biogenic SOA precursors should be critically evaluated. In addition, physico-chemical processes such as heterogeneous reactions have not been accounted for here. These processes may need to be included to improve the accuracy of any SOA model.

Sensitivity simulations suggest that SOA formation from individual aromatic reactions is sensitive to the assumption of first vs. later generation condensable reaction products. Inclusion of expanded aromatic mechanisms did not significantly change base case SOA formation rates, largely because aromatic-SOA formation is low compared to total SOA formation. The SOA grid model should be used to test the representation of monoterpene reactions to form SOA, since these are the predominant SOA precursors.

Sensitivity simulations also suggest that SOA formation is a fairly linear function of Mo concentrations and SOA precursor emissions. SOA formation via hydroxyl and ozone oxidation appears to be limited by precursor availability, confirming why the highest formation rates for these reactions occur in areas of

high emissions. In contrast  $\text{NO}_3$  oxidation of monoterpenes appears to be limited by oxidant availability, and the highest SOA formation rates via this pathway occur just at the edge of areas of biogenic emissions. Nitrate radical formed in urban and industrial areas reacts immediately with available monoterpenes just north of Houston. The sensitivity studies reinforce the importance of accurate existing aerosol mass concentrations and precursor emissions.

Finally, the SOA grid model was used to test the sensitivity of SOA formation to anthropogenic  $\text{NO}_x$  emissions and anthropogenic light-olefin emissions. Reducing  $\text{NO}_x$  emissions has a dual effect on daily SOA formation rates, both increasing them because of higher monoterpene- $\text{O}_3$  oxidation and decreasing them because of lower monoterpene- $\text{NO}_3$  oxidation. Furthermore, changes in SOA formation from reducing  $\text{NO}_x$  occur in and near urban Houston, where  $\text{PM}_{2.5}$  concentrations are high. The effect of  $\text{NO}_x$  reductions on urban SOA concentrations might be significant and should be carefully considered. Changes in base case light-olefin emissions have a negligible effect on SOA formation.

The following chapter summarizes the major accomplishments and conclusions of the research presented in this thesis.

## 7.0 Conclusions and Recommendations

There are three major accomplishments of this research: 1) Development of a conceptual model for  $PM_{2.5}$  for the urban and industrial areas of Southeast Texas, including estimates of secondary organic aerosol (SOA) concentrations, 2) Development of a photochemical grid model tool with both a flexible chemical mechanism and a module to predict SOA formation, and 3) Application of the SOA grid model tool to predict SOA formation in Southeast Texas, and test the sensitivity of SOA formation to various input parameters.

Fine particulate matter pollution ( $PM_{2.5}$ ) is a pollutant of emerging importance in the U.S. and the first step in controlling this pollutant is to understand, conceptually, what sources are contributing to its formation. The conceptual model developed in this research contributes greatly to the understanding of  $PM_{2.5}$  because it characterizes the pollutant in a large urban and industrial area of the country where little  $PM_{2.5}$  characterization data exist.

The conceptual model provided some important general findings. First, mean annual  $PM_{2.5}$  concentrations during the 2000-2001 period were not in violation of the U.S. NAAQS; however, two locations, both in the industrial area of Houston, experienced mean annual  $PM_{2.5}$  concentrations within  $2 \mu\text{g}/\text{m}^3$  of the standard. Mean monthly  $PM_{2.5}$  in Southeast Texas does not vary significantly throughout the year; however, maximum monthly  $PM_{2.5}$  tends to be slightly higher in fall and winter. Diurnal patterns of  $PM_{2.5}$  show a distinct morning maximum that is consistent across the region and in all seasons. Some sites show

a slight secondary maximum during the ozone season. This secondary maximum is particularly strong at rural receptor sites. The relative composition of  $PM_{2.5}$  is also very consistent throughout the region and from season to season. Ammonium sulfate and organic carbon are consistently the dominant mass components of  $PM_{2.5}$ . High  $PM_{2.5}$  mass concentrations can be measured simultaneously at all monitoring sites and independently at certain locations. In the former case, back trajectories indicate a clear predominance of large scale flow of air from the southeastern U.S. The trajectory analysis and the fact that  $PM_{2.5}$  characteristics are consistent throughout the region suggest that regional transport of  $PM_{2.5}$  may be important in Southeast Texas. There are, however, several examples in the datasets of site-to-site variability in composition, diurnal profiles and  $PM_{2.5}$  mass concentrations on a given day. These data indicate that local  $PM_{2.5}$  sources cannot be ignored.

An empirical model for secondary organic aerosol was developed by analysis of relative amounts of organic carbon (OC) and elemental carbon (EC) in  $PM_{2.5}$ . A model for primary OC was developed by eliminating all measurements with possible secondary OC or non-routine OC content, and by assuming that primary OC is, on average, a constant function of EC at a certain location. The analyses showed that, annually, primary OC is the largest fraction of OC in  $PM_{2.5}$  in Southeast Texas; however, secondary OC was as significant as primary OC during the ozone season throughout the region. These distinctions are important for addressing control strategies for  $PM_{2.5}$ , since OC comprises a large fraction of this pollutant.

A major limitation of most photochemical grid models is that the chemical mechanisms are hard-coded into the source code and cannot be easily modified. Modeling secondary organic aerosol formation requires accurate representation of reactions of individual precursors, and this is not possible with common chemical mechanisms used for modeling ozone. A valuable tool was developed in this research that allows a user to define a chemical mechanism of their choice and include this mechanism in CAMx, which is an elaborate photochemical grid model. The chemical mechanism is based on the state-of-the-science SAPRC99 mechanism. This new tool can be used to examine the importance of chemical reactions to ozone and PM<sub>2.5</sub> chemistry in ways that are limited by fixed chemical mechanisms, for example, modeling certain reactants explicitly rather than in a lumped fashion. A unique chemical mechanism was created in this research treating monoterpene and aromatic model species in ways suitable for predicting SOA formation.

The second tool developed in this research was an independent module, added to CAMx, which allows prediction of SOA formation rates from individual reaction pathways of the user's choice. The unique feature of this tool is that it is coupled with the flexible mechanism CAMx, which allows the user to consider different reaction mechanisms of SOA precursors. Furthermore, the gas/particle partitioning framework used to estimate SOA formation uses ambient measurements of particulate OC, rather than highly uncertain emissions inventories of primary OC. The SOA grid model was applied to Southeast Texas

to predict SOA formation from monoterpenes and aromatics, which are traditionally the two predominant precursors in urban areas.

The base case modeling results showed that biogenic monoterpenes dominated SOA formation in Southeast Texas compared to aromatics, predominantly  $\alpha$ -pinene reacting with ozone and  $\beta$ -pinene reacting with the nitrate radical. SOA formation from OH radical oxidation was low compared to formation from  $O_3$  and  $NO_3$  oxidation. Furthermore, SOA formation rates varied substantially throughout the day and were highest in the evening and night-time when mixing heights were low but when oxidant concentrations from photochemical activity were still high.

Although the model considers only SOA formation rates, the estimated contribution of local SOA formation accounted for much of the SOA concentrations predicted by the conceptual model; in general, local SOA formation does not contribute substantially to  $PM_{2.5}$  concentrations. Furthermore, a number of other PM measurements support the spatial distribution and biogenic nature of SOA formation predicted with the model. It is very encouraging that this first attempt to predict SOA is so consistent with ambient data. The base case modeling results contribute greatly to the understanding of SOA formation in general and can be used to guide further research on SOA. It is recommended that emissions inventories of biogenic monoterpenes be critically evaluated, since they are the predominant SOA precursor. It is also recommended that the tool be used to test the significance of other SOA precursors if data for these become available.

Finally, as the understanding of the physico-chemical processes of SOA formation advance, the model for SOA formation should be updated accordingly.

The SOA grid model tool was used to test the sensitivity of SOA formation to various parameters. Most importantly, it was found that SOA formation is directly proportional to precursor emissions, except for SOA formation via nitrate radical oxidation. The latter reactions appear to be limited by the availability of the oxidant. Since biogenic compounds are the predominant SOA precursors, an important reduction strategy will be to reduce the important oxidant concentrations: ozone and nitrate radical. Substantial reductions of anthropogenic NO<sub>x</sub> emissions resulted in both SOA benefits and dis-benefits, and both benefits and dis-benefits occurred in the urban/industrial areas of Houston where PM<sub>2.5</sub> concentrations are highest. The effect of NO<sub>x</sub> emission reductions on PM<sub>2.5</sub> concentrations should be carefully evaluated, and the SOA grid model tool developed here is ideal for this purpose.

## **Appendix A: Emissions Inventory Processing for the TXAQS modeling episode.**

This Appendix summarizes the data sources used to process the emissions for the TXAQS modeling episode. Details on the TXAQS modeling episode are presented in Chapter 5. Input files and run scripts for the emissions processing have been organized in an archive file (.tar) that can be extracted on a UNIX system. These files can be used to re-process the emissions or process emissions with a different chemical mechanism for this episode. The Appendix is meant to help someone that is familiar with emissions processing to re-create emissions for the TXAQS episode. The methods and software used to process the emissions are presented in Chapter 5.

The four major emissions categories are area sources (including off-road mobile source), on-road mobile sources, point sources and biogenic sources. Tables A1 through A4 summarize the data that were used to process each category respectively. All four categories have low-level (ground-level) emissions; point sources also have both elevated emissions and low-level emissions. The emissions for area, on-road mobile and low-level point sources were processed for the 4km domain at 2km resolution, and for the 36km domain at 12km resolution. After emissions processing, the 2km emissions were aggregated to 4km, the 12km emissions were aggregated to 36km, and the 12km emissions were windowed to the size of the 12km domain. The biogenic emissions were processed for the 4km domain at 4km resolution, for the 12km domain at 12km resolution and for the 36km domain at 36km resolution. The size

of the 4km domain for the biogenic emissions was slightly larger than the 4km modeling domain (owing to slightly different dimensions to the GLOBEIS input files); therefore the biogenic emissions were windowed to the appropriate size after processing.

For each anthropogenic emissions category, Tables A1 through A3 list the parts of the inventory that were processed separately, the data files used in the processing, and the sources of those files. The data files are:

- data: AFS, AMS or link emissions file.
- splitf: splitfactor file giving speciation of total VOC to model species.
- c-xref: cross-reference file for assigning the appropriate splitfactor to each emissions source.
- temporal: temporal profiles for non-hourly emissions.
- t-xref: cross-reference file for assigning the appropriate temporal profile to each emissions source.
- spatial: spatial surrogate file for allocating county-level emissions to each model grid cell.
- s-xref: cross-reference file for assigning the appropriate spatial surrogate to each emissions source.

Finally, Table A4 lists the names and sources of the landuse, temperature and photo-active radiation (PAR) input files that were used to process the biogenic emissions.

Table A1: Area & off-road (non-road) sources

grid	type	coverage	input	filename	source
4km	area	Texas	data	ams.TX_00.area_base2	1
			splitfac	splitf.\$mech.txt	2
			c-xref	scc-voc.prf.voc.xref.08Jan02.area.strip	3
			temporal	tmprof.hgmcrcr	1
			t-xref	tmpxref.hgmcrcr.area.jdm	1
			spatial	HG_2km_sur.grdem	1
			s-xref	sti_sur_xref.area.strip	1
4km	off-road	Texas	data	ams.TX_00.NR_base2	1
			splitfac	splitf.\$mech.txt	2
			c-xref	scc-voc.prf.voc.xref.08Jan02.area.strip	3
			temporal	tmprof.hgmcrcr	1
			t-xref	tmpxref.hgmcrcr.areaNR.jdm_strip	1
			spatial	HG_2km_sur.grdem	1
			s-xref	sti_sur_xref.NR.strip	1
4km	off-shore	Texas & Louisiana coast	data	ams.os1990_revised_all	3
			splitfac	splitf.\$mech.txt	2
			c-xref	scc-voc.prf.voc.xref.08Jan02.area.strip	3
			temporal	tmprof.hgmcrcr	1
			t-xref	tmpxref.hgmcrcr.area_os.jdm	1
			spatial	os_2km_sur.grdem	3
			s-xref	os_sur.xref	3
4km	area & off-road	Louisiana	data	ams.LA_in_grid3.net99.3pol	4
			splitfac	splitf.\$mech.txt	2
			c-xref	scc-voc.prf.voc.xref.08Jan02.area.strip	3
			temporal	tmprof.hgmcrcr	1
			t-xref	tmpxref.hgmcrcr.LA_all_area.jdm	1
			spatial	HG_2km_sur.grdem	1
			s-xref	sti_sur_xref.LA_all_area.strip	1
36km & 12km	area & off-road	all states	data	ams.area.national.net99.srt	4
			splitfac	splitf.\$mech.txt	2
			c-xref	chmprf.xref.voc.v0598.98May05.x_tra.a1	4
			temporal	tmprof.regional.net99	4
			t-xref	tmpxref.regional.net99_wsub.m1	5
			spatial	txreg.grdsrg.12km.surg.subrgn.dat.a1	4
			s-xref	sscsrgs.xref.ar+nr.net99_wsub.m1	5
36km & 12km	off-shore	Texas & Louisiana coast	data	ams.os1990_revised_all	3
			splitfac	splitf.\$mech.txt	2
			c-xref	scc-voc.prf.voc.xref.08Jan02.area.strip	3
			temporal	tmprof.hgmcrcr	1
			t-xref	tmpxref.hgmcrcr.area_os.jdm	1
			spatial	os_12km_sur.grdem	3
			s-xref	os_sur.xref	3

1: From TCEQ. Originally in archive: AreaEI\_2000AUG\_20021209.tar which was downloaded from (<ftp://tnrcc.state.tx.us/pub/OEPAA/TAD/Modeling/HGAQSE/Modeling/EI>).

2: Splitfactors that are specific to the chemical mechanism of choice. See Chapter 5 for how these were created.

3: From TCEQ. Directly obtained from a staff member via email or public ftp site.

4: From the 'Texas near non-attainment area' (txna) modeling projects. Residing on CEER systems on disk: /aacog1 (Spring 2003) and originally from ENVIRON under contract to the University of Texas at Austin.

5: Cross-reference files with .m1 suffix were from the txna modeling project (see note 4 above) and were updated to include missing SCC codes that were in the AMS files. These updates were for completeness only and should not have a significant effect on total emissions or model predicted concentrations.

Table A2: On-road (mobile) sources

grid	type	coverage	input	filename	source
4km	on-road	TX & LA excluding 8-county HG non-attainment area	data	ams.onroad.national.net99.srt	4
			splitfac	splitf.\$mech.txt	2
			c-xref	chmprf.xref.voc.v0598.98May05.x_tra.a1	4
			temporal	tmpprof.regional.net99	4
			t-xref	tmpxref.onroad.regional.net99_wsub.m1	5
			spatial	HG_2km_sur.grdem	1
			s-xref	sscsrgs.xref.onroad.net99_wsub	4
4km	on-road	8-county HG non-attainment area	data	mobile6.2000.HGA_8County.\$mdd.lbase_in	3
			splitfac	splitf.\$mech.hg_mobile.txt	2
			c-xref	chmprf.xref.voc.links.UT	6
			temporal		
			t-xref		
			spatial	grdem.surrogate.hg_2km.matt	6
s-xref	m6.9veh.4pol.3road.xref	6			
36km & 12km	on-road	all states	data	ams.onroad.national.net99.srt	4
			splitfac	splitf.\$mech.txt	2
			c-xref	chmprf.xref.voc.v0598.98May05.x_tra.a1	4
			temporal	tmpprof.regional.net99	4
			t-xref	tmpxref.onroad.regional.net99_wsub.m1	5
			spatial	txreg.grdsrg.12km.surg.subrgn.dat.a1	4
			s-xref	sscsrgs.xref.onroad.net99_wsub	4

1: From TCEQ. Originally in archive: AreaEI\_2000AUG\_20021209.tar which was downloaded from ([ftp.tnrc.state.tx.us/pub/OEPAA/TAD/Modeling/HGAQSE/Modeling/EI](http://ftp.tnrc.state.tx.us/pub/OEPAA/TAD/Modeling/HGAQSE/Modeling/EI)).

2: Splitfactors that are specific to the chemical mechanism of choice. See Chapter 5 for how these were created.

3: From TCEQ. Directly obtained from a staff member via email or file transfer ftp site.

4: From the 'Texas near non-attainment area' (txnna) modeling projects. Residing on CEER systems on disk: /aacog1 (Spring 2003) and originally from ENVIRON under contract to the University of Texas at Austin.

5: Cross-reference files with .m1 suffix were from the txnna modeling project (see note 4 above) and were updated to include missing SCC codes that were in the AMS files. These updates were for completeness only and should not have a significant effect on total emissions or model predicted concentrations.

6: These link processing files are slightly modified files that were originally in the archive: mobile6.2000.hga\_8county.eps2x\_input\_files.tar which was downloaded from ([ftp.tnrc.state.tx.us/pub/OEPAA/TAD/Modeling/HGAQSE/Modeling/EI](http://ftp.tnrc.state.tx.us/pub/OEPAA/TAD/Modeling/HGAQSE/Modeling/EI)). chmprf.xref.voc.links.UT is the same as chmprf.xref.voc.MV\_hstn\_upd.m6 except the names of the speciation profiles are slightly different. grdem.surrogate.hg\_2km.matt is based on mobile.2000.dummy.surrogate.hg\_2km with a slightly smaller domain definition. TCEQ's original 4km domain was slightly bigger and these files were not updated to reflect the current 4km domain size.

Table A3: Point sources

grid(s)	type	coverage	input	filename	
36km 12km 4km	E.G.U.	Texas	data splitfac c-xref temporal t-xref	afs.EGU2000withSpecial2000.v4a splitf.\$mech.txt xref.voc.hg2000.pt.all tmpri_prof.hgmc_r_pt_afs_v12a.o3_day tmpri_xref.pt_collapsed_afs_v12a	1 2 3 3 3
36km 12km 4km	N E.G.U.	Texas	data splitfac c-xref temporal t-xref	afs.NEGU2000withSpecial2000.v4a splitf.\$mech.txt xref.voc.hg2000.pt.all tmpri_prof.hgmc_r_pt_afs_v12a.o3_day tmpri_xref.pt_collapsed_afs_v12a	1 2 3 3 3
36km 12km 4km	Upsets.	Texas	data splitfac c-xref temporal t-xref	afs.non81.upsets splitf.\$mech.txt xref.voc.hg2000.pt.all tmpri_prof.hgmc_r_pt_afs_v12a.o3_day tmpri_xref.pt_collapsed_afs_v12a	1 2 3 3 3
36km 12km 4km	E.G.U.	Louisiana	data splitfac c-xref temporal t-xref	hourly_LAegu_000822-000901.afs_v4_lcp.3pols splitf.\$mech.txt xref.voc.hg2000.pt.all tmpri_prof.net99.po tmpri_xref.LA_egu_0999.po_wsub	1 2 3 4 4
36km 12km 4km	N E.G.U.	Louisiana	data splitfac c-xref temporal t-xref	afs.la_negu.000101-010101.v4_lcp.3pols splitf.\$mech.txt xref.voc.hg2000.pt.all tmpri_prof.net99.po tmpri_xref.LADEQ_negu.po_wsub	1 2 3 4 4
36km 12km	E.G.U.	All states excluding Texas & Louisiana	data splitfac c-xref temporal t-xref	hourly_RegionEGU_000822-000901.afs_lcp.3pols splitf.\$mech.txt xref.voc.hg2000.pt.all tmpri_prof.net99.po tmpri_xref.net99.po_wsub	1 2 3 4 4
36km 12km	N E.G.U.	All states excluding Texas & Louisiana	data splitfac c-xref temporal t-xref	afs.points.regional.net99.noTXLA_negu.000822-000901_lcp.3pols splitf.\$mech.txt xref.voc.hg2000.pt.all tmpri_prof.net99.po tmpri_xref.net99.po_wsub	1 2 3 4 4
36km 12km 4km	Offshore sources (see note 6 below)	Gulf coast	data splitfac c-xref temporal t-xref	afs.offshore.93_2_lcp splitf.\$mech.txt xref.voc.hg2000.pt.all tmpri_prof.os.o3_day tmpri_xref.os.new_egu.a0	1 2 3 3 3
36km 12km	E.G.U. & N E.G.U.	Mexico	data splitfac c-xref temporal t-xref	afs.bravo.Mexico.1999_v1.lcp.3pols splitf.\$mech.txt xref.voc.hg2000.pt.all tmpri_prof.pt_mex tmpri_xref.pt_mex	1 2 3 3 3
Elevat ed only	Elevated ship emissions	Gulf coast	data splitfac c-xref temporal t-xref	afs.lcp_ships.base97 splitf.\$mech.txt scc-voc.prf.voc.xref.08Jan02.area.strip tmpri_prof.hgmc_r tmpri_xref.hgmc_r.areaNR_jdm_strip	5 2 3 5 5

1: From TCEQ. Originally in archive: PointEI 2000AUG\_20030108.tar which was downloaded from (<ftp://tnccc.state.tx.us/pub/OEPAA/TAD/Modeling/HGAOSE/Modeling/EI>).

2: Splitfactors that are specific to the chemical mechanism of choice. See Chapter 5 for how these were created.

3: From TCEQ. Directly obtained from a staff member via email or file transfer ftp site. These files were originally in an archive called EPSbase4a.tar.

4: From the 'Texas near non-attainment area' (txnna) modeling projects. Residing on CEER systems on disk: /aacog1 (Spring 2003) and originally from ENVIRON under contract to the University of Texas at Austin.

- 5: The elevated ships, although point sources, were included with the area source emissions, so these files came from TCEQ, originally in archive: AreaEI\_2000AUG\_20021209.tar which was downloaded from (<ftp.tnccc.state.tx.us/pub/OEPA/TAD/Modeling/HGAQSE/Modeling/EI>).
- 6: The offshore sources are also controlled from 1993 to 2000 using the CNTLEM processor and data included in the archive listed in note 3.

Table A4: Biogenic sources

grid	type	input	filename	source
4km*	biogenic	landuse	lus_4km_beld+texmex_hgbpa.txt	1
		temp	hgbpa_YYMMDD_4km_v1_temp.txt	1
		PAR	spar_YYMMDD_hgbpa4km.txt	1
12km	biogenic	landuse	lus_12km_beld+texmex_arklatex.txt	1
		temp	etx_YYMMDD_12km_v1_temp.txt	1
		PAR	spar.YYMMDD.LCP12km.dat	1
36km	biogenic	landuse	lus_36km_beld+texmex_region.txt	1
		temp	reg_YYMMDD_36km_v1_temp.txt	1
		PAR	MDDre36.dat	1

1: From TCEQ. Originally in archive: BioEI\_2000AUG\_20020327.tar which was downloaded from (<ftp.tnrc.state.tx.us/pub/OEPAA/TAD/Modeling/HGAQSE/Modeling/EI>).

\*: The 4km grid dimensions in this data are slightly larger than the 4km modeling grid. The 4km biogenic emissions were windowed to the correct size prior to merging them with the anthropogenic emissions.

## **Appendix B: Integration of a flexible SAPRC99-generated chemical mechanism into CAMx 3.10.**

(This work was jointly performed with Dr. Yosuke Kimura at the Center for Energy and Environmental Resources)

This Appendix summarizes the code development to include a flexible version of the Statewide Air Pollution Research Center's latest chemical mechanism (SAPRC99) into the Comprehensive Air Quality Model with Extensions version 3.10 (CAMx31). Both SAPRC99 and CAMx31 software are available for free at ([pah.cert.ucr.edu/~carter/SAPRC99.htm](http://pah.cert.ucr.edu/~carter/SAPRC99.htm)) and ([www.camx.com](http://www.camx.com)) respectively. Appropriate references are (Carter 1990, 1995, 2000) for SAPRC99, and (ENVIRON International Corporation 2002) for CAMx31.

The first section of this Appendix presents an overview of the concepts being covered. The second section explains how the chemical mechanism is solved in CAMx31. The third section outlines how the SAPRC99 and CAMx31 software were modified to allow coupling of the source code. The fourth and final section serves as a user's guide for implementing a SAPRC99-generated mechanism into CAMx31.

## Overview

The numerical simulation of atmospheric chemistry involves three steps. The first is to define the chemical mechanism, which is a mathematical representation of the chemical and photo-chemical reactions. The second step is to translate the mechanism into a programming language so that it can be solved numerically. This translation can be done either individually for each mechanism or automatically by software that is specifically written for this purpose (mechanism generation software). The third step is to implement a numerical solution scheme, which solves the chemical mechanism for various initial and boundary conditions.

A limitation of most available grid models, including CAMx31, is that the chemical mechanism is 'hard-coded' into the source code. In other words, the mechanism has already been translated to programming language and cannot be changed without extensive changes to the source code. The released version of CAMx31 includes five hard-coded mechanisms to choose from and is not designed to allow the user to readily add new mechanisms. The objective of the software developed for this study is to allow users to implement and solve arbitrary chemical mechanisms in CAMx31. SAPRC99 software was used as the tool to implement the user specified, arbitrary mechanism. Both CAMx31 and SAPRC99 software were modified to accomplish this objective; however, the general approach taken in this research was to minimize changes to CAMx31 to prevent compromising the accuracy of the grid model. As a result, the majority of modifications were additions to the SAPRC99 software.

It is important to distinguish different uses of “SAPRC99” in this Appendix, and some definitions are provided in Table B1 as a guide.

Table B1. Terminology used in the Appendix

<b>Term</b>	<b>Definition</b>
SAPRC99 Software	The original SAPRC99 software system, which is used to develop an arbitrary chemical mechanism. This software generates new source code that solves the mechanism developed by the user. This software was modified to generate source code that conforms to CAMx31.
SAPRC99 generated code	The FORTRAN77 code that solves the chemical mechanism developed by the user. This code is generated by the software described above.
Original SAPRC99 Mechanism (s99 mechanism)	The original, standard, fixed-parameter SAPRC99 mechanism, developed by the makers of SAPRC99 software. Details on the fixed parameter version of SAPRC99 mechanism can be found in the SAPRC99 documentation (Carter 2000).
Modified SAPRC99 Mechanism	A new chemical mechanism developed in this research and designed to model SOA. This new mechanism is a variation of the s99 mechanism described above.

### **The Chemical Mechanism and Its Solver**

The chemical mechanism is a term used to describe the set of chemical and photo-chemical reactions in the model and their mathematical representation. The chemical mechanism is designed to balance accurate prediction of the gas-phase chemistry/photochemistry and computational efficiency. Generally speaking, atmospheric reactions involve radicals, inorganic species and organic compounds (both emitted and intermediate reaction products). Radicals and

inorganic compounds (e.g. NO<sub>x</sub>) are typically treated explicitly in most chemical mechanisms, because the reactions in which they participate are critical for accurately modeling the gas-phase chemistry. Many organic compounds, however, can be grouped (or lumped) into categories that have similar reaction characteristics. This reduces the number of model species and makes the mechanism more computationally efficient. The major difference between different chemical mechanisms is the method used for lumping organic compounds.

There are a small number of chemical mechanisms that are widely used for air quality modeling. The most common, Carbon Bond IV (CB4) (Gery et al. 1989), breaks organic compounds down into a set of ten structural components, and has a relatively small number of model species (20 radical species, 25 non-radical species). The mechanism is very computationally efficient; however, lumping is based on structure, and all molecular-level information is lost. Since SOA formation is highly dependent on individual molecule or structure (especially, but not limited to, molecular weight), the standard CB4 is not a suitable mechanism for modeling SOA.

The original SAPRC99 mechanism (s99) is considered to be chemically up to date and is highly advantageous for SOA modeling because lumping is based on molecules. Furthermore, SAPRC99 is distributed as a software package that allows the user to control the lumping of organic compounds, i.e. to create variations of the original s99 mechanism. One objective of this research is to treat important SOA precursors explicitly, i.e. un lumped. The SAPRC99 software

generates source code based on the reactions, model species and lumping schemes that are chosen for the mechanism. Once compiled, the generated code solves the concentration of species over time. The original s99 mechanism is more computationally demanding than CB4, which is one reason the mechanism is not widely used for regulatory air quality modeling; however, SAPRC99 is a more appropriate system to use to develop mechanisms for this research, because lumping is based on individual molecules. The SAPRC99 software is used to develop these mechanisms.

There are two important points that deserve additional discussion. First, the development of a chemical mechanism for air quality models is not trivial and extreme caution should be exercised in reversing mechanisms. Most mechanisms have been under continual development for many years and model reactions have been extensively tested against experimental data. The reactions of inorganic compounds, radicals, intermediates, and explicit reactive organic compounds (such as ethene and isoprene) comprise the 'base' mechanism in s99. Reactions of lumped organic groups then comprise the remainder of the mechanism. Modifications to the base mechanism reactions or model species will likely have a significant effect on predicted model species concentrations, and caution should be taken when making such modifications. Theoretically, changes can be made to any and all reactions in the mechanism; however, in this research, changes are made only to implement various lumping schemes for organic compounds. This has great importance to modeling SOA, since SOA formation characteristics vary from compound to compound.

The second point is that CAMx31 has a number of features that are directly affected by the chemical mechanism source code, namely probing tools, and a plume module that solves reactions in concentrated NO<sub>x</sub> plumes (Plume-In-Grid). Probing tools are used to analyze the processes that form ozone to, for example, determine what sources are contributing to this formation. Any new mechanism that is implemented in the modified CAMx31 will not be able to use these tools. The modifications required to enable new mechanisms to use these tools went beyond the scope of this research. The Plume-In-Grid module solves concentrations from a subset of the inorganic reactions in the base mechanism. These reactions are already ‘built-in’ to CAMx31 since a standard version of SAPRC99 mechanism is ‘built-in’ to CAMx31. The PiG feature will work for any new mechanism, if and only if these base mechanism reactions are included.

The numerical solution of the chemical mechanism (i.e. the solver) determines, for each grid cell, the concentrations of all models species at the end of a time step given concentrations at the beginning of the time step. CAMx31 offers two numerical schemes to solve each of its five built-in mechanisms. The first scheme requires the mechanism to be implemented with software called Chemical Mechanism Compiler (CMC), which is proprietary to the makers of CAMx. The CMC is not available for scrutiny, and so this numerical scheme is not considered. The second scheme is based on the Implicit-Explicit Hybrid method (IEH) described by Sun et al. (1994). The IEH scheme is used for all modified mechanisms in this research and is discussed below.

Atmospheric chemical reactions can be represented by a system of non-linear, stiff, ordinary differential equations (ODEs). Each ODE represents the time rate of change ( $Y$ ) of a model species ( $i$ ):

$$Y_i = \frac{dC_i}{dt} = \left[ \frac{dC_i}{dt} \right]_{gain} - \left[ \frac{dC_i}{dt} \right]_{loss} = f(C_1, C_2, C_3, \dots, C_i, \dots, C_n) \quad [\text{B.1}]$$

A stable solution to this system of ODE's, given initial conditions, can be found using a 'Gear' solution after Gear (1971). The IEH scheme reduces the number of ODEs that must be solved by solving some model species explicitly and independent of other model species. The version of IEH in CAMx31 splits model species into three groups: steady-state species, fast-reacting species and slow-reacting species.

Steady state species are fast reacting radicals, whose concentrations are approximated by a pseudo-steady state assumption (in terms of gain and loss):

$$C_{steady-state} = \left( \frac{\left[ \frac{dC}{dt} \right]_{gain}}{\left[ \frac{dC}{dt} \right]_{loss} * \frac{1}{C_{t=0}}} \right) \quad [\text{B.2}]$$

Fast species are those that must be solved with a Gear solution because they are highly inter-dependent upon other fast species concentrations. The time rate of change of each species,  $Y_i$ , forms a set of non-linear ODEs. The numerical Gear solver used in CAMx31 to solve the system is the Livermore Solver for

Ordinary Differential Equations (LSODE) (Hindmarsh 1983). The stiff system of ODEs is solved using, in addition to the rate of change vector  $Y$ , the Jacobian matrix  $J$ , whose elements are the partial derivatives of each differential equation with respect to each dependent variable:

$$J = \begin{bmatrix} \frac{\partial Y_1}{\partial C_1} & \cdots & \cdots & \cdots & \frac{\partial Y_n}{\partial C_1} \\ \vdots & \cdot & & & \vdots \\ \vdots & & \cdot & & \vdots \\ \vdots & & & \cdot & \vdots \\ \frac{\partial Y_1}{\partial C_n} & \cdots & \cdots & \cdots & \frac{\partial Y_n}{\partial C_n} \end{bmatrix}$$

Each element in  $J$  is a function of reaction throughputs and rate constants that can be calculated at beginning of each time step. Although LSODE can approximate  $J$  numerically, it is recommended that an external routine be provided that calculates the elements of the matrix.

Finally, slow species are assumed to react slowly enough during the time step that their final concentrations are found by a simple, first-order explicit approximation:

$$C_{t=\Delta t} = \frac{dC}{dt} * \Delta t + C_{t=0} \quad [\text{B.3}]$$

(Note this is different from the IEH method described by Sun et al., which uses an Adams-Bashford second order solution for the ‘slow’ species with intermediate calls to the Gear solver. CAMx31 uses a first order approximation to solve the slow species, and this is done only once after the LSODE call.)

The order of the solution of species is important: an initial approximation of steady-state species is obtained first; fast species are solved next (with continuous updates to steady-state species); slow species are solved last.

The most computationally demanding step is the implicit solution of fast species, and so the number of fast species is typically minimized to a point of acceptable accuracy (when compared to treating all species as fast species). The choice of steady-state vs. fast vs. slow species must be made prior to developing the mechanism source code. In the s99 mechanism built into CAMx31, most fast species are those that participate in the base mechanism reactions, whereas slow species are those lumped organics and other slow reacting inorganics and radicals. The modified SAPRC99 mechanisms used in this research have added/replaced slow species (lumped organics); therefore, the number of steady-state and fast species does not differ from the standard built-in s99 mechanism in CAMx31. As a result, the current IEH scheme is expected to be stable for any modified mechanism. The solution scheme may require modification if significant changes are made to the SAPRC99 base mechanism reactions.

### **Source code modifications**

The general approach for source code modifications was to minimize changes to the grid model code. In other words, the SAPRC99 software was modified whenever possible to generate codes that conform to CAMx31. Figure B.1 shows a diagram of how the chemical mechanism is solved in CAMx31 using the IEH solver. The routines ‘ierxn’, ‘ierate’, ‘iejac’, and ‘ieslow’ are the four

main, mechanism-specific routines that are used in solving concentrations of model species. LSODE solves the set of ODE's for fast species. The SAPRC software generates routines similar to 'ierxn', 'ierate', 'iejac', and 'ieslow' and these are imported to CAMx31. Figure B.2 shows a diagram of how the chemical mechanism is solved in the modified CAMx using the IEH solver and SAPRC generated routines. As shown in the Figure, 'iehsolv' still calls 'ierxn', 'ierate', 'iejac', and 'ieslow' but they are now 'wrapper' routines that simply call the SAPRC generated code.

Several source code modifications were required to integrate the SAPRC generated code into CAMx31. The next two sub-sections detail the changes and additions to the SAPRC99 and CAMx31 software. The sections are written to allow someone who is familiar with the source code of both models to understand how the integration was accomplished. As pointed out in the Overview section of this Appendix, it is important to distinguish SAPRC99 source code from SAPRC99-generated source code. SAPRC99 source code refers to the downloaded FORTRAN77 source code that makes up the SAPRC99 software. This software itself does not immediately solve chemical mechanisms. Rather, one function of the software is to generate *new* mechanism-specific FORTRAN77 source code that can be compiled separately by the user, and that solves the chemical mechanism designed by the user. This is referred to as SAPRC99-generated source code. The modifications detailed in the next section are to the SAPRC99 source code; however, these modifications will also produce SAPRC99-generated code that is slightly different than that produced by

unmodified SAPRC99 source code, so that it will seamlessly integrate into CAMx31.

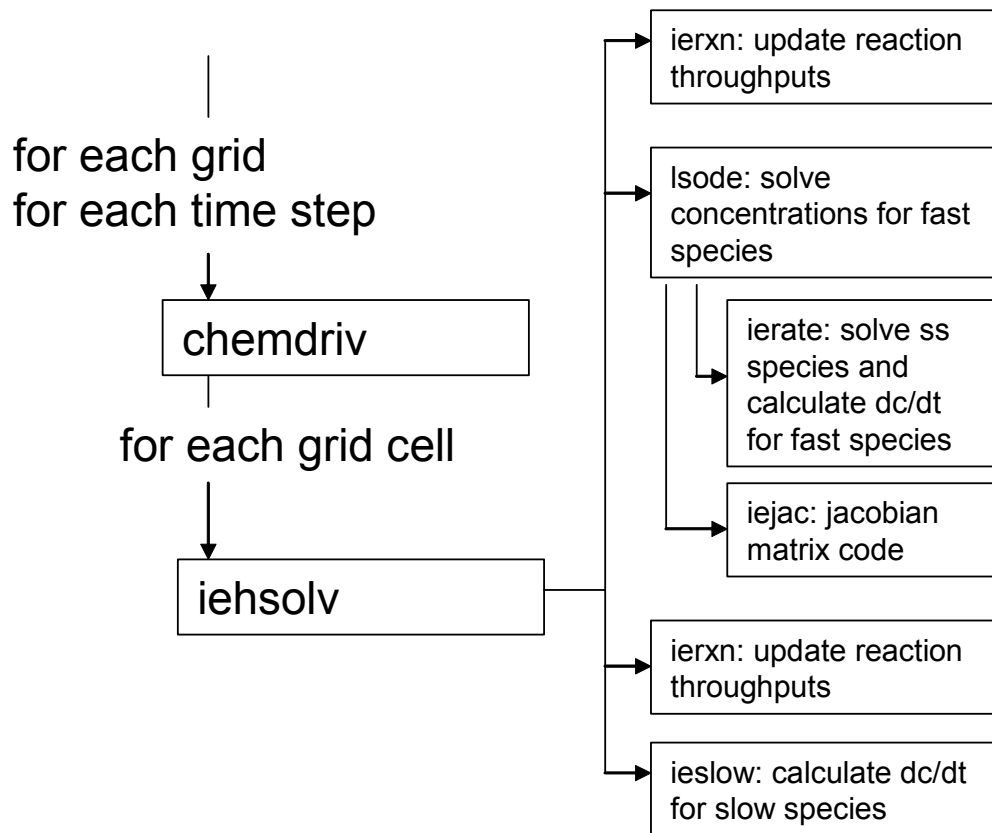


Figure B.1: Algorithm diagram of CAMx solution to chemical mechanism using the IEH solver. Each box represents a subroutine in CAMx31; each arrow represents a subroutine call.

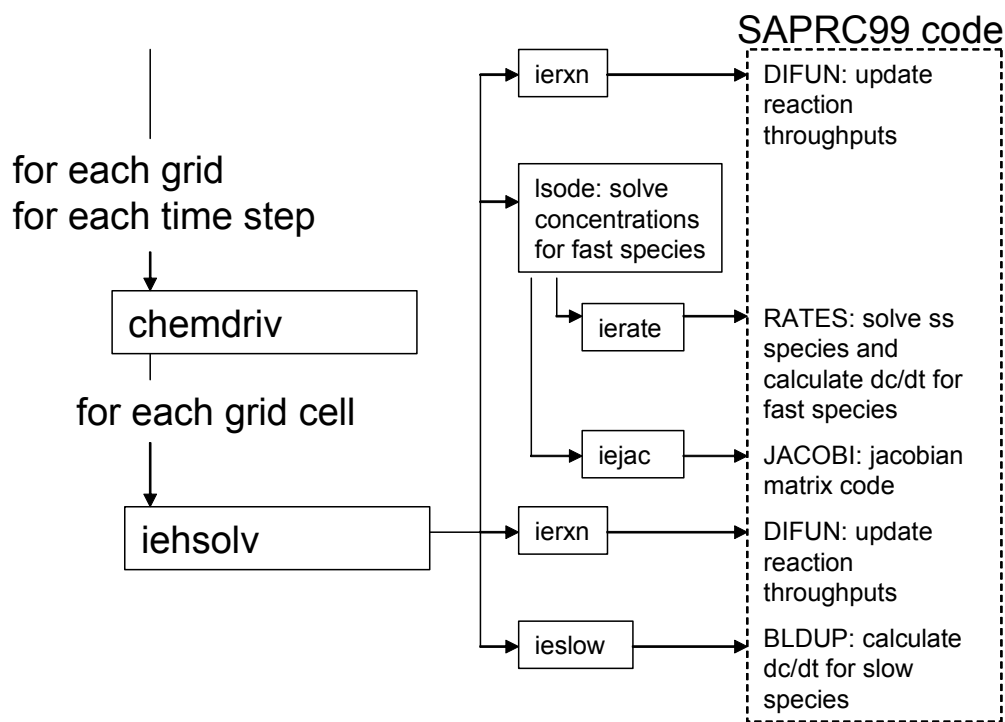


Figure B.2: Algorithm diagram of chemical mechanism solution with the IEH solver using imported SAPRC generated source code. The mechanism specific routines iernx, ierate, iejac and ieslow now are ‘empty’ and simply call the SAPRC generated code. Each box represents a subroutine in CAMx31; each arrow represents a subroutine call.

### Modifications to SAPRC99 Software

The majority of source code modifications were to the SAPRC software, more specifically the PREP modules, which read in the details of the chemical mechanism and generate the source code that solves this mechanism. A new ‘FORMAT’ specifier, ‘FORMAT=C’, was introduced to indicate that PREP is used to produce code for CAMx31. The CAMx modifications are optional, and the original functionality of PREP was maintained if FORMAT is not set equal to

‘C’. Note that once FORMAT=C is specified, the user can no longer use the other functions of the SAPRC99 software, such as the INT functions for box-model simulations. Any other SAPRC99 program that calls PREP, such as PRP, will not function properly. There are five major technical issues that drove the modifications to the SAPRC99 software:

1. Model species are categorized slightly differently for CAMx31 compared to the convention followed in SAPRC99. SAPRC99 software considers four categories: steady state (STS) species, active (ACT) species, build-up (BLD) species and constant (CONST) species. All non steady-state reactants or fast-reacting products are ‘active’ and are solved implicitly using LSODE. Reaction products that do not react are typically designated as build-up species. The IEH method in CAMx31 however allows some reactants to also be slow reacting species to reduce the number of implicit (fast) species. In addition, CAMx31 must distinguish radicals (species that are not emitted, transported or output) from other species. Finally, CAMx31 groups some model species together outside of the chemical mechanism, for example NXOY is used in CAMx31 to conserve NO<sub>y</sub> and represents the sum of N<sub>2</sub>O<sub>5</sub> and NO<sub>3</sub>. These species that are not involved in the chemical mechanism yet must be included in concentration arrays, are thus labeled ‘dummy’ species: DUMACT if they represent active species and DUMSLO if they represent slow reacting species.
2. The chemistry module of CAMx31 expects rate constants to be in mixing-ratio based units, for example, ppm<sup>-1</sup>min<sup>-1</sup>. There are seven different types of

rate constants for the s99 mechanism, which differ on how they depend on temperature and or pressure. Rate constant parameters are typically reported in concentration-based units. SAPRC99 software can convert the parameters from each reaction to give rate constants in mixing-ratio based units; however, the program assumes a standard temperature and pressure for this conversion. CAMx31 converts rate constants while accounting for the effect of actual pressure and temperature, and this adjustment depends on the order of the reaction. As a result, some rate constant parameters in SAPRC99 generated mechanism were ‘un-converted’ to allow CAMx31 to do the conversion at run-time. In addition, SAPRC99 software was modified to output reaction order.

3. CAMx31 requires two separate subroutines to calculate reaction throughputs and species rates ( $dC/dt$ ) respectively. SAPRC99 generated source code originally had only one routine called DIFUN.f that does both, and this was modified to conform to CAMx31 expectations.
4. CAMx31 contains a subroutine for each of its built-in mechanisms that calculate the elements of the Jacobian matrix to solve the fast-reacting species. SAPRC99 generated code relies on LSODE to approximate the Jacobian numerically; however, for consistency SAPRC99 software was modified to generate a Jacobian subroutine that is exported to CAMx31.
5. CAMx31 has mechanism-specific information that is both hard-coded into the model and specified in the chemistry parameters (chemparam) input. Furthermore, a number of model parameters are used to dimension variable

arrays that are related to solving the chemical mechanism and are found in a file camx.prm. If a new mechanism is used, essentially all mechanism specific information must come from SAPRC99 software. The software was modified to print 1) a chemparam file in new format with additional mechanism information, and 2) a new section of model parameters that must be included into camx.prm.

The modifications listed above were accomplished by both modifying existing SAPRC99 software subroutines and adding new subroutines. All modifications/new subroutines are listed in Table B1.

Table B2. Modifications/additions to SAPRC99 software subroutines to produce source code to be integrated into CAMx31.

<b>Subroutine</b>	<b>Function</b>	<b>Modifications/Description</b>
Bldup.for	Generates 'bldup' code.	Minor changes to allow a buildup species to be a reactant and hence use its concentration in calculation of dC/dt.
Listsc.for	Writes info to .mod file.	Minor change to write out name of slow reacting radicals if present. Original SAPRC treats all radicals as active, now they might be slow reacting.
Pnhrxn.for	Driver for routines that generate source code.	Writes new bldup header with additional argument arrays. Writes both rates and difun header. Calls both rates and difun routine. Now writes jacobi, getrk headers and calls jacobi and getrk code. Writes and calls are formatted the same as old writes and calls.
Diffun.for	Generates 'difun' code.	Literally split into two routines rates and difun, where rates sets up reaction throughputs and new difun calculates loss and gain for active species.
Prep.for	Main processing routine for the prep	This program reads the important .prp input file and processes it. If FORMAT=C than it

	modules, it calls all other routines.	sets FORM3=1 (which means separate loss and gain calculations). Also, FORMAT =C calls rdspc,savecpm,saveprm and optionally matchpig,mtchtuv and rdval.
Rdrxn.for	Reads the reactions in the .prp file.	Add a flag to delete certain bldup only species, like XC (“.CAMX DELETE”). Add recognition of new species labels (“.RAD”, “.DUMSLO”, “.DUMACT”, “.DUMBLD”). Keep track of reaction order for later use. Recognize “.CAMX TUV” flag meaning a listing of TUV reactions follows. Recognizes “.CAMX PIG” flag meaning a listing of pig reactions numbers follows. Here you can label species using different names than are specified in the reactions. Can specify “.CAMX VALUE”, which allows to specify values for variables in the mechanism. Finally, you can specify whether to keep or delete pure build-up species using “.CAMX BLD KEEP” or “.CAMX BLD DELETE”. (default is true).
Reordr.for	Determines what type of species are involved in each reaction and puts them in the correct order.	For CAMx, the flags to specify radicals and dummy species are now used to distinguish these species types. The species are ordered as steady-state, fast-reacting (non steady state radicals and active species) and slow-reacting (build-up species that react). For CAMx, true build-up only species (products only) are deleted unless they listed explicitly in the .prp file.
Rxlst1.for	Determine species # matching the names in spname array.	Minor changes to recognize flags for slow, radical and dummy species.
Cspecs.for (New)	Include file.	Include file with common blocks and new variables used by multiple routines.
Getrk.for (New)	Generates ‘getrk’ code.	Creates code called getrk, which fills in photolysis rates in a CAMx array (rk) that has rate constants for all reactions. In the SAPRC chemistry routines, photolysis rates are read from coefficient array, however the PiG routines look in rk. So for PiG to work,

		the photolysis rates are put in the rk array.
Jacobi.for (New)	Generates 'jacobi' code	Creates code called jacobi, which calculates the elements of the Jacobian matrix to solve the fast species.
Rates.for (New)	Generates 'rates' code.	Creates a new code called rates, which was formerly created by difun.for. Difun.for was literally split into two routines: rates.for creates 'rates' code that calculates the reaction throughputs, and difun.for creates 'difun' code that calculates species loss and gain.
Rdspc.for (New)	Reads list of physical constants.	Reads a user-supplied file with .spc extension and that contains physical parameters for all model species. This information is echoed to the .cpm file.
Savecpm.for (New)	Writes new chemparam file.	Save a new modified version of the chemparam input file to CAMx, with the extension .cpm. This file includes: <ul style="list-style-type: none"> <li>• Information that was formally hard-coded into CAMx31 e.g. # of each species type in the mechanism, # of reactions, # of photolysis reactions.</li> <li>• Physical constants for each model species, which must be provided in a separate file with a .spc extension.</li> <li>• The reaction rate constant parameters, including reaction order and adjusted as to let CAMx calculate a conversion factor from concentration to mixing ratio based units.</li> <li>• Stoichiometric coefficients for all reactions</li> </ul>
Saveprm.for (New)	Writes new model parameters section.	Creates a new file with a .prm extension, which is to be included in the camx.prm file. This file gives parameters for array bounds and is used at compile time. The information replaces information in part of the existing camx.prm file.

## Modifications to CAMx31

The majority of the modifications to CAMx31 were to the routine that sets up the IEH solution of the chemical mechanism (iehsolv.f) in each grid cell, and to the routine that reads the chemparam file (readchm.f). As with the SAPRC99 software modifications, the original functionality of CAMx31 is not perturbed if no new mechanism is used, i.e. the modified code produces the exact same results as un-modified CAMx31 if it is not used with a SAPRC-generated mechanism. The new chemparam file contains the text 'VERSION3UT' in the first line if a new modified mechanism is used, which in turn sets the global flag 'camxut' to TRUE. If 'camxut' is TRUE then probing tools will not work, the PiG module will only work if a particular subset of inorganic reactions is included in the new mechanism, and only the IEH solution method may be chosen to solve the chemistry. There are three major technical issues that drove the modifications to CAMx31:

1. CAMx31 uses a working array to pass concentrations to the IEH subroutines. The expected order of species in the working array is different for the SAPRC99-generated subroutines. In iehsolv.f (original CAMx31 mechanisms) the order of species is: fast radicals, fast species, steady-state species, slow species, and finally constant species. In utieh.f (SAPRC99-generated mechanism) the order of species is: fast radicals, fast species, steady-state species, constant species, and finally slow species. Other than this re-ordering, the order/storage of model species concentrations is the same for built-in and SAPRC99-generated mechanisms in CAMx31.

2. CAMx31 stores a reaction rate for each reaction, including photolysis, in an array called rk. The array is populated at each time step and for each grid cell, with rate constants as a function of temperature and pressure. SAPRC generated code stores photolysis rate in a different array, called coeff. This coefficient array is updated for each grid cell and each time step so that SAPRC generated code accesses the photolysis rate appropriately. CAMx31, however, has a driver routine for the PiG submodule, which has a ‘mini’ chemistry solver for the reduced set of reactions that are considered in the NO<sub>x</sub> plumes. Code for this submodule is not created in the modified SAPRC99 software, and the new mechanisms will continue to use the original code in CAMx31. This routine accesses the array rk for photolysis information, hence the new subroutine getrk which is produced by the modified SAPRC99 software. Getrk loads the photolysis rate from the coefficient array into the rk array prior to calling the PiG chemistry routine.
3. CAMx31 has five built-in mechanisms and all the stoichiometric coefficients of reactants and products are hard-coded into the source code. SAPRC99 stores these coefficients in a separate array in a common block and each routine accesses it as needed.

Table B3 lists the modifications made to CAMx3.1.

Table B3: modifications to CAMx31.

<b>Subroutine</b>	<b>Function</b>	<b>Modification/Description</b>
utchem.com (NEW)	Include file	Declares the ‘chmut’ common block with some new global variables.
chemdriv.f	Loops over all grid cells in a time step	If ‘camxut’ is true, calls an alternate version of the IEH solver, called utieh.f.

	and calls chemistry driver.	The new mechanism is implicitly numbered 9. chemdriv.f declares externally ierate9.f, ierxn9.f, ieslow9.f and iejac9.f, which are 'wrapper' routines.
kphoto.f	Calculates photolysis rates for a certain grid cell.	If camxut is true, kphoto reads and writes photolysis rate data in the coefficient array rather than rk.
pigdrive.f	Driver routine for PiG calculations	Runs the SAPRC-generated routine getrk which loads the photolysis rates from the coefficient array into rk. (to allow pigdrive to use rk for all reactions)
readchm.f	Reads information from the chemparam file and assigns values to many global variables	The routine essentially now has two sections, one is executed if camxut is true, the other is executed if camxut is false. The difference in sections reflects the difference between standard or SAPRC-generated chemparam files. New information in modified chemparam file is: <ul style="list-style-type: none"> <li>• # radicals, # steady-state species, # fast species, # constant species</li> <li>• Indices of photolysis rates in variable coefficient array.</li> <li>• # PiG reactions and reaction ID numbers</li> <li>• various indices to reference data in the constant coefficient array</li> <li>• names of radical species</li> <li>• names of constant species and concentrations</li> <li>• stoichiometric coefficients and various other parameters stored in the variable coefficient array</li> </ul>
utieh.f (NEW)	Parent equation for the IEH solution of chemical mechanism for one grid cell.	Based on iehsolv.f and called if camxut is true. The major difference between the two is the order in which concentrations are loaded into the working arrays. Utieh.f calls 'ierxn9', 'ierate9', 'iejac9', and 'ieslow9', which in turn call the SAPRC-generated code.
ierxn9.f	Wrapper that calls	Calls SAPRC-generated rates.f which

(NEW)	rates.f	calculates throughputs of each reaction.
ieslow9.f (NEW)	Wrapper that calls bldup.f	Calls SAPRC-generated bldup.f which calculates loss and gain of slow species. After bldup call, subtracts loss from gain to get overall rate for each slow species. Note ierxn9 is called just prior to ieslow9 in utieh.
ierate9.f (NEW)	Wrapper that calls difun.f	First calls ierxn9.f, then calls SAPRC-generated difun.f which calculates steady state species concentrations first followed by loss and gain of all fast reacting species. After difun call, subtracts loss from gain to get overall rate for each fast species.
iejac9.f (NEW)	Wrapper that calls jacobi.f	First calls ierxn9.f, then calls SAPRC-generated jacobi.f which calculates the elements of the Jacobian matrix, for the implicit solution of fast-reacting model species.
'mechanism'.f (NEW)	SAPRC-generates source code.	Library of routines generated by SAPRC: bldup, rates, difun, jacobi, getrk.

### **Guidelines for implementing a modified chemical mechanism into CAMx31**

This section acts as a guideline for implementing a chemical mechanism into CAMx31 using the modified SAPRC99/CAMx31 software. The user should be aware of the limitations of using this tool that have been discussed in previous sections. The two most important considerations are 1) that significant changes to the base mechanism may lead to unstable numerical solutions and 2) if the user plans to use PiG capabilities of CAMx31, the same subset of inorganic reactions currently in the standard SAPRC99 mechanism must be included in the new mechanism. The guidelines below are oriented toward someone who is already familiar with both the CAMx and SAPRC99 modeling systems.

1. Build the chemical mechanism using SAPRC software (creating <mechanism\_name>.prp file). This involves:
  - a. Lumping and/or treating organic compounds explicitly as needed using various SAPRC99 programs (see SAPRC99 documentation).
  - b. Creating reaction mechanisms for lumped compounds using various SAPRC99 programs (see SAPRC99 documentation).
  - c. Preparing the list of reactions (base mechanism plus lumped species reactions and any explicit species reactions) in the <mechanism\_name>.prp file.
  - d. Listing species types in the <mechanism\_name>.prp file (.ACT, .RAD, .SLO, .STS, .DUMSLO, .DUMACT commands). Listing constant species and their concentrations in the <mechanism\_name>.prp file.
  - e. Renaming any model species to four-letter CAMx names in <mechanism\_name>.prp file (“CAMX REPLACE” command).
  - f. Adding FORMAT=C to the beginning of <mechanism\_name>.prp file
  - g. Preparing a separate file called <mechanism\_name>.spc containing physical constants for all non-radical model species.
  - h. Executing the PREP command which creates <mechanism\_name>.cpm (chemparam file), <mechanism\_name>.prm file (model parameters file) and <mechanism\_name>.f (library of SAPRC routines).

2. Couple the SAPRC99-generated code to CAMx31. This involves:
  - a. Creating a symbolic link called <mechanism\_name>.f in the /CMC directory of the CAMx31 source code to the SAPRC99-generated <mechanism\_name>.f file.
  - b. Creating a symbolic link called saprc.prm.<mechanism\_name> to the SAPRC99-generated <mechanism\_name>.prm.
  - c. Issuing make cammond. It uses the Makefile which has been modified to link the saprc.prm.<mechanism\_name> file to saprc.prm, which replaces the chemistry model parameters in the original camx.prm. The Makefile compiles and links the new SAPRC99-generated source code, utieh.f, ieslow9.f, ierate9.f, ierxn9.f and iejac9.f with the rest of the CAMx31 routines.
3. Prepare CAMx31 emissions, boundary condition and initial condition files that conform to the new chemical mechanism. This last task will likely comprise the bulk of the work and should be carefully thought out before beginning with a new mechanism.

## **Appendix C: Modifications to the Emitdb.xls tool.**

This Appendix explains how software was used to assign individual organic compounds to model species in the chemical mechanism. A Microsoft Excel based tool called 'emitdb.xls' was downloaded at <ftp://ftp.cert.ucr.edu/pub/carter/emitdb/emitdb.xls> and used for this research. Related information can be found at <http://pah.cert.ucr.edu/~carter/emitdb>. (Both sites were accessed on 9/1/03; the version of emitdb.xls used in this research was updated on 7/23/02.) A brief description of Emitdb.xls is given prior to listing the modifications that were made.

Emitdb.xls contains a number of worksheets and Visual Basic Macros that automate the assignment of individual organic compounds to both the standard s99 and cb4 model species. Two important features of this tool are that it recognizes multiple classifications systems for organic compounds/mixtures, and that it breaks down mixtures into individual compounds before allocation to model species. The recognized classifications are: Texas SAROAD classification, EPA SAROAD classification, California Air Resources Board classification or SPECIATE3.2 program classification. The pollutant codes used in the classification system are mapped to internal 'Unique ID's' or UID's, where each UID is either a single compound, a simple (isomeric) mixture, a complex mixture (non-isomeric) or 'poorly defined'. Mixture UID's are broken down into mass fractions of individual compound UID's.

Emitdb.xls assigns compound UID's to s99 model species in three steps. First, UID's are assigned to one of ~700 Detailed Model Species (DMS) recognized by the SAPRC99 software. Second, DMS are in turn mapped to one of 63 SAPRC 'Emissions' groups (S99Emiss). Finally, the S99Emiss groups are assigned to one of 31 s99 model species (S99Lump). The intermediate group of S99Emiss species is not important to this research, however since it is used in the original emitdb.xls, it is used here as well. The most important assignments are made in the 'Compound' worksheet, where all UIDs for single compounds are given an assignment to a SAPRC99 DMS, and in some cases directly to a S99Lump. DMS species are mapped to SAPRC99 emissions groups in the 'DMS worksheet'. Emissions groups are mapped to lumped species in the 'Emissions groups' worksheet. (If a UID represents a mixture it is first mapped to single compound UID and then mapped to model species as above).

It is important to distinguish between a speciation profile and splitfactors. The former refers to the relative mass amounts of individual organic compounds that comprise VOC emissions from a particular source. The latter refers to factors that convert this mass of total VOC to moles of individual model species. Emitdb.xls has macros that can convert a speciation profile (with any number of compounds or mixtures, and in any of the abovementioned classification systems) into a set of splitfactors (one for each model species). This is accomplished using the mapping described in the previous paragraph. Figure C1 is a flowchart of how a speciation profile is mapped to model species and converted to splitfactors.

The two modifications to emitdb.xls for this research were 1) to automate the processing of multiple speciation profiles into splitfactors, and 2) to let the tool create splitfactors in a new chemical mechanism. These two modifications are discussed below.

### **Processing multiple speciation profiles.**

Emitdb.xls has a built in VB Macro called 'ProcessSarEmit' that takes a speciation profile and creates splitfactors in both standard s99 and CB4 species. This Macro is run on the "emit worksheet" sheet. The calculated splitfactors have units of moles of model species per mole of carbon atom in the mixture of compounds. The Macro also calculates the mean molecular weight of the mixture in units of grams per mole Carbon. Dr. Yosuke Kimura at the Center for Energy and Environmental Resources made two modifications to Emitdb.xls to facilitate processing multiple speciation profiles into splitfactors. The first was to allow direct use of the UID to classify organic compounds and mixtures, rather than one of the aforementioned classification systems. This is useful because the UID's for individual compounds are actually Chemical Abstract Service (CAS) numbers.

The second modification was to add a VB Macro that automatically processes any number of speciation profiles of varying classifications through the "emit worksheet", and to calculate splitfactors in units of moles model species per gram total VOC. These are the units required by EPS2, which is the emissions processing software that creates emissions inputs for the grid model. This new

Macro reads the list of speciation profiles from a separate worksheet, and writes splitfactors of s99 and CB4 species to two new worksheets.

### **Calculating splitfactors for s99soa model species.**

The s99soa mechanism is based on standard s99 and uses SAPRC99 model species. Emitdb.xls was modified to process speciation profiles into s99soa species rather than s99 standard species, and this involved a basic reassignment of compound UID's to S99Lump species. The two differences between s99soa and s99 are 1). Five monoterpenes ( $\alpha$ -pinene,  $\beta$ -pinene,  $\Delta^3$ -carene, sabinene and d-limonene) are treated explicitly rather than lumped into the TERP category, and 2) the two lumped aromatic groups ARO1 (low  $k_{OH}$ ) and ARO2 (high  $k_{OH}$ ) are replaced with 6 lumped groups: ARH1 (high-yield aromatics with low  $k_{OH}$ ), ARL1 (low-yield aromatics with low  $k_{OH}$ ), ARH2 (high-yield aromatics with high  $k_{OH}$ ), ARL2 (low-yield aromatics with high  $k_{OH}$ ), ARN1 (no-yield aromatics with low  $k_{OH}$ ), ARN2 (no-yield aromatics with high  $k_{OH}$ ).

The following modifications were made to emitdb.xls to create splitfactors for s99soa model species.

1. A new S99Emiss and S99Lump group was created for each of five explicit monoterpenes (these five monoterpenes already had explicit DMS). The assignments in the "Emissions Groups" and "DMS" worksheets were updated to assign these monoterpenes to explicit species as opposed to the generic TERP species.

2. All aromatic compounds in the internal database were assigned either high-yield, low-yield or no-yield based on predicted aerosol forming characteristics (see Chapter 5 for details). AR1H, AR2H, AR1L, AR2L, AR1N, AR2N were added to the S99Emiss and S99Lump lists to replace ARO1 and ARO2. The first mapping step, from UID to DMS, remains unchanged. Two DMS species (C12-BEN3 and C11-BEN3) contained both high and low yield aromatics compounds. In this case these species are assigned to a high-yield or low-yield S99emiss category based on the number of high- or low-yield compounds assigned to the DMS. All other DMS aromatics contained either high-yield, low-yield or non-yield aromatic compounds exclusively. The assignments of DMS to S99Emiss, and S99Emiss to S99Lump were then updated in the “Emissions Groups” and “DMS” worksheets respectively.
3. The new explicit terpenes and the six replacement aromatics were added to the species list in the ‘Parameters and Commands’ worksheet with appropriate molecular weights, ie AR1H was assigned the MW of ARO1 etc. The internal names ‘S99Lspec’ and ‘S99Lmw’ were reassigned to the expanded list of lumped model species and molecular weights respectively.
4. Finally, additional columns were added to the ‘SAROAD assignments’ sheet to accommodate the expanded list of model species. The array

function that lists these names as 'S99Lspec' was re-entered in the new set of cells.

After the above modifications were made, the 'Merge All Compounds' Macro and the 'Update Mechanism Assignments' Macro were re-run to update assignments to model species. The 'ProcessSarEmir' Macro now creates splitfactors for s99soa species rather than s99 model species.



## **Appendix D: Modifications made to GLOBEIS version 2.2.**

GLOBEIS version 2.2 was used in this research to calculate biogenic emissions. GLOBEIS2.2 is available for free at <http://www.globeis.com/registration/reg.html>, along with several reports and references describing its development (this link was accessed on 10/5/2003). The released version only calculates CB4 emissions.

The mechanism used in this research, s99soa, was based on the standard SAPRC99 chemical mechanism (referred to as s99), but had separate species to explicitly represent  $\alpha$ -pinene,  $\beta$ -pinene, sabinene, d-limonene and  $\Delta^3$ -carene. All other monoterpene compounds are collectively represented by a ‘leftover’ monoterpene species. In contrast, s99 represents all monoterpenes by one model species. Besides the representation of monoterpenes, s99 and s99soa share all other species in common. GLOBEIS2.2 was modified to predict s99 and s99soa model species in addition to CB4 model species.

GLOBEIS2.2 has built-in emissions factors for isoprene, NO, total monoterpenes, and ‘other VOC’ emissions (emissions other than isoprene or monoterpenes, but not including sesquiterpenes) for a large number of tree species. Isoprene and NO are treated explicitly in CB4, s99 and s99soa, so emissions of these compounds can be converted mole-for-mole into equivalent model species. Total monoterpenes and ‘other VOC’ emissions are split into model species using global splitfactors, i.e. the allocation to model species is done after emissions from all tree species have been summed in each grid cell, and is

thus independent of tree species. In this research, total monoterpene emissions are speciated into individual compounds by tree species rather than globally, leading to a very detailed monoterpene emission inventory.

The two modifications to GLOBEIS2.2 for this research were 1) speciation of total monoterpenes to individual compounds by tree species, and 2) calculation of biogenic emissions of s99 and s99soa model species from the biogenic emissions. Each modification is discussed in detail below.

#### **Speciation of total monoterpene emissions by tree species.**

The speciation of total monoterpene emissions into individual monoterpene was done using data summarized in Geron et al. (2000). This reference included a table with the fractions of fourteen individual monoterpene compounds in emissions from 95 tree species and tree genus. The reader is referred to references in Geron et al. (2000) for more details. Although there is a much larger number of tree species in the GLOBEIS2.2 data base, the vast majority of total monoterpenes emissions in Southeast Texas are from tree species in this table (i.e. 91% of total monoterpene emissions in the 4km modeling domain have a specific monoterpene profile).

GLOBEIS2.2 was modified to calculate emissions of  $\alpha$ -pinene,  $\beta$ -pinene, sabinene, d-limonene,  $\Delta^3$ -carene, and a 'leftover' terpene group, which is the sum of all other terpene compounds. Similar modifications could allow calculation of emissions of nine other monoterpenes (camphene, myrcene, p-cymene,  $\alpha$ -terpinene,  $\gamma$ -terpinene, terpinolene,  $\beta$ -phellandrene, ocimene and  $\alpha$ -thujene), since

these compounds are included in the monoterpene profiles. The aerosol forming characteristics of these nine terpenes are not well known relative to the five terpenes that are treated explicitly. Furthermore,  $\alpha$ -pinene,  $\beta$ -pinene, sabinene, d-limonene and  $\Delta^3$ -carene are the most abundant monoterpenes. Table D1 below is imported into GLOBEIS2.2.

Table D1. Percentage of each compound in total monoterpene emissions (Geron et al. 2000). N denotes the number of samples used to determine the speciation. The first row of data is an average speciation profile across all 95 other profiles. mt\_link was added to link each genus/species with internal GLOBEIS emissions factors.

Genus species (Genus groups are succeeded by spp.)	mt_link (code used to link to emission factors in GLOBEIS2.2)	N	$\alpha$ -pinene	$\beta$ -pinene	$\Delta^3$ -carene	d-limonene	camphene	myrcene	$\alpha$ -terpinene	$\beta$ -phellandrene	sabinene	p-cymene	ocimene	$\alpha$ -thujene	terpinolene	$\gamma$ -terpinene
AVERAGE	MEAN		36.9	14.7	6.0	11.1	4.4	5.8	0.5	2.0	2.9	2.8	2.5	0.4	0.7	0.4
Abies balsamea	ABIEBAL*	27	20.7	35.8	1.2	20.3	9.2	1.7	2	5.7	0	3.4	0	0	0	0
Abies concolor	ABIECON*	1	33.3	35	0	6.2	6	4.2	0	2	10	0	0	0	2.9	0.4
Abies fraseri	ABIEFRA*	6	71.9	17	8.6	1.1	0	0.2	0	1.3	0	0	0	0	0	0
Abies grandis	ABIEGRA*	2	56.7	17.9	0.7	4.1	10	5.1	0	3.6	1.3	0	0	0	0.6	0
Abies lasiocarpa	ABIELAS*	2	22.1	13.9	1	29.5	10	1.5	12.5	0	0	8.5	0	1	0	0
Abies procera	ABIEPRO*	1	9.2	13.3	0	30.5	2.4	10	0	30	0	8.5	0	0	1.8	2.7
Acacia spp	Acac	4	87.6	7.1	0	3.4	0	1.8	0	0	0	0	0	0	0	0
Acer spp	Acer	23	21.1	4.3	25	13	5.1	7.9	0.5	0	21.5	0	0	0.8	0	0.7
Alnus spp	Alnu	1	12	44	0	21	0	0	0	0	0	2	19	2	0	0
Amelanchier arborea	AMEARB	1	0	0	0	0	0	0	0	0	0	0	0	0	0	0
Betula alleghaniensis	NOLCVEG	1	28.3	4	0	23.2	26.3	0	4	0	0	14.1	0	0	0	0
Betula papyrifera	NOLCVEG	1	29	0	0	29	21	0	0	0	0	21	0	0	0	0
Carpinus caroliniana	NOLCVEG	2	28.1	23	21.7	9.1	9.1	0	0	0	0	9.1	0	0	0	0
Carya spp	CARY	13	24.1	7.2	33.4	19.2	0.3	6.9	0	0	3	0	0	0.2	5.7	0.1
Celtis occidentalis	CELT	1	2	0	0	0	0	2	0	0	0	0	96	0	0	0
Cercocarpus montanus	Cerc	1	0	0	0	0	0	0	0	0	0	0	0	0	0	0
Chamaecyparis lawsoni	Cham	1	16	64.3	0	19.7	0	0	0	0	0	0	0	0	0	0
Cornus florida	CORN	5	20.3	0.5	38.7	26.8	7.7	0	0	0	0	4.7	0	0	1.4	0

Cupressus spp	CUPRSP*	4	42.5	1.2	0	31.2	0.5	23	0	0.3	0.5	0	0.3	0.5	0	0
Diospyros virginiana	DIOVIR	17	50.7	49.3	0	0	0	0	0	0	0	0	0	0	0	0
Eucalyptus spp	Euca	2	35.4	18.8	0	20.8	0	0	0	0	0	0	25	0	0	0
Fagus grandifolia	Fagu	3	31.5	12	6.2	24.3	4	1.5	8	0	0.3	12	0	0.3	0	0
Fraxinus spp	Frax	4	20.9	8.4	2.7	0.7	0.7	22.2	0	44.4	0	0	0	0	0	0
Ilex opaca	ILEXOPAC*	3	0	0	0	0	0	0	0	0	0	0	0	0	0	0
Juglans spp	JUGSP.	1	29	51.6	0	12.9	0	6.5	0	0	0	0	0	0	0	0
Juniperus monosperma	JUNIMON*	2	24.2	0	25.8	48	0	1.2	0.8	0	0	0	0	0	0	0
Juniperus occidentalis	NOLCVEG	4	0	0	0	0	0	0	0	0	0	0	0	0	0	0
Juniperus scopulorum	NOLCVEG	2	2.6	0	0	1.4	0	1.8	1	0.2	87.5	0	0	2.7	0	2.9
Juniperus virginiana	JUNIVIR*	1	33.3	0	66.7	0	0	0	0	0	0	0	0	0	0	0
Larix occidentalis	Lari	1	0	0	0	0	0	0	0	0	0	0	0	0	0	0
Liquidambar styraciflua	Liqu	28	45.4	6.8	16.3	16.1	0.6	3.7	1.5	3.1	4.4	1.8	0	0.1	0	0
Liriodendron tulipifera	LIRITUL*	19	4.6	6.5	0.4	40.1	1.3	26.8	0	0.9	0	0	9.9	0	8.9	0.4
Magnolia grandiflora	MAGNAGRA*	4	60.6	26.5	1.6	5.6	0.6	5.1	0	0	0	0	0	0	0	0
Malus spp	MALU	1	0	0	0	0	0	0	0	0	0	0	0	0	0	0
Meliaazedarach	MELI	1	35.7	14.3	0	17.9	0	32.1	0	0	0	0	0	0	0	0
Morus spp	MORSP.	5	0	0	0	0	0	0	0	0	0	0	0	0	0	0
Nyssa spp	NYSSP.	4	21.5	17.4	8.9	31.5	6.6	14.1	0	0	0	0	0	0	0	0
Ostrya virginiana	OSTVIR	1	20	0	0	20	40	0	0	0	0	20	0	0	0	0
Oxydendrum arboretum	OXYARB	1	39.2	16.4	12.9	31.4	0	0	0	0	0	0	0	0	0	0
Persea borbonia	Pers	3	61	39	0	0	0	0	0	0	0	0	0	0	0	0
Picea abies	PICEABI*	14	45.3	12.4	8.6	10.1	8.6	6.6	0	4.1	3.3	0.9	0	0	0.1	0.1
Picea engelmannii	PICEENG*	5	36.7	13.4	5.8	8.1	12.3	8.7	3	5.2	0	6.7	0	0	0.1	0
Picea glauca	PICEGLA*	25	24	11.3	5.4	26.5	18.1	8.4	0.1	5.5	0.4	0	0	0	0.2	0.1
Picea mariana	PICEMAR*	10	24.2	2.9	28.1	15.3	23.1	2.1	0.1	0.3	0.1	3.4	0	0	0.2	0.2
Picea pungens	PICEPUN*	16	33.9	27.6	8.8	19.6	5.7	2.7	0.1	0.8	0.6	0.1	0	0	0.1	0.1
Picea rubens	PICERUB*	3	20	8.1	26.2	5.6	28.8	5.8	0	3	0	1.7	0	0	0.4	0.3
Picea sitchensis	PICESIT*	14	17.3	10	0	0.1	2.2	51.6	0	18.8	0	0	0	0	0	0

<i>Pinus albicaulis</i>	PINUALB*	2	38.3	26.4	2.2	10.4	2.9	13.2	0	5.2	0.9	0.1	0	0	0.5	0
<i>Pinus aristata</i>	PINUARI*	1	100	0	0	0	0	0	0	0	0	0	0	0	0	0
<i>Pinus attenuata</i>	PINUATT*	3	37.9	21.4	3.7	15.7	1.3	10.7	0	7.8	0.3	0	1.1	0	0.2	0
<i>Pinus balfouriana</i>	PINUBAL*	2	98.7	0.8	0	0.5	0	0	0	0	0	0	0	0	0	0
<i>Pinus banksiana</i>	PINUBAN*	19	30.4	25	10.4	6	7.3	12.6	0.1	1.7	4.3	0.1	0.1	0	1.8	0
<i>Pinus clausa</i>	PINCLA	8	45.4	54	0	0.1	0.3	0	0	0.1	0	0.1	0	0	0	0
<i>Pinus contorta</i>	PINUCON*	21	22	19.8	5	18.1	5.4	9.7	4.4	10.5	1.4	1.6	0.2	0	1.6	0.3
<i>Pinus coulteri</i>	PINUCOU*	2	29	15.2	2.7	19.4	2	7.6	0	9.6	12.5	0.9	0.2	0	0.9	0.2
<i>Pinus discolor</i>	PINUDIS*	1	98.2	0	0	1.8	0	0	0	0	0	0	0	0	0	0
<i>Pinus echinata</i>	PINUECH*	5	55	14.1	5	22.8	0.5	2.3	0.1	0	0.1	0	0	0	0	0
<i>Pinus edulis</i>	PINUEDU*	2	90.7	4.1	0.5	0	0.7	0	0	0	0	0	0	0	0	0
<i>Pinus elliotii</i>	PINUELL*	29	47.3	37.7	7.5	5.7	0.1	0.5	0	1.1	0	0	0	0	0	0
<i>Pinus engelmannii</i>	PINUENG*	3	69	17.7	0	0.1	3.4	5.9	0	2.9	0.1	0.1	0	0	0.2	0.1
<i>Pinus flexilis</i>	PINUFLE*	1	100	0	0	0	0	0	0	0	0	0	0	0	0	0
<i>Pinus glabra</i>	PINGLA	1	50	50	0	0	0	0	0	0	0	0	0	0	0	0
<i>Pinus jeffreyi</i>	PINUJEF*	2	44.6	6.6	0	23.2	6.8	16.2	0	1.5	0.3	0.5	0.3	0	0.2	0
<i>Pinus lambertiana</i>	PINULAM*	1	83	17	0	0	0	0	0	0	0	0	0	0	0	0
<i>Pinus leiophylla</i>	PINULEI*	1	94.2	0	5.8	0	0	0	0	0	0	0	0	0	0	0
<i>Pinus monticola</i>	PINUMON*	8	29.7	26.1	32.5	3.4	0	8.2	0	0	0	0	0	0	0	0
<i>Pinus nigra</i>	PINUNIG*	1	97.2	0	0	2.8	0	0	0	0	0	0	0	0	0	0
<i>Pinus palustris</i>	PINUPAL*	34	42	53.7	2.7	1.4	0	0.1	0	0	0	0	0	0	0	0
<i>Pinus ponderosa</i>	PINUPON*	27	21.7	33.3	41.3	1.4	0	1.8	0.1	0	0.4	0	0	0	0	0
<i>Pinus pungens</i>	PINUPUN*	1	75.3	17.1	7.7	0	0	0	0	0	0	0	0	0	0	0
<i>Pinus radiata</i>	PINURAD*	8	38.7	41.7	0.1	10.7	0.1	8.1	0	0.7	0	0	0	0	0	0
<i>Pinus resinosa</i>	PINURES*	2	9.8	0.2	1.8	34.9	19.3	7.3	4.6	0	0	22	0	0	0	0
<i>Pinus rigida</i>	PINRIG	2	73.5	18	8.5	0	0	0	0	0	0	0	0	0	0	0
<i>Pinus sabiniana</i>	PINUSAB*	1	60.3	39.7	0	0	0	0	0	0	0	0	0	0	0	0
<i>Pinus serotina</i>	PINSER	2	16.8	20.9	0	61.4	0.5	0	0	0.4	0	0.1	0	0	0	0
<i>Pinus strobus</i>	PINSTR	12	25.3	19.7	0.1	0.1	14.2	29.1	0	6.8	0.8	0	0	3.9	0	0

<i>Pinus sylvestris</i>	PINSYL	50	20.7	21.4	30.5	7.8	0.4	9.4	1.9	7.6	0.2	0	0	0	0.1	0
<i>Pinus taeda</i>	PINUTAE*	36	58	24.1	1	6.9	0.8	8.4	0.2	0	0	0.5	0	0	0.1	0
<i>Pinus virginiana</i>	PINUVIR*	7	33.1	12.8	34.2	12.3	4.5	3	0	0	0.1	0	0	0	0	0
<i>Populus</i> spp	POPU	7	32.1	7.5	0.9	27.1	16.9	2.7	0.9	0	0	12	0	0	0	0
<i>Prunus</i> spp	PRUN	5	37.6	15.7	1.2	9.7	12	9	0	0	0	0.4	25	0	0	0
<i>Pseudotsuga menziesii</i>	PSEUMEN*	37	64.2	21.2	2.7	5.3	1	2.5	0	0.1	3	0	0	0	0	0
<i>Quercus</i> spp	QUER	86	34.8	6.1	0.4	13.4	6.8	0.4	0	0	0.7	10.9	14.7	0	11.7	0
<i>Robinia pseudoacacia</i>	ROBIPSE*	2	0	0	0	0	0	100	0	0	0	0	0	0	0	0
<i>Salix</i> spp	SALI	12	10.9	0	0	21.4	0	0	0	0	0	19.6	48	0	0	0
<i>Sassafras albidum</i>	Sassp.	2	0	10.4	0	0	9.6	0	0	0	9.6	43	0	0	27.4	0
<i>Sequoia sempervirens</i>	NOLCVEG	33	25.7	0.9	0	12.3	0.3	5.7	0.6	4.4	28.5	1	0.8	0.1	0.8	19.1
<i>Sequoiadendron giganteum</i>	NOLCVEG	14	98.5	0	0	1.2	0	0	0	0	0	0	0	0	0.2	0
<i>Taxodium distichum</i>	TAXODIS*	23	51.8	0.4	4.3	2.4	0	2.5	0	0	0	0	0	0	0	0
<i>Taxodium mucronatum</i>	NOLCVEG	1	86.3	1	0	8.8	0.9	3	0	0	0	0	0	0	0	0
<i>Thuja occidentalis</i>	THUJOCC*	4	35.7	6.8	1.4	13	16.4	1.3	0	0	6.8	8.5	0	9.5	0	0.5
<i>Tilia americana</i>	TILIAME*	1	0	0	0	0	0	0	0	0	0	0	0	0	0	0
<i>Tsuga canadensis</i>	TSUSP.	5	14.5	5.9	0.7	15.8	27.8	1.3	0.4	0	0	21.5	0	12	0	0
<i>Ulmus</i> spp	ULMU	5	8.7	31.8	0	11	0	1.4	0	0	42	0	0	5.1	0	0
<i>Umbellularia californica</i>	UMBCALI*	12	26	13.5	0	1.3	0.3	5.5	4.2	0	35.1	2.2	0	0	0.6	11.1

The most significant modification made to GLOBEIS2.2 was to link the monoterpene profiles to the total monoterpene emissions factors. The table ‘link lcCode VegCode’ contains the field “lcVeg”, which has the most detailed classification of vegetation types in GLOBEIS2.2. “lcVeg” codes are linked to “vegib2” codes in the table ‘vegCode char’, which contains ‘total monoterpene’ emission factor for each “vegib2” code. This is a many-to-one mapping because several tree species (i.e. “lcVeg” codes) have the same emission factor.

The monoterpene profiles are linked to “vegib2” codes via the “mt\_link” field in ‘vegCode char’. All 95 monoterpene profiles had corresponding “lcveg” codes but many did not have specific “vegib2” codes. As a result, several new more specific “vegib2” codes were added to ‘vegCode char’ (these codes are succeeded by an asterisk in Table D1 above). The new “vegib2” codes were also linked to the appropriate “lcVeg” code in ‘link lcCode VegCode’.

Finally, “vegib2” codes without a specific monoterpene profile were linked to the AVERAGE profile, i.e. average fractions of monoterpene compounds from all 95 profiles. As noted above, however, the majority of total monoterpene emissions in the area of interest are from tree species with specific monoterpene profiles. Additional modifications are listed in Table D2 below.

Table D2. Modifications made to GLOBEIS2.2 to calculate emissions of individual monoterpene compounds.

<b>Name</b>	<b>Type</b>	<b>Modifications</b>
‘lcCode char’	query	Add the monoterpene table. Add 6 new fields: apin, bpin, sabi, dlim, dcar and otrp which represent emissions of $\alpha$ -pinene, $\beta$ -pinene, sabinene, d-limonene and $\Delta^3$ -carene and the leftover group. Each field contains an expression similar to the ‘total

		monoterpene' field, but multiplied by the appropriate fraction for that monoterpene compound. The 'leftover' field uses the sum of the fractions of the nine non-explicit monoterpenes as the multiplier. The resulting emission number is thus specific to tree species.
'Make ANNUAL Grid'	query	Add 6 new fields: apin, bpin, sabi, dlim, dcar and otrp. Each column contains an expression similar to that for all other species fields in the query.
'CTM parameters'	query	Add 6 new fields: apin, bpin, sabi, dlim, dcar and otrp. Each column contains an expression similar to that for all other species fields in the query.
'Make Emissions'	module	Add commands (.Fields.Append .CreateField) to create 6 new fields when creating the 'EMISSIONS' table: one each for apin, bpin, sabi, dlim, dcar and otrp. Add calculations of the emissions of apin, bpin, sabi, dlim, dcar and sabi, similar to the calculations for the other emitted species.

Figures D1 through D14 show the spatial distributions of  $\alpha$ -pinene,  $\beta$ -pinene, d-limonene,  $\Delta^3$ -carene, sabinene,  $\alpha$ -terpinene,  $\beta$ -phellandrene, camphene,  $\gamma$ -terpinene, myrcene, ocimene, p-cymene, terpinolene, and  $\alpha$ -thujene respectively in the 4km TXAQS modeling for September 1<sup>st</sup>, 2000. The Figures show that the spatial distribution of emissions is not the same for all monoterpenes. This is a result of different monoterpene profiles from different tree species that have non-uniform spatial distributions. A global monoterpene speciation profile, i.e. the same profile for each grid cell, is not accurate. This monoterpene emissions inventory is the most detailed to date in this area. It should be noted that the spatial distributions of the three most abundant monoterpenes ( $\alpha$ -pinene,  $\beta$ -pinene and limonene) are very similar, and so, in this domain, the majority of monoterpenes are distributed the same.

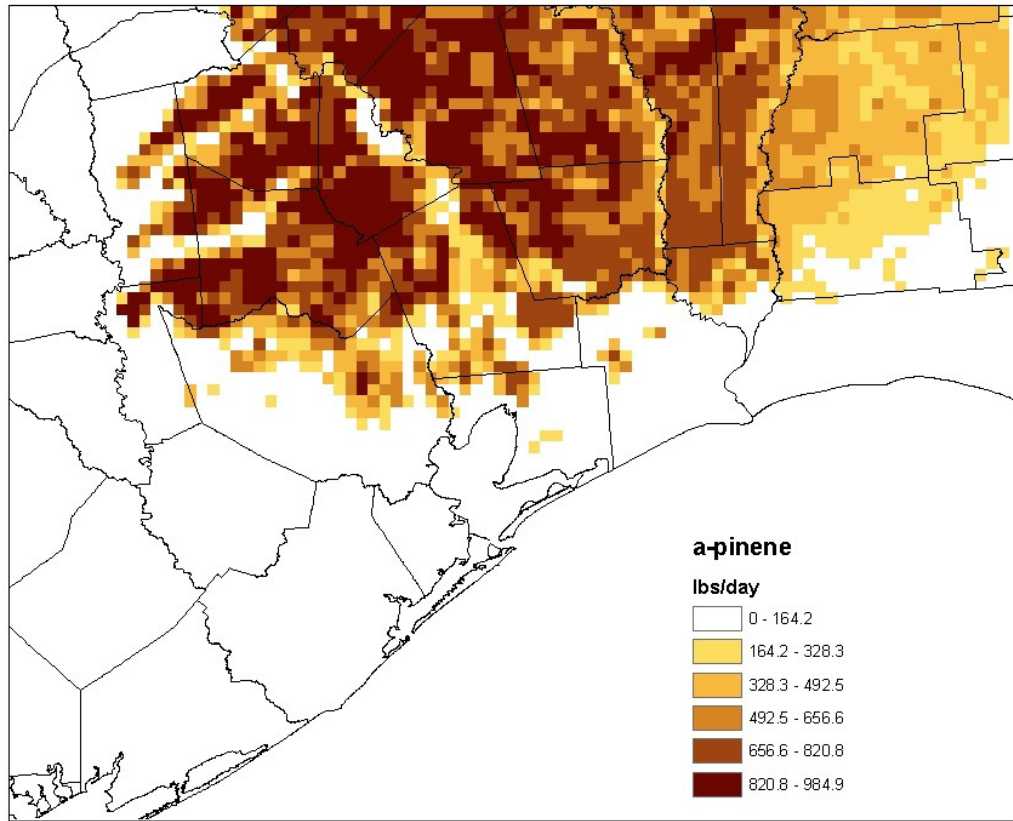


Figure D1. Spatial distribution of  $\alpha$ -pinene emissions in Southeast Texas, in lbs/day on Sep 1<sup>st</sup>, 2000.

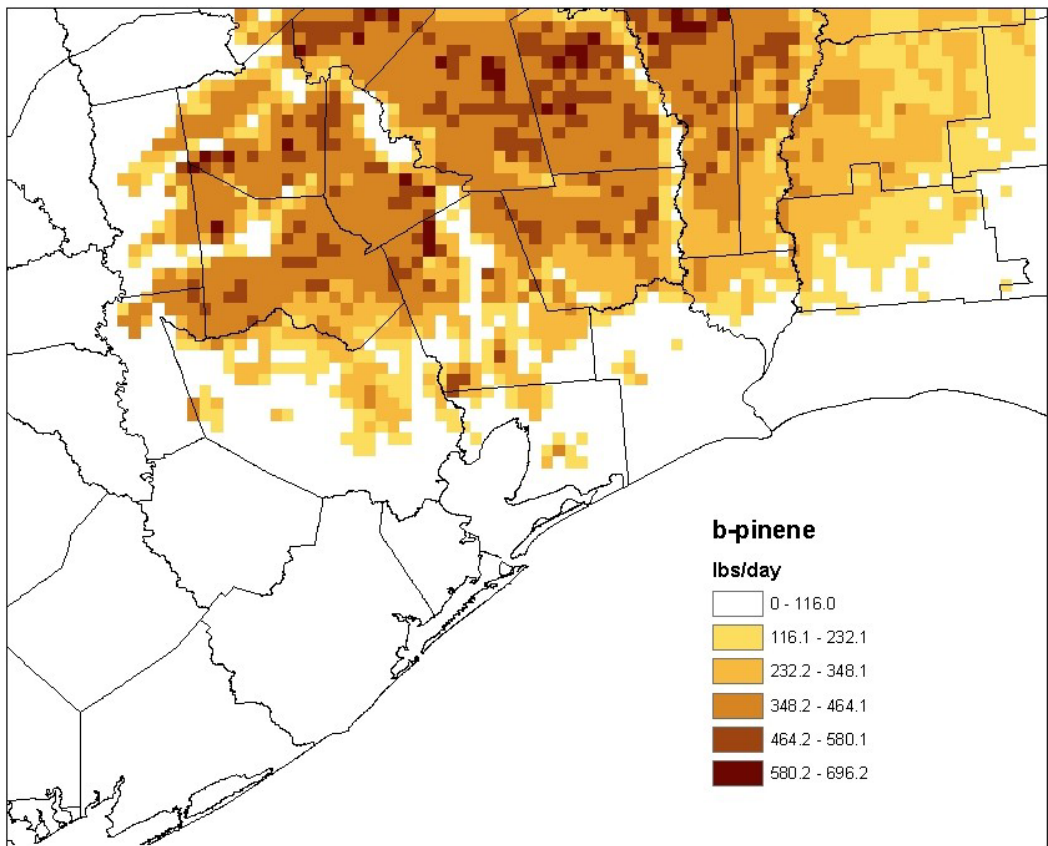


Figure D2. Spatial distribution of  $\beta$ -pinene emissions in Southeast Texas, in lbs/day on Sep 1<sup>st</sup>, 2000.

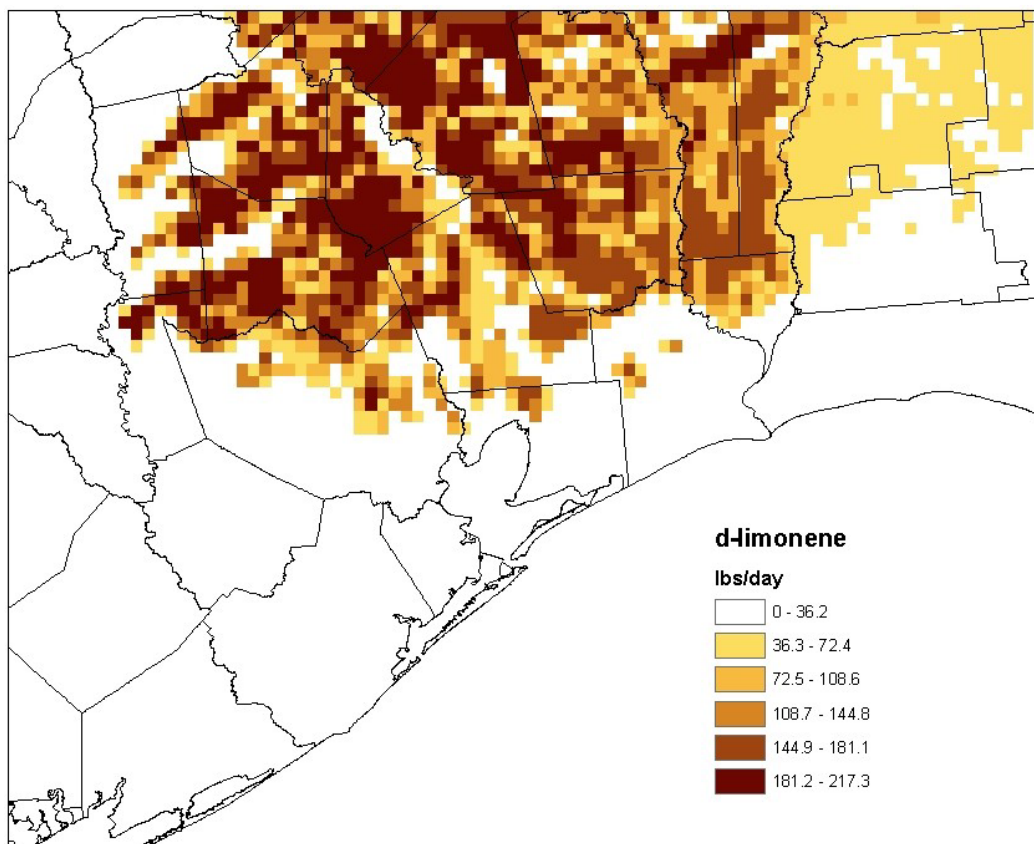


Figure D3. Spatial distribution of d-limonene emissions in Southeast Texas, in lbs/day on Sep 1<sup>st</sup>, 2000.

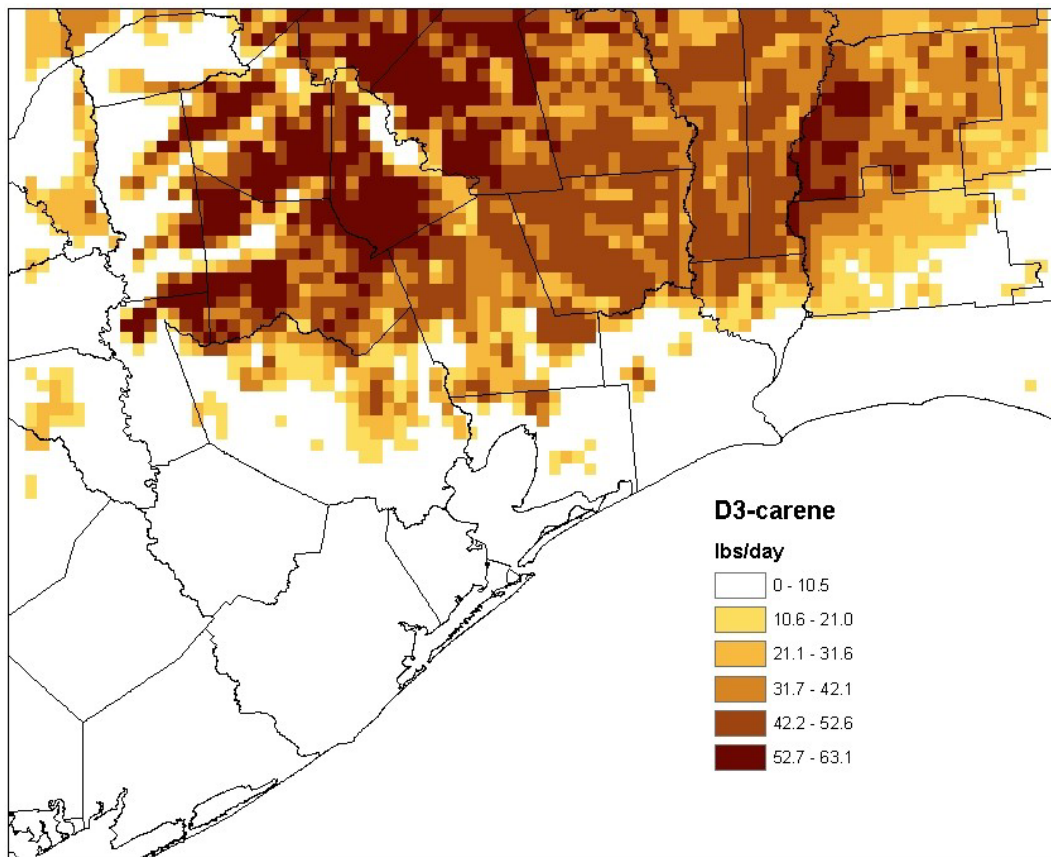


Figure D4. Spatial distribution of  $\Delta^3$ carene emissions in Southeast Texas, in lbs/day on Sep 1<sup>st</sup>, 2000.

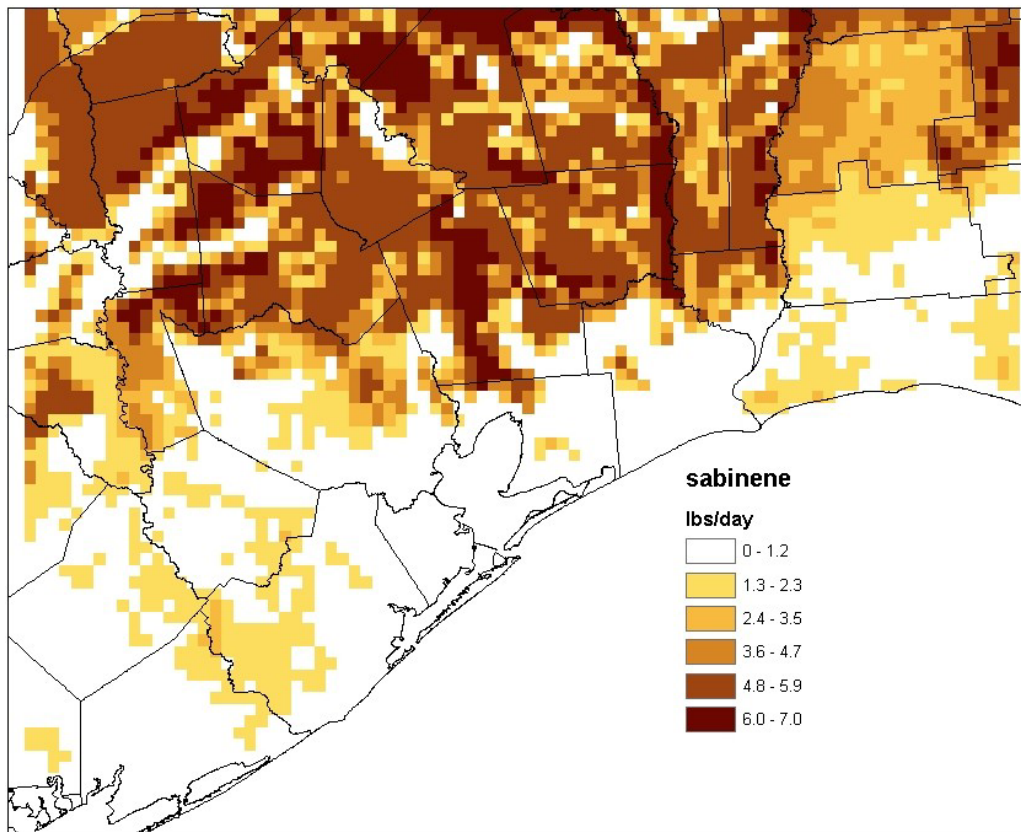


Figure D5. Spatial distribution of sabinene emissions in Southeast Texas, in lbs/day on Sep 1<sup>st</sup>, 2000.

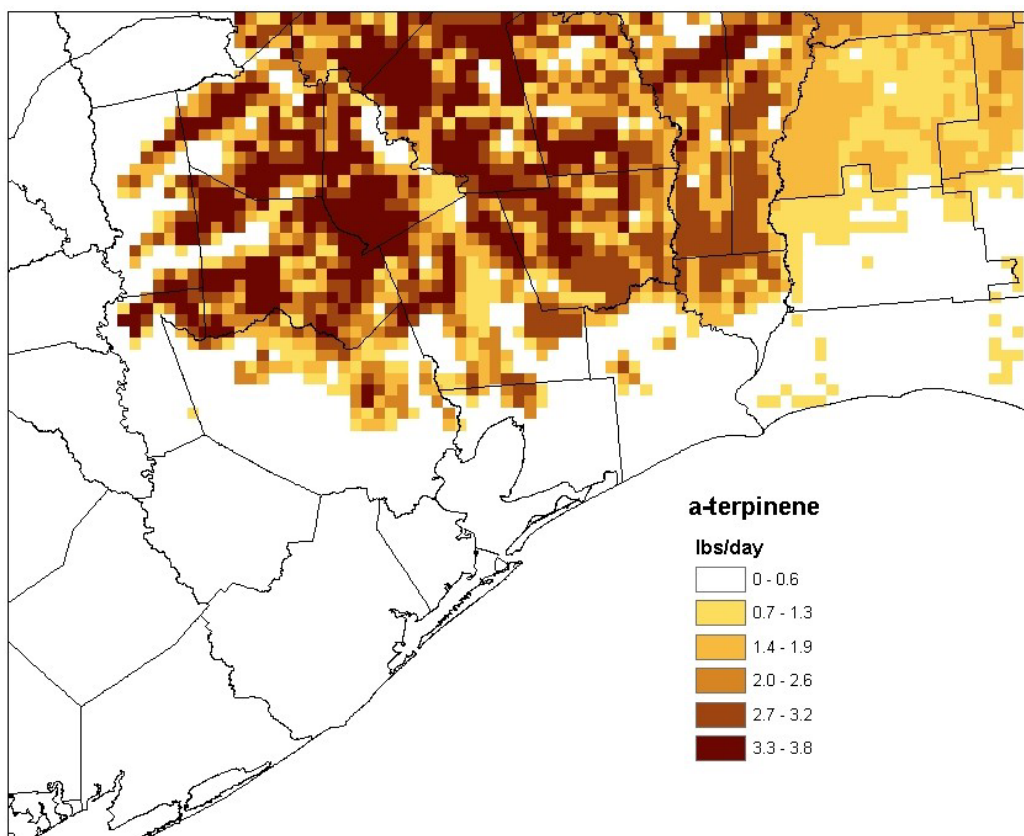


Figure D6. Spatial distribution of  $\alpha$ -terpinene emissions in Southeast Texas, in lbs/day on Sep 1<sup>st</sup>, 2000.

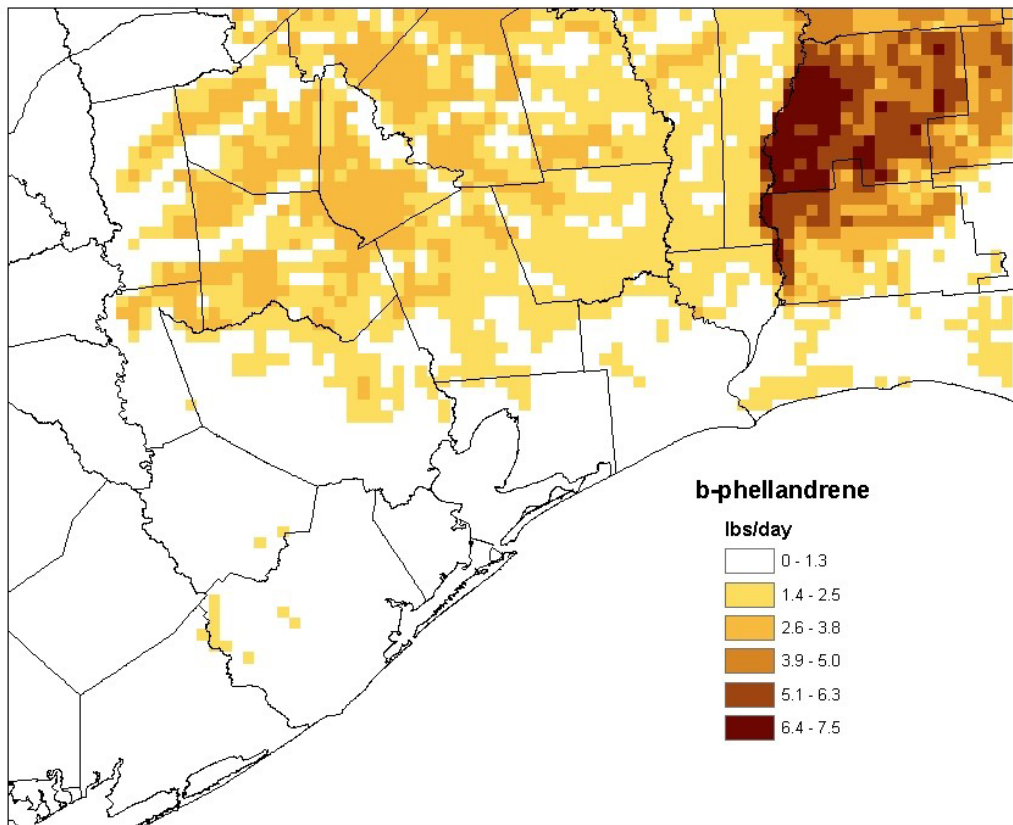


Figure D7. Spatial distribution of  $\beta$ -phellandrene emissions in Southeast Texas, in lbs/day on Sep 1<sup>st</sup>, 2000.

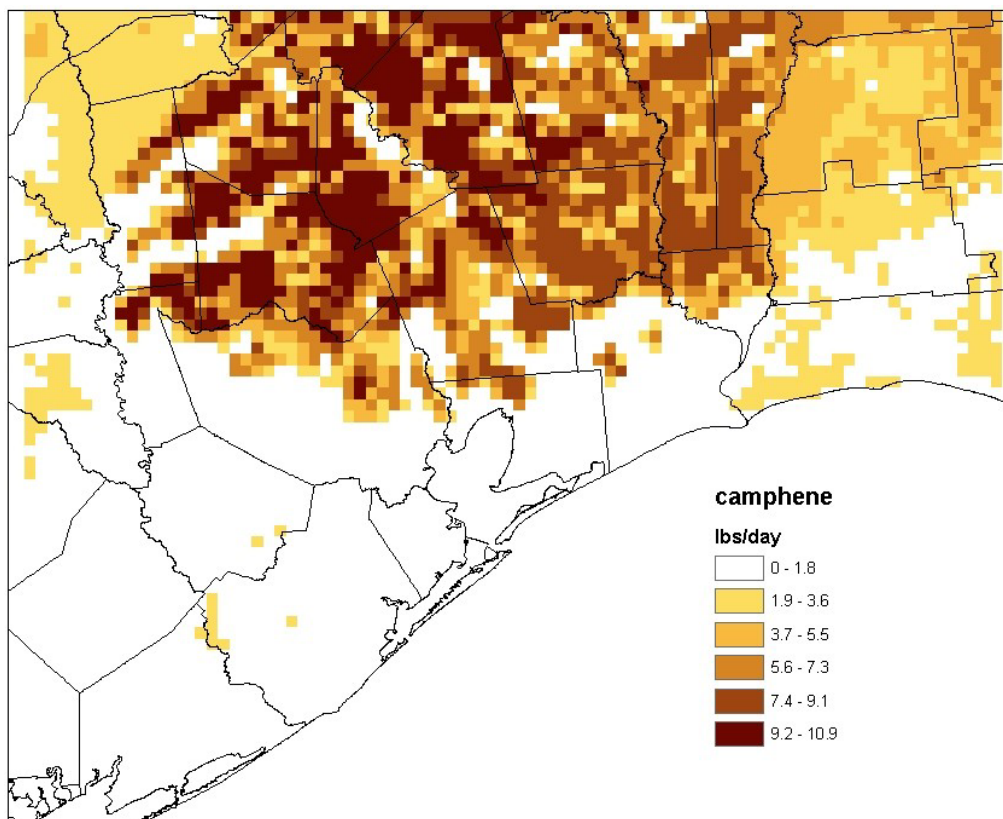


Figure D8. Spatial distribution of camphene emissions in Southeast Texas, in lbs/day on Sep 1<sup>st</sup>, 2000.

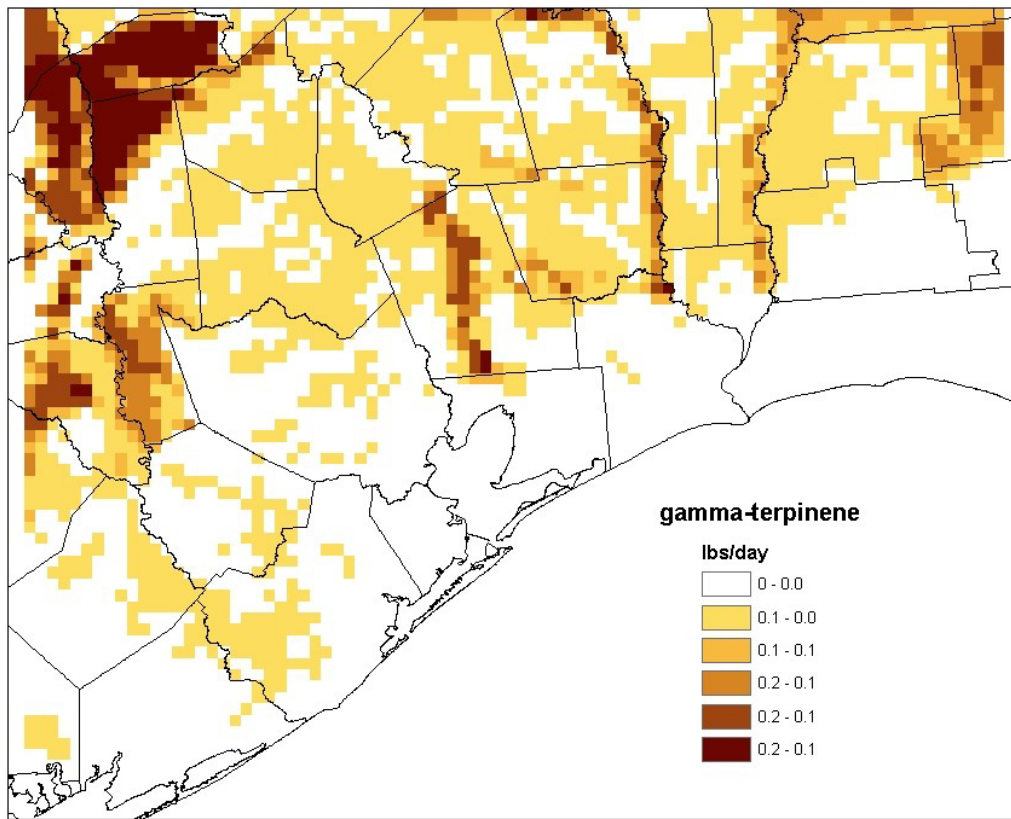


Figure D9. Spatial distribution of  $\gamma$ -terpinene emissions in Southeast Texas, in lbs/day on Sep 1<sup>st</sup>, 2000.

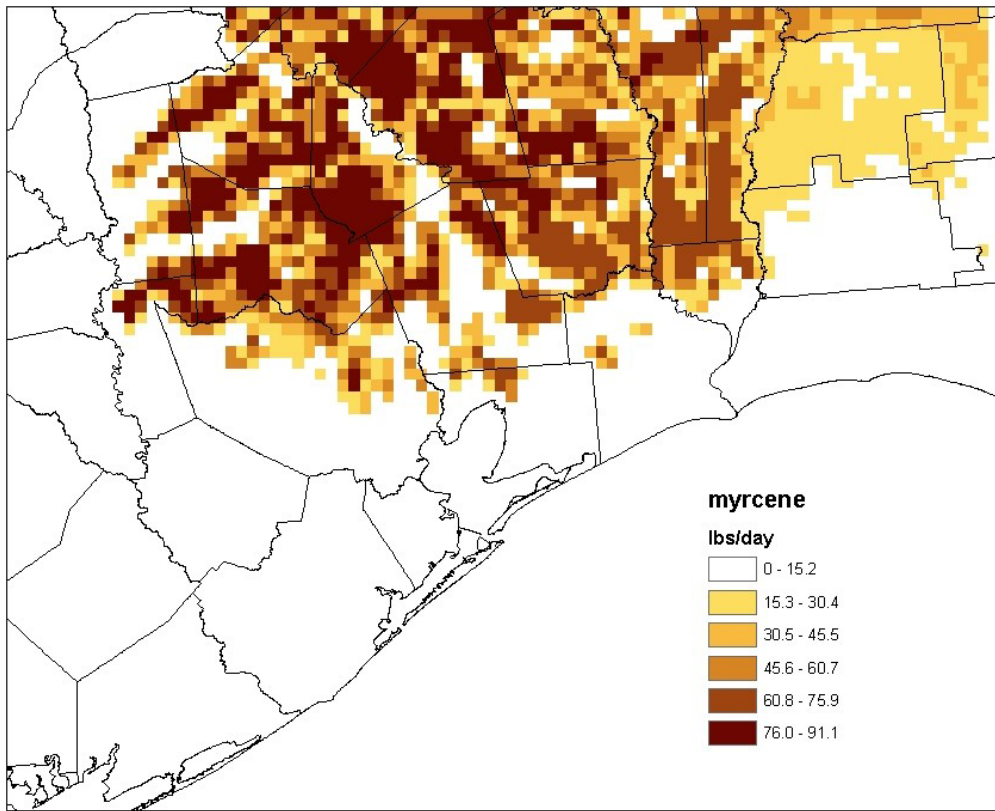


Figure D10. Spatial distribution of myrcene emissions in Southeast Texas, in lbs/day on Sep 1<sup>st</sup>, 2000.

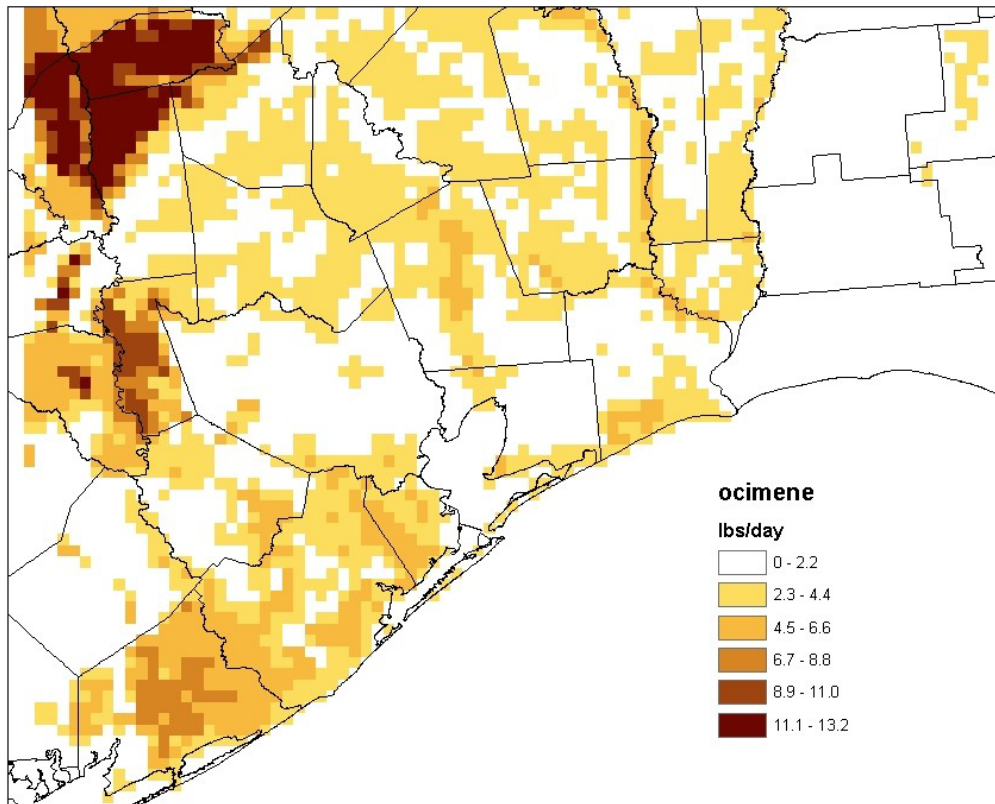


Figure D11. Spatial distribution of ocimene emissions in Southeast Texas, in lbs/day on Sep 1<sup>st</sup>, 2000.

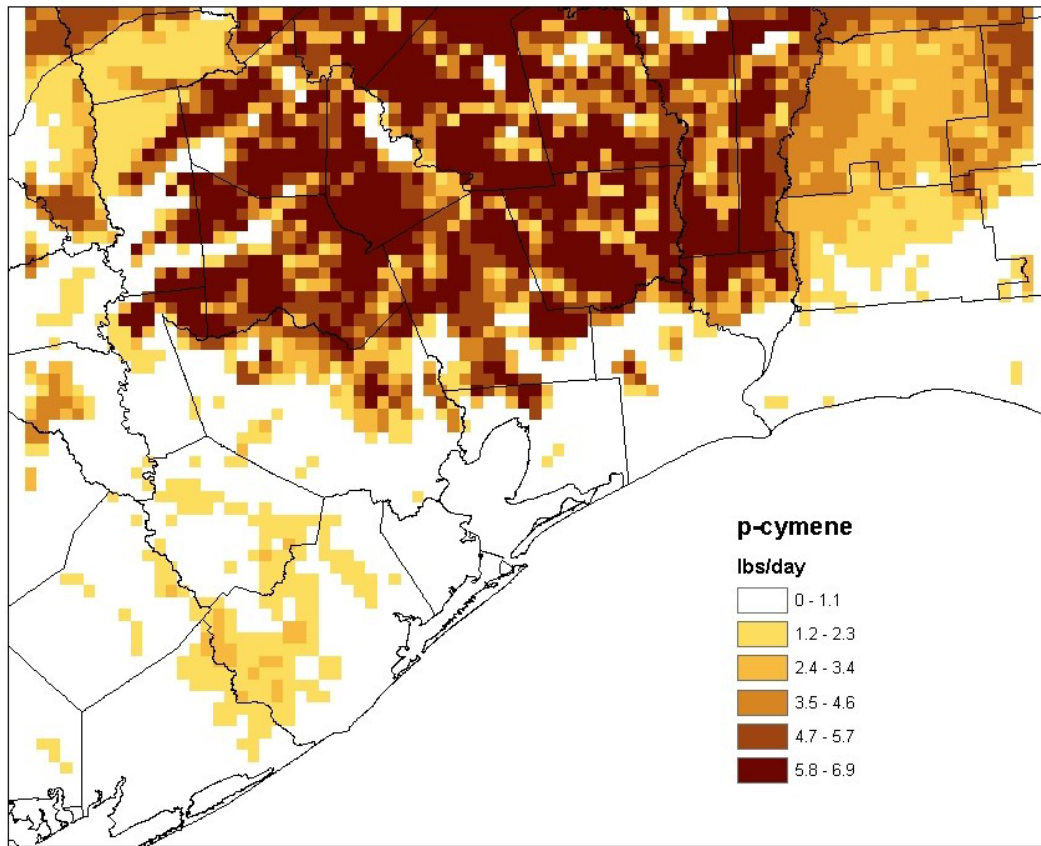


Figure D12. Spatial distribution of p-cymene emissions in Southeast Texas, in lbs/day on Sep 1<sup>st</sup>, 2000.

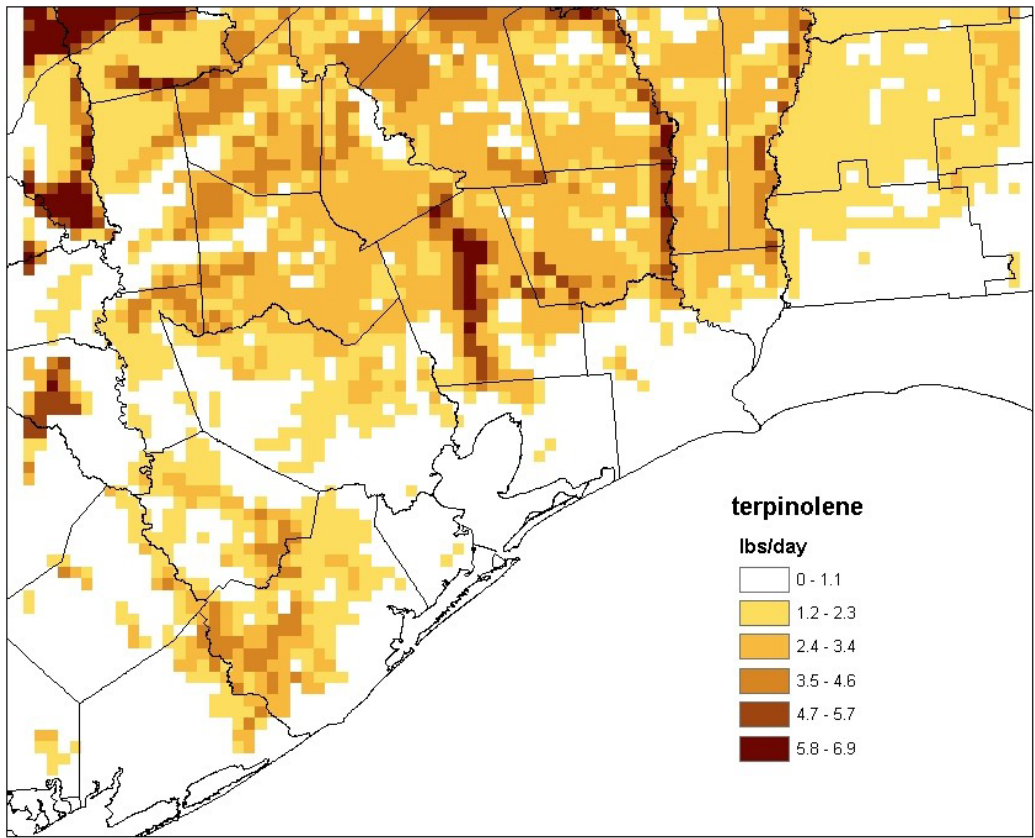


Figure D13. Spatial distribution of terpinolene emissions in Southeast Texas, in lbs/day on Sep 1<sup>st</sup>, 2000.

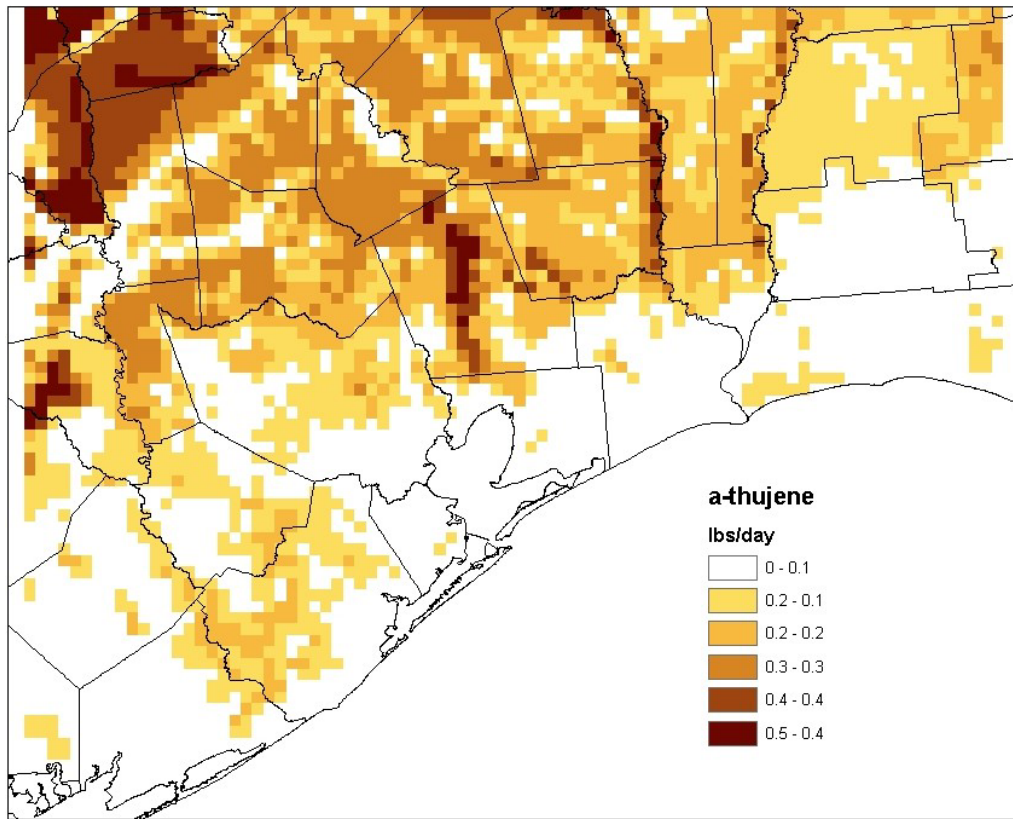


Figure D14. Spatial distribution of  $\alpha$ -thujene emissions in Southeast Texas, in lbs/day on Sep 1<sup>st</sup>, 2000.

### **Calculation of s99 and s99soa emissions from biogenic sources.**

The second set of modifications allowed GLOBEIS2.2 to calculate model species for the s99 and s99soa mechanisms. The model was modified to let the user choose between CB4, s99 or s99soa model species; however, the modifications listed here could easily be implemented to let GLOBEIS2.2 predict emissions for any variation on the SAPRC99 mechanism.

The main difference between s99 and s99soa was that s99soa had five explicit compounds ( $\alpha$ -pinene,  $\beta$ -pinene, sabinene, d-limonene and  $\Delta^3$ -carene), and a 'leftover' monoterpene group. S99 and s99soa had the same model species to represent 'other VOC' emissions. Similar to the CB4 case, a global splitfactor will be included in GLOBEIS2.2 to convert 'other VOC' emissions to s99/s99soa model species. This global splitfactor, presented in Table D3, is based on an average speciation profile of non-isoprene, non-terpene biogenic VOC's and is taken from Guenther et al. (2003). Table D3 also presents the model species associated with this profile, which were created using the emitdb.xls spreadsheet (see Appendix C).

GLOBEIS2.2 was modified to let the user choose to export model species for the cb4, s99, or s99soa mechanism. The choice is made in a new option box in the 'Model Parameters' form, shown in Figure D15. All modifications were designed to allow the original functions of GLOBEIS2.2 to remain undisturbed. All modifications are listed in Table D4.

Table D3: Speciation profile of non-isoprene, non-terpene biogenic VOC's. The original profile was given in mass C. Also shown is mass of each compound (input to emit\_db.xls) and splitfactors for s99/s99soa species (output from emit\_db.xls).

294

compound (1)	mass C (1)	equivalent name in emit_db.xls	unique ID (CAS number)	moles C	C #	moles compound	MW g/mol (2)	total mass of each compound (input to 'Emit Worksheet' in emit_db.xls)	s99 / s99soa species	mols/ g total VOC	
methanol	0.5	methyl alcohol	C67-56-1	0.041628507	1	0.04163	32	1.33211	}		
Ethanol	0.06	ethyl alcohol	C64-17-5	0.004995421	2	0.00250	46.1	0.11514			
acetone	0.1	acetone	C67-64-1	0.008325701	3	0.00278	58.1	0.16124		MEOH	41.59
butanone	0.02	methyl ethyl ketone (mek) (2-butanone)	C78-93-3	0.00166514	4	0.00042	72.1	0.03001		ALK3	2.50
ethane	0.01	ethane	C74-84-0	0.00083257	2	0.00042	30.1	0.01253		ACET	2.78
hexenyl acetate	0.03	n-Hexyl Acetate	C142-92-7	0.00249771	8	0.00031	144.2	0.04502		MEK	0.42
ethene	0.05	ethylene	C74-85-1	0.004162851	2	0.00208	28.1	0.05849		ALK1	0.42
hexenal	0.03	hexanal	C66-25-1	0.00249771	6	0.00042	100.2	0.04171		ALK5	0.73
hexenol	0.03	1-hexanol (n-hexanol)	C111-27-3	0.00249771	6	0.00042	102.2	0.04254		ETHE	2.09
acetaldehyde	0.05	acetaldehyde	C75-07-0	0.004162851	2	0.00208	44.1	0.09179		RCHO	0.69
propene	0.04	propylene	C115-07-1	0.003330281	3	0.00111	42.1	0.04673		CCHO	2.08
butene	0.02	1-butene	C106-98-9	0.00166514	4	0.00042	56.1	0.02335		OLE1	1.53
formaldehyde	0.02	formaldehyde	C50-00-0	0.00166514	1	0.00167	30	0.04995		HCHO	1.66
hexanal	0.02	hexanal	C66-25-1	0.00166514	6	0.00028	100.2	0.02781		ALK2	1.25
acetic acid	0.01	acetic acid	C64-19-7	0.00083257	2	0.00042	60.1	0.02502			
formic acid	0.01	formic acid	C64-18-6	0.00083257	1	0.00083	46	0.03830			

1. Average speciation of non-isoprene, non-terpene biogenic VOC's from Guenther et al. (2003)

2. www.chemfinder.com

Figure D15. ‘Model Parameters’ window in updated version of GLOBEIS2.2. There is now an option box for choosing which mechanism to consider.

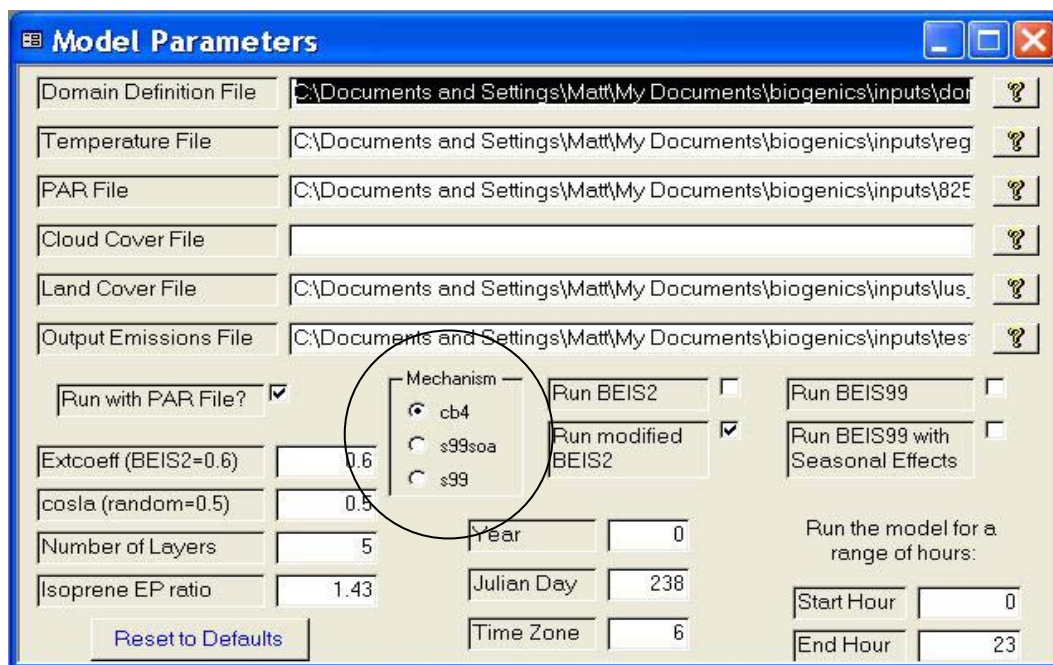


Table D4. Modifications to GLOBEIS2.2 to produce s99 or s99soa model species. These were made in addition to those listed in Table D2 above.

Name	type	Modifications
‘Model_parameters’	table	Added a field ‘Mechanism’ to designate which mechanism to consider.
‘Model_parameters’	form	Added an option box to choose between cb4, s99soa or s99 mechanism. This sets the value of ‘Mechanism’ to 1, 2 or 3 respectively. See Figure D2.
‘Make EMISSIONS mech’ (NEW)	module	Replaces, and similar to ‘Make EMISSIONS CB4’. This module opens ‘Model_parameters’ and checks the value of ‘Mechanism’. If ‘Mechanism’ is equal to 1 (CB4), the module opens the ‘CB4 Constants’ (splitfactors) table and runs the ‘Make CB4 Emissions’ query. If ‘Mechanism’ is equal to 2 or 3, the module

		opens the ‘S99 Constants’ table and runs the ‘Make S99 Emissions’ query.
‘Make S99 Emissions’ (NEW)	query	Similar to ‘Make CB4 Emissions’. This query produces s99 and s99soa model species emissions for each grid cell. TERP, or total monoterpenes, is included, but it is only used if the mechanism is set to s99. The 5 explicit terpenes and a leftover terpene group are also included, but are used only if the mechanism is s99soa. All other model species are common to both s99 and s99soa.
‘S99 Constants’ (NEW)	table	Similar to ‘CB4 Constants’ the table contains the splitfactors for ‘Other VOC’ emissions (reported in Table D3). Note there are no splitfactors for total monoterpenes, because these are explicitly represented in s99 (as TERP) and s99soa (as the five explicit terpenes and ‘leftover’ terpene group).
‘Export Mech Emissions’ (NEW)	module	Replaces, and similar to ‘Export CB4 Emissions’. This module opens ‘Model_parameters’ and checks the value of ‘Mechanism’. Depending on the mechanism the module opens a mechanism-specific query and exports the model species using mechanism-specific export specifications.
‘S99 Emissions to string’ (NEW)	query	Similar to ‘CB4 Emissions to string’ but for s99 model species. The query just formats the model species emissions per grid cell as text. The format specifier ‘0.000’ was added to each field to avoid too many decimal places.
‘S99soa Emissions to string’ (NEW)	query	Similar to ‘CB4 Emissions to string’ but for s99soa model species. The query formats the model species emissions per as text. The format specifier ‘0.000’ was added to each field to avoid too many decimal places.
‘S99 EMISSIONS Export Specification’ (NEW)	ACCESS export spec. file	Similar to ‘CB4 EMISSIONS Export Specification’. Used to export the text s99 species emissions to a comma-separated text file.
‘S99soa EMISSIONS Export	ACCESS export spec. file	Similar to ‘CB4 EMISSIONS Export Specification’. Used to export the text s99soa species emissions to a comma-separated text

Specification' (NEW)		file.
'Cleanup'	module	This module now opens 'Model_parameters' and checks the value of 'Mechanism'. Depending on the mechanism the module deletes the appropriate table.
'Banner'	form	Changed label 'Calculate CB4 Emissions' to 'Calculate Mech Emissions'. The form's code was also modified to open 'Model_parameters' and check the value of 'Mechanism'. Depending on the value of 'Mechanism' the code checks for the existence of the correct table of model species before running the 'Export Mech Emissions' module. Also changed names of variables and module calls to not be specific to CB4.
'CB4 Emissions to string'	query	The query just formats the model species emissions per grid cell as text. The format specifier '0.000' was added to each field to avoid too many decimal places.
'CB4 Constants'	table	Updated splitfactors for 'Other VOC' emissions to data in GLOBEIS version 3 ( <a href="http://www.globeis.com">www.globeis.com</a> ). These new splitfactors are based on the speciation profile given in Table D3 above.

There are a number of features in GLOBEIS2.2 that were not updated to accommodate new mechanisms, such as generating reports and using a user interface to update mechanism-specific splitfactors. These will not work for the additional mechanisms that were added; however, they do not affect the calculation of model species emissions.

## Appendix E: SAPRC99 .RXN Input files for the s99soa and s99soa2 chemical mechanisms

This Appendix contains the .rxn SAPRC input files for both the s99soa and s99soa2 mechanisms. The .rxn files are used to create the source code for the model mechanism, and these files list all reactions, rate constants and stoichiometric coefficients in the mechanism. These files are provided for someone wishing to recreate the mechanisms, and are intended for those familiar with the SAPRC99 modeling software.

### s99soa.rxn

```
!This .rxn includes all reactions in the s99soa mechanism.
!It is based on the original fixed parameter version of SAPRC99
!and is similar to SAPRC99f.rxn, which is distributed with SAPRC99
!
!The following modifications were made for inclusion in CAMx:
!
!1. Modifications to be consistent with CAMx3.10-mech 5:
!   Using only 6 primary photolysis reactions used in mech5
!   The ACROLEIN photolysis reactions equivalent to ISPD in mech5
!   QF for secondary photolysis reactions from mech5 chemparam file
!   Apparant error in mech 5 corrected here: reaction isn3
!       produces 0.813 XN and not 0.813 RNO3 as in mech5.
!   Reaction rates involving HNO4 (or PNA) set to 0 as in mech5
!       i.e. reactions 35,36,37,38. Reaction 37 is assigned
!       a primary photolysis reaction with QY=0.0
!   Specification of STS,ACT,RAD,BLD,CON species to match mech5
!       (listed below)
!
!2. Modifications for modeling SOA:
!   Explicit reactions for APINENE, BPINENE, SABINENE, 3CARENE,
!       LIMONENE
!   Separate reactions for high-yield ARO1, low-yield ARO2
!       high-yield ARO2, no-yield ARO1, no-yield ARO2
!   I relabeled the AR2L (low-yield ARO2) reactions as L2OH to
!       avoid label conflict
!   All lumped model species parameters derived with Texas
!       anthropogenic emissions profile
!
!
!Rate constant in cm3/molec-s units
!
```

```

.STS
O*1D2
O3P
.ACT
= NO + NO2 + O3
= PAN + PAN2 + MA-PAN + PBZN + NPHE + RNO3
= CRES + DCB2 + DCB3 + HNO4
.RAD
= HOCOO. + TBU-O.
= BZ-O. + BZ(NO2)-O.
= N2O5 + NO3 + HO. + HO2. + C-O2.
= RO2-R. + RO2-N. + R2O2.
= CCO-O2. + RCO-O2. + BZCO-O2. + MA-RCO3.
.BLD
= HONO + HNO3 + XN + HO2H + HCHO + CCHO
= RCHO + BALD + BACL + PROD2 + DCB1 + PHEN
= ISOPRENE + ISO-PROD + MVK + METHACRO
= MGLY + GLY + HCOOH + CCO-OH
= CCO-OOH + RCO-OH + RCO-OOH + ACET
= MEK + MEOH + COOH + ROOH + CO + ETHENE
= ALK1 + ALK2 + ALK3 + ALK4 + ALK5
= AR1H + AR2H + AR2L + AR1N + AR2N
= OLE1 + OLE2 + TERP
= A-PINENE + B-PINENE + D-LIMONE
= 3-CARENE + SABINENE
= SO2 + SULF
.DUMSLO
NXOY
.CON
O2      2.09e+5
M        1.00e+6
H2O     2.00e+4
H2       0.50e+0
HV       1.00e+0
CH4     1.75e+0
.RXN
1)      PF=NO2                ;NO2 + HV = NO + O3P
2)      5.68e-34 0.000 -2.80   ;O3P + O2 + M = O3 + M
3)      8.00e-12 4.094 0.00    ;O3P + O3 = #2 O2
4)      1.00e-31 0.000 -1.60   ;O3P + NO + M = NO2 + M
5)      6.50e-12 -0.238 0.00   ;O3P + NO2 = NO + O2
6)      FALLOFF                ;O3P + NO2 = NO3 + M
      9.00e-32 0.000 -2.00
      2.20e-11 0.000 0.00
      0.80 1.0
8)      1.80e-12 2.722 0.00    ;O3 + NO = NO2 + O2
9)      1.40e-13 4.908 0.00    ;O3 + NO2 = O2 + NO3
10)     1.80e-11 -0.219 0.00   ;NO + NO3 = #2 NO2
11)     3.30e-39 -1.053 0.00   ;NO + NO + O2 = #2 NO2
12)     FALLOFF                ;NO2 + NO3 = N2O5
      2.80e-30 0.000 -3.50
      2.00e-12 0.000 0.20
      0.45 1.0
13)     FALLOFF                ;N2O5 = NO2 + NO3
      1.00e-03 21.859 -3.50
      9.70e+14 22.018 0.10
      0.45 1.0
14)     2.60e-22                ;N2O5 + H2O = #2 HNO3
17)     4.50e-14 2.504 0.00    ;NO2 + NO3 = NO + NO2 + O2
18)     PF=NO2 QY=2.379E+0     ;NO3 + HV = NO + O2
19)     PF=NO2 QY=2.199E+1     ;NO3 + HV = NO2 + O3P
20)     PF=NO2 QY=5.063E-2     ;O3 + HV = O3P + O2

```

21) PF=O3O1D ;O3 + HV = O\*1D2 + O2  
 22) 2.20e-10 ;O\*1D2 + H2O = #2 HO.  
 23) 2.09e-11 -0.189 0.00 ;O\*1D2 + M = O3P + M  
 24) FALLOFF ;HO. + NO = HONO  
 7.00e-31 0.000 -2.60  
 3.60e-11 0.000 -0.10  
 0.60 1.0  
 25) PF=NO2 QY=1.923E-1 ;HONO + HV = HO. + NO  
 26) PF=ACROLEIN QY=1.190E+2 ;HONO + HV = HO2. + NO2  
 27) 2.70e-12 -0.517 0.00 ;HO. + HONO = H2O + NO2  
 28) FALLOFF ;HO. + NO2 = HNO3  
 2.43e-30 0.000 -3.10  
 1.67e-11 0.000 -2.10  
 0.60 1.0  
 29) 2.00e-11 ;HO. + NO3 = HO2. + NO2  
 30) K0+K3M/1+K3M/K2 ;HO. + HNO3 = H2O + NO3  
 7.20e-15 -1.560 0.00  
 4.10e-16 -2.862 0.00  
 1.90e-33 -1.441 0.00  
 31) PF=HCHO\_R QY=2.177E-2 ;HNO3 + HV = HO. + NO2  
 32) K1+K2[M] ;HO. + CO = HO2. + CO2  
 1.30e-13  
 3.19e-33  
 33) 1.90e-12 1.987 0.00 ;HO. + O3 = HO2. + O2  
 34) 3.40e-12 -0.537 0.00 ;HO2. + NO = HO. + NO2  
 35) 0.0 ;HO2. + NO2 = HNO4  
 36) 0.0 ;HNO4 = HO2. + NO2  
 37) PF=HCHO\_R QY=0.0 ;HNO4 + HV = #.61 [HO2. + NO2] + #.39 [HO. + NO3]  
 38) 0.0 ;HNO4 + HO. = H2O + NO2 + O2  
 39) 1.40e-14 1.192 0.00 ;HO2. + O3 = HO. + #2 O2  
 40A) K1+K2[M] ;HO2. + HO2. = HO2H + O2  
 2.20e-13 -1.192 0.00  
 1.85e-33 -1.947 0.00  
 40B) K1+K2[M] ;HO2. + HO2. + H2O = HO2H + O2 + H2O  
 3.08e-34 -5.564 0.00  
 2.59e-54 -6.319 0.00  
 41) 4.00e-12 ;NO3 + HO2. = #.8 [HO. + NO2 + O2] + #.2 [HNO3 + O2]  
 42) 8.50e-13 4.869 0.00 ;NO3 + NO3 = #2 NO2 + O2  
 43) PF=HCHO\_M QY=1.709E-1 ;HO2H + HV = #2 HO.  
 44) 2.90e-12 0.318 0.00 ;HO2H + HO. = HO2. + H2O  
 45) 4.80e-11 -0.497 0.00 ;HO. + HO2. = H2O + O2  
 S2OH) FALLOFF ;HO. + SO2 = HO2. + SULF  
 4.00e-31 0.000 -3.30  
 2.00e-12 0.000 0.00  
 0.45 1.0  
 H2OH) 7.70e-12 4.173 0.00 ;HO. + H2 = HO2. + H2O  
 MER1) 2.80e-12 -0.566 0.00 ;C-O2. + NO = NO2 + HCHO + HO2.  
 MER4) 3.80e-13 -1.550 0.00 ;C-O2. + HO2. = COOH + O2  
 MEN3) 1.30e-12 ;C-O2. + NO3 = HCHO + HO2. + NO2  
 MER5) 2.45e-14 -1.410 0.00 ;C-O2. + C-O2. = MEOH + HCHO + O2  
 MER6) 5.90e-13 1.011 0.00 ;C-O2. + C-O2. = #2 [HCHO + HO2.]  
 RRNO) 2.70e-12 -0.715 0.00 ;RO2-R. + NO = NO2 + HO2.  
 RRH2) 1.90e-13 -2.583 0.00 ;RO2-R. + HO2. = ROOH + O2 + #-3 XC  
 RRN3) 2.30e-12 ;RO2-R. + NO3 = NO2 + O2 + HO2.  
 RRME) 2.00e-13 ;RO2-R. + C-O2. = HO2. + #.75 HCHO + #.25 MEOH  
 RRR2) 3.50e-14 ;RO2-R. + RO2-R. = HO2.  
 R2NO) SAMEK RRNO ;R2O2. + NO = NO2  
 R2H2) SAMEK RRH2 ;R2O2. + HO2. = HO2.  
 R2N3) SAMEK RRN3 ;R2O2. + NO3 = NO2  
 R2ME) SAMEK RRME ;R2O2. + C-O2. = C-O2.  
 R2RR) SAMEK RRR2 ;R2O2. + RO2-R. = RO2-R.

R2R3) SAMEK RRR2 ;R2O2. + R2O2. =  
RNN0) SAMEK RRNO ;RO2-N. + NO = RNO3  
RNH2) SAMEK RRH2 ;RO2-N. + HO2. = ROOH + #3 XC  
RNME) SAMEK RRME ;RO2-N. + C-O2. = HO2. + #.25 MEOH + #.5 [MEK +  
PROD2] + #.75 HCHO + XC  
RNN3) SAMEK RRN3 ;RO2-N. + NO3 = NO2 + O2 + HO2. + MEK + #2 XC  
RNR2) SAMEK RRR2 ;RO2-N. + R2O2. = RO2-N.  
RNRN) SAMEK RRR2 ;RO2-N. + RO2-N. = MEK + HO2. + PROD2 + O2 + #2 XC  
APN2) FALLOFF ;CCO-O2. + NO2 = PAN  
2.70e-28 0.000 -7.10  
1.20e-11 0.000 -0.90  
0.30 1.0  
DPAN) FALLOFF ;PAN = CCO-O2. + NO2  
4.90e-03 24.045 0.00  
4.00e+16 27.026 0.00  
0.30 1.0  
APNO) 7.80e-12 -0.596 ;CCO-O2. + NO = C-O2. + CO2 + NO2  
APH2) 4.30e-13 -2.067 0.00 ;CCO-O2. + HO2. = #.75 [CCO-OOH +O2] +  
#.25 [CCO-OH + O3]  
APN3) 4.00e-12 ;CCO-O2. + NO3 = C-O2. + CO2 + NO2 + O2  
APME) 1.80e-12 -0.994 0.00 ;CCO-O2. + C-O2. = CCO-OH + HCHO + O2  
APRR) 7.50e-12 ;CCO-O2. + RO2-R. = CCO-OH  
APR2) SAMEK APRR ;CCO-O2. + R2O2. = CCO-O2.  
APRN) SAMEK APRR ;CCO-O2. + RO2-N. = CCO-OH + PROD2  
APAP) 2.90e-12 -0.994 0.00 ;CCO-O2. + CCO-O2. = #2 [C-O2. + CO2] + O2  
PPN2) 1.20e-11 0.000 -0.90 ;RCO-O2. + NO2 = PAN2  
PAN2) 2.00e+15 25.436 0.00 ;PAN2 = RCO-O2. + NO2  
PPNO) 1.25e-11 -0.477 ;RCO-O2. + NO = NO2 + CCHO + RO2-R. + CO2  
PPH2) SAMEK APH2 ;RCO-O2. + HO2. = #.75 [RCO-OOH + O2] +  
#.25 [RCO-OH + O3]  
PPN3) SAMEK APN3 ;RCO-O2. + NO3 = NO2 + CCHO + RO2-R. + CO2 + O2  
PPME) SAMEK APME ;RCO-O2. + C-O2. = RCO-OH + HCHO + O2  
PPRR) SAMEK APRR ;RCO-O2. + RO2-R. = RCO-OH + O2  
PPR2) SAMEK APRR ;RCO-O2. + R2O2. = RCO-O2.  
PPRN) SAMEK APRR ;RCO-O2. + RO2-N. = RCO-OH + PROD2 + O2  
PPAP) SAMEK APAP ;RCO-O2. + CCO-O2. = #2 CO2 + C-O2. + CCHO +  
RO2-R. + O2  
PPPP) SAMEK APAP ;RCO-O2. + RCO-O2. = #2 [CCHO + RO2-R. + CO2]  
BPN2) 1.37e-11 ;BZCO-O2. + NO2 = PBZN  
BPAN) 7.90e+16 27.821 0.00 ;PBZN = BZCO-O2. + NO2  
BPNO) SAMEK PPNO ;BZCO-O2. + NO = NO2 + CO2 + BZ-O. + R2O2.  
BPH2) SAMEK APH2 ;BZCO-O2. + HO2. = #.75 [RCO-OOH + O2] +  
#.25 [RCO-OH + O3] + #4 XC  
BPN3) SAMEK APN3 ;BZCO-O2. + NO3 = NO2 + CO2 + BZ-O. + R2O2. + O2  
BPME) SAMEK APME ;BZCO-O2. + C-O2. = RCO-OH + HCHO + O2 + #4 XC  
BPRR) SAMEK APRR ;BZCO-O2. + RO2-R. = RCO-OH + O2 + #4 XC  
BPR2) SAMEK APRR ;BZCO-O2. + R2O2. = BZCO-O2.  
BPRN) SAMEK APRR ;BZCO-O2. + RO2-N. = RCO-OH + PROD2 + O2 + #4 XC  
BPAP) SAMEK APAP ;BZCO-O2. + CCO-O2. = #2 CO2 + C-O2. + BZ-O. +  
R2O2.  
BPPP) SAMEK APAP ;BZCO-O2. + RCO-O2. = #2 CO2 + CCHO + RO2-R. +  
BZ-O. + R2O2.  
BBBP) SAMEK APAP ;BZCO-O2. + BZCO-O2. = #2 [BZ-O. + R2O2. + CO2]  
MPN2) SAMEK PPN2 ;MA-RCO3. + NO2 = MA-PAN  
MPPN) 1.60e+16 26.800 0.00 ;MA-PAN = MA-RCO3. + NO2  
MPNO) SAMEK PPNO ;MA-RCO3. + NO = NO2 + CO2 + HCHO + CCO-O2.  
MPH2) SAMEK APH2 ;MA-RCO3. + HO2. = #.75 [RCO-OOH + O2] +  
#.25 [RCO-OH + O3] + XC  
MPN3) SAMEK APN3 ;MA-RCO3. + NO3 = NO2 + CO2 + HCHO + CCO-O2. + O2  
MPME) SAMEK APME ;MA-RCO3. + C-O2. = RCO-OH + HCHO + XC + O2

MPRR) SAMEK APRR ;MA-RCO3. + RO2-R. = RCO-OH + XC  
 MPR2) SAMEK APRR ;MA-RCO3. + R2O2. = MA-RCO3.  
 MPRN) SAMEK APRR ;MA-RCO3. + RO2-N. = #2 RCO-OH + O2 + #4 XC  
 MPAP) SAMEK APAP ;MA-RCO3. + CCO-O2. = #2 CO2 + C-O2. + HCHO +  
 CCO-O2. + O2  
 MPPP) SAMEK APAP ;MA-RCO3. + RCO-O2. = HCHO + CCO-O2. + CCHO +  
 RO2-R. + #2 CO2  
 MPBP) SAMEK APAP ;MA-RCO3. + BZCO-O2. = HCHO + CCO-O2. + BZ-O. +  
 R2O2. + #2 CO2  
 MPMP) SAMEK APAP ;MA-RCO3. + MA-RCO3. = #2 [HCHO + CCO-O2. + CO2]  
 TBON) 2.40e-11 ;TBU-O. + NO2 = RNO3 + #-2 XC  
 TBOD) 7.50e+14 16.200 0.00 ;TBU-O. = ACET + C-O2.  
 BRN2) 2.30e-11 -0.298 0.00 ;BZ-O. + NO2 = NPHE  
 BRH2) SAMEK RRH2 ;BZ-O. + HO2. = PHEN  
 BRXX) 1.00e-03 ;BZ-O. = PHEN  
 BNN2) SAMEK BRN2 ;BZ(NO2)-O. + NO2 = #2 XN + #6 XC  
 BNH2) SAMEK RRH2 ;BZ(NO2)-O. + HO2. = NPHE  
 BNXX) SAMEK BRXX ;BZ(NO2)-O. = NPHE  
 FAHV) PF=HCHO\_R ;HCHO + HV = #2 HO2. + CO  
 FAVS) PF=HCHO\_M ;HCHO + HV = H2 + CO  
 FAOH) 8.60e-12 -0.040 0.00 ;HCHO + HO. = HO2. + CO + H2O  
 FAH2) 9.70e-15 -1.242 0.00 ;HCHO + HO2. = HOCOO.  
 FAHR) 2.40e+12 13.910 0.00 ;HOCOO. = HO2. + HCHO  
 FAHN) SAMEK MER1 ;HOCOO. + NO = HCOOH + NO2 + HO2.  
 FAN3) 2.00e-12 4.830 0.00 ;HCHO + NO3 = HNO3 + HO2. + CO  
 AAOH) 5.60e-12 -0.616 0.00 ;CCHO + HO. = CCO-O2. + H2O  
 AAHV) PF=CCHO\_R ;CCHO + HV = CO + HO2. + C-O2.  
 AAN3) 1.40e-12 3.696 0.00 ;CCHO + NO3 = HNO3 + CCO-O2.  
 PAOH) 2.00e-11 ;RCHO + HO. = #.034 RO2-R. + #.001 RO2-N. +  
 #.965 RCO-O2. + #.034 CO + #.034 CCHO +  
 #-0.003 XC  
 PAHV) PF=HCHO\_R QY=5.749E-1 ;RCHO + HV = CCHO + RO2-R. + CO + HO2.  
 PAN3) 1.40e-12 3.520 ;RCHO + NO3 = HNO3 + RCO-O2.  
 K3OH) 1.10e-12 1.033 0.00 ;ACET + HO. = HCHO + CCO-O2. + R2O2.  
 K3HV) PF=CCHO\_R QY=9.448E-2 ;ACET + HV = CCO-O2. + C-O2.  
 K4OH) 1.30e-12 0.050 2.00 ;MEK + HO. = #.37 RO2-R. + #.042 RO2-N. +  
 #.616 R2O2. + #.492 CCO-O2. + #.096 RCO-O2. +  
 #.115 HCHO + #.482 CCHO + #.37 RCHO + #.287 XC  
 K4HV) PF=CCHO\_R QY=3.507E-1 ;MEK + HV = CCO-O2. + CCHO + RO2-R.  
 MeOH) 3.10e-12 0.715 2.00 ;MEOH + HO. = HCHO + HO2.  
 MER9) 2.90e-12 -0.378 0.00 ;COOH + HO. = H2O + #.35 [HCHO + HO.] + #.65 C-O2.  
 MERA) PF=HCHO\_M QY=1.193E-1 ;COOH + HV = HCHO + HO2. + HO.  
 LPR9) 1.10e-11 ;ROOH + HO. = H2O + RCHO + #.34 RO2-R. + #.66 HO.  
 LPRA) PF=HCHO\_M QY=1.193E-1 ;ROOH + HV = RCHO + HO2. + HO.  
 GLHV) PF=ACROLEIN QY=6.181E+1 ;GLY + HV = #2 [CO + HO2.]  
 GLVM) PF=NO2 QY=1.582E-3 ;GLY + HV = HCHO + CO  
 GLOH) 1.10e-11 ;GLY + HO. = #.63 HO2. + #1.26 CO + #.37 RCO-O2. +  
 #- .37 XC  
 GLN3) 2.80e-12 4.722 ;GLY + NO3 = HNO3 + #.63 HO2. + #1.26 CO +  
 #.37 RCO-O2. + #- .37 XC  
 MGHV) PF=NO2 QY=1.631E-2 ;MGLY + HV = HO2. + CO + CCO-O2.  
 MGOH) 1.50e-11 ;MGLY + HO. = CO + CCO-O2.  
 MGN3) 1.40e-12 3.765 ;MGLY + NO3 = HNO3 + CO + CCO-O2.  
 BAHV) PF=NO2 QY=2.800E-2 ;BACL + HV = #2 CCO-O2.  
 PHOH) 2.63e-11 ;PHEN + HO. = #.24 BZ-O. + #.76 RO2-R. + #.23 GLY +  
 #4.1 XC  
 PHN3) 3.78e-12 ;PHEN + NO3 = HNO3 + BZ-O.  
 CROH) 4.20e-11 ;CRES + HO. = #.24 BZ-O. + #.76 RO2-R. +  
 #.23 MGLY + #4.87 XC  
 CRN3) 1.37e-11 ;CRES + NO3 = HNO3 + BZ-O. + XC  
 NPN3) SAMEK PHN3 ;NPHE + NO3 = HNO3 + BZ(NO2)-O.  
 BZOH) 1.29e-11 ;BALD + HO. = BZCO-O2.

BZHV) PF=ACROLEIN QY=2.250E+1;BALD + HV = #7 XC  
 BZNT) 1.40e-12 3.720 0.00 ;BALD + NO3 = HNO3 + BZCO-O2.  
 MAOH) 1.86e-11 -0.350 0.00 ;METHACRO + HO. = #.5 RO2-R. + #.416 CO +  
 #.084 HCHO + #.416 MEK + #.084 MGLY +  
 #.5 MA-RCO3. + #-0.416 XC  
 MAO3) 1.36e-15 4.200 0.00 ;METHACRO + O3 = #.008 HO2. + #.1 RO2-R. +  
 #.208 HO. + #.1 RCO-O2. + #.45 CO + #.117 CO2 +  
 #.2 HCHO + #.9 MGLY + #.333 HCOOH + #-0.1 XC  
 MAN3) 1.50e-12 3.430 0.00 ;METHACRO + NO3 = #.5 [HNO3 + RO2-R. + CO +  
 MA-RCO3.] + #1.5 XC + #.5 XN  
 MAOP) 6.34e-12 ;METHACRO + O3P = RCHO + XC  
 MAHV) PF=ACROLEIN QY=1.000 ;METHACRO + HV = #.34 HO2. + #.33 RO2-R. +  
 #.33 HO. + #.67 CCO-O2. + #.67 CO + #.67 HCHO +  
 #.33 MA-RCO3. + #-0 XC  
 MVOH) 4.14e-12 -0.900 0.00 ;MVK + HO. = #.3 RO2-R. + #.025 RO2-N. +  
 #.675 R2O2. + #.675 CCO-O2. + #.3 HCHO +  
 #.675 RCHO + #.3 MGLY + #-0.725 XC  
 MVO3) 7.51e-16 3.020 0.00 ;MVK + O3 = #.064 HO2. + #.05 RO2-R. + #.164 HO. +  
 #.05 RCO-O2. + #.475 CO + #.124 CO2 + #.1 HCHO +  
 #.95 MGLY + #.351 HCOOH + #-0.05 XC  
 MVOP) 4.32e-12 ;MVK + O3P = #.45 RCHO + #.55 MEK + #.45 XC  
 MVHV) PF=ACROLEIN QY=5.122E-1;MVK + HV = #.3 C-O2. + #.7 CO + #.7 PROD2 +  
 #.3 MA-RCO3. + #-2.4 XC  
 IPOH) 6.19e-11 ;ISO-PROD + HO. = #.67 RO2-R. + #.041 RO2-N. +  
 #.289 MA-RCO3. + #.336 CO + #.055 HCHO +  
 #.129 CCHO + #.013 RCHO + #.15 MEK + #.332 PROD2 +  
 #.15 GLY + #.174 MGLY + #-0.504 XC  
 IPO3) 4.18e-18 ;ISO-PROD + O3 = #.4 HO2. + #.048 RO2-R. +  
 #.048 RCO-O2. + #.285 HO. + #.498 CO + #.14 CO2 +  
 #.125 HCHO + #.047 CCHO + #.21 MEK + #.023 GLY +  
 #.742 MGLY + #.1 HCOOH + #.372 RCO-OH + #-0.33 XC  
 IPN3) 1.00e-13 ;ISO-PROD + NO3 = #.799 RO2-R. + #.051 RO2-N. +  
 #.15 MA-RCO3. + #.572 CO + #.15 HNO3 +  
 #.227 HCHO + #.218 RCHO + #.008 MGLY +  
 #.572 RNO3 + #.28 XN + #-0.815 XC  
 IPHV) PF=ACROLEIN ;ISO-PROD + HV = #1.233 HO2. + #.467 CCO-O2. +  
 #.3 RCO-O2. + #1.233 CO + #.3 HCHO + #.467 CCHO +  
 #.233 MEK + #-0.233 XC  
 K6OH) 1.50e-11 ;PROD2 + HO. = #.379 HO2. + #.473 RO2-R. +  
 #.07 RO2-N. + #.029 CCO-O2. + #.049 RCO-O2. +  
 #.213 HCHO + #.084 CCHO + #.558 RCHO + #.115 MEK +  
 #.329 PROD2 + #.886 XC  
 K6HV) PF=HCHO\_M QY=1.590E-2 ;PROD2 + HV = #.96 RO2-R. + #.04 RO2-N. +  
 #.515 R2O2. + #.667 CCO-O2. + #.333 RCO-O2. +  
 #.506 HCHO + #.246 CCHO + #.71 RCHO + #.299 XC  
 RNOH) 7.80e-12 ;RNO3 + HO. = #.338 NO2 + #.113 HO2. +  
 #.376 RO2-R. + #.173 RO2-N. + #.596 R2O2. +  
 #.01 HCHO + #.439 CCHO + #.213 RCHO + #.006 ACET +  
 #.177 MEK + #.048 PROD2 + #.31 RNO3 + #.351 XN +  
 #.56 XC  
 RNHV) PF=HCHO\_R QY=9.686E-2 ;RNO3 + HV = NO2 + #.341 HO2. + #.564 RO2-R. +  
 #.095 RO2-N. + #.152 R2O2. + #.134 HCHO +  
 #.431 CCHO + #.147 RCHO + #.02 ACET + #.243 MEK +  
 #.435 PROD2 + #.35 XC  
 D1OH) 5.00e-11 ;DCB1 + HO. = RCHO + RO2-R. + CO  
 D1O3) 2.00e-18 ;DCB1 + O3 = #1.5 HO2. + #.5 HO. + #1.5 CO +  
 #.5 CO2 + GLY  
 D2OH) 5.00e-11 ;DCB2 + HO. = R2O2. + RCHO + CCO-O2.  
 D2HV) PF=NO2 QY=1.095E-1 ;DCB2 + HV = RO2-R. + #.5 [CCO-O2. + HO2.] + CO +  
 R2O2. + #.5 [GLY + MGLY + XC]  
 D3OH) 5.00e-11 ;DCB3 + HO. = R2O2. + RCHO + CCO-O2.  
 D3HV) PF=ACROLEIN QY=1.780E+3;DCB3 + HV = RO2-R. + #.5 [CCO-O2. + HO2.] + CO +

```

R2O2. + #.5 [GLY + MGLY + XC]
c1OH) 2.15e-12 3.448 0.00 ;CH4 + HO. = H2O + C-O2.
etOH) 1.96e-12 -0.870 0.00 ;ETHENE + HO. = RO2-R. + #1.61 HCHO + #.195 CCHO
etO3) 9.14e-15 5.127 0.00 ;ETHENE + O3 = #.12 HO. + #.12 HO2. + #.5 CO +
#.13 CO2 + HCHO + #.37 HCOOH
etN3) 4.39e-13 4.535 2.00 ;ETHENE + NO3 = RO2-R. + RCHO + #-1 XC + XN
etOA) 1.04e-11 1.574 0.00 ;ETHENE + O3P = #.5 HO2. + #.2 RO2-R. + #.3 C-O2. +
#.491 CO + #.191 HCHO + #.25 CCHO + #.009 GLY +
#.5 XC
isOH) 2.50e-11 -0.810 0.00 ;ISOPRENE + HO. = #.907 RO2-R. + #.093 RO2-N. +
#.079 R2O2. + #.624 HCHO + #.23 METHACRO +
#.32 MVK + #.357 ISO-PROD + #-0.167 XC
isO3) 7.86e-15 3.800 0.00 ;ISOPRENE + O3 = #.266 HO. + #.066 RO2-R. +
#.008 RO2-N. + #.126 R2O2. + #.192 MA-RCO3. +
#.275 CO + #.122 CO2 + #.592 HCHO + #.1 PROD2 +
#.39 METHACRO + #.16 MVK + #.204 HCOOH +
#.15 RCO-OH + #-0.259 XC
isN3) 3.03e-12 0.890 0.00 ;ISOPRENE + NO3 = #.187 NO2 + #.749 RO2-R. +
#.064 RO2-N. + #.187 R2O2. + #.936 ISO-PROD +
#-0.064 XC + #.813 XN
isOP) 3.60e-11 ;ISOPRENE + O3P = #.01 RO2-N. + #.24 R2O2. +
#.25 C-O2. + #.24 MA-RCO3. + #.24 HCHO +
#.75 PROD2 + #-1.01 XC
A1OH) 9.819E-12 2.181 0.00 ;ALK1 + HO. = RO2-R. + #.001 CO + #.048 HCHO +
#.902 CCHO + #.048 RCHO + #.001 HCOOH
A2OH) 8.896E-12 1.244 0.00 ;ALK2 + HO. = #.154 HO. + #.076 HO2. +
#.715 RO2-R. + #.026 RO2-N. + #.033 R2O2. +
#.028 CCO-O2. + #.001 TBU-O. + #.102 CO +
#.028 HCHO + #.187 RCHO + #.498 ACET +
#.155 GLY + #.001 MGLY + #.077 HCOOH +
#.029 CCO-OH + #.002 INERT + #.149 XC
A3OH) 8.546E-12 0.737 0.00 ;ALK3 + HO. = #.031 HO2. + #.743 RO2-R. +
#.072 RO2-N. + #.507 R2O2. + #.008 C-O2. +
#.003 RCO-O2. + #.143 TBU-O. + #.001 CO2 +
#.036 HCHO + #.514 CCHO + #.121 RCHO +
#.023 ACET + #.361 MEK + #.003 CCO-OH +
#.008 INERT + #.02 XC
A4OH) 6.123E-12 0.193 0.00 ;ALK4 + HO. = #.003 HO. + #.025 HO2. +
#.786 RO2-R. + #.144 RO2-N. + #.902 R2O2. +
#.009 C-O2. + #.008 CCO-O2. + #.005 RCO-O2. +
#.02 TBU-O. + #.002 CO + #.046 HCHO +
#.38 CCHO + #.218 RCHO + #.425 ACET +
#.101 MEK + #.168 PROD2 + #.003 MGLY +
#.002 HCOOH + #.005 CCO-OH + #.001 INERT +
#-0.157 XC
A5OH) 1.065E-11 0.032 0.00 ;ALK5 + HO. = #.201 HO2. + #.58 RO2-R. +
#.214 RO2-N. + #.565 R2O2. + #.003 C-O2. +
#.001 RCO-O2. + #.001 CO + #.143 HCHO +
#.082 CCHO + #.439 RCHO + #.045 ACET +
#.054 MEK + #.281 PROD2 + #.001 INERT +
#2.042 XC
O1OH) 6.008E-12 -0.926 0.00 ;OLE1 + HO. = #.002 HO2. + #.959 RO2-R. +
#.039 RO2-N. + #.049 R2O2. + #.915 HCHO +
#.574 CCHO + #.352 RCHO + #.005 ACET +
#.022 PROD2 + #.001 MGLY + #.001 BAEL +
#.012 INERT + #.484 XC + #.002 XN
O1O3) 3.643E-15 3.484 0.00 ;OLE1 + O3 = #.228 HO. + #.059 HO2. +
#.018 RO2-R. + #.15 C-O2. + #.417 CO +
#.105 CO2 + #.499 HCHO + #.301 CCHO +
#.207 RCHO + #.001 ACET + #.037 PROD2 +
#.001 MGLY + #.185 HCOOH + #.098 CCO-OH +
#.148 RCO-OH + #.048 INERT + #.504 XC

```

O1N3)	1.538E-13	1.534	0.00	;OLE1 + NO3 = #.002 HO2. + #.895 RO2-R. + #.091 RO2-N. + #.19 R2O2. + #.012 RCO-O2. + #.015 CCHO + #.042 RCHO + #.022 ACET + #.002 PROD2 + #.002 BACL + #.305 RNO3 + #.012 CCO-OH + #1.326 XC + #.697 XN
O1OA)	1.166E-11	0.605	0.00	;OLE1 + O3P = #.449 RCHO + #.528 MEK + #.02 PROD2 + #.001 RCO-OH + #.419 XC
O2OH)	1.569E-11	-0.871	0.00	;OLE2 + HO. = #.938 RO2-R. + #.062 RO2-N. + #.192 HCHO + #.685 CCHO + #.341 RCHO + #.178 ACET + #.017 MEK + #.003 BACL + #.032 BALD + #.125 METHACRO + #.125 ISO-PROD + #.075 XC
O2O3)	9.518E-16	1.065	0.00	;OLE2 + O3 = #.357 HO. + #.016 HO2. + #.018 RO2-R. + #.001 RO2-N. + #.148 R2O2. + #.173 C-O2. + #.145 CCO-O2. + #.005 RCO-O2. + #.262 CO + #.098 CO2 + #.307 HCHO + #.41 CCHO + #.224 RCHO + #.058 ACET + #.006 MEK + #.046 PROD2 + #.001 MGLY + #.001 BACL + #.022 BALD + #.131 METHACRO + #.098 MVK + #.075 HCOOH + #.113 CCO-OH + #.141 RCO-OH + #.046 INERT + #.037 XC
O2N3)	1.888E-12	0.000	0.00	;OLE2 + NO3 = #.431 NO2 + #.455 RO2-R. + #.108 RO2-N. + #.573 R2O2. + #.005 C-O2. + #.002 RCO-O2. + #.02 HCHO + #.501 CCHO + #.171 RCHO + #.158 ACET + #.003 MGLY + #.008 BALD + #.24 MVK + #.179 RNO3 + #.233 XC + #.39 XN
O2OA)	2.497E-11	0.000	0.00	;OLE2 + O3P = #.065 HO2. + #.06 RO2-R. + #.005 RO2-N. + #.06 CO + #.015 RCHO + #.608 MEK + #.311 PROD2 + #.06 METHACRO + #.323 XC
B1OH)	5.910E-12	0.000	0.00	;AR1N + HO. = #.236 HO2. + #.764 RO2-R. + #.207 GLY + #.236 PHEN + #.764 DCB1 + #1.114 XC
B2OH)	5.347E-12	-0.945	0.00	;AR2N + HO. = #.367 HO2. + #.176 RO2-R. + #.091 RO2-N. + #.365 RCO-O2. + #.084 GLY + #.367 PHEN + #.081 DCB1 + #.048 DCB2 + #.048 DCB3 + #5.184 XC
L2OH)	2.734E-11	0.000	0.00	;AR2L + HO. = #.181 HO2. + #.81 RO2-R. + #.009 RO2-N. + #.091 GLY + #.303 MGLY + #.077 BACL + #.181 CRES + #.052 BALD + #.628 DCB1 + #.05 DCB2 + #.079 DCB3 + #1.754 XC
C1OH)	5.910E-12	0.000	0.00	;AR1H + HO. = #.229 HO2. + #.762 RO2-R. + #.009 RO2-N. + #.029 PROD2 + #.119 GLY + #.124 MGLY + #.014 PHEN + #.215 CRES + #.07 BALD + #.483 DCB1 + #.128 DCB2 + #.053 DCB3 + #1.253 XC
C2OH)	1.981E-11	0.000	0.00	;AR2H + HO. = #.193 HO2. + #.799 RO2-R. + #.008 RO2-N. + #.106 GLY + #.288 MGLY + #.044 BACL + #.193 CRES + #.046 BALD + #.444 DCB1 + #.197 DCB2 + #.113 DCB3 + #1.706 XC
t1OH)	1.83e-11	-0.893	0.00	;TERP + HO. = #.75 RO2-R. + #.25 RO2-N. + #.5 R2O2. + #.276 HCHO + #.474 RCHO + #.276 PROD2 + #5.146 XC
t1O3)	1.08e-15	1.632	0.00	;TERP + O3 = #.567 HO. + #.033 HO2. + #.031 RO2-R. + #.18 RO2-N. + #.729 R2O2. + #.123 CCO-O2. + #.201 RCO-O2. + #.157 CO + #.037 CO2 + #.235 HCHO + #.205 RCHO + #.13 ACET + #.276 PROD2 + #.001 GLY + #.031 BACL + #.103 HCOOH + #.189 RCO-OH + #4.183 XC

t1N3)	3.66e-12	-0.347	0.00	;TERP + NO3 = #.474 NO2 + #.276 RO2-R. + #.25 RO2-N. + #.75 R2O2. + #.474 RCHO + #.276 RNO3 + #5.421 XC + #.25 XN
t1OP)	3.27e-11			;TERP + O3P = #.147 RCHO + #.853 PROD2 + #4.441 XC
M1OH)	1.210E-11	-0.882	0.00	;A-PINENE + HO. = #.75 RO2-R. + #.25 RO2-N. + #.5 R2O2. + #.75 RCHO + #6.5 XC
M1O3)	1.010E-15	1.455	0.00	;A-PINENE + O3 = #.7 HO. + #.081 RO2-R. + #.321 RO2-N. + #1.375 R2O2. + #.298 RCO-O2. + #.051 CO + #.339 HCHO + #.218 RCHO + #.345 ACET + #.002 GLY + #.081 BA CL + #.3 RCO-OH + #3.875 XC
M1N3)	1.190E-12	-0.974	0.00	;A-PINENE + NO3 = #.75 NO2 + #.25 RO2-N. + #.75 R2O2. + #.75 RCHO + #6.25 XC + #.25 XN
M1OA)	3.200E-11	0.000	0.00	;A-PINENE + O3P = PROD2 + #4 XC
M2OH)	2.380E-11	-0.709	0.00	;B-PINENE + HO. = #.75 RO2-R. + #.25 RO2-N. + #.5 R2O2. + #.75 HCHO + #.75 PROD2 + #3.25 XC
M2O3)	1.010E-15	2.493	0.00	;B-PINENE + O3 = #.34 HO. + #.09 HO2. + #.05 RO2-N. + #.2 R2O2. + #.2 RCO-O2. + #.375 CO + #.1 CO2 + #.25 HCHO + #.75 PROD2 + #.28 HCOOH + #3.595 XC
M2N3)	2.510E-12	0.000	0.00	;B-PINENE + NO3 = #.75 RO2-R. + #.25 RO2-N. + #.75 R2O2. + #.75 RNO3 + #4 XC + #.25 XN
M2OA)	2.700E-11	0.000	0.00	;B-PINENE + O3P = #.4 RCHO + #.6 PROD2 + #.5.2 XC
M3OH)	1.640E-11	-0.994	0.00	;3-CARENE + HO. = #.75 RO2-R. + #.25 RO2-N. + #.5 R2O2. + #.75 RCHO + #6.25 XC
M3O3)	1.010E-15	1.958	0.00	;3-CARENE + O3 = #.7 HO. + #.161 RO2-N. + #.539 R2O2. + #.482 CCO-O2. + #.058 RCO-O2. + #.058 HCHO + #.482 RCHO + #.3 RCO-OH + #.5.492 XC
M3N3)	9.100E-12	0.000	0.00	;3-CARENE + NO3 = #.75 NO2 + #.25 RO2-N. + #.75 R2O2. + #.75 RCHO + #6.25 XC + #.25 XN
M3OA)	3.200E-11	0.000	0.00	;3-CARENE + O3P = PROD2 + #4 XC
M4OH)	2.190E-11	-0.994	0.00	;SABINENE + HO. = #.75 RO2-R. + #.25 RO2-N. + #.5 R2O2. + #.75 HCHO + #.75 PROD2 + #3.25 XC
M4O3)	1.010E-15	1.459	0.00	;SABINENE + O3 = #.34 HO. + #.09 HO2. + #.05 RO2-N. + #.2 R2O2. + #.2 RCO-O2. + #.375 CO + #.1 CO2 + #.25 HCHO + #.75 PROD2 + #.28 HCOOH + #3.595 XC
M4N3)	1.000E-11	0.000	0.00	;SABINENE + NO3 = #.75 RO2-R. + #.25 RO2-N. + #.75 R2O2. + #.75 RNO3 + #4 XC + #.25 XN
M4OA)	1.690E-11	0.000	0.00	;SABINENE + O3P = #.4 RCHO + #.6 PROD2 + #.5.2 XC
M5OH)	3.190E-11	-0.994	0.00	;D-LIMONE + HO. = #.75 RO2-R. + #.25 RO2-N. + #.5 R2O2. + #.75 RCHO + #6.25 XC
M5O3)	3.710E-15	1.729	0.00	;D-LIMONE + O3 = #.7 HO. + #.161 RO2-N. + #.539 R2O2. + #.482 CCO-O2. + #.058 RCO-O2. + #.058 HCHO + #.482 RCHO + #.3 RCO-OH + #.5.492 XC
M5N3)	1.220E-11	0.000	0.00	;D-LIMONE + NO3 = #.75 NO2 + #.25 RO2-N. + #.75 R2O2. + #.75 RCHO + #6.25 XC + #.25 XN
M5OA)	7.200E-11	0.000	0.00	;D-LIMONE + O3P = PROD2 + #4 XC

## s99soa2

```
!This .rxn includes all reactions in the s99soa mechanism.
!It is based on the original fixed parameter version of SAPRC99
!and is similar to SAPRC99f.rxn, which is distributed with SAPRC99
!
!The following modifications were made for inclusion in CAMx:
!
!1. Modifications to be consistent with CAMx3.10-mech 5:
!   Using only 6 primary photolysis reactions used in mech5
!   The ACROLEIN photolysis reactions equivalent to ISPD in mech5
!   QF for secondary photolysis reactions from mech5 chemparam file
!   Apparant error in mech 5 corrected here: reaction isn3
!       produces 0.813 XN and not 0.813 RNO3 as in mech5.
!   Reaction rates involving HNO4 (or PNA) set to 0 as in mech5
!       i.e. reactions 35,36,37,38. Reaction 37 is assigned
!       a primary photolysis reaction with QY=0.0
!   Specification of STS,ACT,RAD,BLD,CON species to match mech5
!       (listed below)
!
!2. Modifications for modeling SOA:
!   Explicit reactions for APINENE, BPINENE, SABINENE, 3CARENE,
!       LIMONENE
!   Separate reactions for high-yield ARO1, low-yield ARO2
!       high-yield ARO2, no-yield ARO1, no-yield ARO2
!   I relabeled the AR2L (low-yield ARO2) reactions as L2OH to
!       avoid label conflict
!   All lumped model species parameters derived with Texas
!       anthropogenic emissions profile
!
!Rate constant data consistent with cm3/molec-s units
!
.STS
O*1D2
O3P
.ACT
= NO + NO2 + O3
= PAN + PAN2 + MA-PAN + PBZN + NPHE + RNO3
= CRES + DCB2 + DCB3 + HNO4
.RAD
= HOCOO. + TBU-O.
= BZ-O. + BZ(NO2)-O.
= N2O5 + NO3 + HO. + HO2. + C-O2.
= RO2-R. + RO2-N. + R2O2.
= CCO-O2. + RCO-O2. + BZCO-O2. + MA-RCO3.
.BLD
= HONO + HNO3 + XN + HO2H + HCHO + CCHO
= RCHO + BALD + BA CL + PROD2 + DCB1 + PHEN
= ISOPRENE + ISO-PROD + MVK + METHACRO
= MGLY + GLY + HCOOH + CCO-OH
= CCO-OOH + RCO-OH + RCO-OOH + ACET
= MEK + MEOH + COOH + ROOH + CO + ETHENE
= ALK1 + ALK2 + ALK3 + ALK4 + ALK5
= AR1H + AR2H + AR2L + AR1N + AR2N
= OLE1 + OLE2 + TERP
= A-PINENE + B-PINENE + D-LIMONE
= 3-CARENE + SABINENE
= SO2 + SULF
.DUMSLO
```

```

NXOY
.CON
O2      2.09e+5
M       1.00e+6
H2O     2.00e+4
H2      0.50e+0
HV      1.00e+0
CH4     1.75e+0
.RXN
1)      PF=NO2      ;NO2 + HV = NO + O3P
2)      5.68e-34 0.000 -2.80 ;O3P + O2 + M = O3 + M
3)      8.00e-12 4.094 0.00 ;O3P + O3 = #2 O2
4)      1.00e-31 0.000 -1.60 ;O3P + NO + M = NO2 + M
5)      6.50e-12 -0.238 0.00 ;O3P + NO2 = NO + O2
6)      FALLOFF    ;O3P + NO2 = NO3 + M
      9.00e-32 0.000 -2.00
      2.20e-11 0.000 0.00
      0.80 1.0
8)      1.80e-12 2.722 0.00 ;O3 + NO = NO2 + O2
9)      1.40e-13 4.908 0.00 ;O3 + NO2 = O2 + NO3
10)     1.80e-11 -0.219 0.00 ;NO + NO3 = #2 NO2
11)     3.30e-39 -1.053 0.00 ;NO + NO + O2 = #2 NO2
12)     FALLOFF    ;NO2 + NO3 = N2O5
      2.80e-30 0.000 -3.50
      2.00e-12 0.000 0.20
      0.45 1.0
13)     FALLOFF    ;N2O5 = NO2 + NO3
      1.00e-03 21.859 -3.50
      9.70e+14 22.018 0.10
      0.45 1.0
14)     2.60e-22      ;N2O5 + H2O = #2 HNO3
17)     4.50e-14 2.504 0.00 ;NO2 + NO3 = NO + NO2 + O2
18)     PF=NO2 QY=2.379E+0 ;NO3 + HV = NO + O2
19)     PF=NO2 QY=2.199E+1 ;NO3 + HV = NO2 + O3P
20)     PF=NO2 QY=5.063E-2 ;O3 + HV = O3P + O2
21)     PF=O3O1D    ;O3 + HV = O*1D2 + O2
22)     2.20e-10      ;O*1D2 + H2O = #2 HO.
23)     2.09e-11 -0.189 0.00 ;O*1D2 + M = O3P + M
24)     FALLOFF    ;HO. + NO = HONO
      7.00e-31 0.000 -2.60
      3.60e-11 0.000 -0.10
      0.60 1.0
25)     PF=NO2 QY=1.923E-1 ;HONO + HV = HO. + NO
26)     PF=ACROLEIN QY=1.190E+2;HONO + HV = HO2. + NO2
27)     2.70e-12 -0.517 0.00 ;HO. + HONO = H2O + NO2
28)     FALLOFF    ;HO. + NO2 = HNO3
      2.43e-30 0.000 -3.10
      1.67e-11 0.000 -2.10
      0.60 1.0
29)     2.00e-11      ;HO. + NO3 = HO2. + NO2
30)     K0+K3M/1+K3M/K2 ;HO. + HNO3 = H2O + NO3
      7.20e-15 -1.560 0.00
      4.10e-16 -2.862 0.00
      1.90e-33 -1.441 0.00
31)     PF=HCHO_R QY=2.177E-2 ;HNO3 + HV = HO. + NO2
32)     K1+K2[M]    ;HO. + CO = HO2. + CO2
      1.30e-13
      3.19e-33
33)     1.90e-12 1.987 0.00 ;HO. + O3 = HO2. + O2
34)     3.40e-12 -0.537 0.00 ;HO2. + NO = HO. + NO2
35)     0.0          ;HO2. + NO2 = HNO4
36)     0.0          ;HNO4 = HO2. + NO2

```

```

37) PF=HCHO_R QY=0.0 ;HNO4 + HV = #.61 [HO2. + NO2] + #.39 [HO. + NO3]
38) 0.0 ;HNO4 + HO. = H2O + NO2 + O2
39) 1.40e-14 1.192 0.00 ;HO2. + O3 = HO. + #2 O2
40A) K1+K2[M] ;HO2. + HO2. = HO2H + O2
      2.20e-13 -1.192 0.00
      1.85e-33 -1.947 0.00
40B) K1+K2[M] ;HO2. + HO2. + H2O = HO2H + O2 + H2O
      3.08e-34 -5.564 0.00
      2.59e-54 -6.319 0.00
41) 4.00e-12 ;NO3 + HO2. = #.8 [HO. + NO2 + O2] + #.2 [HNO3 +
      O2]
42) 8.50e-13 4.869 0.00 ;NO3 + NO3 = #2 NO2 + O2
43) PF=HCHO_M QY=1.709E-1 ;HO2H + HV = #2 HO.
44) 2.90e-12 0.318 0.00 ;HO2H + HO. = HO2. + H2O
45) 4.80e-11 -0.497 0.00 ;HO. + HO2. = H2O + O2
S2OH) FALLOFF ;HO. + SO2 = HO2. + SULF
      4.00e-31 0.000 -3.30
      2.00e-12 0.000 0.00
      0.45 1.0
H2OH) 7.70e-12 4.173 0.00 ;HO. + H2 = HO2. + H2O
MER1) 2.80e-12 -0.566 0.00 ;C-O2. + NO = NO2 + HCHO + HO2.
MER4) 3.80e-13 -1.550 0.00 ;C-O2. + HO2. = COOH + O2
MEN3) 1.30e-12 ;C-O2. + NO3 = HCHO + HO2. + NO2
MER5) 2.45e-14 -1.410 0.00 ;C-O2. + C-O2. = MEOH + HCHO + O2
MER6) 5.90e-13 1.011 0.00 ;C-O2. + C-O2. = #2 [HCHO + HO2.]
RRNO) 2.70e-12 -0.715 0.00 ;RO2-R. + NO = NO2 + HO2.
RRH2) 1.90e-13 -2.583 0.00 ;RO2-R. + HO2. = ROOH + O2 + #-3 XC
RRN3) 2.30e-12 ;RO2-R. + NO3 = NO2 + O2 + HO2.
RRME) 2.00e-13 ;RO2-R. + C-O2. = HO2. + #.75 HCHO + #.25 MEOH
RRR2) 3.50e-14 ;RO2-R. + RO2-R. = HO2.
R2NO) SAMEK RRNO ;R2O2. + NO = NO2
R2H2) SAMEK RRH2 ;R2O2. + HO2. = HO2.
R2N3) SAMEK RRN3 ;R2O2. + NO3 = NO2
R2ME) SAMEK RRME ;R2O2. + C-O2. = C-O2.
R2RR) SAMEK RRR2 ;R2O2. + RO2-R. = RO2-R.
R2R3) SAMEK RRR2 ;R2O2. + R2O2. =
R2NO) SAMEK RRNO ;RO2-N. + NO = RNO3
R2NH2) SAMEK RRH2 ;RO2-N. + HO2. = ROOH + #3 XC
R2NME) SAMEK RRME ;RO2-N. + C-O2. = HO2. + #.25 MEOH + #.5 [MEK +
      PROD2] + #.75 HCHO + XC
R2N3) SAMEK RRN3 ;RO2-N. + NO3 = NO2 + O2 + HO2. + MEK + #2 XC
R2NRR) SAMEK RRR2 ;RO2-N. + RO2-R. = HO2. + #.5 [MEK + PROD2] + O2 +
      XC
R2NR2) SAMEK RRR2 ;RO2-N. + R2O2. = RO2-N.
R2NRN) SAMEK RRR2 ;RO2-N. + RO2-N. = MEK + HO2. + PROD2 + O2 + #2 XC
APN2) FALLOFF ;CCO-O2. + NO2 = PAN
      2.70e-28 0.000 -7.10
      1.20e-11 0.000 -0.90
      0.30 1.0
DPAN) FALLOFF ;PAN = CCO-O2. + NO2
      4.90e-03 24.045 0.00
      4.00e+16 27.026 0.00
      0.30 1.0
APNO) 7.80e-12 -0.596 ;CCO-O2. + NO = C-O2. + CO2 + NO2
APH2) 4.30e-13 -2.067 0.00 ;CCO-O2. + HO2. = #.75 [CCO-OOH + O2] +
      #.25 [CCO-OH + O3]
APN3) 4.00e-12 ;CCO-O2. + NO3 = C-O2. + CO2 + NO2 + O2
APME) 1.80e-12 -0.994 0.00 ;CCO-O2. + C-O2. = CCO-OH + HCHO + O2
APRR) 7.50e-12 ;CCO-O2. + RO2-R. = CCO-OH
APR2) SAMEK APRR ;CCO-O2. + R2O2. = CCO-O2.
APRN) SAMEK APRR ;CCO-O2. + RO2-N. = CCO-OH + PROD2
APAP) 2.90e-12 -0.994 0.00 ;CCO-O2. + CCO-O2. = #2 [C-O2. + CO2] + O2

```



AAN3) 1.40e-12 3.696 0.00 ;CCHO + NO3 = HNO3 + CCO-O2.  
 PAOH) 2.00e-11 ;RCHO + HO. = #.034 RO2-R. + #.001 RO2-N. +  
 #.965 RCO-O2. + #.034 CO + #.034 CCHO +  
 #-0.003 XC  
 PAHV) PF=HCHO\_R QY=5.749E-1 ;RCHO + HV = CCHO + RO2-R. + CO + HO2.  
 PAN3) 1.40e-12 3.520 ;RCHO + NO3 = HNO3 + RCO-O2.  
 K3OH) 1.10e-12 1.033 0.00 ;ACET + HO. = HCHO + CCO-O2. + R2O2.  
 K3HV) PF=CCHO\_R QY=9.448E-2 ;ACET + HV = CCO-O2. + C-O2.  
 K4OH) 1.30e-12 0.050 2.00 ;MEK + HO. = #.37 RO2-R. + #.042 RO2-N. +  
 #.616 R2O2. + #.492 CCO-O2. + #.096 RCO-O2. +  
 #.115 HCHO + #.482 CCHO + #.37 RCHO + #.287 XC  
 K4HV) PF=CCHO\_R QY=3.507E-1 ;MEK + HV = CCO-O2. + CCHO + RO2-R.  
 MeOH) 3.10e-12 0.715 2.00 ;MEOH + HO. = HCHO + HO2.  
 MER9) 2.90e-12 -0.378 0.00 ;COOH + HO. = H2O + #.35 [HCHO + HO.] + #.65 C-O2.  
 MERA) PF=HCHO\_M QY=1.193E-1 ;COOH + HV = HCHO + HO2. + HO.  
 LPR9) 1.10e-11 ;ROOH + HO. = H2O + RCHO + #.34 RO2-R. + #.66 HO.  
 LPRA) PF=HCHO\_M QY=1.193E-1 ;ROOH + HV = RCHO + HO2. + HO.  
 GLHV) PF=ACROLEIN QY=6.181E+1 ;GLY + HV = #2 [CO + HO2.]  
 GLVM) PF=NO2 QY=1.582E-3 ;GLY + HV = HCHO + CO  
 GLOH) 1.10e-11 ;GLY + HO. = #.63 HO2. + #1.26 CO + #.37 RCO-O2. +  
 #- .37 XC  
 GLN3) 2.80e-12 4.722 ;GLY + NO3 = HNO3 + #.63 HO2. + #1.26 CO +  
 #.37 RCO-O2. + #- .37 XC  
 MGHV) PF=NO2 QY=1.631E-2 ;MGLY + HV = HO2. + CO + CCO-O2.  
 MGOH) 1.50e-11 ;MGLY + HO. = CO + CCO-O2.  
 MGN3) 1.40e-12 3.765 ;MGLY + NO3 = HNO3 + CO + CCO-O2.  
 BAHV) PF=NO2 QY=2.800E-2 ;BALD + HV = #2 CCO-O2.  
 PHOH) 2.63e-11 ;PHEN + HO. = #.24 BZ-O. + #.76 RO2-R. + #.23 GLY +  
 #4.1 XC  
 PHN3) 3.78e-12 ;PHEN + NO3 = HNO3 + BZ-O.  
 CROH) 4.20e-11 ;CRES + HO. = #.24 BZ-O. + #.76 RO2-R. +  
 #.23 MGLY + #4.87 XC  
 CRN3) 1.37e-11 ;CRES + NO3 = HNO3 + BZ-O. + XC  
 NPN3) SAMEK PHN3 ;NPHE + NO3 = HNO3 + BZ(NO2)-O.  
 BZOH) 1.29e-11 ;BALD + HO. = BZCO-O2.  
 BZHV) PF=ACROLEIN QY=2.250E+1 ;BALD + HV = #7 XC  
 BZNT) 1.40e-12 3.720 0.00 ;BALD + NO3 = HNO3 + BZCO-O2.  
 MAOH) 1.86e-11 -0.350 0.00 ;METHACRO + HO. = #.5 RO2-R. + #.416 CO +  
 #.084 HCHO + #.416 MEK + #.084 MGLY +  
 #.5 MA-RCO3. + #-0.416 XC  
 MAO3) 1.36e-15 4.200 0.00 ;METHACRO + O3 = #.008 HO2. + #.1 RO2-R. +  
 #.208 HO. + #.1 RCO-O2. + #.45 CO + #.117 CO2 +  
 #.2 HCHO + #.9 MGLY + #.333 HCOOH + #-0.1 XC  
 MAN3) 1.50e-12 3.430 0.00 ;METHACRO + NO3 = #.5 [HNO3 + RO2-R. + CO +  
 MA-RCO3.] + #1.5 XC + #.5 XN  
 MAOP) 6.34e-12 ;METHACRO + O3P = RCHO + XC  
 MAHV) PF=ACROLEIN QY=1.000 ;METHACRO + HV = #.34 HO2. + #.33 RO2-R. +  
 #.33 HO. + #.67 CCO-O2. + #.67 CO + #.67 HCHO +  
 #.33 MA-RCO3. + #-0 XC  
 MVOH) 4.14e-12 -0.900 0.00 ;MVK + HO. = #.3 RO2-R. + #.025 RO2-N. +  
 #.675 R2O2. + #.675 CCO-O2. + #.3 HCHO +  
 #.675 RCHO + #.3 MGLY + #-0.725 XC  
 MVO3) 7.51e-16 3.020 0.00 ;MVK + O3 = #.064 HO2. + #.05 RO2-R. + #.164 HO. +  
 #.05 RCO-O2. + #.475 CO + #.124 CO2 + #.1 HCHO +  
 #.95 MGLY + #.351 HCOOH + #-0.05 XC  
 MVOP) 4.32e-12 ;MVK + O3P = #.45 RCHO + #.55 MEK + #.45 XC  
 MVHV) PF=ACROLEIN QY=5.122E-1 ;MVK + HV = #.3 C-O2. + #.7 CO + #.7 PROD2 +  
 #.3 MA-RCO3. + #-2.4 XC  
 IPOH) 6.19e-11 ;ISO-PROD + HO. = #.67 RO2-R. + #.041 RO2-N. +  
 #.289 MA-RCO3. + #.336 CO + #.055 HCHO +  
 #.129 CCHO + #.013 RCHO + #.15 MEK + #.332 PROD2 +  
 #.15 GLY + #.174 MGLY + #-0.504 XC

IPO3) 4.18e-18 ;ISO-PROD + O3 = #.4 HO2. + #.048 RO2-R. +  
#.048 RCO-O2. + #.285 HO. + #.498 CO + #.14 CO2 +  
#.125 HCHO + #.047 CCHO + #.21 MEK + #.023 GLY +  
#.742 MGLY + #.1 HCOOH + #.372 RCO-OH + #-.33 XC

IPN3) 1.00e-13 ;ISO-PROD + NO3 = #.799 RO2-R. + #.051 RO2-N. +  
#.15 MA-RCO3. + #.572 CO + #.15 HNO3 +  
#.227 HCHO + #.218 RCHO + #.008 MGLY +  
#.572 RNO3 + #.28 XN + #-.815 XC

IPHV) PF=ACROLEIN ;ISO-PROD + HV = #1.233 HO2. + #.467 CCO-O2. +  
#.3 RCO-O2. + #1.233 CO + #.3 HCHO + #.467 CCHO +  
#.233 MEK + #-.233 XC

K6OH) 1.50e-11 ;PROD2 + HO. = #.379 HO2. + #.473 RO2-R. +  
#.07 RO2-N. + #.029 CCO-O2. + #.049 RCO-O2. +  
#.213 HCHO + #.084 CCHO + #.558 RCHO + #.115 MEK +  
#.329 PROD2 + #.886 XC

K6HV) PF=HCHO\_M QY=1.590E-2 ;PROD2 + HV = #.96 RO2-R. + #.04 RO2-N. +  
#.515 R2O2. + #.667 CCO-O2. + #.333 RCO-O2. +  
#.506 HCHO + #.246 CCHO + #.71 RCHO + #.299 XC

RNOH) 7.80e-12 ;RNO3 + HO. = #.338 NO2 + #.113 HO2. +  
#.376 RO2-R. + #.173 RO2-N. + #.596 R2O2. +  
#.01 HCHO + #.439 CCHO + #.213 RCHO + #.006 ACET +  
#.177 MEK + #.048 PROD2 + #.31 RNO3 + #.351 XN +  
#.56 XC

RNHV) PF=HCHO\_R QY=9.686E-2 ;RNO3 + HV = NO2 + #.341 HO2. + #.564 RO2-R. +  
#.095 RO2-N. + #.152 R2O2. + #.134 HCHO +  
#.431 CCHO + #.147 RCHO + #.02 ACET + #.243 MEK +  
#.435 PROD2 + #.35 XC

D1OH) 5.00e-11 ;DCB1 + HO. = RCHO + RO2-R. + CO

D1O3) 2.00e-18 ;DCB1 + O3 = #1.5 HO2. + #.5 HO. + #1.5 CO +  
#.5 CO2 + GLY

D2OH) 5.00e-11 ;DCB2 + HO. = R2O2. + RCHO + CCO-O2.

D2HV) PF=NO2 QY=1.095E-1 ;DCB2 + HV = RO2-R. + #.5 [CCO-O2. + HO2.] + CO +  
R2O2. + #.5 [GLY + MGLY + XC]

D3OH) 5.00e-11 ;DCB3 + HO. = R2O2. + RCHO + CCO-O2.

D3HV) PF=ACROLEIN QY=1.780E+3 ;DCB3 + HV = RO2-R. + #.5 [CCO-O2. + HO2.] + CO +  
R2O2. + #.5 [GLY + MGLY + XC]

c1OH) 2.15e-12 3.448 0.00 ;CH4 + HO. = H2O + C-O2.

etOH) 1.96e-12 -0.870 0.00 ;ETHENE + HO. = RO2-R. + #1.61 HCHO + #.195 CCHO

etO3) 9.14e-15 5.127 0.00 ;ETHENE + O3 = #.12 HO. + #.12 HO2. + #.5 CO +  
#.13 CO2 + HCHO + #.37 HCOOH

etN3) 4.39e-13 4.535 2.00 ;ETHENE + NO3 = RO2-R. + RCHO + #-1 XC + XN

etOA) 1.04e-11 1.574 0.00 ;ETHENE + O3P = #.5 HO2. + #.2 RO2-R. + #.3 C-O2. +  
#.491 CO + #.191 HCHO + #.25 CCHO + #.009 GLY +  
#.5 XC

isOH) 2.50e-11 -0.810 0.00 ;ISOPRENE + HO. = #.907 RO2-R. + #.093 RO2-N. +  
#.079 R2O2. + #.624 HCHO + #.23 METHACRO +  
#.32 MVK + #.357 ISO-PROD + #-0.167 XC

isO3) 7.86e-15 3.800 0.00 ;ISOPRENE + O3 = #.266 HO. + #.066 RO2-R. +  
#.008 RO2-N. + #.126 R2O2. + #.192 MA-RCO3. +  
#.275 CO + #.122 CO2 + #.592 HCHO + #.1 PROD2 +  
#.39 METHACRO + #.16 MVK + #.204 HCOOH +  
#.15 RCO-OH + #-0.259 XC

isN3) 3.03e-12 0.890 0.00 ;ISOPRENE + NO3 = #.187 NO2 + #.749 RO2-R. +  
#.064 RO2-N. + #.187 R2O2. + #.936 ISO-PROD +  
#-0.064 XC + #.813 XN

isOP) 3.60e-11 ;ISOPRENE + O3P = #.01 RO2-N. + #.24 R2O2. +  
#.25 C-O2. + #.24 MA-RCO3. + #.24 HCHO +  
#.75 PROD2 + #-1.01 XC

A1OH) 9.819E-12 2.181 0.00 ;ALK1 + HO. = RO2-R. + #.001 CO + #.048 HCHO +  
#.902 CCHO + #.048 RCHO + #.001 HCOOH

A2OH) 8.896E-12 1.244 0.00 ;ALK2 + HO. = #.154 HO. + #.076 HO2. +  
#.715 RO2-R. + #.026 RO2-N. + #.033 R2O2. +

				#.028 CCO-O2. + #.001 TBU-O. + #.102 CO + #.028 HCHO + #.187 RCHO + #.498 ACET + #.155 GLY + #.001 MGLY + #.077 HCOOH + #.029 CCO-OH + #.002 INERT + #.149 XC
A3OH)	8.546E-12	0.737	0.00	;ALK3 + HO. = #.031 HO2. + #.743 RO2-R. + #.072 RO2-N. + #.507 R2O2. + #.008 C-O2. + #.003 RCO-O2. + #.143 TBU-O. + #.001 CO2 + #.036 HCHO + #.514 CCHO + #.121 RCHO + #.023 ACET + #.361 MEK + #.003 CCO-OH + #.008 INERT + #.02 XC
A4OH)	6.123E-12	0.193	0.00	;ALK4 + HO. = #.003 HO. + #.025 HO2. + #.786 RO2-R. + #.144 RO2-N. + #.902 R2O2. + #.009 C-O2. + #.008 CCO-O2. + #.005 RCO-O2. + #.02 TBU-O. + #.002 CO + #.046 HCHO + #.38 CCHO + #.218 RCHO + #.425 ACET + #.101 MEK + #.168 PROD2 + #.003 MGLY + #.002 HCOOH + #.005 CCO-OH + #.001 INERT + #-0.157 XC
A5OH)	1.065E-11	0.032	0.00	;ALK5 + HO. = #.201 HO2. + #.58 RO2-R. + #.214 RO2-N. + #.565 R2O2. + #.003 C-O2. + #.001 RCO-O2. + #.001 CO + #.143 HCHO + #.082 CCHO + #.439 RCHO + #.045 ACET + #.054 MEK + #.281 PROD2 + #.001 INERT + #2.042 XC
O1OH)	6.008E-12	-0.926	0.00	;OLE1 + HO. = #.002 HO2. + #.959 RO2-R. + #.039 RO2-N. + #.049 R2O2. + #.915 HCHO + #.574 CCHO + #.352 RCHO + #.005 ACET + #.022 PROD2 + #.001 MGLY + #.001 BACL + #.012 INERT + #.484 XC + #.002 XN
O1O3)	3.643E-15	3.484	0.00	;OLE1 + O3 = #.228 HO. + #.059 HO2. + #.018 RO2-R. + #.15 C-O2. + #.417 CO + #.105 CO2 + #.499 HCHO + #.301 CCHO + #.207 RCHO + #.001 ACET + #.037 PROD2 + #.001 MGLY + #.185 HCOOH + #.098 CCO-OH + #.148 RCO-OH + #.048 INERT + #.504 XC
O1N3)	1.538E-13	1.534	0.00	;OLE1 + NO3 = #.002 HO2. + #.895 RO2-R. + #.091 RO2-N. + #.19 R2O2. + #.012 RCO-O2. + #.015 CCHO + #.042 RCHO + #.022 ACET + #.002 PROD2 + #.002 BACL + #.305 RNO3 + #.012 CCO-OH + #1.326 XC + #.697 XN
O1OA)	1.166E-11	0.605	0.00	;OLE1 + O3P = #.449 RCHO + #.528 MEK + #.02 PROD2 + #.001 RCO-OH + #.419 XC
O2OH)	1.569E-11	-0.871	0.00	;OLE2 + HO. = #.938 RO2-R. + #.062 RO2-N. + #.192 HCHO + #.685 CCHO + #.341 RCHO + #.178 ACET + #.017 MEK + #.003 BACL + #.032 BALD + #.125 METHACRO + #.125 ISO-PROD + #.075 XC
O2O3)	9.518E-16	1.065	0.00	;OLE2 + O3 = #.357 HO. + #.016 HO2. + #.018 RO2-R. + #.001 RO2-N. + #.148 R2O2. + #.173 C-O2. + #.145 CCO-O2. + #.005 RCO-O2. + #.262 CO + #.098 CO2 + #.307 HCHO + #.41 CCHO + #.224 RCHO + #.058 ACET + #.006 MEK + #.046 PROD2 + #.001 MGLY + #.001 BACL + #.022 BALD + #.131 METHACRO + #.098 MVK + #.075 HCOOH + #.113 CCO-OH + #.141 RCO-OH + #.046 INERT + #.037 XC
O2N3)	1.888E-12	0.000	0.00	;OLE2 + NO3 = #.431 NO2 + #.455 RO2-R. + #.108 RO2-N. + #.573 R2O2. + #.005 C-O2. + #.002 RCO-O2. + #.02 HCHO + #.501 CCHO + #.171 RCHO + #.158 ACET + #.003 MGLY + #.008 BALD + #.24 MVK + #.179 RNO3 + #.233 XC + #.39 XN

O2OA)	2.497E-11	0.000	0.00	;OLE2 + O3P = #.065 HO2. + #.06 RO2-R. + #.005 RO2-N. + #.06 CO + #.015 RCHO + #.608 MEK + #.311 PROD2 + #.06 METHACRO + #.323 XC
B1OH)	5.910E-12	0.000	0.00	;AR1N + HO. = #.236 HO2. + #.764 RO2-R. + #.207 GLY + #.236 PHEN + #.764 DCB1 + #1.114 XC
B2OH)	5.347E-12	-0.945	0.00	;AR2N + HO. = #.367 HO2. + #.176 RO2-R. + #.091 RO2-N. + #.365 RCO-O2. + #.084 GLY + #.367 PHEN + #.081 DCB1 + #.048 DCB2 + #.048 DCB3 + #5.184 XC
L2OH)	2.734E-11	0.000	0.00	;AR2L + HO. = #.181 HO2. + #.81 RO2-R. + #.009 RO2-N. + #.091 GLY + #.303 MGLY + #.077 BACL + #.181 CRES + #.052 BALD + #.628 DCB1 + #.05 DCB2 + #.079 DCB3 + #1.754 XC
C1OH)	5.910E-12	0.000	0.00	;AR1H + HO. = #.229 HO2. + #.762 RO2-R. + #.009 RO2-N. + #.029 PROD2 + #.119 GLY + #.124 MGLY + #.014 PHEN + #.215 CRES + #.07 BALD + #.483 DCB1 + #.128 DCB2 + #.053 DCB3 + #1.253 XC
C2OH)	1.981E-11	0.000	0.00	;AR2H + HO. = #.193 HO2. + #.799 RO2-R. + #.008 RO2-N. + #.106 GLY + #.288 MGLY + #.044 BACL + #.193 CRES + #.046 BALD + #.444 DCB1 + #.197 DCB2 + #.113 DCB3 + #1.706 XC
t1OH)	1.83e-11	-0.893	0.00	;TERP + HO. = #.75 RO2-R. + #.25 RO2-N. + #.5 R2O2. + #.276 HCHO + #.474 RCHO + #.276 PROD2 + #5.146 XC
t1O3)	1.08e-15	1.632	0.00	;TERP + O3 = #.567 HO. + #.033 HO2. + #.031 RO2-R. + #.18 RO2-N. + #.729 R2O2. + #.123 CCO-O2. + #.201 RCO-O2. + #.157 CO + #.037 CO2 + #.235 HCHO + #.205 RCHO + #.13 ACET + #.276 PROD2 + #.001 GLY + #.031 BACL + #.103 HCOOH + #.189 RCO-OH + #4.183 XC
t1N3)	3.66e-12	-0.347	0.00	;TERP + NO3 = #.474 NO2 + #.276 RO2-R. + #.25 RO2-N. + #.75 R2O2. + #.474 RCHO + #.276 RNO3 + #5.421 XC + #.25 XN
t1OP)	3.27e-11			;TERP + O3P = #.147 RCHO + #.853 PROD2 + #4.441 XC
M1OH)	1.210E-11	-0.882	0.00	;A-PINENE + HO. = #.75 RO2-R. + #.25 RO2-N. + #.5 R2O2. + #.75 RCHO + #6.5 XC
M1O3)	1.010E-15	1.455	0.00	;A-PINENE + O3 = #.7 HO. + #.081 RO2-R. + #.321 RO2-N. + #1.375 R2O2. + #.298 RCO-O2. + #.051 CO + #.339 HCHO + #.218 RCHO + #.345 ACET + #.002 GLY + #.081 BACL + #.3 RCO-OH + #3.875 XC
M1N3)	1.190E-12	-0.974	0.00	;A-PINENE + NO3 = #.75 NO2 + #.25 RO2-N. + #.75 R2O2. + #.75 RCHO + #6.25 XC + #.25 XN
M1OA)	3.200E-11	0.000	0.00	;A-PINENE + O3P = PROD2 + #4 XC
M2OH)	2.380E-11	-0.709	0.00	;B-PINENE + HO. = #.75 RO2-R. + #.25 RO2-N. + #.5 R2O2. + #.75 HCHO + #.75 PROD2 + #3.25 XC
M2O3)	1.010E-15	2.493	0.00	;B-PINENE + O3 = #.34 HO. + #.09 HO2. + #.05 RO2-N. + #.2 R2O2. + #.2 RCO-O2. + #.375 CO + #.1 CO2 + #.25 HCHO + #.75 PROD2 + #.28 HCOOH + #3.595 XC
M2N3)	2.510E-12	0.000	0.00	;B-PINENE + NO3 = #.75 RO2-R. + #.25 RO2-N. + #.75 R2O2. + #.75 RNO3 + #4 XC + #.25 XN
M2OA)	2.700E-11	0.000	0.00	;B-PINENE + O3P = #.4 RCHO + #.6 PROD2 + #5.2 XC
M3OH)	1.640E-11	-0.994	0.00	;3-CARENE + HO. = #.75 RO2-R. + #.25 RO2-N. + #.5 R2O2. + #.75 RCHO + #6.25 XC
M3O3)	1.010E-15	1.958	0.00	;3-CARENE + O3 = #.7 HO. + #.161 RO2-N. +

				#.539 R2O2. + #.482 CCO-O2. + #.058 RCO-O2. + #.058 HCHO + #.482 RCHO + #.3 RCO-OH + #5.492 XC
M3N3)	9.100E-12	0.000	0.00	;3-CARENE + NO3 = #.75 NO2 + #.25 RO2-N. + #.75 R2O2. + #.75 RCHO + #6.25 XC + #.25 XN
M3OA)	3.200E-11	0.000	0.00	;3-CARENE + O3P = PROD2 + #4 XC
M4OH)	2.190E-11	-0.994	0.00	;SABINENE + HO. = #.75 RO2-R. + #.25 RO2-N. + #.5 R2O2. + #.75 HCHO + #.75 PROD2 + #3.25 XC
M4O3)	1.010E-15	1.459	0.00	;SABINENE + O3 = #.34 HO. + #.09 HO2. + #.05 RO2-N. + #.2 R2O2. + #.2 RCO-O2. + #.375 CO + #.1 CO2 + #.25 HCHO + #.75 PROD2 + #.28 HCOOH + #3.595 XC
M4N3)	1.000E-11	0.000	0.00	;SABINENE + NO3 = #.75 RO2-R. + #.25 RO2-N. + #.75 R2O2. + #.75 RNO3 + #4 XC + #.25 XN
M4OA)	1.690E-11	0.000	0.00	;SABINENE + O3P = #.4 RCHO + #.6 PROD2 + #5.2 XC
M5OH)	3.190E-11	-0.994	0.00	;D-LIMONE + HO. = #.75 RO2-R. + #.25 RO2-N. + #.5 R2O2. + #.75 RCHO + #6.25 XC
M5O3)	3.710E-15	1.729	0.00	;D-LIMONE + O3 = #.7 HO. + #.161 RO2-N. + #.539 R2O2. + #.482 CCO-O2. + #.058 RCO-O2. + #.058 HCHO + #.482 RCHO + #.3 RCO-OH + #5.492 XC
M5N3)	1.220E-11	0.000	0.00	;D-LIMONE + NO3 = #.75 NO2 + #.25 RO2-N. + #.75 R2O2. + #.75 RCHO + #6.25 XC + #.25 XN
M5OA)	7.200E-11	0.000	0.00	;D-LIMONE + O3P = PROD2 + #4 XC

## References

- Andersson-Skold, Y., Simpson, D. (2001). "Secondary organic aerosol formation in northern Europe: A model study." Journal of Geophysical Research-Atmospheres **106**(D7): 7357-7374.
- Barthelmie, R. J., Pryor, S. C. (1999). "A model mechanism to describe oxidation of monoterpenes leading to secondary organic aerosol - 1. alpha-pinene and beta-pinene." Journal of Geophysical Research-Atmospheres **104**(D19): 23657-23669.
- Birch, M. E., Cary, R. A. (1996). "Elemental carbon-based method for occupational monitoring of particulate diesel exhaust: Methodology and exposure issues." Analyst **121**(9): 1183-1190.
- Bowman, F. M., Karamalegos, A. M. (2002). "Estimated effects of composition on secondary organic aerosol mass concentrations." Environmental Science & Technology **36**(12): 2701-2707.
- Bowman, F. M., Odum, J. R., Seinfeld, J. H., Pandis, S. N. (1997). "Mathematical model for gas-particle partitioning of secondary organic aerosols." Atmospheric Environment **31**(23): 3921-3931.
- Brock, C. A., Trainer, M., Ryerson, T. B., Neuman, J. A., Parrish, D. D., Holloway, J. S., Nicks, D. K., Frost, G. J., Hubler, G., Fehsenfeld, F. C., Wilson, J. C., Reeves, J. M., Lafleur, B. G., Hilbert, H., Atlas, E. L., Donnelly, S. G., Schauffler, S. M., Stroud, V. R., Wiedinmyer, C. (2003). "Particle growth in urban and industrial plumes in Texas." Journal of Geophysical Research-Atmospheres **108**(D3): -.
- Carter, W. P. L. (1990). "A Detailed Mechanism for the Gas-Phase Atmospheric Reactions of Organic-Compounds." Atmospheric Environment Part a-General Topics **24**(3): 481-518.
- Carter, W. P. L. (1995). "Computer Modeling of Environmental Chamber Measurements of Maximum Incremental Reactivities of Volatile Organic-Compounds." Atmospheric Environment **29**(18): 2513-2527.
- Carter, W. P. L. (2000). DOCUMENTATION OF THE SAPRC-99 CHEMICAL MECHANISM FOR VOC REACTIVITY ASSESSMENT, Report to California Air Resources Board.
- Castro, L. M., Pio, C. A., Harrison, R. M., Smith, D. J. T. (1999). "Carbonaceous aerosol in urban and rural European atmospheres: estimation of secondary organic carbon concentrations." Atmospheric Environment **33**(17): 2771-2781.

- Chow, J. C., Watson, J. G., Crow, D., Lowenthal, D. H., Merrifield, T. (2001). "Comparison of IMPROVE and NIOSH carbon measurements." Aerosol Science and Technology **34**(1): 23-34.
- Chow, J. C., Watson, J. G., Pritchett, L. C., Pierson, W. R., Frazier, C. A., Purcell, R. G. (1993). "The Dri Thermal Optical Reflectance Carbon Analysis System - Description, Evaluation and Applications in United-States Air-Quality Studies." Atmospheric Environment Part a-General Topics **27**(8): 1185-1201.
- Cocker, D. R., Clegg, S. L., Flagan, R. C., Seinfeld, J. H. (2001a). "The effect of water on gas-particle partitioning of secondary organic aerosol. Part I: alpha-pinene/ozone system." Atmospheric Environment **35**(35): 6049-6072.
- Cocker, D. R., Mader, B. T., Kalberer, M., Flagan, R. C., Seinfeld, J. H. (2001b). "The effect of water on gas-particle partitioning of secondary organic aerosol: II. m-xylene and 1,3,5-trimethylbenzene photooxidation systems." Atmospheric Environment **35**(35): 6073-6085.
- Cousins, I. T., Mackay, D. (2001). "Gas - Particle partitioning of organic compounds and its interpretation using relative solubilities." Environmental Science & Technology **35**(4): 643-647.
- Dechapanya, W., Eusebi, A., Kimura, Y., Allen, D. T. (2003a). "Secondary organic aerosol formation from aromatic precursors. 1. Mechanisms for individual hydrocarbons." Environmental Science & Technology **37**(16): 3662-3670.
- Dechapanya, W., Eusebi, A., Kimura, Y., Allen, D. T. (2003b). "Secondary organic aerosol formation from aromatic precursors. 2. Mechanisms for lumped aromatic hydrocarbons." Environmental Science & Technology **37**(16): 3671-3679.
- Dechapanya, W., Russell, M. M., Allen, D. T. (2003c). "Estimates of anthropogenic secondary organic aerosol formation in Houston, Texas." Aerosol Science and Technology **In press**.
- Edney, E. O., Driscoll, D. J., Speer, R. E., Weathers, W. S., Kleindienst, T. E., Li, W., Smith, D. F. (2000). "Impact of aerosol liquid water on secondary organic aerosol yields of irradiated toluene/propylene/NO<sub>x</sub>/(NH<sub>4</sub>)<sub>2</sub> SO<sub>4</sub>/air mixtures." Atmospheric Environment **34**(23): 3907-3919.
- ENVIRON International Corporation (2002). User's guide. Comprehensive Air Quality Model with Extensions (CAMx) version 3.1. Novato.
- Fraser, M. P., Yue, Z. W., Tropp, R. J., Kohl, S. D., Chow, J. C. (2002). "Molecular composition of organic fine particulate matter in Houston, TX." Atmospheric Environment **36**(38): 5751-5758.

- Gear, C. W. (1971). Numerical Initial Value Problems in Ordinary Differential Equations. Englewood Cliffs, N.J., Prentice-Hall.
- Geron, C., Rasmussen, R., R. Arnts, R., Guenther, A. (2000). "A review and synthesis of monoterpene speciation from forests in the United States." Atmospheric Environment **34**(11): 1761-1781.
- Gery, M. W., Whitten, G. Z., Killus, J. P., Dodge, M. C. (1989). "A Photochemical Kinetics Mechanism for Urban and Regional Scale Computer Modeling." Journal of Geophysical Research-Atmospheres **94**(D10): 12925-12956.
- Gray, H. A., Cass, G. R., Huntzicker, J. J., Heyerdahl, E. K., Rau, J. A. (1986). "Characteristics of Atmospheric Organic and Elemental Carbon Particle Concentrations in Los-Angeles." Environmental Science & Technology **20**(6): 580-589.
- Griffin, R. J., Cocker, D. R., Flagan, R. C., Seinfeld, J. H. (1999). "Organic aerosol formation from the oxidation of biogenic hydrocarbons." Journal of Geophysical Research-Atmospheres **104**(D3): 3555-3567.
- Griffin, R. J., Dabdub, D., Kleeman, M. J., Fraser, M. P., Cass, G. R., Seinfeld, J. H. (2002a). "Secondary organic aerosol - 3. Urban/regional scale model of size- and composition-resolved aerosols." Journal of Geophysical Research-Atmospheres **107**(D17): art. no.-4334.
- Griffin, R. J., Dabdub, D., Seinfeld, J. H. (2002b). "Secondary organic aerosol - 1. Atmospheric chemical mechanism for production of molecular constituents." Journal of Geophysical Research-Atmospheres **107**(D17): art. no.-4332.
- Grosjean, D., Seinfeld, J. H. (1989). "Parameterization of the Formation Potential of Secondary Organic Aerosols." Atmospheric Environment **23**(8): 1733-1747.
- Guenther, A., Wiedinmyer, C., Karl, T. (2003). "A global model of methanol, ethanol, acetone, acetaldehyde, ethene, propene and butene emissions from vegetation." In preparation.
- Hatakeyama, S., Izumi, K., Fukuyama, T., Akimoto, H. (1989). "Reactions of Ozone with Alpha-Pinene and Beta-Pinene in Air - Yields of Gaseous and Particulate Products." Journal of Geophysical Research-Atmospheres **94**(D10): 13013-13024.
- Hindmarsh, A. C. (1983). Odepack, a systematized collection of ode solvers. Scientific Computing. R. S. e. a. Stepleman. Amsterdam, North-Holland: 55-64.
- Hoffmann, T., Odum, J. R., Bowman, F., Collins, D., Klockow, D., Flagan, R. C., Seinfeld, J. H. (1997). "Formation of organic aerosols from the oxidation of biogenic hydrocarbons." Journal of Atmospheric Chemistry **26**(2): 189-222.

- Izumi, K., Fukuyama, T. (1990). "Photochemical Aerosol Formation from Aromatic-Hydrocarbons in the Presence of Nox." Atmospheric Environment Part a-General Topics **24**(6): 1433-1441.
- Jacobson, M. C., Hansson, H. C., Noone, K. J., Charlson, R. J. (2000). "Organic atmospheric aerosols: Review and state of the science." Reviews of Geophysics **38**(2): 267-294.
- Jang, M., Kamens, R. M. (1998). "A thermodynamic approach for modeling partitioning of semivolatile organic compounds on atmospheric particulate matter: Humidity effects." Environmental Science & Technology **32**(9): 1237-1243.
- Jang, M., Kamens, R. M., Leach, K. B., Strommen, M. R. (1997). "A thermodynamic approach using group contribution methods to model the partitioning of semivolatile organic compounds on atmospheric particulate matter." Environmental Science & Technology **31**(10): 2805-2811.
- Jang, M. S., Czoschke, N. M., Lee, S., Kamens, R. M. (2002). "Heterogeneous atmospheric aerosol production by acid-catalyzed particle-phase reactions." Science **298**(5594): 814-817.
- Jaoui, M., Kamens, R. M. (2001). "Mass balance of gaseous and particulate products analysis from alpha-pinene/NOx/air in the presence of natural sunlight." Journal of Geophysical Research-Atmospheres **106**(D12): 12541-12558.
- Jenkin, M. E., Saunders, S. M., Pilling, M. J. (1997). "The tropospheric degradation of volatile organic compounds: A protocol for mechanism development." Atmospheric Environment **31**(1): 81-104.
- Junge, C. E. (1977). Basic considerations about trace constituents in the atmosphere as related to the fate of global pollutants. Fate of Pollutants in the Air and Water Environments, Part I. N. Y. Wiley: 7-26.
- Kalberer, M., Yu, J., Cocker, D. R., Flagan, R. C., Seinfeld, J. H. (2000). "Aerosol formation in the cyclohexene-ozone system." Environmental Science & Technology **34**(23): 4894-4901.
- Kamens, R., Jang, M., Chien, C. J., Leach, K. (1999). "Aerosol formation from the reaction of alpha-pinene and ozone using a gas-phase kinetics aerosol partitioning model." Environmental Science & Technology **33**(9): 1430-1438.
- Kamens, R. M., Jaoui, M. (2001). "Modeling aerosol formation from alpha-pinene plus NOx in the presence of natural sunlight using gas-phase kinetics and gas-particle partitioning theory." Environmental Science & Technology **35**(7): 1394-1405.
- Khalil, M. A. K., Rasmussen, R. A. (2003). "Tracers of wood smoke." Atmospheric Environment **37**(9-10): 1211-1222.

- Lemire, K. R., Allen, D. T., Klouda, G. A., Lewis, C. W. (2002). "Fine particulate matter source attribution for Southeast Texas using C-14/C-13 ratios." Journal of Geophysical Research-Atmospheres **107**(D22): art. no.-4613.
- Liang, C. K., Pankow, J. F., Odum, J. R., Seinfeld, J. H. (1997). "Gas/particle partitioning of semivolatile organic compounds to model inorganic, organic, and ambient smog aerosols." Environmental Science & Technology **31**(11): 3086-3092.
- Lim, H. J., Turpin, B. J. (2002). "Origins of primary and secondary organic aerosol in Atlanta: Results of time-resolved measurements during the Atlanta supersite experiment." Environmental Science & Technology **36**(21): 4489-4496.
- Lurmann, F. W., Wexler, A. S., Pandis, S. N., Musarra, S., Kumar, N., Seinfeld, J. H. (1997). "Modelling urban and regional aerosols .2. Application to California's South Coast Air Basin." Atmospheric Environment **31**(17): 2695-2715.
- Meng, Z. Y., Dabdub, D., Seinfeld, J. H. (1998). "Size-resolved and chemically resolved model of atmospheric aerosol dynamics." Journal of Geophysical Research-Atmospheres **103**(D3): 3419-3435.
- NIOSH (1996). Elemental Carbon (Diesel Particulate): Method 5040. NIOSH Manual of Analytical Methods. Publication No 96-135. P. M. Eller and M. E. Cassinelli. Cincinnati, OH, (National Institute for Occupational Safety and Health).
- NIOSH (1998). NIOSH Method 5040, Elemental Carbon (Diesel Particulate). NIOSH Manual of Analytical Methods. Cincinnati, OH, (National Institute for Occupational Safety and Health).
- NOAA (2003a). Environmental Technology Lab. At: [http://www.etl.noaa.gov/et2/data/data\\_pages/texaq/air\\_aerosol.html](http://www.etl.noaa.gov/et2/data/data_pages/texaq/air_aerosol.html), National Oceanic Atmospheric Administration. **2003**.
- NOAA (2003b). National Climatic Data Center. At: [www.ncdc.noaa.gov/oa/ncdc.html](http://www.ncdc.noaa.gov/oa/ncdc.html), National Oceanic Atmospheric Administration. **2003**.
- NOAA (2003c). TexAQS 2000 Phase II, Analysis of NOAA Data, Final Report., National Oceanic Atmospheric Administration Aeronomy Labs. **2003**.
- Odum, J. R., Hoffmann, T., Bowman, F., Collins, D., Flagan, R. C., Seinfeld, J. H. (1996). "Gas/particle partitioning and secondary organic aerosol yields." Environmental Science & Technology **30**(8): 2580-2585.
- Odum, J. R., Jungkamp, T. P. W., Griffin, R. J., Flagan, R. C., Seinfeld, J. H. (1997a). "The atmospheric aerosol-forming potential of whole gasoline vapor." Science **276**(5309): 96-99.

- Odum, J. R., Jungkamp, T. P. W., Griffin, R. J., Forstner, H. J. L., Flagan, R. C., Seinfeld, J. H. (1997b). "Aromatics, reformulated gasoline, and atmospheric organic aerosol formation." Environmental Science & Technology **31**(7): 1890-1897.
- Pandis, S. N., Harley, R. A., Cass, G. R., Seinfeld, J. H. (1992). "Secondary Organic Aerosol Formation and Transport." Atmospheric Environment Part a-General Topics **26**(13): 2269-2282.
- Pandis, S. N., Paulson, S. E., Seinfeld, J. H., Flagan, R. C. (1991). "Aerosol Formation in the Photooxidation of Isoprene and Beta-Pinene." Atmospheric Environment Part a-General Topics **25**(5-6): 997-1008.
- Pankow, J. F. (1987). "Review and Comparative-Analysis of the Theories on Partitioning between the Gas and Aerosol Particulate Phases in the Atmosphere." Atmospheric Environment **21**(11): 2275-2283.
- Pankow, J. F. (1994). "An Absorption-Model of Gas-Particle Partitioning of Organic-Compounds in the Atmosphere." Atmospheric Environment **28**(2): 185-188.
- Pankow, J. F., Seinfeld, J. H., Asher, W. E., Erdakos, G. B. (2001). "Modeling the formation of secondary organic aerosol. 1. Application of theoretical principles to measurements obtained in the alpha-pinene/, beta-pinene/, sabinene/, Delta(3)-carene/, and cyclohexene/ozone systems." Environmental Science & Technology **35**(6): 1164-1172.
- Pilinis, C., Seinfeld, J. H. (1988). "Development and Evaluation of an Eulerian Photochemical Gas Aerosol Model." Atmospheric Environment **22**(9): 1985-2001.
- Pun, B. K., Griffin, R. J., Seigneur, C., Seinfeld, J. H. (2002a). "Secondary organic aerosol - 2. Thermodynamic model for gas/particle partitioning of molecular constituents." Journal of Geophysical Research-Atmospheres **107**(D17): art. no.-4333.
- Pun, B. K., Wu, S. Y., Seigneur, C. (2002b). "Contribution of biogenic emissions to the formation of ozone and particulate matter in the eastern united states." Environmental Science & Technology **36**(16): 3586-3596.
- Russell, A., Dennis, R. (2000). "NARSTO critical review of photochemical models and modeling." Atmospheric Environment **34**(12-14): 2283-2324.
- Saxena, P., Hildemann, L. M., McMurry, P. H., Seinfeld, J. H. (1995). "Organics Alter Hygroscopic Behavior of Atmospheric Particles." Journal of Geophysical Research-Atmospheres **100**(D9): 18755-18770.

- Schell, B., Ackermann, I. J., Hass, H., Binkowski, F. S., Ebel, A. (2001). "Modeling the formation of secondary organic aerosol within a comprehensive air quality model system." Journal of Geophysical Research-Atmospheres **106**(D22): 28275-28293.
- Seinfeld, J. H., Erdakos, G. B., Asher, W. E., Pankow, J. F. (2001). "Modeling the formation of secondary organic aerosol (SOA). 2. The predicted effects of relative humidity on aerosol formation in the alpha-pinene-, beta-pinene-, sabinene-, Delta(3)-Carene-, and cyclohexene-ozone systems." Environmental Science & Technology **35**(9): 1806-1817.
- Seinfeld, J. H., Pandis, S. N. (1998). Atmospheric Chemistry and Physics, From Air Pollution to Climate Change, John Wiley and Sons, Inc. NY.
- Sheehan, P. E., Bowman, F. M. (2001). "Estimated effects of temperature on secondary organic aerosol concentrations." Environmental Science & Technology **35**(11): 2129-2135.
- Stockwell, W. R., Kirchner, F., Kuhn, M., Seefeld, S. (1997). "A new mechanism for regional atmospheric chemistry modeling." Journal of Geophysical Research-Atmospheres **102**(D22): 25847-25879.
- Stockwell, W. R., Middleton, P., Chang, J. S., Tang, X. Y. (1990). "The 2nd Generation Regional Acid Deposition Model Chemical Mechanism for Regional Air-Quality Modeling." Journal of Geophysical Research-Atmospheres **95**(D10): 16343-16367.
- Strader, R., Lurmann, F., Pandis, S. N. (1999). "Evaluation of secondary organic aerosol formation in winter." Atmospheric Environment **33**(29): 4849-4863.
- Sun, P., Chock, D. P., Winkler, S. L. (1994). "An Implicit-Explicit Hybrid Solver for a System of Stiff Kinetic Equations." Journal of Computational Physics **115**(2): 515-523.
- Tropp, R. J., Kohl, S. D., Chow, J. C., Frazier, C. A. (1998). Final Report for the Texas PM<sub>2.5</sub> Sampling and Analysis Study, Desert Research Institute and TRC Environmental Corporation.
- Turpin, B. J., Huntzicker, J. J. (1991). "Secondary Formation of Organic Aerosol in the Los-Angeles Basin - a Descriptive Analysis of Organic and Elemental Carbon Concentrations." Atmospheric Environment Part a-General Topics **25**(2): 207-215.
- Turpin, B. J., Huntzicker, J. J. (1995). "Identification of Secondary Organic Aerosol Episodes and Quantitation of Primary and Secondary Organic Aerosol Concentrations During Scaqs." Atmospheric Environment **29**(23): 3527-3544.

- Turpin, B. J., Lim, H. J. (2001). "Species contributions to PM<sub>2.5</sub> mass concentrations: Revisiting common assumptions for estimating organic mass." Aerosol Science and Technology **35**(1): 602-610.
- Turpin, B. J., Saxena, P., Andrews, E. (2000). "Measuring and simulating particulate organics in the atmosphere: problems and prospects." Atmospheric Environment **34**(18): 2983-3013.
- USEPA (2002). Aerometric Information Retrieval System (AIRS) Database. At: [www.epa.gov/air/data/airfdb.html](http://www.epa.gov/air/data/airfdb.html), U.S. Environmental Protection Agency. **2002**.
- Vizueté, W., Junquera, V., Allen, D. T. (2003). "Sesquiterpene emissions and secondary organic aerosol formation potentials for Southeast Texas." Aerosol Science and Technology **In press**.
- Walk, C. J., Katchick, J. W., Loos, K., Crow, W. L., Dattner, S., Price, J., Lambeth, B., Jr., M. A., McMullen, G., Chow, J. C., Tropp, R. J. (1999). The Results of a Collaborative Effort to Measure and Speciate PM<sub>2.5</sub> in Houston and other Texas Cities. 92 Annual Air & Waste Management Conference.
- Yamasaki, H., Kuwata, K., Miyamoto, H. (1982). "Effects of Ambient-Temperature on Aspects of Airborne Polycyclic Aromatic-Hydrocarbons." Environmental Science & Technology **16**(4): 189-194.
- Yu, J. Z., Cocker, D. R., Griffin, R. J., Flagan, R. C., Seinfeld, J. H. (1999). "Gas-phase ozone oxidation of monoterpenes: Gaseous and particulate products." Journal of Atmospheric Chemistry **34**(2): 207-258.
- Zhang, S. H., Shaw, M., Seinfeld, J. H., Flagan, R. C. (1992). "Photochemical Aerosol Formation from Alpha-Pinene- and Beta-Pinene." Journal of Geophysical Research-Atmospheres **97**(D18): 20717-20729.

## **Vita**

Matthew Maclean Russell was born in Ottawa, Canada on March 26<sup>th</sup>, 1974, the son of Linda Joyce Russell and Neil Maclean Russell. Matthew was raised on the Caribbean Island of St. Maarten and earned a V.W.O (Voorbereidend Wetenschappelijk Onderwijs) degree from the Milton Peters College. After high school, Matthew returned to Ottawa and earned a Bachelor of Engineering in Environmental Engineering from Carleton University, graduating in 1996. Matthew entered the University of Texas at Austin in 1997 and earned a Master's of Science in Engineering in Environmental and Water Resources Engineering in 1999. Matthew started the Ph.D program in Civil Engineering at the University of Texas at Austin in 2000.

Permanent address: 807-2400 Carling Avenue, Ottawa, CANADA K2B7H2

This dissertation was typed by the author.